Table of Contents

I. Symmetry and Group Theory.

All of the topics covered in this course make extensive use of molecular symmetry and group theory - topics of entire books by themselves. It is the aim of this text to present group theory in sufficient detail so that the student can solve most day to day spectroscopic problems and read the spectroscopy literature.

A **symmetry operation** is a rotation and/or reflection which leaves the molecule unchanged. It is performed about a **symmetry element**: a point, a line or a plane. The square planar $PtCl_4^{2-}$ ion is said to be a higly symmetric ion because it contains a large number of symmetry elements. All of the symmetry operations that apply to a molecule or ion constitute its *point group*. It is the point group to which the molecule belongs that designates its symmetry. In the next section, it will be shown that sixteen symmetry operations can be performed on the $PtCl_4^{2-}$ ion. These sixteen operations constitute what is known as the D_{4h} point group, *i.e.*, $PtCl_4^{2-}$ has D_{4h} symmetry. In a treatment of the spectroscopy or bonding of an inorganic compound, one must first determine the point group to which the system belongs. A full appreciation of what D_{4h} symmetry implies requires the visualization of the symmetry elements and operations as well as an understanding of groups. In the following two sections, the various symmetry operations and groups will be discussed while the point group definitions are given in section I.4. The remainder of the chapter is devoted to representations of the point groups and to some simple applications of group theory to spectroscopy and bonding.

I.1 Symmetry operations and symmetry elements

There are only five *types* of symmetry operations required for the systems covered in this course, and the $PtCl_4^{2-}$ ion contains examples of each. In this section, each type of operation will be discussed in terms of its effect on this ion. The effect of the operations on the chlorine p_z orbitals will also be considered in order to better illustrate the effects of the operations. Thus, in the figures that follow, ① will represent chlorine atom 1 with the positive lobe of the p_z orbital out of the plane of the paper while ❶ will imply that the negative lobe of the p_z orbital is out of the plane of the paper for chlorine atom 1.

1. The **Identity Operation** (**E**) does nothing and has no symmetry element but it is a required member of each symmetry group. Thus, operation with **E** will change neither the positions of the atoms nor the phases of the p_z orbitals.

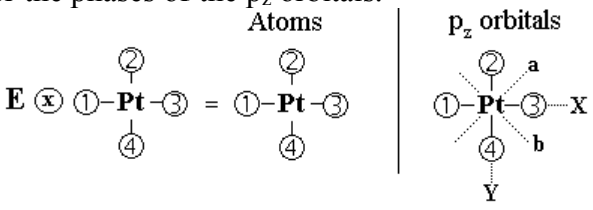

Figure I-1. The effect of the identity operation on the atoms and the chlorine p_z orbitals in $PtCl_4^{2-}$. Also the definitions of the X, Y, a and b axes relevant to other discussions are defined.

2. An **n-fold rotation** ($\mathbf{C}_n$) is a rotation of $2\pi/n$ radians about an axis. The axis with the **highest value of n is the principle axis** and is designated as the z-axis. Thus the z-axis in $PtCl_4^{2-}$ is perpendicular to the plane of the ion. This axis is actually three symmetry elements since rotations by $\pi/2$, π, and $3\pi/2$ about this axis all result in no change in the molecule. These

three axes are referred to as C_4, $C_4^2 = C_2$ and C_4^3, respectively.[1] Rotation about the z-axis will not change the phase of the p_z orbitals. The X, Y, a and b axes defined in figure I-1 are also C_2 rotational axes. It will be shown later that the C_2 rotations in this group can be grouped into three *classes* which are differentiated with the use of ' and " {$C_2(Z)$},{$C_2'(X)$ & $C_2'(Y)$}, {$C_2''(a)$ & $C_2''(b)$}. Since the C_2' and C_2'' axes are perpendicular to the z-axis, rotation about any one of them will invert the p_z orbitals as shown in figure I-2.

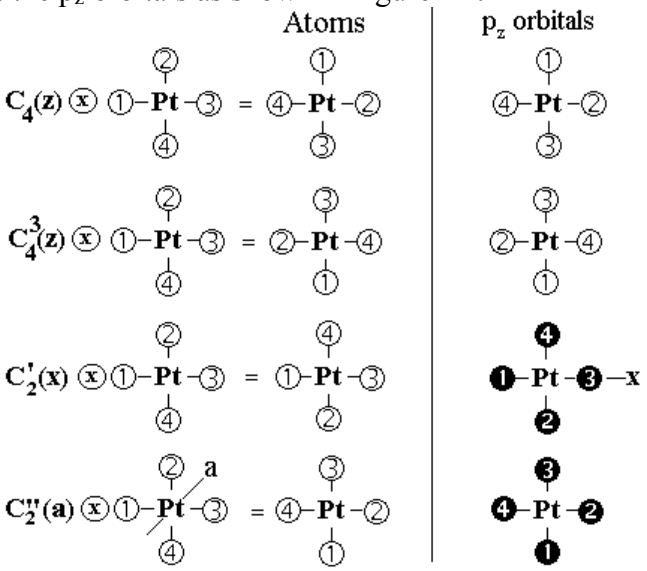

Figure I-2. The effect of some of the C_n operations on the atoms and the chlorine p_z orbitals in $PtCl_4^{2-}$.

Thus the ion contains C_4 , C_4^3 , $C_4^2 = C_2$, $C_2'(x)$,$C_2'(y)$, $C_2''(a)$ and $C_2''(b)$ or 7 rotational axes.

3. **Reflections** can be made through three different types of planes: vertical planes (σ_v) contain the principle axis**,** horizontal planes (σ_h) are perpendiuclar to the principle axis and dihedral planes (σ_d) contain the principle axis and bisect two C_2 axes. The distinction between vertical and dihedral is often unclear. Where appropriate, planes bisecting bond angles will be designated as dihedral while those containing bonds will be designated as vertical. See figure I-3.

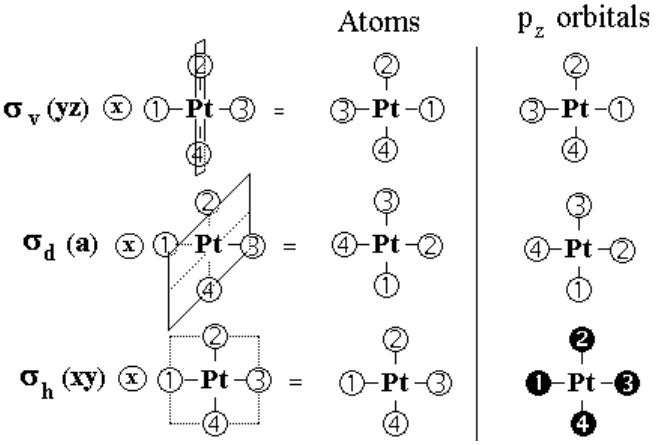

[1] Since the clockwise C_4^3 operation is equivalent to a counterclockwise C_4 rotation, the C_4 and C_4^3 operations are also referred to as the C_4^+ and C_4^- operations, respectively.

Figure I-3. The effect of reflection through the symmetry planes on the atoms and the chlorine p_z orbitals in $PtCl_4^{2-}$.

In $PtCl_4^{2-}$, the planes containing the z-axis (σ_v and σ_d) will not change the phase of the p_z-orbitals while reflection through the plane perpendicular to the z-axis (σ_h) does invert them (figure I-3). Thus, $PtCl_4^{2-}$ contains: σ_v(XZ)and σ_v(YZ), σ_h(XY) and σ_d (a) and σ_d (b) or five planes of symmetry. Note that the a and b planes are defined as those planes perpendicular to the plane of the ion and containing the a and b rotational axes.

4. An **improper rotation or a rotary reflection** ($\mathbf{S_n}$) is a C_n followed by a σ_h. Since $PtCl_4^{2-}$ is a planar ion, the Z-axis is an element for both proper and improper rotations. See figure I-4. Note that an S_4 results in the same numbering as a C_4, but the phases of the p_z orbitals are changed.

5. A **Center of Inversion** (**i**) takes all (x,y,z) → (-x,-y,-z). This operation can be performed by a C_2(z) which takes (x,y,z) → (-x,-y,+z) followed by a σ(xy) which inverts z, i.e., $\mathbf{i = C_2\sigma_h = S_2}$. Since i and S_2 are equivalent, S_2 is not usually used.

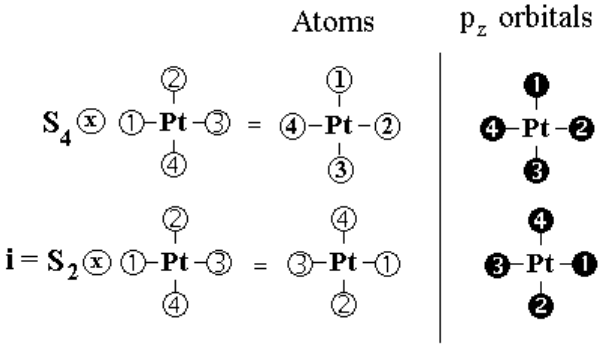

Figure I-4. The effect of improper rotations on the atoms and the chlorine p_z orbitals in $PtCl_4^{2-}$.

$PtCl_4^{2-}$ contains E, C_4 , C_4^3 , $C_4^2 = C_2$, C_2'(x) ,C_2'(y), C_2''(a), C_2''(b), i, S_4, S_4^3 ,σ_v(XZ), σ_v(YZ), σ_h, σ_d (a) and σ_d (b). These sixteen symmetry elements specify the symmetry of the ion.

Show that trigonal bipyramidal MX_5 contains the following symmetry elements: E,C_3, C_3^2, C_2, C_2', C_2'', σ_v, σ_v', σ_v'', S_3, and S_3^2

Successive Operations. In some of the following discussion, the result of applying more than one operation will be important. The result of performing a C_4 rotation followed by a reflection through the XZ plane ($\sigma_v C_4$) is the same as a single σ_d(a) operation.

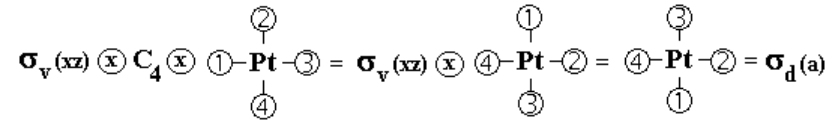

However, if the order of the operations is reversed, *i.e.*, $C_4\sigma_v$, the result is equivalent to a σ_d(b).

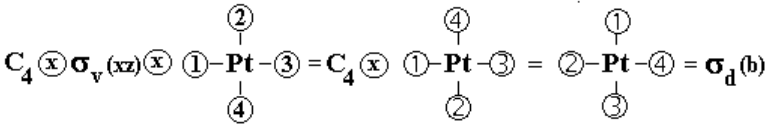

It is important to note that in this case the order of the operation is important, *i.e.*, $C_4\sigma_v \neq \sigma_v C_4$. In some instances, the order of operation is not important. Two operations **commute** if the result of successive application of the two operators is the same irrespective of the order in which they were carried out. Thus, C_4 and σ_v do not commute, but, as shown below, C_4 and σ_h do commute, *i.e.*, $C_4\sigma_h = S_4 = \sigma_h C_4$.

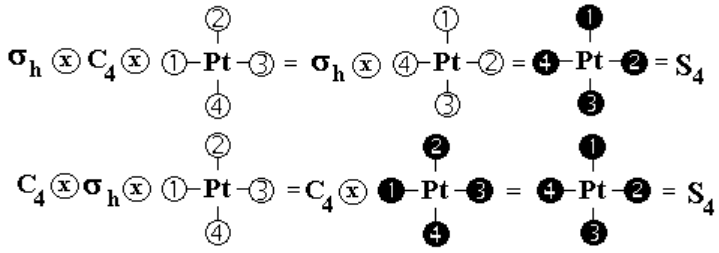

Show that $\sigma_v(XZ)C_2(X) = \sigma_h$ for the trigonal bipyramidal MX_5.

I.2 Groups

A set of operations like those above form a group if they meet the following requirements:

1. The set contains the identity operation, **E**. **RE** = **ER** = **R**.

2. The **product of any two operations of the group must also be a member of the group**. From above, it should be clear that $C_4\sigma_v(XZ) = \sigma_d(b)$ while $\sigma_v(XZ)C_4 = \sigma_d(a)$. Verify that $C_2(a)\sigma_v(XZ) = S_4^3$.

3. **Multiplication is associative for all members of the group**. The triple product $C_2(a)\sigma_v(XZ)C_4$ can be written either as $\{C_2(a)\sigma_v(XZ)\}C_4 = S_4^3C_4 = \sigma_h$ or as $C_2(a)\{\sigma_v(XZ)C_4\} = C_2(a)\sigma_d(a) = \sigma_h$

4. The **inverse of every operation is a member of the group**. The inverse of an operation is that operation which returns the system to its original form, *i.e.*, $RR^{-1} = E$. A reflection through a plane and a two-fold rotation are each their own inverse.

The sixteen symmetry operations discussed for the $PtCl_4^{2-}$ ion satisfy all of these requirements and constitute a group. **Groups of symmetry operations are called point groups**. As mentioned previously, the point group to which $PtCl_4^{2-}$ belongs is called D_{4h}. The **number of members of the group is called the order** of the group and given the **symbol h**. For the D_{4h} point group, h=16.

A **multiplication table** presents the results of the multiplication, *i.e.*, the successive application of two operations. By convention, the first operation performed is given at the top of the column and the second operation involved is at the beginning of the row. The multiplication table for the E, C_4, C_2 and C_4^3 operations of the D_{4h} point group is given below.

first → / second ↓	E	C_4	C_2	C_4^3
E	E	C_4	C_2	C_4^3
C_4	C_4	C_2	C_4^3	E

C_2	C_2	C_4^3	E	C_4
C_4^3	C_4^3	E	C_4	C_2

These operations satisfy all of the requirements of a group of order 4 (h=4). Indeed, they comprise the C_4 point group. Since all of the members of the C_4 point group are also found in the D_{4h} point group (h=16), C_4 is said to be a **subgroup** of D_{4h}. Note that the order of a subgroup must be an integral divisor of the order of the group.

Problem I.1. Water belongs to the C_{2v} point group, $\{C_{2v} | E, C_2, \sigma(XZ), \sigma(YZ)\}$. Define the molecular plane as the XZ plane and generate the multiplication table for the C_{2v} point group.

In the following section, extensive use of the multiplication table will be made, but since the point group is so large, its multiplication table is cumbersome (16x16). We will, therefore, consider the ammonia molecule which has lower symmetry. NH_3 belongs to the C_{3v} point group of order 6, $\{C_{3v}| E, C_3, C_3^2, \sigma_v, \sigma_v', \sigma_v''\}$. The effect of each of the symmetry operations of the C_{3v} point group on the ammonia molecule is shown in figure I.5

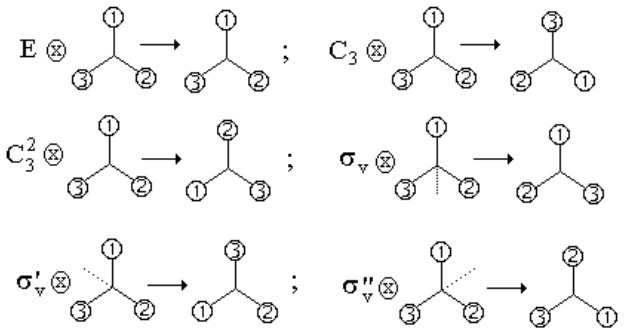

Figure I.5. The effect of each of the symmetry operations of the C_{3v} point group on the ammonia molecule as viewed down the C_3 axis.

The student should verify that the multiplication table for the C_{3v} point group is,

first → / second ↓	E	C_3	C_3^2	σ_v	σ_v'	σ_v''
E	E	C_3	C_3^2	σ_v	σ_v'	σ_v''
C_3	C_3	C_3^2	E	σ_v''	σ_v	σ_v'
C_3^2	C_3^2	E	C_3	σ_v'	σ_v''	σ_v
σ_v	σ_v	σ_v'	σ_v''	E	C_3	C_3^2
σ_v'	σ_v'	σ_v''	σ_v	C_3^2	E	C_3
σ_v''	σ_v''	σ_v	σ_v'	C_3	C_3^2	E

I.3 Similarity Transformations

The operations, **X** and **Y** are said to be *conjugate* if they are related by a *similarity transfomation*, *i.e.*, if $\mathbf{Z^{-1}XZ} = \mathbf{Y}$, where **Z** is at least one operation of the group**.** A **class** is a complete set of operations which are conjugate to one another. The operations of a class have a "similar" effect and are therefore treated together. To determine which operations of the group are in the same class as C_3, one must determine which operations are conjugate to C_3. The results of the similarity transformation of C_3 with every other member of the group are determined from the multiplication table above to be,

$E^{-1}C_3 E = C_3$	$C_3^{-1}C_3C_3 = C_3^2C_3C_3 = C_3^2C_3^2 = C_3$
$(C_3^2)^{-1}C_3C_3^2 = C_3C_3C_3^2 = C_3^2C_3^2 = C_3$	$\sigma_v^{-1}C_3\sigma_v = \sigma_vC_3\sigma_v = \sigma_v\sigma_v'' = C_3^2$

$(\sigma_v')^{-1}C_3\sigma_{v'} = \sigma_v'C_3\sigma_v' = \sigma_v'\sigma_v = C_3^2$	$(\sigma_v'')^{-1}C_3\sigma_v'' = \sigma_v''C_3\sigma_v'' = \sigma_v''\sigma_v' = C_3^2$

Thus, C_3 and C_3^2 are conjugate and are members of the same class. In a similar manner, it can be shown that σ_v, σ_v', and σ_v'' are also conjugate and these three operations form another class of the C_{3v} point group. The C_{3v} point group is then written as $\{C_{3v} \mid E, 2C_3, 3\sigma_v\}$. The *order of a class must be an integral divisor of the order of the group*. Similar considerations allow us to write the D_{4h} point group as $\{D_{4h} \mid E, 2C_4, C_2, 2C_2', 2C_2'', i, 2S_4, \sigma_h, 2\sigma_v, 2\sigma_d\}$.

Problem I.2 Identify the identity operator and the inverse of each function, and determine the classes for a group with the following multiplication table.

	M	N	P	Q	R	S
M	P	S	Q	M	N	R
N	R	Q	S	N	M	P
P	Q	R	M	P	S	N
Q	M	N	P	Q	R	S
R	S	P	N	R	Q	M
S	N	M	R	S	P	Q

I.4 The Point Groups

The following groups all contain the identity operation and only the minimum operations required to define the group are given. In many cases, these minimum operations lead to other operations. In the following, "k" is an integer ≥ 2.

C_1: No symmetry

C_s: Only a plane of symmetry.

C_k: Only a C_k rotational axis:

C_i: Only an inversion center.

C_{kh}: A C_k rotational axis and a σ_h.

C_{kv}: A C_k rotational axis and a σ_v.

D_k: One C_k and kC_2 rotational axes. The kC_2 axes are perpendicular to the C_k and at equal angles to one another.

D_{kh}: The D_k operations plus a σ_h but this combination also results in $k\sigma_v$'s.

D_{kd}: The D_k operations plus $k\sigma_d$'s containing the C_k and bisecting the angles between adjacent C_2's.

S_k: Only the improper rotation, S_k. Note k must be an even number since an odd number would require a σ_h.

T_d: The tetrahedral point group contains three mutally perpendicular C_2 axes, four C_3 axes and a σ_d through each pair of C_3's.

O_h: The octahedral point group has three mutally perpendicular C_4 axes, four C_3 axes and a center of symmetry.

Determining the point group to which a molecule belongs will be the first step in a treatment of the molecular orbitals or spectra of a compound. It is therefore important that this be done somewhat systematically. The flow chart in figure I-6 is offered as an aid, and a few examples should clarify the process. We will first determine the point groups for the following Pt(II) ions,

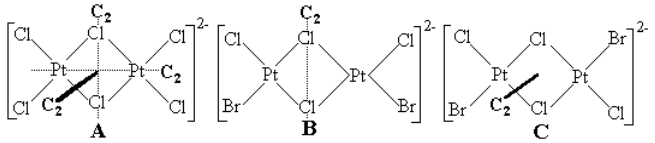

A contains three C_2 axes, *i.e.*, $[C_k?]$ is yes with k=2. It contains a plane of symmetry so $[\sigma?]$ is yes. The three C_2 axes are perpendicular, *i.e*, there is a C_2 axis and two perpendicular C_2's which means that $[\perp C_2?]$ is yes. There is a plane of symmetry perpendicular to the C_2 so $[\sigma_h?]$ is yes and we arrive at the D_{2h} point group. **B** contains only one C_2 axis, no $\perp C_2$'s, no σ_h, but it does

have two σ_v's and is therefore a C_{2v} ion. **C** contains a single C_2 axis and a horizontal plane (the plane of the ion) and therefore has C_{2h} symmetry.

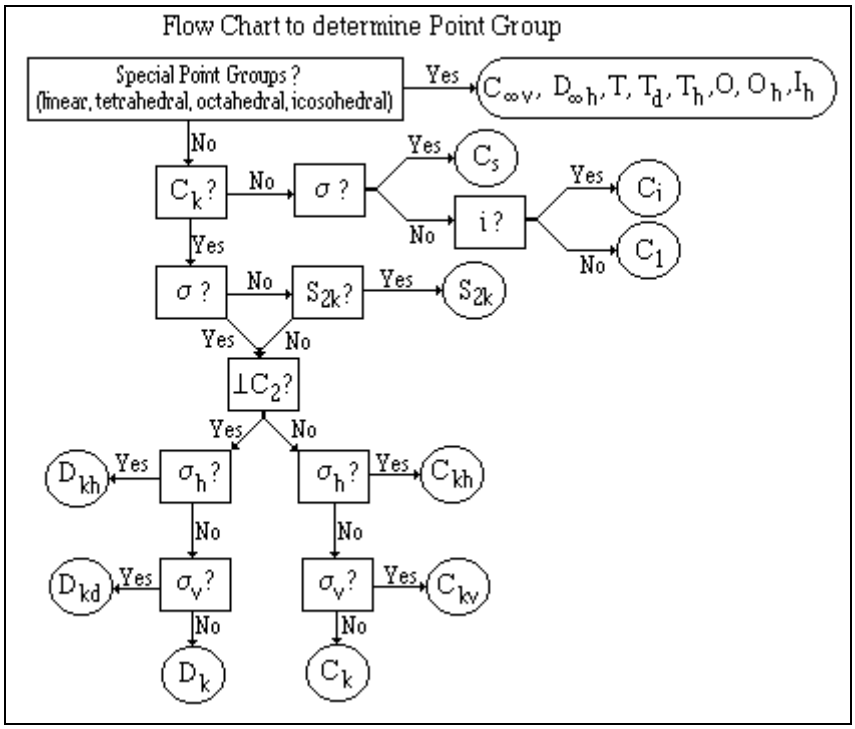

Figure 1-6. Flow chart for the determination of molecular point groups

Next we determine the point group to which the staggered and eclipsed forms of octachlorodirhenate belong.

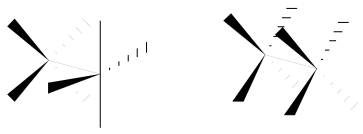

Staggered Eclipsed

Both forms of $[Re_2Cl_8]^{2-}$ contain a C_4 axis (Re-Re bond) so the answer to [C_k?] is yes with k=4. Both contain planes of symmetry so [σ?] is also yes. The four ⊥ C_2's passing through the center of the Re-Re bond are more apparent for the eclipsed form (2 parallel to the ReCl bonds and 2 parallel to their bisectors). Although less apparent than in the eclipsed form, there are also four ⊥ C_2's in the staggered form. As shown below the ⊥ C_2's bisect the Cl-Re-Re-Cl dihedral angles.

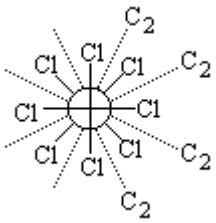

Both forms also contain vertical planes, but the eclipsed form also has a horizontal plane which is absent in the staggered form. The point groups are therefore, D_{4h} for the eclipsed form and D_{4d} for the staggered form.

It is important to become proficient with this skill, but only practice will do it.

Problem I.3 Determine the point group to which each of the following belongs.

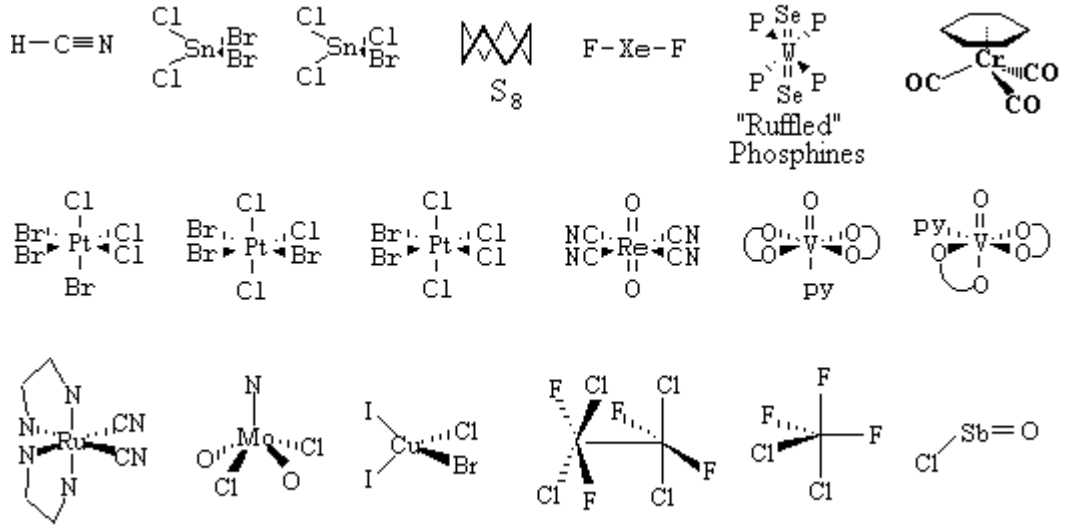

I.5 Matrix Representations of Groups

There are an infinite number of ways of choosing matrices to represent the symmetry operations. The choice of representation is determined by its **basis**, *i.e.*, by the labels or functions attached to the objects. The number of basis functions or labels is called the **dimension** of the representation.

A convenient basis to use when dealing with the motions of molecules is the set of Cartesian displacement vectors. Each atom has three degrees of motional freedom so a molecule with N atoms will generate a basis of dimension 3N. For the water molecule, a 9-dimensional basis results and thus each operation will be represented by a 9x9 matrix. These 9-basis vectors are shown below along with the results of the C_2 (z) rotation.

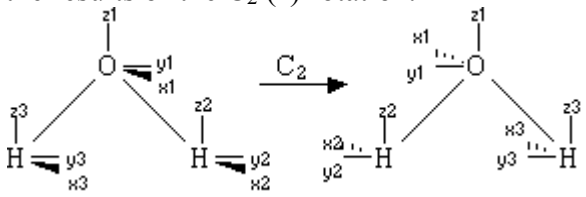

The result of this operation is: ($x_i \rightarrow -x_j$), ($y_i \rightarrow -y_j$), and ($z_i \rightarrow +z_j$) where i = j for the oxygen atom coordinates since the oxygen lies on the C_2 axis and therefore does not change its position, but i ≠ j for the hydrogen atoms since they are do not lie on the C_2 axis and are therefore rotated into one another, *e.g.*, $x_2 \rightarrow -x_3$. We can represent this transformation in matrix notation where each atom will have a 3x3 matrix,

$$\begin{pmatrix} x_i \\ y_i \\ z_i \end{pmatrix} = \begin{pmatrix} -1 & 0 & 0 \\ 0 & -1 & 0 \\ 0 & 0 & +1 \end{pmatrix} \begin{pmatrix} x_j \\ y_j \\ z_j \end{pmatrix}$$

which must be placed into the 9x9 matrix representation of the C_2 operation. The oxygen atom is not moved by the rotation (i = j = 1), so its 3x3 matrix remains in its original position (1,1) on the diagonal while the hydrogen atoms are exchanged by the rotation so their 3x3 matrices are rotated off of the diagonal to the (2,3) and (3,2) positions.

The matrix representation of this C_2 rotation is:

$$C_2 \begin{pmatrix} x_1 \\ y_1 \\ z_1 \\ x_2 \\ y_2 \\ z_2 \\ x_3 \\ y_3 \\ z_3 \end{pmatrix} = \begin{pmatrix} -1 & 0 & 0 & 0 & 0 & 0 & 0 & 0 & 0 \\ 0 & -1 & 0 & 0 & 0 & 0 & 0 & 0 & 0 \\ 0 & 0 & +1 & 0 & 0 & 0 & 0 & 0 & 0 \\ 0 & 0 & 0 & 0 & 0 & 0 & -1 & 0 & 0 \\ 0 & 0 & 0 & 0 & 0 & 0 & 0 & -1 & 0 \\ 0 & 0 & 0 & 0 & 0 & 0 & 0 & 0 & +1 \\ 0 & 0 & 0 & -1 & 0 & 0 & 0 & 0 & 0 \\ 0 & 0 & 0 & 0 & -1 & 0 & 0 & 0 & 0 \\ 0 & 0 & 0 & 0 & 0 & +1 & 0 & 0 & 0 \end{pmatrix} \begin{pmatrix} x_1 \\ y_1 \\ z_1 \\ x_2 \\ y_2 \\ z_2 \\ x_3 \\ y_3 \\ z_3 \end{pmatrix}$$

For reflection through the plane of the molecule (σ_v = YZ), only the x-coordinate is changed and no atoms are moved so the matrix representation is

$$\sigma \begin{pmatrix} x_1 \\ y_1 \\ z_1 \\ x_2 \\ y_2 \\ z_2 \\ x_3 \\ y_3 \\ z_3 \end{pmatrix} = \begin{pmatrix} -1 & 0 & 0 & 0 & 0 & 0 & 0 & 0 & 0 \\ 0 & +1 & 0 & 0 & 0 & 0 & 0 & 0 & 0 \\ 0 & 0 & +1 & 0 & 0 & 0 & 0 & 0 & 0 \\ 0 & 0 & 0 & -1 & 0 & 0 & 0 & 0 & 0 \\ 0 & 0 & 0 & 0 & +1 & 0 & 0 & 0 & 0 \\ 0 & 0 & 0 & 0 & 0 & +1 & 0 & 0 & 0 \\ 0 & 0 & 0 & 0 & 0 & 0 & -1 & 0 & 0 \\ 0 & 0 & 0 & 0 & 0 & 0 & 0 & +1 & 0 \\ 0 & 0 & 0 & 0 & 0 & 0 & 0 & 0 & +1 \end{pmatrix} \begin{pmatrix} x_1 \\ y_1 \\ z_1 \\ x_2 \\ y_2 \\ z_2 \\ x_3 \\ y_3 \\ z_3 \end{pmatrix}$$

Thus, 9x9 matrices like those above could serve as the representations of the operations for the water molecule in this basis. Fortunately, only the **trace** of this matrix needs to be specified, *i.e.*, the sum of the diagonal elements. The resulting number is called the **character**, and the character of an operation **R** is given the symbol $\chi(\mathbf{R})$. In this example, $\chi(C_2) = -1$ and $\chi(\sigma_v) = 3$. Two important points about the character should be apparent from the above:

1. Only those atoms which remain in the same position can contribute to the trace since otherwise their 3x3 matrices will be rotated off of the diagonal.

2. Each operation contributes the same amount to the trace for each atom since all atoms have the same 3x3 matrix.

For a reflection through the plane bisecting the H-O-H bond angle, $\chi(\sigma_v') = +1$ since only the O is unshifted and a plane contributes +1 for each unshifted atom. The **character for the identity element will always be the dimension of the basis** since all labels are unchanged. For water then, $\chi(E) = 9$.

The representation (Γ) for water **in this basis** is:

	E	C_2	σ_v = YZ	σ_v' = XZ
Γ	9	-1	3	1

The s-orbitals can also serve as a basis,

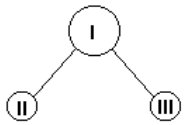

In this basis, each atom has 1 and not 3 labels so each operation is a 3x3 matrix as opposed to the 9x9 matrices of the previous basis. In addition, there can be no sign change for an s-orbital. The resulting representation is,

$$E = \begin{pmatrix}1&0&0\\0&1&0\\0&0&1\end{pmatrix};\quad C_2 = \begin{pmatrix}1&0&0\\0&0&1\\0&1&0\end{pmatrix};\quad \sigma_v = \begin{pmatrix}1&0&0\\0&1&0\\0&0&1\end{pmatrix};\quad \sigma_v' = \begin{pmatrix}1&0&0\\0&0&1\\0&1&0\end{pmatrix}$$

$$\Gamma \qquad\qquad 3 \qquad\qquad\qquad 1 \qquad\qquad\qquad 3 \qquad\qquad\qquad 1$$

If one basis (f ') is a linear combination of another basis (f) or f ' = Cf, then the representation in one basis should be *similar* to that in the other. It can be shown that the matrix representations of operator **R** in these two basis sets (D(**R**) and D'(**R**)) are related by a similarity transformation: $D'(R) = C^{-1}D(R)C$ and $D(R) = CD'(R)C^{-1}$, *i.e.*, the matrices D(R) and D'(R) are conjugate. For example, the linear combination of s-orbitals: X = I + II, Y = I + III and Z = II + III which can be expressed in matrix form as

$$f' = C\,f$$

$$\begin{pmatrix}X\\Y\\Z\end{pmatrix} = \begin{pmatrix}1&1&0\\1&0&1\\0&1&1\end{pmatrix}\begin{pmatrix}I\\II\\III\end{pmatrix} \text{ and the inverse of C is } C^{-1} = \begin{pmatrix}+0.5&+0.5&-0.5\\+0.5&-0.5&+0.5\\-0.5&+0.5&+0.5\end{pmatrix}$$

The matrix representation of C_2 ($D'(C_2)$) in the new basis then is given by $D'(C_2) = C^{-1}D(C_2)C$

or $$D'(C_2) = \begin{pmatrix}+0.5&+0.5&-0.5\\+0.5&-0.5&+0.5\\-0.5&+0.5&+0.5\end{pmatrix}\begin{pmatrix}1&0&0\\0&0&1\\0&1&0\end{pmatrix}\begin{pmatrix}1&1&0\\1&0&1\\0&1&1\end{pmatrix} = \begin{pmatrix}0&1&0\\1&0&0\\0&0&1\end{pmatrix}$$ similarly,

$$D'(\sigma_v') = \begin{pmatrix}0&1&0\\1&0&0\\0&0&1\end{pmatrix} \text{ and } D'(E) = D'(\sigma_v) = \begin{pmatrix}1&0&0\\0&1&0\\0&0&1\end{pmatrix}.$$

Note that the representation for C_2 and σ' have changed, but in all cases **the character is invariant with the similarity transformation**. Thus, *all the members of a class of operations can be treated together since they are related by a similarity transformation and must have the same characters*. The two 3x3 bases used to this point can be viewed as consisting of a 1x1matrix (one basis vector is not rotated into any of the others by any operation of the group - I & Z) and a 2x2 submatrx (two basis vectors are rotated into one another by at least one operation of the group). Thus, the 3x3 representation has been reduced to a 1x1 and a 2x2. Indeed, the 2x2 matrix can be reduced into two 1x1 matrices. In this process, a large **reducible representation** is *decomposed* into smaller (usually 1x1 but sometimes 2x2 and 3x3) **irreducible representations**.

Consider the *symmetry adapted linear combinations (SALC's)*: A = I, B = II + III and C = II - III.

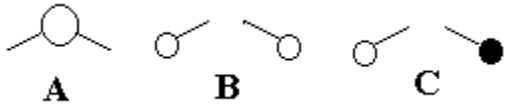

In this basis, a C_2 rotation and a reflection through the plane perpendicular to the molecular plane do not change A or B, and change only the sign of C while reflection through the molecular plane leaves all three unchanged.

$E = \sigma = \begin{pmatrix} 1 & 0 & 0 \\ 0 & 1 & 0 \\ 0 & 0 & 1 \end{pmatrix}$ while $C_2 = \sigma' = \begin{pmatrix} 1 & 0 & 0 \\ 0 & 1 & 0 \\ 0 & 0 & -1 \end{pmatrix}$. In this basis, no basis vector is changed into another by a symmetry operation, *i.e.*, this basis is *symmetry adapted*. Now, our 3x3 representation consists of three 1x1 matrices and we have converted our reducible representation Γ into three irreducible representations, Γ_1; Γ_2 and Γ_3. *i.e.*, $\Gamma = \Gamma_1 + \Gamma_2 + \Gamma_3$

	E	C_2	σ	σ'
Γ_1	1	1	1	1
Γ_2	1	1	1	1
Γ_3	1	-1	1	-1
Γ	3	1	3	1

The term "irreducible representation" is used so frequently that it is often abbreviated as "irrep". We will also use this abbreviation throughout this book,

irrep ≡ irreducible representation

Decomposing a reducible representation into irreps is a very important process, and a procedure to accomplish the decomposition will be described later in this chapter.

I.6 Point Group Representations

A point group representation is a basis set in which the irreducible representations are the basis vectors. As **i**, **j**, and **k** form a complete, orthonormal basis for three-dimensional space, so too do the irreps form the a complete orthonormal basis for an m-dimensional space, where m is the number of irreducible representations and is equal to the number of classes in the group. These considerations are summarized by the following rules.

1. The number of basis vectors or irreps (m) equals the number of classes.
2. The sum of the squares of the dimensions of the m irreps equals the order,

$$\sum_{i=1}^{m} d_i^2 = h$$

   The character of the identity operation equals the dimension of the representation, $\chi(E) = d_i$ which is referred to as the degeneracy of the irrep. The degeneracy of most irreducible representations is 1(non-degenerate representations are 1x1 matrices) but can sometimes be 2 or 3. The icosahedral point group to which C_{60} (Buckminster fulerene or "Buckyball") belongs, has irreducible representations with degeneracies of 4 and 5. No character in an irreducible representation can exceed the dimension of the representation. Thus, in non-degenenerate representations, all characters must be ±1.
3. The member irreps are orthonormal, *i.e.*, the sum of the squares of the characters in any irrep is equal to the order (row normalization), while the sum of the product of the characters over all operations in two different irreps is zero (orthogonality).

$$\sum_{R} g(R)\chi_i(R)\chi_j(R) = h\delta_{ij}$$

where the sum is over all of the *classes* of operations, g(R) is the number of operations, R, in the class, $\chi_i(R)$ and $\chi_j(R)$ are the characters of the operation R in the i^{th} and j^{th} irreps, h is the order of the group and δ_{ij} is the Kroniker delta (0 when $i \neq j$ and 1 when i=j).

4. The sum of the squares of the characters of any operation over all of the irreps times the number of operations in the class is equal to h, *i.e.*, columns of the representation are also normalized.

$$\sum_{i=1}^{m} g(R)\chi_i^2(R) = h$$

where m is the number of irreducible representations.

5. The sum of the products of the characters of any two different operations over all of the irreps is zero, *i.e.*, columns of the representation are also orthoganol.

$$\sum_{i=1}^{m} \chi_i(R')\chi_i(R) = 0$$

6. The first representation is always the totally symmetric representation in which all characters are +1.
7. Any reducible representation in the point group can be expressed as a linear combination of the irreducible representations - the completeness of the set.

We will now generate the C_{2v} point group, $\{C_{2v} \mid E, C_2, \sigma, \sigma'\}$. The order of the group is four and the number of classes in the group is four, *i.e.*, h = m = 4. Each class has only one operation, *i.e.*, g(R)=1 in all cases. Rule 2 states that $d_1^{2+} d_2^2 + d_3^2 + d_4^2 = 4$ so that $d_1 = d_2 = d_3 = d_4 = 1$ - there are no degenerate representations in C_{2v}. The character of the identity operation is always the dimension of the representation, $\chi_i(E) = d_i$. Therefore, all of the characters under the E operation are known. From rule 6 we may write the characters of Γ_1 as +1's only. Thus, we may write the following,

C_{2v}	E	C_2	σ_v	σ_v'
Γ_1	1	1	1	1
Γ_2	1	a	b	c
Γ_3	1	d	e	f
Γ_4	1	g	h	i

and since there are no degenerate representations, characters **a** through **i** must all be +1 or -1. In order to maintain orthogonality of rows and columns, only one of the remaining characters in each row and in each column may be +1 while the other two in each column and row must each be -1, *i.e.*, there are only three remaining +1's and no two can be in the same column or row. We will make **a**, **e** and **i** the +1's and then others must be -1.

The C_{2v} **character table** is then determined to be:

C_{2v}	E	C_2	σ_v	σ_v'
Γ_1	1	1	1	1
Γ_2	1	1	-1	-1
Γ_3	1	-1	1	-1
Γ_4	1	-1	-1	1

Mulliken symbols for irreps:

- "A" means the irrep is symmetric with respect to rotation about the principle axis ($\chi[C_n(z)] = +1$)
- "B" means the irrep is antisymmetric with respect to rotation about the principle axis ($\chi[C_n(z)] = -1$)
- "E" implies a doubly degenerate representation ($d = 2 \Rightarrow \chi(E) = 2$)
- "T" implies a triply degenerate representation ($d = 3 \Rightarrow \chi(E) = 3$)
- "G" and "H" imply degeneracies of 4 and 5, respectively.

In many instances there are more than one A, B, E , etc. irreps present in the point group so subscripts and superscripts are used.

- g or u subscripts are used in point groups with centers of symmetry (i) to denote ***g****erade* (symmetric) and ***u****ngerade* (antisymmetric) with respect to inversion.
- ' and " are used to designate symmetric and antisymmetric with respect to inversion through a σ_h plane
- numerical subscripts are used otherwise.

In the C_{2v} point group then, the irreps are designated as $\Gamma_1 = A_1$; $\Gamma_2 = A_2$; $\Gamma_3 = B_1$; $\Gamma_4 = B_2$.

In the treatment of molecular systems, one generates a reducible representation using an appropriate basis (*e.g.*, atomic orbitals or cartesian displacement vectors) and then decomposes this reducible representation into its component irreps to arrive at a description of the system which contains the information available from the molecular symmetry. There are certain symmetry properties which are very important and do not change so long as the point group remains the same (the metal orbitals for metals on all of the symmetry elements, the translations and rotations, and the dipole operators). Since the symmetries of these various aspects are used frequently, they are also included in the character table. We will now demonstrate the determination of these symmetries for the water molecule.

Since the s-orbital on the oxygen atom lies on all of the symmetry elements and is spherically symmetric, it is unchanged by a rotation about the C_2 axis or reflections through the planes thus the representation for the s-orbital is:

C_{2v}	E	C_2	σ_v	σ_v'
s-orb	+1	+1	+1	+1

which is the A_1 irrep. **s-orbitals on central elements will always transform as the totally symmetric representation but are not included in character tables.**

The three p-orbitals, translation along the x- ,y- and z-axes, and the three components of the electric dipole operator (μ_x, μ_y, μ_z) all transform in the same manner. The p_x and p_y orbitals will change sign with a C_2 operation and with reflection through the perpendicular plane, yz and xz, respectively. The p_z orbital is not affected by any operation.

p_x p_z p_y

C_{2v}	E	$C_2(z)$	$\sigma_v(xz)$	$\sigma_v(yz)$
p_z	+1	+1	+1	+1

p_x	+1	-1	+1	-1
p_y	+1	-1	-1	+1

Thus, $\Gamma_p = A_1 + B_1 + B_2$. The p_x orbital is said to

- form the basis for the B_1 represention,
- have B_1 symmetry, or
- transform as B_1.

Translations along the x, y and z directions (x, y, z) transform in the same way as p_x, p_y and p_z. To see this simply translate the water molecule slightly in the x-direction without moving any of the symmetry elements. In this new position, C_2 and $\sigma(yz)$ are destroyed and the characters are those of p_x above.

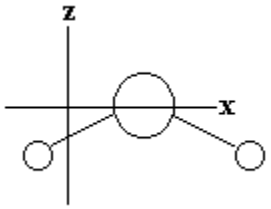

Rotation of the water molecule slightly about the z-axis moves the H's out of the plane. In this orientation, the C_2 axis is still preserved, but both planes of symmetry are destroyed, *i.e.*, R_z transforms as A_2. Rotation about the x-axis preserves the yz plane but destroys both the C_2 rotation and the xz reflection while rotation about the y-axis preserved the xz-plane and destroys the C_2 rotation and yz reflection.

C_{2v}	E	$C_2(z)$	$\sigma_v(xz)$	$\sigma_v(yz)$
R_z	+1	+1	-1	-1
R_x	+1	-1	-1	+1
R_y	+1	-1	+1	-1

Thus, the rotations in the C_{2v} point group transform as $A_2 + B_1 + B_2$. In most character tables, C_{2v} has the following form:

C_{2v}	E	C_2	σ_v	σ_v'		
A_1	1	1	1	1	z	x^2, y^2, z^2
A_2	1	1	-1	-1	R_z	xy
B_1	1	-1	1	-1	x, R_y	xz
B_2	1	-1	-1	1	y, R_x	yz

The final column gives the squares and binary products of the coordinates and represent the transformation properties of the d-orbitals.

A set of character tables is given in the appendix A. This set is only a minimal set having only those point groups encountered in this course. More complete sets are available in other texts.

As a final example, the C_{3v} point group will be generated. The operations of C_{3v} are E, C_3, C_3^2, σ_v, σ_v', and σ_v'', which can now be writen as E, $2C_3$, and $3\sigma_v$ since C_3 and C_3^2 are conjugate as are all three σ_v. This group has an order of six and contains three classes (h=6, m=3) $\Rightarrow d_1^2 + d_2^2 + d_3^2 = 6 \Rightarrow d_1 = d_2 = 1$ and $d_3 = 2$. Since the dimensions of the irreps are the χ(E) and every group contains the totally symmetric irrep,

C_{3v}	**1**E	**2**C_3	**3**σ_v

Γ_1	1	1	1
Γ_2	1	j	k
Γ_3	2	m	n

Orthogonality with Γ_1 requires that $\Sigma g(R)\chi(R) = 0$ for Γ_2 [(**1**)(1)(1) + (**2**)(1)(j) + (**3**)(1)(k) = 0] and for Γ_3 [(**1**)(1)(2) + (**2**)(1)(m) + (**3**)(1)(n) = 0]. Γ_2 is non-degenerate (j and k must each be ±1) so the orthogonality condition implies that j = +1 and k = -1. Normalization of Γ_3 means $(1)(2)^2 + 2(m^2) + 3(n^2) = 6$ so m = -1 and n =0. Alternatively, we can use the fact that $g(R)\Sigma\chi(R)^2 = h$ down any column so $2(1^2 + 1^2 + m^2) = 6$ or $m^2 = 1$ and $3(1^2 + (-1)^2 + n^2) = 6$ so $n^2 = 0$.

C_{3v}	E	$2C_3$	$3\sigma_v$
A_1	1	1	1
A_2	1	1	-1
E	2	-1	0

The ammonia molecule (C_{3v} point group) and the coordinate system used in the following discussion is given below (one N-H bond in the XZ plane).

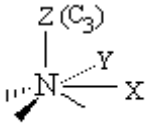

The p_z orbital is not changed by any of the operations of the group, *i.e.*, it is totally symmetric and transforms as A_1. However, it should be apparent that p_x and p_y are neither symmetric nor antisymmetric with respect to the C_3 or σ_v operations, but rather go into linear combinations of one another and must therefore be considered together as components of a 2 dimensional representation. The matrices in this irreducible representation will be 2x2 and not 1x1. The character of the identity operation will then be 2 (the trace of a 2x2 matrix with 1's on the diagonal), *i.e.*, $\chi(E)=2$. A rotation through an angle $2\pi/n$ can be represented by the following transformation: $\begin{pmatrix} x' \\ y' \end{pmatrix} = \begin{pmatrix} \cos(2\pi/n) & \sin(2\pi/n) \\ -\sin(2\pi/n) & \cos(2\pi/n) \end{pmatrix} \begin{pmatrix} x \\ y \end{pmatrix}$ the trace of the C_n rotation matrix is $2\cos(2\pi/n)$ which for n=3 is $2\cos(2\pi/3) = 2(-0.5) = -1$, *i.e.*, $\chi(C_3) = -1$. The character for reflection through a plane can be determined by the effect of reflection through any one of the three planes since they are all in the same class. The easiest operation to use is the reflection through the XZ plane which results in $p_x \rightarrow p_x$ and $p_y \rightarrow -p_y$ or $\begin{pmatrix} x' \\ y' \end{pmatrix} = \begin{pmatrix} 1 & 0 \\ 0 & -1 \end{pmatrix} \begin{pmatrix} x \\ y \end{pmatrix}$ which has a trace of 0, $\chi(\sigma_v)=0$. The transformation properties of the p_x and p_y orbitals are represented as,

	E	$2C_3$	$3\sigma_v$
(x,y)	2	-1	0

which is the E irreducible representation. The p_x and p_y orbitals are degenerate in C_{3v} symmetry and are taken **together** to form a basis for the two-dimensional irreducible representation, E. Treating rotations and binary products as before, we can represent the C_{3v} point group as

C_{3v}	E	$2C_3$	$3\sigma_v$		
A_1	1	1	1	z	x^2+y^2; z^2

A_2	1	1	-1	R_z	
E	2	-1	0	$(x,y);(R_x,R_y)$	$(x^2\text{-}y^2,xy);(xz,yz)$

Thus the x^2-y^2 and xy orbitals are also degenerate as are the xz and yz orbitals.

Problem I.4. What are the dimensions of the irreducible representations of a group with the following classes: E, R_1, $2R_2$, $2R_3$, $2R_4$, $2R_5$, $5R_6$, $5R_7$?

Problem I.5. Generate the D_4 point group. $\{D_4 \mid E, 2C_4, C_2, 2C_2', 2C_2''\}$

Problem I.6 By convention, the z-axis is the principle symmetry axis, however, for planar molecules, it is also common to define the z-axis as the axis perpendicular to the plane. Determine the irreps to which the metal d-orbitals belong for *cis*-Cl_2PtBr_2 (C_{2v}) using the latter convention (z perpencicular to molecular plane). Define the x-axis as bisecting the Cl-Pt-Cl bond and the y-axis as bisecting the Cl-Pt-Br bonds.

I.7 Decomposing Reducible Representations

In the determination of molecular orbital or vibrational symmetries, a reducible representation is generated from an appropriate basis set and then decomposed into its constituent irreducible representations. The process is analagous to determining the projection of a vector on the x,y or z axis in three space where the dot product of the vector with **i**, **j** or **k** yields the result. Decomposing a reducible representation can be viewed as determining the projection of the reducible representation along one of the irreps and the process is similar to taking the dot product of the two. The actual method is given here without proof.

$$a_i = \frac{1}{h}\sum_R g(R)\chi_i(R)\chi(R)$$

a_i : the number of times that the i^{th} irrep appears in the reducible representation
h : the order of the group
R : an operation of the group
g(R) : the number of operations in the class
$\chi_i(R)$: the character of the R^{th} operation in the i^{th} irrep
$\chi(R)$: the character of the R^{th} operation in the reducible representation

As an example, we will decompose the reducible representation: Γ_{red} = 7 1 1 of the C_{3v} point group, *i.e.*, we will determine the number of times (a_i) that each irrep is contained in Γ_{red} . The order of the point group is 6.

C_{3v}	**1**E	**2**C_3	**3**σ_v
A_1	1	1	1
Γ_{red}	7	1	1

C_{3v}	**1**E	**2**C_3	**3**σ_v
A_2	1	1	-1
Γ_{red}	7	1	1

$$a(A_1) = \frac{1}{6}\{(\mathbf{1})(1)(7)+(\mathbf{2})(1)(1)+(\mathbf{3})(1)(1)\} = \frac{1}{6}\{12\} = 2$$

$$a(A_2) = \frac{1}{6}\{(\mathbf{1})(1)(7)+(\mathbf{2})(1)(1)+(\mathbf{3})(-1)(1)\} = \frac{1}{6}\{6\} = 1$$

C_{3v}	**1**E	**2**C_3	**3**σ_v
E	2	-1	0

Γ_{red}	7	1	1

$$a(E) = \frac{1}{6}\{(\mathbf{1})(2)(7) + (\mathbf{2})(-1)(1) + (\mathbf{3})(0)(+1)\} = \frac{1}{6}\{12\}=2$$

The reducible representation can be decomposed as follows: $\Gamma_{red} = 2A_1 + A_2 + 2E$. The results can be verified by adding the characters of the irreps,

C_{3v}	E	$2C_3$	$3\sigma_v$
$2A_1$	2	2	2
A_2	1	1	-1
2E	4	-2	0
Γ_{red}	7	1	1

Problem I.7 Decompose the following reducible representations of the C_{4v} point group.

C_{4v}	E	$2C_4$	C_2	$2\sigma_v$	$2\sigma_d$
Γ_1	11	1	-1	5	1
Γ_2	6	0	2	0	0
Γ_3	5	1	-3	-1	-1
Γ_4	4	-4	4	0	0

The reducible representation of the Cartesian displacement vectors for water was determined earlier (see page I.8 - I.10) and is given in the following table as Γ_{cart}

C_{2v}	E	C_2	σ_v	σ'_v	
A_1	1	1	1	1	z
A_2	1	1	-1	-1	R_z
B_1	1	-1	1	-1	x, R_y
B_2	1	-1	-1	1	y,R_x
Γ_{cart}	9	-1	3	1	

Decomposition of Γ_{cart} yields,

$a(A_1) = 1/4\ \{(1)(1)(9) + (1)(1)(-1) + (1)(1)(3) + (1)(1)(1)\} = 1/4\ \{12\} = 3$
$a(A_2) = 1/4\ \{(1)(1)(9) + (1)(1)(-1) + (1)(-1)(3) + (1)(-1)(1)\} = 1/4\ \{4\} = 1$
$a(B_1) = 1/4\ \{(1)(1)(9) + (1)(-1)(-1) + (1)(1)(3) + (1)(-1)(1)\} = 1/4\ \{12\} = 3$
$a(B_2) = 1/4\ \{(1)(1)(9) + (1)(-1)(-1) + (1)(-1)(3) + (1)(1)(1)\} = 1/4\ \{8\} = 2$

i.e., $\Gamma_{cart} = 3A_1 + A_2 + 3B_1 + 2B_2$

Linear combinations of the 3N displacement vectors represent the degrees of motional freedom of the molecule. Of these 3N degrees of freedom, three are translational, three are rotational and the remaining 3N-6 are the vibrational degrees of freedom. Thus, to get the symmetries of the vibrations, the irreducible representations of translation and rotation need only be subtracted from Γ_{cart}, but the irreps of rotation and translation are available from the character table. For the water molecule, $\Gamma_{vib} = \Gamma_{cart} - \Gamma_{trans} - \Gamma_{rot} = \{3A_1 + A_2 + 3B_1 + 2B_2\} - \{A_1 + B_1 + B_2\} - \{A_2 + B_1 + B_2\} = 2A_1 + B_1$. Construction of these "symmetry coordinates" will be

discussed in detail in the Vibrational Spectroscopy chapter, but we will draw them below and note that S_1 (symmetric stretch) and S_2 (bending mode) both preserve the symmetry of the molecule, *i.e.*, are totally symmetric, while S_3 (antisymmetric stretch) destroys the plane perpendicular to the molecule and the C_2 axis but retains the plane of the molecule, *i.e.*, it has B_1 symmetry.

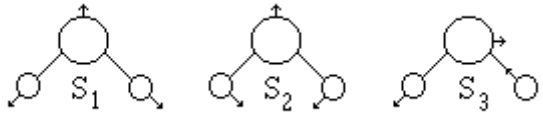

Problem I.8 Determine the symmetries of the vibrations of NH_3, $PtCl_4^{2-}$ and SbF_5.

I.8. Direct Products.

It is often necessary to determine the symmetry of the product of two irreps, *i.e.*, to determine their direct product.

Direct Products: The representation of the product of two representations is given by the product of the characters of the two representations.

Verify that under C_{2v} symmetry $A_2 \otimes B_1 = B_2$

C_{2v}	E	C_2	σ_v	σ_v'
A_2	1	1	-1	-1
B_1	1	-1	1	-1
$A_2 \otimes B_1$	1	-1	-1	1

As can be seen above, the characters of $A_2 \otimes B_1$ are those of the B_2 irrep.

Verify that $A_2 \otimes B_2 = B_1$, $B_2 \otimes B_1 = A_2$. Also verify that

- the product of any non degenerate representation with itself is totally symmetric and
- the product of any representation with the totally symmetric representation yields the original representation.

Note that,

- A x B = B; while A x A = B x B = A
- "1" x "2" = "2" while "1" x "1" = "2" x "2" = "1"
- g x u = u while g x g = u x u =g.

A table of Direct Products for the groups pertinent to this course is given in Appendix B.

The basis of *selection rules* (see Chapter III) is that the transition between two states a and b is *electric dipole allowed* if the electric dipole moment matrix element is non-zero, *i.e.*,

$$\langle a|\mu|b\rangle = \int_{\infty} \psi_a^* \mu \psi_b \, d\tau \neq 0$$

where $\mu = \mu_x, + \mu_y + \mu_z$ is the electric dipole moment operator which transforms in the same manner as the p-orbitals (x, y and z in the character table). A necessary condition for this inequality is that the direct product of the integrand, $\psi_a \otimes \mu \otimes \psi_b = \psi_a \otimes (\mu_x, + \mu_y + \mu_z) \otimes \psi_b$, must contain the totally symmetric representation.

Is the orbital transition $d_{yz} \rightarrow p_x$ electric dipole allowed in C_{2v} symmetry? The C_{2v} character table indicates that the d_{yz} orbital forms the basis for the B_2 irrep while the p_x orbital transforms as B_1 so the question is whether or not a transition between a B_2 orbital and a B_1 orbital is electric dipole allowed? Such a transition is allowed only if the product $B_1 \otimes \mu \otimes B_2$ contains the A_1 representation. In C_{2v}, the electric dipole transforms as $b_1 + b_2 + a_1$. The direct products are determined to be $B_1 \otimes \begin{pmatrix} b_1 \\ b_2 \\ a_1 \end{pmatrix} \otimes B_2 = \begin{pmatrix} a_1 \\ a_2 \\ b_1 \end{pmatrix} \otimes B_2 = \begin{pmatrix} b_2 \\ b_1 \\ a_2 \end{pmatrix}$. None of the three components contains the a_1 representation, so this transition is forbidden.

Since the irreps are orthogonal, the direct product of two different irreps will always contain -1's and thus cannot be totally symmetric. The only way to get +1's exclusively is to square the individual characters, *i.e.*, the **direct product of two non-dengerate irreps can be a_1 only if they are the same irrep**. A triple product will transform as A_1 only if the direct product of two irreps is the same irrep as the third. We may therefore state the following:

A transition between two non-degenerate states will be allowed only if the direct product of the two state symmetries is the same irrep as one of the components of the electric dipole.

The transition $d_{yz} \rightarrow p_x$ will be allowed only if the direct product $B_1 \otimes B_2$ transforms the same as x,y or z. Since $B_1 \otimes B_2 = a_2$ and x nor y nor z transform as a_2 the transition is not allowed. An $A_1 \rightarrow B_2$ transition is allowed however since $A_1 \otimes B_2 = B_2$, and y transforms as b_2. In this case, the transition is said to be "y-allowed". Show that the $A_2 \rightarrow B_1$ transition is also "y-allowed".

Problem I.9. Indicate whether each of the following metal localized transitions is electric dipole allowed in $PtCl_4^{2-}$. (a) $d_{xy} \rightarrow p_z$ (b) $d_{yz} \rightarrow d_{z2}$ (c) $d_{x2-y2} \rightarrow p_x, p_y$ (d) $p_z \rightarrow s$

I.9 Symmetry Adapted Linear Combinations

We will construct molecular orbitals as linear combinations of atomic orbitals, but these *molecular orbitals must form the bases for the irreps of the molecular point group* (chapter II), and we have already shown that the vibrational modes are constructed as linear combinations of the Cartesian basis vectors in such a way that they too form the bases for the irreducible representations of the molecular point group. Since these linear combinations form the bases for the irreps of the molecular point group, we call them **s**ymmetry **a**dapted **l**inear **c**ombinations or SALC's. The construction of these SALC's is mandatory if all of the information available from the molecular symmetry is to be obtained.

SALC's are formed from symmetrically complete sets. Each **member of a symmetrically complete set can be carried into every other member by some operations of the group**. For example, compare square planar $[PtCl_3Br]^{2-}$ of C_{2v} symmetry with tetrahedral $[CoCl_3Br]^{2-}$ of C_{3v} symmetry. In the C_{2v} ion, the three chlorines are not symmetrically equivalent since there is no operation of the C_{2v} point group which can exchange trans- and cis-chlorines and thus they must be in different sets. In the C_{3v} ion, all three chlorines can be exchanged by a C_3 rotation and thus all belong in the same set.

We state without proof the method for construction of a set of SALC's ψ_k from an m-dimension set, $\{\phi_i | j = 1,2,...m\}$ which is symmetrically complete:

$$\psi_k = N_k \sum_{j=1}^{m} \chi_{jk}(R^{\phi_s \rightarrow \phi_j})\phi_j$$

where ψ_k is the SALC belonging to the k^{th} irrep
$\chi_{jk}(R^{\phi_s \rightarrow \phi_j})$ is the character of the operation R which carries a reference vector, ϕ_s into the vector ϕ_j in the kth irrep
N_k is a normalization constant

More simply put, one vector of the symmetrically equivalent set is chosen as the reference then the coefficent on the j^{th} member of the set in the SALC is the character of the operation of the point group which carries the reference vector into the j^{th} member of the set. The reference vector is carried into itself with the identity operation and therefore has a coefficient of +1.

To determine SALC's of the s-orbitals in water,

1. Determine the point group of the molecule. H_2O belongs to the C_{2v} point group.
2. Identify the symmetrically complete sets. H(1) and H(2) form one set while the O forms the other
3. Determine the operation which converts the reference vector into each of the others. $H(1) \xrightarrow{E} H(1)$; $H(1) \xrightarrow{C_2} H(2)$; $O \xrightarrow{E} O$
4. Determine the reducible representation of the complete sets.

C_{2v}	E	C_2	σ_v	σ'_v	
Γ(H)	2	0	2	0	A_1+B_1
Γ(O)	1	1	1	1	A_1

5. Determine the character of the appropriate operation for each of the irreps

	A_1	B_1
E	1	1
C_2	1	-1

6. Construct SALC's

A_1: $\psi_1 = N_1\{H(1) + H(2)\}$ & $\psi_2 = N_2\{O\}$ $\quad$ B_1: $\psi_3 = N_3\{H(1) - H(2)\}$

7. Normalize the SALC's - the sum of the squares of the coefficients must be unity.

$$2N_1^2 = 1 \Rightarrow N_1 = \frac{1}{\sqrt{2}};\ N_2^2 = 1 \Rightarrow N_2 = 1;\ 2N_3^2 = 1 \Rightarrow N_3 = \frac{1}{\sqrt{2}}$$

To convert H(1) into H(2) we chose the C_2 rotation, but the σ'_v could also have been used. In this example it did not matter since the characters of the C_2 and σ'_v operations are the same in both A_1 and B_1. However this will not always be the case and the above method will not lead to a unique SALC. In these cases, the *complete projection operator* should be used, *i.e.*, the effect of **every** operation in the group on the reference vector must be determined and the effect then multiplied by the character of the operation in the irreducible representation. For the H(1) reference in A_1 and B_1 representations,

	E	C_2	σ_v	σ'_v
effect on H(1)	H(1)	H(2)	H(1)	H(2)

A_1	1	1	1	1
B_1	1	-1	1	-1

Thus the A_1 SALC would be $N_1\{2H(1) + 2H(2)\} = 0.707\{H(1) + H(2)\}$, and the B_1 SALC would be $N_2\{2H(1) - 2H(2)\} = 0.707\{H(1) - H(2)\}$ - the same results as before. This method can be somewhat more tedious then the former method, but it will always yield unambiguous results.

The SALC's for the s-orbitals for the three H's of NH_3 are determined in the same manner with the added complication of degeneracy. The reducible representation is

C_{3v}	E	$2C_3$	$3\sigma_v$
A_1	1	1	1
A_2	1	1	-1
E	2	-1	0
$\Gamma(1s)$	3	0	1

Which can be decomposed into $\Gamma(1s) = A_1 + E$. We will use ϕ_1 as the reference vector and the C_3 rotation to convert it into ϕ_2 and ϕ_3 ($\chi(C_3) = -1$ in the E' representation). The normalized SALC of A_1 symmetry is then $\psi_1 = \frac{1}{\sqrt{3}}(\phi_1 + \phi_2 + \phi_3)$ while the two components of the doubly degenerate pair of E' symmetry are obtained in an analgous manner by using two different reference vectors, for example ϕ_2 and ϕ_3,

$$\psi_2^{a'} = \frac{1}{\sqrt{6}}(-\phi_1 + 2\phi_2 - \phi_3) \text{ and } \psi_2^{b'} = \frac{1}{\sqrt{6}}(-\phi_1 - \phi_2 + 2\phi_3)$$

The two components of a doubly degenerate set form the basis for a 2-dimensional representation and must therefore be orthogonal to one another, but the two derived above are not orthogonal. To generate two orthogonal components, linear combinations of the above are taken, $\psi_2^{a'} \pm \psi_2^{b'}$ yielding,

$$\psi_2^{a} = -\frac{1}{\sqrt{6}}(2\phi_1 - \phi_2 - \phi_3) \text{ and } \psi_2^{b} = \frac{1}{\sqrt{2}}(\phi_2 - \phi_3)$$

Note that since only the relative phases of the orbitals are important, the minus sign in ψ_2^{a} is usually dropped. A quick check of orthogonality can be done by looking at the nodal planes.

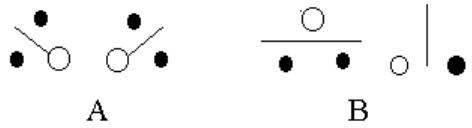

A B

In A, $\Psi_2^{a'}$ and $\Psi_2^{b'}$ the nodal planes interesect at an angle of 120° - they are not orthogonal while in B, Ψ_2^{a} and Ψ_2^{b}, the nodal planes are perpendicular, *i.e.*, orthogonal, as are the two basis vectors.

Using the complete **projection operator** for this problem (see page I.5 for the definitions of the planes) we would write,

	E	C_3	C_3^2	σ_v	σ_v'	σ_v''
effect on ϕ_1	ϕ_1	ϕ_2	ϕ_3	ϕ_1	ϕ_3	ϕ_2
A_1	1	1	1	1	1	1
E	2	-1	-1	0	0	0

Remember that the effect of **EVERY** operation must be considered! The SALC's are then

$\psi_1 = N_1\{\phi_1 + \phi_2 + \phi_3 + \phi_1 + \phi_2 + \phi_3\}$ or $\psi_1 = \frac{1}{\sqrt{3}}(\phi_1 + \phi_2 + \phi_3)$ and

$\psi_2 = N_2\{2\phi_1 - \phi_2 - \phi_3\}$ which can be manipulated as in the previous method to give the same degenerate SALC's.

Problem I.10 Construct the SALC's for the s-orbitals on the chlorine atoms in $Mo(O)Cl_4^{2-}$, a tetragonal pyramid with C_{4v} symmetry.

The rest of the course will be dealing with these and other applications of symmetry and group theory, but at this stage you should be able to do the following:

1. Determine the molecular point group.
2. Generate reducible representations for various systems.
3. Decompose a reducible representation into its irreducible representations.
4. Determine the direct product of several representations.
5. Generate SALC's from symmetrically complete sets

Chapter II - Molecular Orbital Theory

II.1 Quantum Theory: a brief tour

All information concerning the structure, energetics and dynamics of a molecule is contained in the molecular wavefunction, ψ, the wave property of matter. The physical significance of the wavefunction is that ψ*ψdτ is proportional to the probability that the particle can be found in the interval dτ. Thus, the integral of ψ*ψdτ over all space, $\int_{-\infty}^{+\infty} \psi_n^* \psi_n d\tau$, is proportional to the probability that the particle exists in space. For a well constructed wavefunction, this integral is unity and the wavefunction is said to be **normalized**.

Perhaps the most encountered quantum mechanical expression is the Schrödinger equation:

$$\mathbf{H\Psi_n = E_n\Psi_n} \qquad \text{Eq II.1}$$

where **H** is the Hamiltonian or energy operator, Ψ_n is the stationary state wavefunction of the n^{th} state, and E_n is the energy of that state. Theoretically, there are an infinite number of Ψ_n (n=1,...,∞) and as solutions to the above equation they form a **complete set** of **basis functions** which means that any function, ϕ, can be expressed as a linear combination of the members of the set, $\phi = \sum_{j=1}^{\infty} c_j \psi_j$. Since the normalized functions are also orthogonal, they form an **orthonormal basis**. The orthonormality condition is $\int_{-\infty}^{+\infty} \psi_m^* \psi_n d\tau = \delta_{mn}$. where δ_{mn} is the Kroniker delta which is equal to zero for n≠m (orthogonal) and equal to 1 for m=n (normalized).

You have encountered orthonormal basis sets before; the irreducible representations form the basis for a point group and the vectors **i**, **j**, and **k** form a basis for three-space. Any reducible representation can be written as a linear combination of the irreducible representations and any vector, **p**, in three space can be written as a linear combination of the basis vectors, **p** = a**i** + b**j** + c**k**, where a = **p**•**i** is the amount of the basis vector,**i**, that is *mixed into the vector*, **p**. The similarities of the properties of vectors and wavefunctions can be used to advantage by representing the wavefunction, Ψ_n, as a vector |n>, called the **ket** of n and its complex conjugate as <n|, the **bra** of n. The integral over all space then becomes a dot product $\int_{-\infty}^{+\infty} \psi_m^* \psi_n d\tau = \langle m|n\rangle = \delta_{mn}$ where <m|n> is a (bra)(ket). Operation on a vector results in a change of its length and/or its direction. For example, a C_8 operation on **i** (rotation by 45° about the z-axis), generates a new vector, $C_8\mathbf{i} = \frac{1}{\sqrt{2}}(\mathbf{i} + \mathbf{j})$. The dot product of this vector with the each of the basis vectors could be represented as

$$\langle j|C_8|i\rangle = \left\langle \mathbf{j} \middle| \frac{1}{\sqrt{2}}(\mathbf{i} + \mathbf{j}) \right\rangle = \frac{1}{\sqrt{2}}\left(\langle j|i\rangle + \langle j|j\rangle\right) = \frac{1}{\sqrt{2}}(0 + 1) = \frac{1}{\sqrt{2}}$$

$$\langle k|C_8|i\rangle = \left\langle k \middle| \frac{1}{\sqrt{2}}(\mathbf{i} + \mathbf{j}) \right\rangle = \frac{1}{\sqrt{2}}\left(\langle k|i\rangle + \langle k|j\rangle\right) = \frac{1}{\sqrt{2}}(0 + 0) = 0$$

so the operator C_8 is said to remove the orthogonality of **i** and **j** by mixing them. The resulting vector, however is still orthogonal to **k**.

We can view quantum mechanical operators in the same way so Eq II.1 can now be written,

$$\mathbf{H}n\rangle = E_n n\rangle \qquad \text{Eq II.2}$$

The operation, **H**, changes only the length of the vector, n>, *i.e.*, it yields a scalar, E_n, times the initial vector. In cases like this, the vectors represented by **n> are said to be eigenvectors of the operator H with eigenvalues E_n**. It is often the case that n> is not an eigenvector of an operator, **O**, or $\mathbf{O}n\rangle = \Sigma_j c_{ij} j\rangle$, *i.e.*, n> is rotated into a linear combination of the basis vectors just as **i** was rotated into a linear combination of **i** and **j** by the C_8 rotation.

If n> is an eigenvector of **H** but not of **O**, then the observable O is not a constant of the motion, *i.e.*, its value is changing while the energy remains constant. In this case it is the average value of the physical observable, designated <O>, that is determined,

$$\langle O \rangle = \frac{\int_{-\infty}^{+\infty} \Psi_n^* O \Psi_n \, d\tau}{\int_{-\infty}^{+\infty} \Psi_n^* \Psi_n \, d\tau} = \frac{\langle n|O|n\rangle}{\langle n|n\rangle} = \langle n|O|n\rangle \qquad \text{Eq II.3}$$

<O> = <n|**O**n> is also called the **expectation value** of the observable O (momentum, position, energy, spin, etc.) in the n^{th} state, but these numbers are simply the diagonal elements of a matrix of such elements, $\langle \mathbf{O} \rangle_{mn} = \langle m|\mathbf{O}n\rangle$ - if the n> are eigenvectors of **O** than the matrix is diagonalized. Indeed, a frequently used procedure for the determination of the eigenvalues and eigenvectors of a system is to assume a basis set which closely approximates the actual system, generate the Hamiltonian matrix in the selected basis and then diagonalize it. This procedure results in both the eigenvalues and the eigenvectors of the matrix.

Problem II.1 (a) Given that $|j\rangle$, $|k\rangle$, and $|n\rangle$ are all members of the same basis set and that $\mathbf{O}|n\rangle = \Sigma_k c_k |k\rangle$ show that $c_j = \langle j|\mathbf{O}|n\rangle$. (b) Assume $\langle \phi_i | \phi_j \rangle = \delta_{ij}$ and show that SALC, $\Psi_a = 2\phi_1 - \phi_2 - \phi_3$ is orthogonal to $\Psi_b = \phi_2 - \phi_3$ (the other member of the degenerate pair) but not to $\Psi_c = -\phi_1 + 2\phi_2 - \phi_3$ (one of the functions used to generarte Ψ_b in section I.9.

II.2 Wavefunctions as bases for irreducible representations

The energy of a system will not change when identical particles (electrons or nuclei) are interchanged, so the Hamiltonian must be invariant with respect to any of the operations of the group, *i.e.*, R**H** = +1**H** so **H** transforms as the totally symmetric representation. The physical properties of the system are contained in ψ^2, so it too must be invariant, *i.e.*, $R\psi^2 = +1\psi^2$ which means that for a non-degenerate wavefunction, $R\psi = \pm 1\psi$. Thus the application of each of the operations of the group to an eigenfunction/eigenvector will generate one of the irreducible representations of the molecular point group.

The eigenvectors form bases for the irreducible representations of the molecular point group.

In general, symmetry operations will rotate one member of a degenerate representation into a linear combination of all members of the degenerate representation. It can be shown that a k-dimensional representation is generated by a k-fold degenerate set of eigenvectors. The trace of the k-dimensional representation then forms the basis for a degenerate representation.

Determining whether two functions can be mixed by an operator is an important application of group theory. We have already encountered one such application: selection rules are based on whether two states can be mixed by the electric dipole operator, $\langle\psi_i | \boldsymbol{\mu} | \psi_j\rangle \neq 0$. Remember that in order for an integral over all space to be non-zero, the integrand must contain the A_1 irreducible representation. Thus, the integral $\langle\psi_i | \mathbf{H} | \psi_j\rangle \neq 0$ only if the direct product of $\Gamma_i \times \Gamma_H \times \Gamma_j$ contains the A_1 irreducible representation. Since Γ_H is A_1, the direct product will contain A_1 only if $\Gamma_i \otimes \Gamma_j$ is A_1 and for non-degenerate irreducible representations that implies that $\Gamma_i = \Gamma_j$. Therefore,

$H_{ij} = \langle\psi_i | H | \psi_j\rangle \neq 0$ only if ψ_i and ψ_j form the basis for the same irreducible representation.

II.3 Quantum Mechanical Approach to Molecular Orbitals

Molecular orbitals are formed by taking a **L**inear **C**ombination of **A**tomic **O**rbitals (LCAO). Just as atomic orbitals are solutions to the hydrogen atom wave equation, molecular orbitals are based of the solution to hydrogen molecule ion, H_2^+,

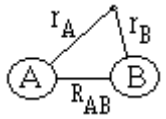

The Hamilitonian for this two proton, one electron system is

$$H = -\frac{\hbar^2}{2m_e}\nabla_e^2 - \frac{\hbar^2}{2m_A}\nabla_A^2 - \frac{\hbar^2}{2m_B}\nabla_B^2 - \frac{e^2}{r_A} - \frac{e^2}{r_B} + \frac{e^2}{R_{AB}}$$

or E = (kinetic energy of the electron) + (kinetic energy of nucleus A) + (kinetic energy of nucleus B) - (the Coulombic attraction of nucleus A for the electron) - (the Coulombic attraction of nucleus B for the electron) + (the Coulombic repulsion of the two nuclei).

The problem can be simplified considerably with Born-Oppenheimer approximation.

Born Oppenheimer Approximation: Electronic motion is so much faster than nuclear motion that the two are independent, *i.e.*, the nuclear and electronic kinetic energies can be separated.

The result of this approximation is to remove the nuclear kinetic energy terms and allow R_{AB} to be treated as a constant, *i.e.*, the electronic energy can be calculated at given values of R_{AB}.

The two H's are in the ground state so the 1s orbitals will be used to construct the mo's (LCAO).

$$\Psi_{mo} = \Sigma C_i \phi_i = C_A \phi_A + C_B \phi_B = C_A 1s_{(A)} + C_B 1s_{(B)}$$

The expectation value (eq II.3) for the energy of the system is given as:

$$\langle E \rangle = \frac{\langle \Psi_{MO} | H | \Psi_{MO} \rangle}{\langle \Psi_{MO} | \Psi_{MO} \rangle} = \frac{C_A^2 \langle \phi_A | H | \phi_A \rangle + 2C_A C_B \langle \phi_A | H | \phi_B \rangle + C_B^2 \langle \phi_B | H | \phi_B \rangle}{C_A^2 + 2C_A C_B \langle \phi_A \| \phi_B \rangle + C_B^2}$$

Eq II.4

$$\langle E \rangle = \frac{C_A^2 H_{AA} + 2C_A C_B H_{AB} + C_B^2 H_{AA}}{C_A^2 + 2C_A C_B S_{AB} + C_B^2}$$

where $H_{AA} = \langle\phi_A | H | \phi_A\rangle = \langle\phi_B | H | \phi_B\rangle = H_{BB} = \alpha > 0$ - the Coulomb integral;

$H_{AB} = \langle\phi_A | H | \phi_B\rangle = \beta < 0$ - the Resonance ;
and $S = \langle\phi_A | \phi_B\rangle = \langle\phi_B | \phi_A\rangle$ - the overlap integral.

$C_A$and C_B are then determined by applying the **Variation principle:** The expectation energy calculated with any acceptable, approximate wavefunction can never be less than the true ground state energy. Or, the best wavefunctions are the ones that yield the lowest energy. The values of C_A and C_B are determined to be those that minimize the energy (Eq II.4). Minimizing E with respect to C_A and C_B, *i.e.*, $(E/\partial C_A)_{C_B} = 0$ and $(\partial E/\partial C_B)_{C_A} = 0$, yields two equations:

$$(\alpha - E)C_A + (\beta - SE)C_B = 0 = (H_{AA} - E)C_A + (H_{AB} - SE)C_B$$
$$(\beta - SE)C_A + (\alpha - E)C_B = 0 = (H_{AB} - SE)C_A + (H_{AA} - E)C_B$$

Both equations can be satisfied with non-trivial solutions only if the determinant of the coefficients of C_A and C_B is 0 which yields the **Secular Equation**:

$$\begin{vmatrix} H_{AA} - E & H_{AB} - SE \\ H_{AB} - SE & H_{AA} - E \end{vmatrix} = 0 .$$

which has the following eigenvalues and normalized eigenvectors:

$$E_+ = \frac{H_{AA} + H_{AB}}{1+S} \Rightarrow \Psi_+ = \frac{\phi_A + \phi_B}{\sqrt{2+2S}} \qquad \& \qquad E_- = \frac{H_{AA} - H_{AB}}{1-S} \Rightarrow \Psi_- = \frac{\phi_A - \phi_B}{\sqrt{2-2S}} \qquad \text{Eq II.5}$$

Since the coulomb integral is positive and the exchange integral is negative, $E_+ < E_-$.

Figure II.1 shows the square of the two wavefunctions. Ψ_-^2 has a nodal plane perpendicular to the internuclear axis which means that electron density is excluded from this region. *Ψ_- is, therefore, an antibonding orbital*. Ψ_+^2 has no nodal plane perpendicular to R_{AB} and has an accumulation of electron density between the atoms - *Ψ_+ is a bonding orbital.* In addition, **t**he internuclear axis is not contained in a nodal plane which makes this type of interaction a σ interaction**.** We therefore refer to *Ψ_+ as a σ orbital* and *Ψ_- as a σ^* orbital*.

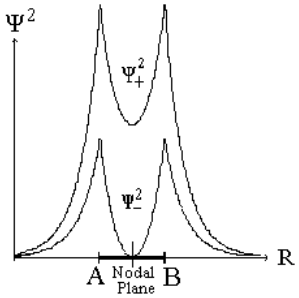

Figure II. 1 Plots of the radial portions of Ψ_+^2, and Ψ_-^2

The energy of each separated atom is H_{AA}. E_+ has a lower energy than H_{AA} and is therefore stabilized relative to the unbound atoms by the amount $H_{AA} - E_+ = \Delta_+$ (see figure II.2). E_- is greater than H_{AA} and thus is destabilized. The extent of the destabilization is $E_- - H_{AA} = \Delta_-$. The magnitudes of stabilization and destabilization are given as,

$$\Delta_\pm = \frac{SH_{AA} - H_{AB}}{1 \pm S} \qquad \text{Eq II.6}$$

The magnitude of H_{AB} is dependent upon the overlap, $H_{AB} = 0$ if $S = 0$. If the overlap is not zero, however, $\Delta_+ < \Delta_-$ and a four electron bond would not form since the total stabilization, $\Delta_+ - \Delta_-$ is negative, *i.e.*, the destabilization resultling from the double occupancy of the antibonding orbital is greater than the stabilization resulting from two electrons in the bonding

mo. This means that the energy of the separated atoms will be less than that of the "bound" atoms.

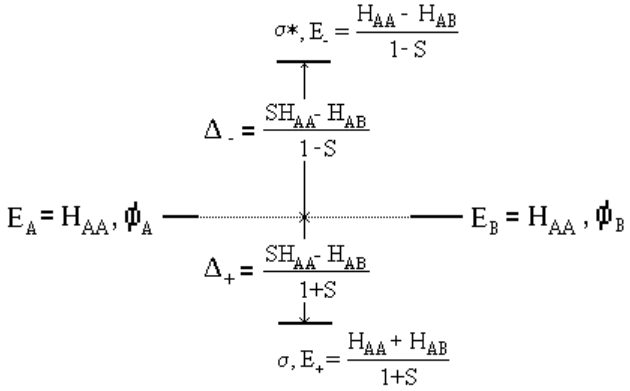

Figure II.2 Interaction of two degenerate atomic orbitals forming one bonding mo, σ, which is stabilized by Δ_+ relative to the ao's and one antibonding mo, σ*, destabilized by an amount Δ_-.

To better picture the difference between the bonding and antibonding mo's, consider the energy of each as a function of the internuclear separation as shown in figure II.3. E_+ reaches a minimum at R_e, the equilibrium bond length, and is, therefore, a *bound state*. E_- is unbound (no minimum) and excitation into this anti-bonding orbital would be dissociative.

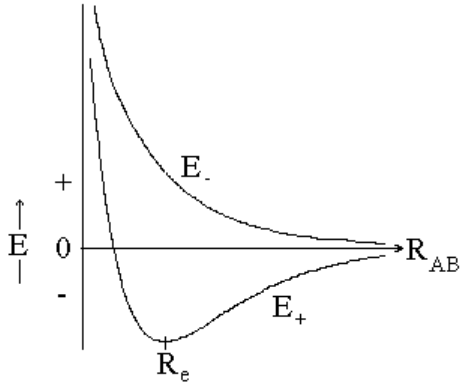

Figure II .3. The energies of the bonding mo (E_+) and the dissociative antibonding mo (E_-) as a function of the internuclear separation.

Similar considerations can be made for the p-orbitals. Since the bonding axis is the C $_\infty$ or z-axis, interaction of the p_z's will also result in a σ-bond (figure II.4). Interactions of the p_x or p_y orbitals result in mo's with substantial electron density between the atoms, but, in this case, the internuclear axis is contained in a nodal plane. The resulting mo is called a π mo with a corresponding π* antibonding mo.

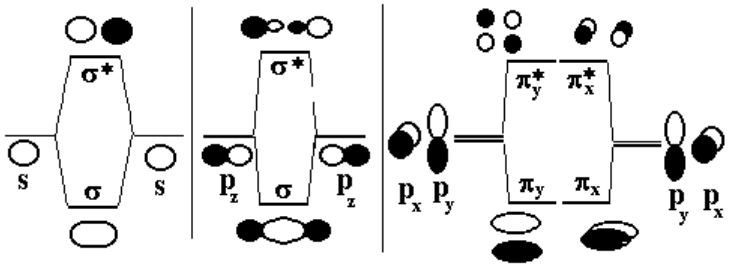

Figure II.4. Interactions of s- and p-orbitals showing the formation of σ and σ* mo's from interaction of s or p_z ao's and the formation of π and π* mo's from interaction of p_x or p_y ao's.

Interactions in which the bond axis contains two nodal planes are called δ-bonds (see Problem II.3).

Remember from the discussion of the Hamiltonian matrix at the beginning of this chapter that the matrix element H_{ij} can be non-zero only when ψ_i and ψ_j form the basis for the same irreducible representation. Thus, $H_{AB} \neq 0$ only if ψ_a and ψ_b have the same symmetry. In other words,

Only orbitals of the same irreducible representation can mix!

The same conclusion is reached by realizing that the value of H_{ij} depends on the extent of overlap. For example, an s-orbital on one atom will not mix with a p_x on another atom (z-axis is bond) as regions of positive overlap are cancelled by regions of negative overlap (figure II.5).

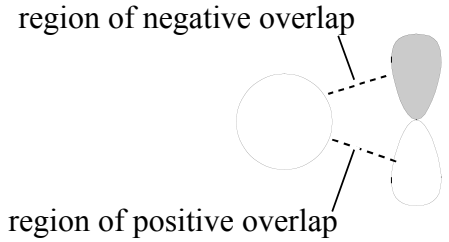

Figure II.5 Zero overlap resulting from the cancellation of the positive overlap by the negative overlap.

Problem II.2 Indicate the result (σ,π, δ or none) of mixing the following pairs of orbitals on two different atoms in a diatomic molecule:

a) $s + p_z$ b) $d_{xz} + p_x$ c) $d_{x^2-y^2} + p_x$ d) $d_{z^2} + d_{xz}$.

Draw the bonding and anti-bonding combinations for all **interacting** pairs. Remember the bond axis is the z-axis.

II.4 Homonuclear Diatomic Molecules

The mo's form bases for the irreducible representations of the molecular point group so the construction of mo's from the ao's is a matter of constructing SALC's (symmetry adapted linear combinations) from the ao's of symmetrically complete sets. Homonuclear diatomic molecules belong to the $D_{\infty h}$ point group, a *partial* group table is given here.

$D_{\infty h}$	E	$2C_\infty^\phi$	$\infty\sigma_v$	i	$2S_\infty^\phi$	∞C_2
Σ_g^+	1	1	1	1	1	1
Σ_g^-	1	1	-1	1	1	-1
Π_g	2	2cosϕ	0	2	-2cosϕ	0
Σ_u^+	1	1	1	-1	-1	-1
Σ_u^-	1	1	-1	-1	-1	1
Π_u	2	2cosϕ	0	-2	2cosϕ	0

The mo's for a diatomic molecule composed of first or second row elements will consist of LCAO's of the s, p_x, p_y and p_z orbitals on the two atoms. The p_z and s reducible representations are straightforward, but since rotation of p_x or p_y about the C_∞ axis leads to a combination of p_x and p_y, these orbitals are degenerate and must be considered together. For a

rotation by an angle ϕ, $C_\infty^\phi \begin{pmatrix} p_x \\ p_y \end{pmatrix} = \begin{pmatrix} \cos\phi & \sin\phi \\ -\sin\phi & \cos\phi \end{pmatrix} \begin{pmatrix} p_x \\ p_y \end{pmatrix}$ the character of which is 2cosϕ for each (p_x,p_y) pair on the C_∞ axis, *i.e.*, a character of 4cosϕ for a homonuclear diatomic. Only one of the $\infty\,\sigma_v$'s need be considered and the easiest to see is the xz plane. $\sigma(xz)\begin{pmatrix} p_x \\ p_y \end{pmatrix} = \begin{pmatrix} 1 & 0 \\ 0 & -1 \end{pmatrix} \begin{pmatrix} p_x \\ p_y \end{pmatrix}$ which has a character of zero. The remaining characters of the reducible representation can be determined in a similar manner.

$D_{\infty h}$	E	$2C_\infty^\phi$	$\infty\sigma_v$	i	$2S_\infty^\phi$	∞C_2	
s	2	2	2	0	0	0	$\Sigma_g^+ + \Sigma_u^+$
p_z	2	2	2	0	0	0	$\Sigma_g^+ + \Sigma_u^+$
p_x, p_y	4	4cosϕ	0	0	0	0	$\Pi_g + \Pi_u$

So group theoretical considerations yield the same results we arrived at earlier: mixing of two s- or two p_z-orbitals results in two mo's of one of σ_g^+ (σ) and one of σ_u^+ (σ*) symmetry[1], while mixing p_x or p_y orbitals results in mo's of symmetry π_u (π) and π_g (π*) mo's.

Problem II.3 $Mo_2Cl_8^{4-}$ is reported to contain a Mo-Mo quadruple bond formed from the interaction of the Mo d-orbitals. Assume D_{4h} symmetry for the ion and use the metal d-orbitals as the basis to determine the symmetries of the mo's. Draw pictures like those in figure II.4 to describe the quadruple bond. Label each orbital with the appropriate symmetry and interaction type, σ, π or δ. Order the mo's in increasing energy and place the appropriate number of electrons into the orbitals. **Do not include the x^2-y^2 as they are involved in the Mo-Cl σ-bonds.**

Ordering of mo energies

The predictions of mo theory are based on the orbital occupancy which is dictated by the relative energy ordering of the mo's (mo energy diagram) and the number of electrons in the system. The homonuclear diatomic molecules represent an informative yet relatively simple example of the utility of the method.

The extent of stabilization of an mo depends on the overlap between the ao's involved (S_{ij}). Sigma interactions will have a greater overlap than pi interactions at longer distance due to their directional nature, but the overlap will increase more rapidly for the pi interactions as the internuclear distance shortens. Thus, at longer bond lengths, σ-mo's are stabilized more than π-mo's. Another factor affecting the energy of an mo is mixing - two mo's can mix resulting in one mo being stabilized while the other mo is destabilized. The 2σg and the 3σg have the correct symmetry to mix with the result that the 3σg will be destabilized while the 2σg are stabilized. Since the origin of these mo's are the s and the pz orbitals, this mixing is the equivalent of mixing the s and p first to form sp hybrid orbitals. A combination of differing bond lengths and orbital mixing results in two different energy schemes for the homonuclear diatomic molecules of the atoms of the first and second row (Figure II.6).

[1] Capital Greek letters (*e,g.*, Σ, Π, Δ) are reserved for states (to be discussed in Chapter VI) while lower case (*e.g.*, σ, π, δ) are used for orbitals.

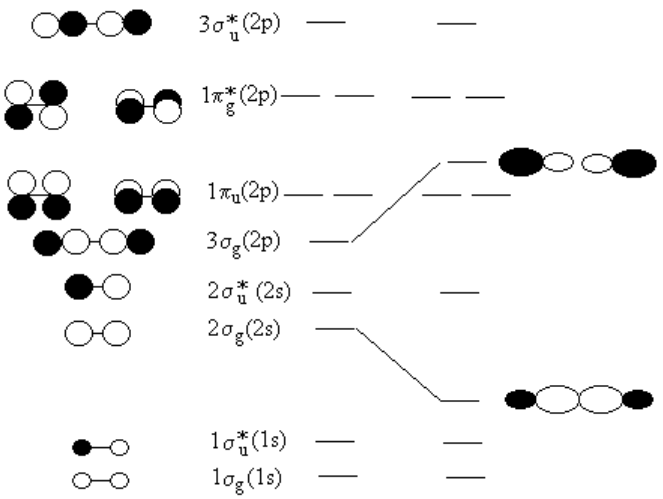

Figure II.6. The two energy diagrams used to describe the bonding in the homonuclear diatomics formed from atoms in the 1st and 2nd rows.

Since there will be many mo's with the same designation, σ_g, σ_u^*, etc., we must distinguish between them. There are two ways of doing this: designate the ao's from which they are derived or simply number the mo's. Both schemes are shown above. However, designating the ao's would be cumbersome when extensive mixing of many ao's occurs, so the latter method is the one most commonly encountered.

Determining the electron configurations of molecules is completely analagous to determining the electron configurations of atoms. The electrons go into the lowest energy orbital available, only two electrons per orbital and electrons remain unpaired in degenerate orbitals if possible (maximum multiplicity). In the case of diboron (B_2), the energy differences between the $1\pi_u$, $2\sigma_u^*$ and 3σ orbitals is evidently less than the pairing energy (Coulombic repulsion between two electrons in the same orbital) resulting in an electron configuration with one electron in each of these orbitals (Figure II.7). One of the major successes of mo theory was the explanation of the paramagnetism of O_2. Figure II.7 also shows the O_2 occupancy which clearly demonstrates the presence of two unpaired elecrtons in the $1\pi_g^*$.

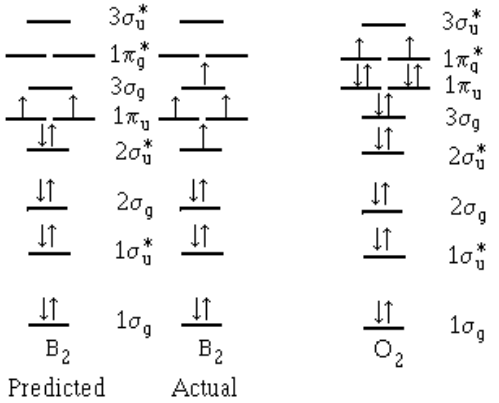

Figure II.7. Examples of orbital occupancy. The predicted and actual cases for B_2 are given as well as the O_2 case to demonstrate its paramagnetism.

One of the important properties of the bond which is readily determined from the electron configuration is the **bond order which is defined as the number of PAIRS of bonding electrons minus the number of PAIRS of antibonding electrons**. Higher bond orders imply stronger, shorter bonds with higher vibrational force constants (frequencies).

Molecule	Predicted Electronic Configuration	Bond Order	Bond Length (pm)	Bond Strength (kJ/mol)
H_2^+	$(1\sigma_g)^1$	1/2	106	260
H_2	$(1\sigma_g)^2$	1	74	431
He_2^+	$(1\sigma_g)^2(1\sigma_u^*)^1$	1/2	108	250
He_2	$(1\sigma_g)^2(1\sigma_u^*)^2$	0	-	-
Li_2	$[He_2](2\sigma_g)^2$	1	267	111
Be_2	$[He_2](2\sigma_g)^2(2\sigma_u^*)^2$	0	-	-
B_2	$[He_2](2\sigma_g)^2(2\sigma_u^*)^1(1\pi_u)^2(3\sigma_g)^1$	2	159	290
C_2	$[He_2](2\sigma_g)^2(2\sigma_u^*)^2(1\pi_u)^4$	2	131	628
N_2	$[He_2](2\sigma_g)^2(2\sigma_u^*)^2(1\pi_u)^4(3\sigma_g)^2$	3	110	941
O_2	$[He_2](2\sigma_g)^2(2\sigma_u^*)^2(3\sigma_g)^2(1\pi_u)^4(1\pi_g^*)^2$	2	121	494
F_2	$[He_2](2\sigma_g)^2(2\sigma_u^*)^2(3\sigma_g)^2(1\pi_u)^4(1\pi_g^*)^4$	1	142	150
Ne_2	$[He_2](2\sigma_g)^2(2\sigma_u^*)^2(3\sigma_g)^2(1\pi_u)^4(1\pi_g^*)^4(3\sigma_u)^2$	0	-	-

Problem II.4 Explain the trends in the following table based on mo considerations.

	$R_{O\text{-}O}$ (pm)	$\bar{\nu}$ (cm^{-1})	
$[O_2^+]AsF_6$	112	1858	dioxygenyl
O_2	121	1555	dioxygen
$K[O_2^-]$	128	1108	superoxide
$Na_2[O_2^{2-}]$	149	760	peroxide

$\bar{\nu}$ is the vibrational wavenumber (frequency).

II.5 Orbital mixing in the non-degenerate case

To this point, we have been discussing the case of mixing two degenerate orbitals, *i.e.*, the ao's involved in the LCAO have had the same energy. Most orbital mixings, however, occur between non-degenerate orbitals, *e.g.*, mixing p_z and s orbitals on atoms of the same element or simply mixing any orbitals on different atoms in a heteroatomic molecule. The mixing of two ao's of the same irreducible representation but of different energies is shown in figure II.8. Again, the destablization, Δ_2 is greater than the stabilization, Δ_1, due to overlap of the ao's similar to the description in Eq II.5.

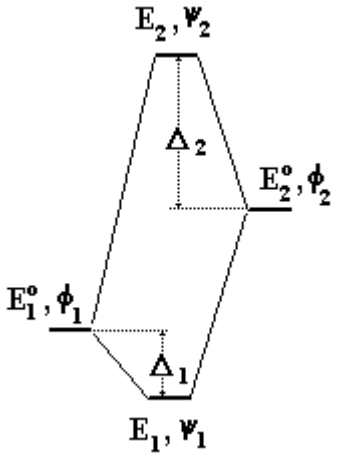

Figure II.8. Energy diagram for mixing non-degenerate ao's ϕ_1 and ϕ_2 on different atoms.

The secular equation for the non-degenerate case is $\left(E_1^o - E\right)\left(E_2^o - E\right) - \left(H_{12} - ES\right)^2 = 0$.

Which yields energies of

$$E_1 = E_1^o - \frac{\left(H_{12} - E_1^o S\right)^2}{E_2^o - E_1^o} = E_1^o - \Delta_1 \quad \& \quad E_2 = E_2^o + \frac{\left(H_{12} - E_2^o S\right)^2}{E_2^o - E_1^o} = E_2^o + \Delta_2 .$$

The molecular wavefunctions (not normalized) are $\psi_1 = \phi_1 + t_1\phi_2$ and $\psi_2 = -t_2\phi_1 + \phi_2$,

where, $t_1 = \frac{(H_{12} - E_1^o S)}{(E_1^o - E_2^o)}$ and $t_2 = \frac{(H_{12} - E_2^o S)}{(E_1^o - E_2^0)}$. The numerators and denominators are all negative so t_1 and t_2 are both positive. t_1 represents the extent to which ϕ_2 is mixed into ϕ_1 to form the ψ_1 mo while t_2 is the extent of mixing of ϕ_1 into ϕ_2 in the ψ_2 mo. Unlike the degenerate case where the mo is an equal mixture of the ao's, these mo's retain more character of the ao which is closer in energy, *i.e.*, the $t_i < 1$. It should be noted that both the extent of mixing of the ao's and, as a consequence, the extent of stabilization of the mo's depends on the difference $\Delta E = E_2^o - E_1^o$, *i.e.*, on the **energy compatibility** of the orbitals.

In order for mixing of orbitals to occur, (1) the orbitals must form the bases for the same irreducible representation of the molecular point group (2) they should be energetically compatibile and (3) they must overlap.

II.6 Orbital Energies

Electronic energies fall into three classes: core levels are those occupied by electrons close to the nucleus and therefore have very high binding energies (BE > 400 eV); valence levels are occupied by the bonding electrons which are much farther from the nucleus and have binding energies in the 10 - 40 eV range; the virtual levels are unoccupied by electrons in the molecular ground state. The most common procedure for the measurement of orbital energies is photoelectron spectroscopy (PES). In a PES experiment, the kinetic energy of an electron which has been ejected from the species by a high energy photon is measured. Due to the conservation of energy, the energy of the photon is equal to the kinetic energy of the ejected electron plus the binding energy of the electron $h\nu = T_e + BE$. The binding energy then is determined as $BE = h\nu - T_e$. Orbital energies are then inferred from Koopman's Theorem.

Koopman's Theorem: the energy of an occupied orbital is equal to minus the ionization energy for that orbital. The energy of a virtual (unoccupied) orbital is equal to minus the electron affinity of that orbital.

When constructing mo energy diagrams, it is helpful to have an idea of the energy of the interacting orbitals, *i.e.*, the H_{aa} values. To aid you in this respect, a table of Valence Oribital H_{ii} values (calculated) is presented in Appendix D.

Most questions pertaining to relative orbital energies can be answered by simple Coulombic (Crystal field) considerations. Atomic orbitals are increasingly stabilized by increasing nuclear charge, *i.e.*, **as electron density is removed from a system, the orbital energies drop and as electron density increases, the orbital energies rise**.

The mo diagram for HF is shown below as an example of a heteroatom diatomic.

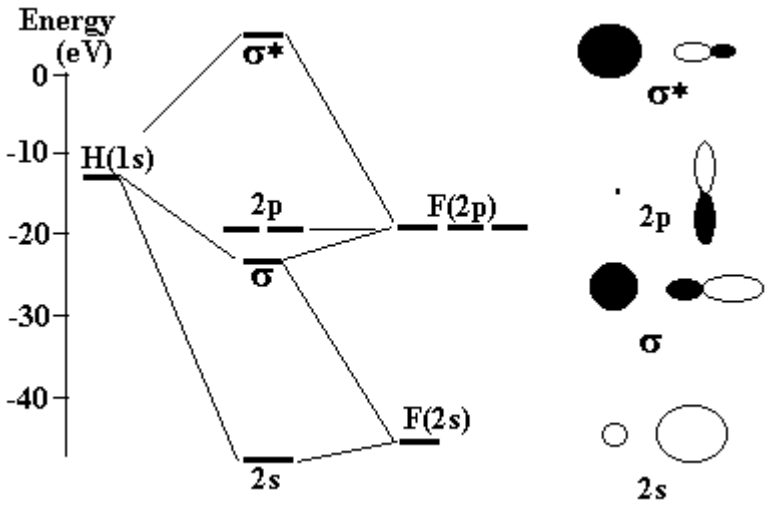

Figure II.9. mo diagram for HF. The HF ionization energies for the occupied orbitals were determined from PES while the energy of the 4σ orbital was calculated.

Energies and ao coefficients for HF from simple Hückel calculations.

Orbital	E (eV)	H(1s)	F(2s)	F(2p)
σ^*	+5.78	-0.804	0.191	0.558
σ	-20.50	-0.515	0.240	-0.824
2s	-45.53	0.292	0.951	0.095

The polarity of the H-F bond can be understood in mo terms since the electron density is much larger near the F - a result of it being the more electronegative element and thus having the lower lying orbitals which dominate the description of the filled mo's.

CO, NO and CN^- are important ligands and their spectroscopy can serve as an excellent probe into metal-ligand interaction The mo diagrams for CO and NO are shown in figure II.10. CO or CN^- interact with the metal in two ways:

- π-acidity: the 2π orbitals are available to accept electron density from the metal orbitals. Since the 2π orbitals are antibonding in nature, increasing the electron density in them will lower the bond order and thus lower the vibrational frequency of the C≡X bond.
- σ-basicity: the 5σ orbitals can donate electron density to the metal. It should be noted however that the 5σ orbital is slightly antibonding in character which means that removal of electron density will increase the vibrational frequency of the C≡X bond - the CO stretch in CO^+ is nearly 50 cm^{-1} higher than in CO.

Carbonyls and cyanides can therefore serve as sensitive probes of the electron density on the metal. We will examine this behavior in detail in chapter V.

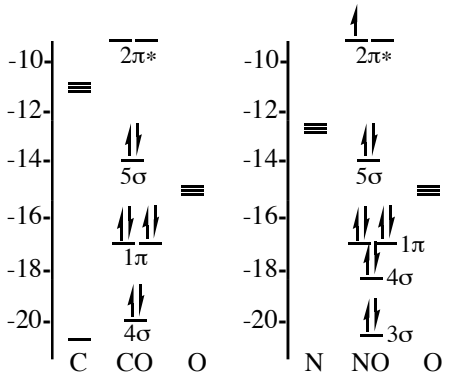

Figure II.10. The VOIE's of C,O and N as well as PES ionization energies of CO and NO. It should be noted that due to the unpaired electron in the 2π orbital of NO, the states that are derived by ionization of NO are complicated resulting in uncertainties in the energy positions of the mo's. The 1σ orbital will be at much lower energy - H_{ii} for the O 2s orbital is -32.3 eV..

Problem II.5 (a) Sketch the orbitals of CO - include the 1σ.
(b) In octahedral complexes, the d-orbitals of t_{2g} symmetry are referred to as the dπ-orbitals since they have the appropriate symmetry to π-bond to the ligands while the e_g orbitals are the dσ's. Draw a diagram showing the effect on the CO 5σ and 2π orbitals and the intreracting Os d-orbitals when an Os-CO bond is formed. The resulting energy difference in the d-orbitals is called the crystal field splitting, 10Dq. Label all orbitals indicating with * those that are anti-bonding. Clearly indicate 10Dq. Suggest an alternate explanation for σ-interaction increasing the CO stretching frequency. Your mo diagram should contain only four mo's: 5σ, 2π, dσ and dπ.
(c) Cyanide is a better σ-donor and a worse π-acceptor than carbonyl. Explain.

II.7 Polyatomic Molecules

For polyatomic molecules, the symmetrically equivalent sets of valence orbitals must be identified and then the appropriate SALC's generated. For example, water belongs to the C_{2v} point group, and the valence ao's are the 2H(1s) + O(2s) + O($2p_x$) + O($2p_y$) + O($2p_z$). Since the oxygen atom is on every symmetry element, the irreducible representations of the oxygen orbitals can be obtained directly from the character table, but two SALC's must be generated for the 2H(1s) orbitals.

C_{2v} character table and the reducible representation for the 2H(1s) orbitals in water

C_{2v}	E	C_2	$\sigma_v(xz)$	$\sigma_v(yz)$	
A_1	1	1	1	1	z
A_2	1	1	-1	-1	
B_1	1	-1	1	-1	x
B_2	1	-1	-1	1	y
Γ[H(1s)]	2	0	2	0	

Remember that s-orbitals are totally symmetric, so the s-orbital of an atom on all symmetry elements will transform as a_1. From the character table, we deduce that p_x, p_y, and p_z

transform as b_1, b_2, and a_1, respectively. Decomposing the reducible representation for Γ(1s) yields $a_1 + b_1$. The following mo diagram applies to the H_2O molecule.

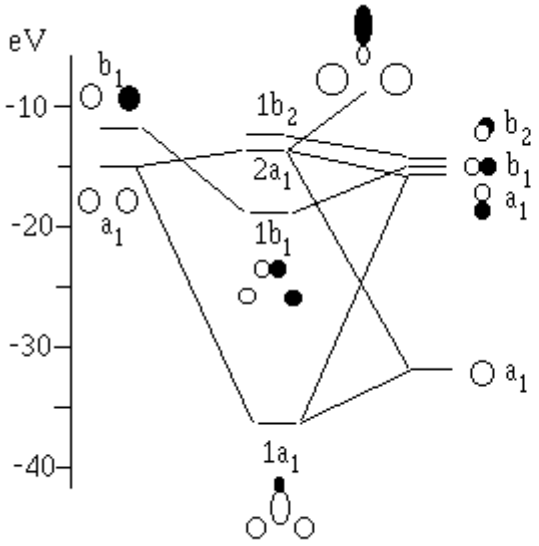

SCF Energies and atomic coefficients for H_2O

mo	E(eV)	O(2s)	O(pz)	H(a1)	O(px)	H(b1)	O(py)
$1a_1$	-36	0.85	0.13	0.21	0	0	0
$1b_1$	-19	0	0	0	0.54	0.61	0
$2a_1$	-13	-0.46	0.83	0.39	0	0	0
$1b_2$	-12	0	0	0	0	0	1

Figure II.11. MO diagram for the water molecule showing orbital energies and pictoral representations of the mo's determined by a self-consistent field (SCF) calculation. Orbital coefficients and energies are given in the table.

As can be seen from figure II.11, $1a_1$ and $1b_1$ are bonding orbitals while $2a_1$ and $1b_2$ are non-bonding - the two "lone pairs" on the oxygen.

Problem II.6 Construct an mo diagram for phosphine. Draw approximate mo's and fill with the approrpriate number of electrons. Discuss the π-accepting abilities of phosphine. Which is a better π-acid, PH_3 or PF_3? Explain.

Organic molecules play an important role in coordination chemistry and an understanding of the bonding in them is also important to the inorganic chemist. Two examples to be considered in this course will be Zeise's salt [$KPtCl_3(C_2H_4)$] and sandwhich compounds. As a result, an understanding of the mo's of ethylene and benzene is essential.

Ethylene: C_2H_4 has D_{2h} symmetry. All four hydrogens are interchangeable by symmetry operations so the four hydrogen 1s orbitals form a symmetrically complete set. The two carbons are also symmetrically equivalent so their valence orbitals also represent symmetrically complete sets (2s, $2p_x$, $2p_y$ and $2p_z$). Figure II.12 defines the system used.

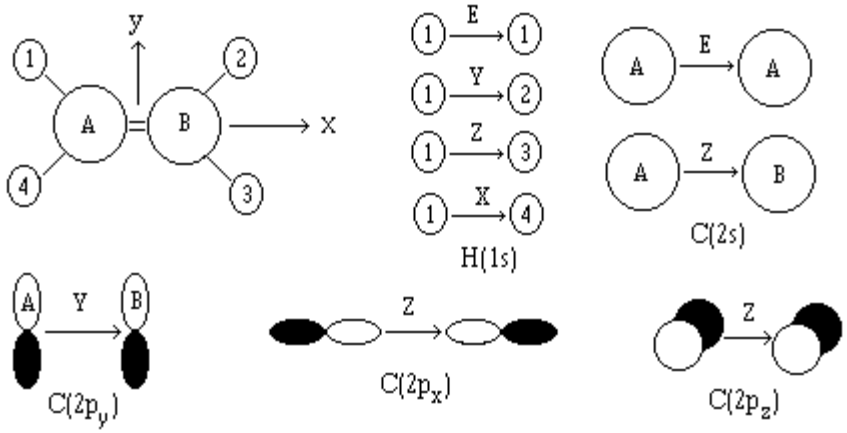

Figure II.12. The coordinate system used for ethylene and the operations which transform each reference orbital (on H_1 and C_A) into each member orbital of the set. Note that Z = C_2(z).

The reducible representations of the symmetrically equivalent sets formed for the valence ao's in ethylene can then be determined and decomposed into the corresponding irreps.

D_{2h}	E	Z	Y	X	i	XY	XZ	YZ	Irreps
H(1s)	4	0	0	0	0	4	0	0	$a_g+b_{1g}+b_{2u}+b_{3u}$
C(2s)	2	0	0	2	0	2	2	0	$a_g + b_{3u}$
C($2p_z$)	2	0	0	-2	0	-2	2	0	$b_{2g} + b_{1u}$
C($2p_x$)	2	0	0	2	0	2	2	0	$a_g + b_{3u}$
C($2p_y$)	2	0	0	-2	0	2	-2	0	$b_{1g} + b_{2u}$

Since the members of all sets can be exchanged completely with only the rotational operations, only the C_2 characters in the irreducible representations generated above need to be considered.

D_{2h}	E	Y	Z	X
a_g	+1	+1	+1	+1
b_{1g}	+1	-1	+1	-1
b_{2g}	+1	+1	-1	-1
b_{1u}	+1	-1	+1	-1
b_{2u}	+1	+1	-1	-1
b_{3u}	+1	-1	-1	+1

The normalized SALC's can now be constructed.

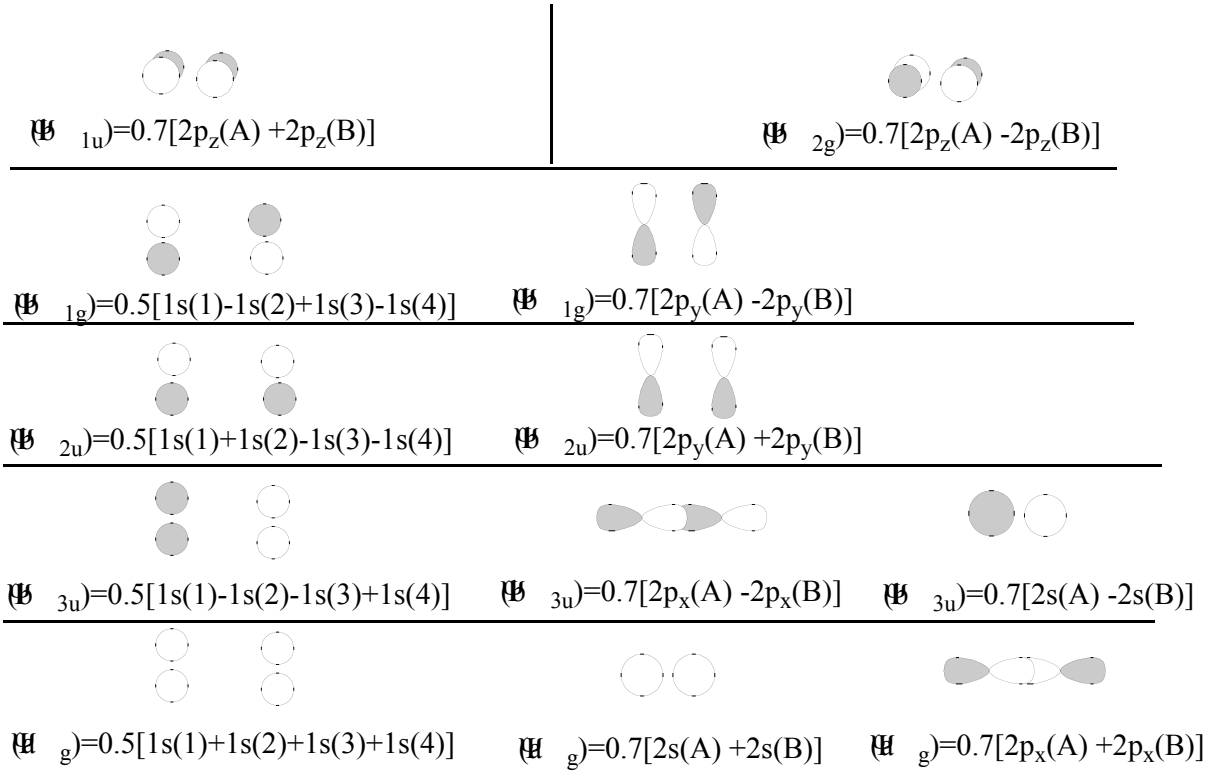

Figure II.13. The normalized SALC's for the ethylene molecule.

Calculations yield the following energies and mo's.

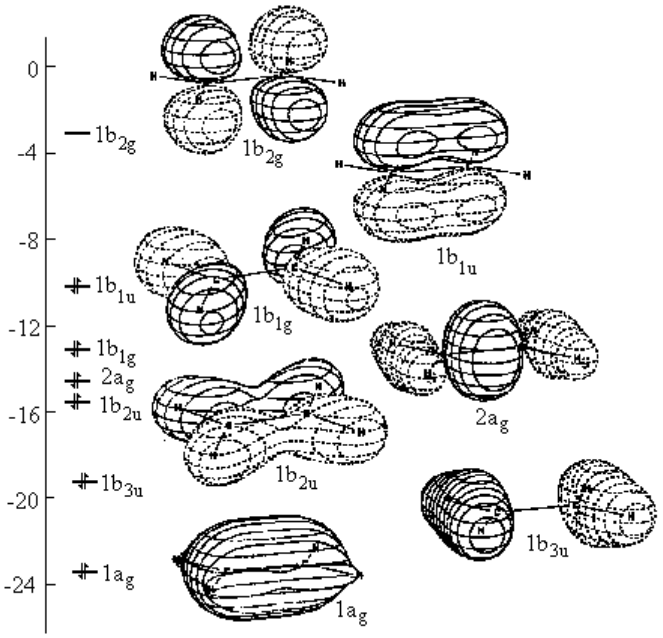

Figure II.14. An mo diagram for ethylene. Occupied orbital energies are PES measurements while the LUMO energy is estimated from the energy of the $\pi \rightarrow \pi^*$ transition in the uv. Contours are from Jorgensen; W.L., Salem, L., *The Organic Chemist's Book of Orbitals*, Academic Press, 1973.

Problem II.7 Construct mo's and an mo diagram for formaldehyde by combining a CO fragment (problem II.5 & figure II.10) with the HH fragment. Hint: one of the π-bonds of CO becomes a non-bonding orbital in H_2CO. Do not try to be precise (you can't know the coefficients without calculation) just roughly sketch the mo's up through the LUMO [CO π*]. Be sure to label each orbital with its symmetry.

Most of the spectroscopy and bonding involving benzene is centered around its π-system, and to a good approximation, the π- and σ-systems can be separated. Our treatment will therefore deal only with the π-orbitals. C_6H_6 has D_{6h} symmetry. The atom numbering system and the symmetry element definitions used are given below:

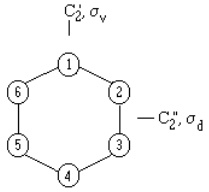

The following reducible representation, Γ_π, is obtained for the six p_z orbitals.

D_{6h}	E	$2C_6$	$2C_3$	C_2	$3C_2'$	$3C_2''$	i	$2S_3$	$2S_6$	σ_h	$3\sigma_v$	$3\sigma_d$	Irreps
Γ_π	6	0	0	0	-2	0	0	0	0	-6	2	0	$a_{2u}+b_{2g}+e_{1g}+e_{2u}$

The operation required to carry the reference p-orbital, ①, into each of the other p-orbitals as well as the character of that operation in each of irreducible representations is given below.

Atom	Operation	a_{2u}	b_{2g}	e_{1g}	e_{2u}
1	E	+1	+1	+2	+2
2	C_6	+1	-1	+1	-1
3	C_3	+1	+1	-1	-1
4	C_2	+1	-1	-2	+2
5	C_3	+1	+1	-1	-1
6	C_6	+1	-1	+1	-1

The SALC's can now be constructed. In order of decreasing energy (number of nodal planes):

$$\Psi(b_{2g}) = \frac{1}{\sqrt{6}}\{p_x(1) - p_x(2) + p_x(3) - p_x(4) + p_x(5) - p_x(6)\}$$

$$\Psi_a(e_{1u}) = \frac{1}{\sqrt{12}}\{2p_x(1) - p_x(2) - p_x(3) + 2p_x(4) - p_x(5) - p_x(6)\}$$

$$\Psi_b(e_{1u}) = \frac{1}{2}\{p_x(2) - p_x(3) + p_x(5) - p_x(6)\}$$

$$\Psi_a(e_{1g}) = \frac{1}{\sqrt{12}}\{2p_x(1) + p_x(2) - p_x(3) - 2p_x(4) - p_x(5) + p_x(6)\}$$

$$\Psi_b(e_{1g}) = \frac{1}{2}\{p_x(2) + p_x(3) - p_x(5) - p_x(6)\}$$

$$\Psi(a_{2u}) = \frac{1}{\sqrt{6}}\{p_x(1) + p_x(2) + p_x(3) + p_x(4) + p_x(5) + p_x(6)\}$$

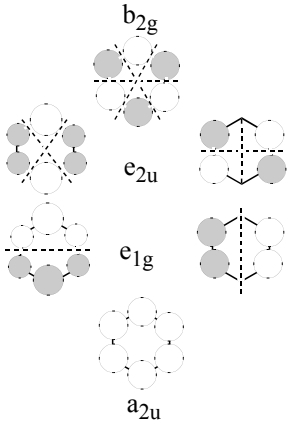

Figure II.15. Pictorial representaion of the of benzene

Problem II.8 Construct mo's (as pictures and functions) and an mo diagram for the π-systems of the cyclopentadienyl anion ($C_5H_5^-$) and pyrazine. Include the lone pairs of the pyrazine. Review section I-9 on how to construct the

SALC's for the degenerate pairs of the cyclopentadienyl anion, use atoms 3 & 4 as references and verify that one of the components of one of the degenerate SALC's is:

$$\Psi = 0.60\phi_2 + 0.37\phi_3 - 0.37\phi_4 - 0.60\phi_5$$

II.8 Hückel MO Theory

Hückel Molecular Orbital (HMO) Theory is quite useful for calculation of molecular properties of conjugated organic molecules.

HMO is used to describe π-type bonding only. Therefore, only collinear, conjugated p-orbitals are used for the basis. Obviously, σ bonding is not considered. The overlap integral between two contiguous p-orbitals is set to zero. This approximation dramatically simplifies the math without destroying the utility of the calculations.

The method for determining HMO results using symmetry is described in the procedure below:

1. Determine the molecular point group. This might require drawing the molecule in a symmetric conformation.
2. Determine the normalized symmetry-adapted linear combinations (SALCs) for each symmetrically-complete set of atomic orbitals using the projection operator method. If there is only one symmetrically complete set, then the SALCs are the molecular orbitals (MOs).
3. Use the SALCs to determine the elements of the Hückel secular determinant:

$$\det|H_{ij} - E_\pi S_{ij}| = 0$$

where E_π is the energy, H is the coulomb integral for i=j and the resonance integral for i≠j, and S is the overlap integral and equals δ_{ij} (Kroneker delta; $S_{i=j}=1$, $S_{i\neq j}=0$). By using SALCs, integrals $\int\psi_I|H_\pi|\psi_j d\tau$ where ψ_i and ψ_j belong to different irreducible representations are zero. Thus, the determinant is either diagonalized (one symmetrically complete set) or block diagonalized (more than one symmetrically complete set).

4. Simplify the mathematical symbolism by letting $H_{ii} = \alpha$, $H_{ij} = \beta$. Divide each element by β and let $x = (\alpha - E)/\beta$. Solve each block for x. If the determinant is diagonal, each diagonal element is an eigenvalue. If the SALCs are the MOs, then you are finished.
5. For each eigenvalue, solve for the eigenvectors (coefficients). These are the contributions of each SALC to the MO. This is achieved using the following secular equations:

$$\Sigma|H_{ij} - ES_{ij}|C_{ij} = 0$$

$$\Sigma(C_{ij})^2 = 1$$

II.8a. An Example: Butadiene.

<u>STEP 1: CONSTRUCT SALCs from 2p orbitals</u>

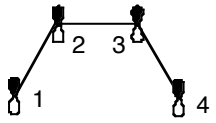

Two symmetrically-complete sets of $2p_z$ orbitals (ϕ_1/ϕ_4 and ϕ_2/ϕ_3)

C_{2v}	E	C_2	$\sigma_v(xz)$	$\sigma_v(yz)$
A_1	1	1	1	1
A_2	1	1	-1	-1
B_1	1	-1	1	-1
B_2	1	-1	-1	1
ϕ_1	ϕ_1	$-\phi_4$	$-\phi_1$	ϕ_4
ϕ_2	ϕ_2	$-\phi_3$	$-\phi_2$	ϕ_2

$$\begin{bmatrix} \alpha - E & \beta & 0 & 0 \\ \beta & \alpha - E & \beta & 0 \\ 0 & \beta & \alpha - E & \beta \\ 0 & 0 & \beta & \alpha - E \end{bmatrix} = 0$$

$\Gamma_\pi(\phi_1/\phi_4) = 2 \quad 0 \quad -2 \quad 0$

$= a_2 + b_2$

$SALC_{14}(a_2) = \phi_1-\phi_4+\phi_1-\phi_4 = 0.707(\phi_1-\phi_4)$

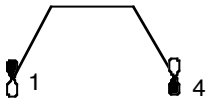

$SALC_{14}(b_2) = \phi_1+\phi_4+\phi_1+\phi_4 = 0.707(\phi_1+\phi_4)$

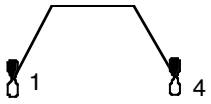

$\Gamma_\pi(\phi_2/\phi_3) = 2 \quad 0 \quad -2 \quad 0$

$= a_2 + b_2$

$SALC_{23}(a_2) = \phi_2-\phi_3+\phi_2-\phi_3 = 0.707(\phi_2-\phi_3)$

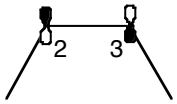

$SALC_{23}(b_2) = \phi_2+\phi_3+\phi_2+\phi_3 = 0.707(\phi_2+\phi_3)$

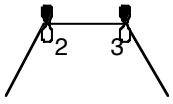

SALC(1) = $0.707(\phi_1 - \phi_4)$; (a_2)
SALC(2) = $0.707(\phi_2 - \phi_3)$; (a_2)
SALC(3) = $0.707(\phi_1 + \phi_4)$; (b_2)
SALC(4) = $0.707(\phi_2 + \phi_3)$; (b_2)

STEP 2: CONSTRUCT SYMMETRIZED HUCKEL SECULAR DETERMINANT

Note that "unsymmetrized" Huckel determinant is 4x4 — time consuming to solve, and a forth-order polynomial results. The determinant is dramatically simplified using symmetry. First, determine the elements H_{ij} using the SALCs.

$H_{11} = 0.5\int(\phi_1-\phi_4)H(\phi_1-\phi_4) = 0.5(\alpha-0-0+\alpha) = \alpha$

$H_{12} = 0.5\int(\phi_1-\phi_4)H(\phi_2-\phi_3) = 0.5(\beta-0-0+\beta) = \beta$

$H_{13} = H_{31} = H_{23} = H_{32} = H_{14} = H_{41} = H_{24} = H_{42} = 0$; SALCs are orthogonal (they transform as different irreps)

$H_{21} = H_{12} = 0.5\int(\phi_1-\phi_4)H(\phi_2-\phi_3) = 0.5(\beta\text{-}0\text{-}0+\beta) = \beta$

$H_{22} = 0.5\int(\phi_2-\phi_3)H(\phi_2-\phi_3) = 0.5(\alpha\text{-}\beta\text{-}\beta+\alpha) = \alpha-\beta$

$H_{33} = 0.5\int(\phi_1+\phi_4)H(\phi_1+\phi_4) = 0.5(\alpha+0+0+\alpha) = \alpha$

$H_{34} = 0.5\int(\phi_1+\phi_4)H(\phi_2+\phi_3) = 0.5(\beta+0+0+\beta) = \beta$

$H_{43} = 0.5\int(\phi_1+\phi_4)H(\phi_2+\phi_3) = 0.5(\beta+0+0+\beta) = \beta$

$H_{44} = 0.5\int(\phi_2+\phi_3)H(\phi_2+\phi_3) = 0.5(\alpha+\beta+\beta+\alpha) = \alpha+\beta$

The symmetrized determinant is:

$$\begin{bmatrix} H_{11}-E & H_{12} & H_{13} & H_{14} \\ H_{21} & H_{22}-E & H_{23} & H_{24} \\ H_{31} & H_{32} & H_{33}-E & H_{34} \\ H_{41} & H_{42} & H_{43} & H_{44}-E \end{bmatrix} = \begin{bmatrix} \alpha-E & \beta & 0 & 0 \\ \beta & \alpha-\beta-E & 0 & 0 \\ 0 & 0 & \alpha-E & \beta \\ 0 & 0 & \beta & \alpha+\beta-E \end{bmatrix} = 0$$

Divide by β and let $x = (\alpha-E)/\beta$:

$$\begin{bmatrix} x & 1 & 0 & 0 \\ 1 & x-1 & 0 & 0 \\ 0 & 0 & x & 1 \\ 0 & 0 & 1 & x+1 \end{bmatrix} = 0$$

The original 4x4 determinant is now block diagonalized into a 2x2 (a_2) and 2x2 (b_2).

STEP 3: DETERMINE THE ORBITAL ENERGIES

The eigenvalues come from the two 2x2 sub-determinants. For the a_2 block:

$$\begin{bmatrix} x & 1 \\ 1 & x-1 \end{bmatrix} = x(x-1)-1 = x^2-x-1 = 0$$

The solutions are $x = (1 \pm 2.24)/2 = 1.62, -0.62$.

Thus,

$$E_+(a_2) = \alpha\text{-}1.62\beta$$
$$E_-(a_2) = \alpha+0.62\beta$$

From the b_2 sub-determinant:

$$\begin{bmatrix} x & 1 \\ 1 & x+1 \end{bmatrix} = x^2+x-1 = 0$$

The solutions are $x = (-1\pm2.24)/2 = -1.62, +0.62$.

Thus,

$$E_-(b_2) = \alpha+1.62\beta$$
$$E_+(b_2) = \alpha\text{-}0.62\beta$$

STEP 4: DETERMINE THE EIGENVECTORS

The eigenvectors represent the contribution of a SALC to the MO. Note that only SALCs of the same irrep can contribute to the same MO.

For the a_2 block and x = 1.62:

$$\begin{bmatrix} 1.62 & 1 \\ 1 & 1.62-1 \end{bmatrix}\begin{bmatrix} c_{11} \\ c_{21} \end{bmatrix} = \begin{bmatrix} 1.62 & 1 \\ 1 & 0.62 \end{bmatrix}\begin{bmatrix} c_{11} \\ c_{21} \end{bmatrix} = 0$$

$1.62c_{11} + c_{21} = 0$ and $c_{11} + 0.62c_{21} = 0$

$1.62c_{11} = -c_{21}$ $c_{11} = -0.62c_{21}$

and

$c_{11}^2 + c_{21}^2 = 1$

So,

$$(-0.62c_{21})^2 + c_{21}^2 = 1$$
$$1.384c_{21}^2 = 1$$
$$c_{21} = 0.85 \quad \text{and} \quad c_{11} = -0.53$$

The MO is $-0.53[(0.707(\phi_1 - \phi_4))] + 0.85[(0.707(\phi_2 - \phi_3))] = -0.37(\phi_1 - \phi_4) + 0.60(\phi_2 - \phi_3) =$

$$\psi_+(a_2) = -0.37\phi_1 + 0.60\phi_2 - 0.60\phi_3 + 0.37\phi_4$$

with

$$E_+(a_2) = \alpha - 1.62\beta$$

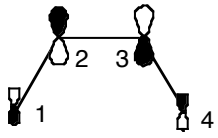

For the a_2 block, and x = -0.62:

$$\begin{bmatrix} -0.62 & 1 \\ 1 & -0.62-1 \end{bmatrix}\begin{bmatrix} c_{12} \\ c_{22} \end{bmatrix} = \begin{bmatrix} -0.62 & 1 \\ 1 & -1.62 \end{bmatrix}\begin{bmatrix} c_{12} \\ c_{22} \end{bmatrix} = 0$$

$-0.62c_{12} + c_{22} = 0$ and $c_{12} - 1.62c_{22} = 0$

$0.62c_{12} = c_{22}$ $c_{12} = 1.62c_{22}$

and

$c_{12}^2 + c_{22}^2 = 1$

So,

$$(1.62c_{22})^2 + c_{22}^2 = 1$$
$$3.62c_{22}^2 = 1$$
$$c_{22} = 0.53 \quad \text{and} \quad c_{12} = 0.85$$

The MO is $0.85[0.707(0.707(\phi_1 - \phi_4))] + 0.53[(0.707(\phi_2 - \phi_3))] = 0.6(\phi_1 - \phi_4) + 0.37(\phi_2 - \phi_3)$ =

$$\psi_-(a_2) = 0.60\phi_1 + 0.37\phi_2 - 0.37\phi_3 - 0.60\phi_4$$

with

$$E_-(a_2) = \alpha + 0.62\beta$$

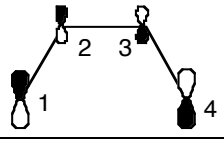

For the b_2 block, and x = -1.62:

$$\begin{bmatrix} -1.62 & 1 \\ 1 & -1.62+1 \end{bmatrix}\begin{bmatrix} c_{33} \\ c_{43} \end{bmatrix} = \begin{bmatrix} -1.62 & 1 \\ 1 & -0.62 \end{bmatrix}\begin{bmatrix} c_{33} \\ c_{43} \end{bmatrix} = 0$$

$-1.62c_{33} + c_{43} = 0$ and $c_{33} - 0.62c_{43} = 0$

$1.62c_{33} = c_{43}$ $c_{33} = 0.62c_{43}$

and

$$c_{33}^2 + c_{43}^2 = 1$$

So,

$$(0.62c_{43})^2 + c_{43}^2 = 1$$
$$1.38c_{43}^2 = 1$$
$$c_{43} = 0.85 \quad \text{and} \quad c_{33} = 0.53$$

The MO is $0.53[0.707(0.707(\phi_1+\phi_4))] + 0.85[(0.707(\phi_2+\phi_3))] = 0.37(\phi_1+\phi_4) + 0.60(\phi_2+\phi_3) =$

$$\psi_-(b_2) = 0.37\phi_1 + 0.60\phi_2 + 0.60\phi_3 + 0.37\phi_4$$

with

$$E_-(b_2) = \alpha+1.62\beta$$

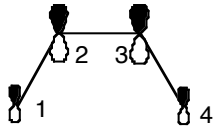

For the b_2 block, and x = 0.62:

$$\begin{bmatrix} 0.62 & 1 \\ 1 & 0.62+1 \end{bmatrix}\begin{bmatrix} c_{34} \\ c_{44} \end{bmatrix} = \begin{bmatrix} 0.62 & 1 \\ 1 & 1.62 \end{bmatrix}\begin{bmatrix} c_{34} \\ c_{44} \end{bmatrix} = 0$$

$0.62c_{34} + c_{44} = 0$ and $c_{34} + 1.62c_{44} = 0$

$0.62c_{34} = -c_{44}$ $c_{34} = -1.62c_{44}$

and

$$c_{34}^2 + c_{44}^2 = 1$$

So,

$$(-1.62c_{44})^2 + c_{44}^2 = 1$$
$$3.62c_{44}^2 = 1$$
$$c_{44} = 0.53 \quad \text{and} \quad c_{34} = -0.85$$

The MO is $-0.85[0.707(0.707(\phi_1+\phi_4))] + 0.53[(0.707(\phi_2+\phi_3))] = -0.60(\phi_1+\phi_4) + 0.37(\phi_2+\phi_3) =$

$$\psi_+(b_2) = -0.60\phi_1 + 0.37\phi_2 + 0.37\phi_3 - 0.60\phi_4$$

with

$$E_+(a_2) = \alpha+0.62\beta$$

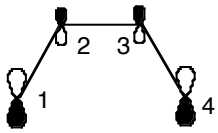

SUMMARY

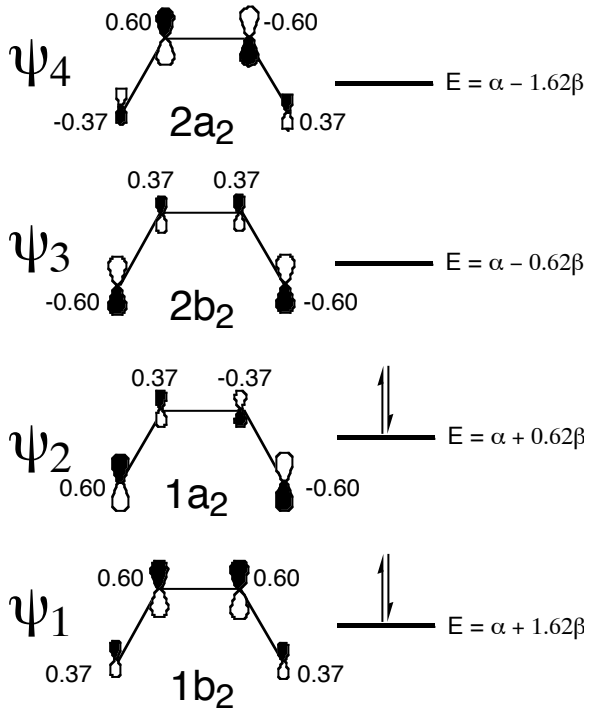

II.8b. Bond Orders, Electron and Charge Densities, and π Energies

The eigenvalues and eigenvectors can be used to calculate important molecular properties. The π bond-order (ρ_{ij}) is simply the product of coefficients of two contiguous atoms summed over all occupied orbitals.

$$\rho_{ij} = \sum_{occ,k} n_k c_{ik} c_{jk}$$

where ***n*** is the number of electrons in the occupied MO *k*, and
c_{ik} and c_{jk} are the coefficients on atoms i and j in MO *k*.

For butadiene the π bond-order for C1-C2 (and C3-C4) is:

$$\rho_{12} = \rho_{34} = 2(0.37 \bullet 0.60) + 2(0.60 \bullet 0.37) = 0.888$$

…or 88.8% of the π bonding in ethylene (ρ = 1)

For the C2-C3 bond in butadiene:

$$\rho_{23} = 2(0.60 \bullet 0.60) + 2(0.37 \bullet -0.37) = 0.446$$

The total amount of π bonding is 2(0.888) + (0.446) = 2.222. This value is greater than the π bonding in two ethylenes (total π bond order = 2x1= 2) and is a manifestation of stabilization by delocalization.

Electron densities (q_i) and charge densities (Q_i) can also be calculated using the coefficients. The electron density for an atom is simply the number of electrons in an MO times the square of the coefficient summed over all occupied MOs.

$$q_i = \sum_{occ,k} n_k c_{ik}^2$$

For butadiene:

$$q_1 = q_4 = 2(0.37^2) + 2(0.60^2) \approx 1$$

$$q_2 = q_3 = 2(0.60^2) + 2(0.37^2) \approx 1$$

This is consistent with the Lewis dot structure.

The charge densities represent the difference between the electron density for a singly-occupied p-orbital, and the electron density calculated by the Hückel method.

$$Q_i = 1 - q_i$$

For butadiene, all Q = 0. For anions, cations, and odd-membered rings, $q \neq 0$ and $Q \neq 0$.

The π energy is simply the sum of the one-electron energies:

$$E_\pi = \sum_{occ,k} n_k E_k$$

For butadiene:

$$E_\pi = 2(\alpha+1.62\beta) + 2(\alpha+0.62\beta) = 4\alpha+4.48\beta$$

Without proof, the π energy for two ethylenes is = 4α+4β. The difference between E_π for butadiene and E_π for two ethylenes (0.48β) is the butadiene delocalization energy. Delocalization energies can be used to explain Huckel's rule for aromaticity (monocyclic 4n+2 π-systems are aromatic, and 4n are antiaromatic). For example:

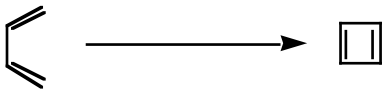

butadiene	cyclobutadiene
$E_\pi = 4\alpha+4.48\beta$	$E_\pi = 4\alpha+4\beta$

Cyclobutadiene and butadiene have the same number of atoms and the same number of π-electrons. However, butadiene has resonance stabilization, and cyclobutadiene does not. In fact, delocalization is lost by "cyclizing" butadiene. This is one way of defining aromaticity, antiaromaticity, and nonaromaticity: aromatic structures are more stable than their open-chain analogs, antiaromatic structures are less stable than their open-chain analogs, and nonaromatic structures are approximately as stable as their open-chain analogs.

For benzene, 1β of stabilization results from "cyclizing" hexatriene.

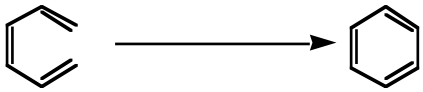

hexatriene	benzene
$E_\pi = 6\alpha+6.99\beta$	$E_\pi = 6\alpha+8\beta$

For cyclooctatetraene, only a small stabilization results, and cyclooctatetraene is considered nonaromatic. Furthermore, any stabilization by delocalization is removed by the molecule's nonplanar conformation (it is tub shaped).

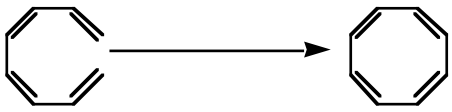

octatetraene	cyclooctatetraene
$E_\pi = 8\alpha+9.52\beta$	$E_\pi = 8\alpha+9.66\beta$

Problem II.9 Construct HMOs for cyclopropenium cation. Calculate electron and charge densities, π bond-orders, and the delocalization energy.

II.9 Crystal Field Theory

The precursor to molecular orbital theory of inorganic complexes was the crystal field theory (CFT). Due to the relative ease of its use and to its qualitative success, CFT remains in common use. All of the predictions of CFT are also made by molecular orbital theory in a more general way, but many times the two different theories use different terminology in coming to the same conclusion. It is important to understand both so we begin our study of inorganic complexes with a review of crystal field theory and then in the following section the molecular orbital approach will be considered.

CFT assumes that all interactions are purely Coulombic (electrostatic). In the absence of the field presented by the ligands, the metal d-orbitals are degenerate. In the presence of a spherically symmetric field created by electron rich ligands, the energy of the d-orbitals rises, but the orbitals remain degenerate. As the symmetry of the field is lowered by the typical four to six ligands, the degeneracy of the d-orbitals is lifted as they "feel" differing amounts of the ligand field. In the case of an ML_6 complex, with the ligands lying on the x-, y- and z-axes, the e_g orbitals (z^2 and x^2-y^2) will be repelled to a higher energy as the charge is concentrated along the bonding axes while the t_{2g} orbitals (xy, xz, yz) are stabilized since they are now directed to locations between the ligands. The extent to which the d-orbitals are split (the energy difference between the e_g and the t_{2g}) is the crystal field or ligand field splitting energy and is denoted by 10Dq. The magnitude of 10Dq is dependent on the nature of both the ligand and the metal. This splitting is such that the barycenter (center of energy) of the orbitals is unchanged so the three t_{2g} orbitals are stabilized by -4Dq while the two e_g orbitals are destabilized by +6Dq (3(-4) + 2(+6) = 0).

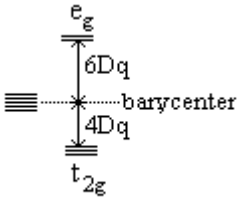

Figure II.16. The splitting of the d-orbitals in an octahedral field..

The crystal field stabilization energy (CFSE) is then -4Dq for every electron in a t_{2g} orbital, +6Dq for every electron in an e_g orbital and +P (electron pairing energy = 12 to 25 kK or 140 to 300 kJ/mol) for every set of paired of electrons. The system will adopt the apropriate configuration to obtain the maximum stabilization - minimum energy. Clearly, the first three d-electrons in an octahedral field will enter into the t_{2g} orbitals, but there are two possible configurations for the four electron system: high spin, $(t_{2g})^3e_g^1$ or low spin $(t_{2g})^4$ which have CFSE's of -6Dq and -16Dq + P. If 10Dq > P - the strong field case - then the low spin configuration will result. Similar arguments can be made for d^5, d^6 and d^7 - in all cases, if 10Dq > P, the system is low spin. d^8, d^9 and d^{10} are not subject to different configurations. A tetrahedral ligand field can be treated in the same manner except for two important facts: the e orbitals are lower than the t_2 orbitals so d^3 can be high spin or low spin while d^7 has only one possible configuration - $(e)^4(t_2)^3$; and the metal orbitals are not directed toward the ligand orbitals as well in T_d as they are in O_h symmetry so that, for the same metal ion, $10Dq(T_d) \approx (4/9)10Dq(O_h)$. The values of 10Dq in kK for several compounds of Co, Rh and Ir are give in the following table.

Species	M=Co	M=Rh	M=Ir
MCl_6^{3-}	-	20.3	25.0
$M(H_2O)_6^{3+}$	18.2	27.0	-
$M(NH_3)_6^{3+}$	22.9	34.1	41.0
$M(en)_3^{3+}$	23.2	34.6	41.4
$M(CN)_6^{3-}$	33.5	45.5	-

10 Dq in kK fromTable in Huheey, J.E., "Inorganic Chemistry: Principles of Structure and Reactivity", Harper & Row, NY, 1983, p384.

Factors dictating 10Dq

- *Oxidation state of the metal*. As the metal increases in oxidation state, it will increase the interaction with the ligands and increase 10Dq.
- *Number and geometry of the ligands*. The more ligands, the stronger the field at the metal. Also, as indicated above, the overlap differences between an octahedral and a tetrahedral field are substantial.
- *Nature of the ligand*. The relative field strengths of various ligands is given by the spectrochemical series which is presented near the end of this chapter.
- *Nature of the metal*. 10Dq increases about 40% in going from the 1st row to the 2nd row and another 25% on going to the third row. Second and third row transition metal complexes are always low spin (strong field).
- *Metal ligand distance*. 10Dq is inversely proportional to the fifth power of the metal-ligand bond length. Thus small ions which can get close to the metal and result in a much stronger field.

Consider figure II.17 which shows a tetragonal distortion of an octahedral complex in which the M-L bond length is increased along the z-axis (axial elongation) and then decreased along the x- and y-axes (equatorial compression). The resulting species has D_{4h} symmetry and the d-orbitals transform as a_{1g} (z^2) + b_{1g}(x^2-y^2) + b_{2g}(xy) + e_g (xz,yz). The ordering of the d-orbital energies in this situation will depend on how compressed the equatorial bond lengths become and on the nature of the ligand. Removal of electron density from the z-axis will stabilize the z^2 dramatically, but the effect on (xz,yz) will depend on the nature of the ligand. If the ligand is a σ-donor only, there will be little electron density in the xz or yz plane other than along the z-axis and (xz,yz) will not be affected. In mo parlance we would say that there are no low lying ligand orbitals of the appropriate symmetry to interact with xy or yz. If, on the other hand, the axial ligand is π-donor, axial elongation will result in some stabilization of (xz,yz). Equatorial compression will destabilize the x^2-y^2 dramatically but have little effect on the other orbitals if the ligand has no π-interaction. If the ligand is a π-donor, then the xy will be destabilized as will (xz,yz), i.e., there are low lying ligand orbitals with the correct symmetry to interact. The order of the d-orbitals will then depend on the length of the M-L bond and on how strong a π-donor the ligand is. In some cases, the z^2 will be the lowest energy d-orbital while in most cases it is the (xz,yz) pair which is lowest in energy. The relative order of the xy and the z^2 will depend on similar considerations.

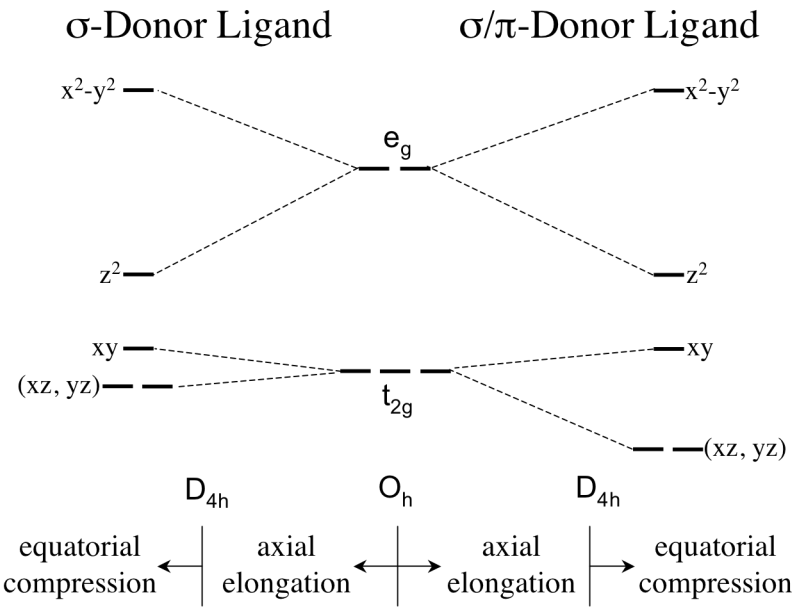

Figure II.17. The change in energy of the d-orbitals as the ligands in the octahedral complex ML_6 are removed along the z-axis and compressed in the xy plane.

Problem II.9a Draw a diagram like figure II.17 for the case where the ligand is a σ-donor and a π-acceptor.

Problem II.9b Arrange the d-orbitals of a D_{3h} (trigonal bipyramid) ion in order of increasing energy.

Electron Counting

It is imperitive that the correct number of electrons be placed in the mo energy level diagram and that they are placed into the correct orbitals. One misconception about the identity of the orbitals used in transition metal complexes is that the ns-orbitals are of lower energy than are the (n-1)d orbitals as is the case in the free atom. In the presence of a ligand field, however, the (n-1)d orbitals are lower in energy and fill before the ns orbitals. Consider iron as an example, the electron configuration of an iron atom is $4s^2 3d^6$, yet the VOIE's given in Appendix D indicate that the energies of the orbitals in iron compounds is 4s orbital: -7.1eV and 3d orbital: -8.7 eV, *i.e.*, the 3d orbitals are 1.6 eV *lower* than the 4s! This difference gets greater in going across the period as the d-electrons are stabilized by the increasing nuclear charge while the s-electrons, screened by the d-electrons, are unaffected - the 3d are 3 eV lower than the 4s in copper. Thus, **in all mo diagrams for transition metals the order of energy is (n-1)d < ns < np**.

The electron configuration of the metal is also of importance and is determined by assigning oxidation states to all of the the ligands and then assigning one to the metal with the realization that *all of the valence electrons for a transition metal are d-electrons*. Consider $(Me_3P)_4WS_2$. Me_3P is a neutral molecule and does not affect the oxidation state of the tungsten. The two sulfurs are each -2 and the molecule is neutral so tungsten must be in the +4 oxidation state - a d^2 configuration. In $[Co(CN)_3CO]^{2-}$, the cobalt is Co(I) which makes it d^8. The Co contributes 8 valence electrons, each CN^- contributes (4+5+1) = 10 electrons and the carbonyl contributes (4+6) = 10 electrons for a total of 48 valence electrons. This should be distinguished from the sum of the bonding and non-bonding electrons on the metal which is typically 18. The eighteen electron rule is based on the fact that the most stable situation is one in which all of the the bonding (or at worst non-bonding) metal orbitals - the dπ - are

filled but none of the dσ* are occupied. Thus the octahedral environment of a metal will consist of six dπ electrons plus six pairs of σ-bonding electrons from the ligands for a total of 18-electrons. As an example, consider $[PtCl_6]^{2-}$: Pt(IV) is d^6 and each chloride donates two electrons so the metal environment consists of 6 + 6(2) = 18 electrons. $[Co(CN)_3CO]^{2-}$, on the other hand, is a 16-electron system.

II.10 Molecular Orbitals in Inorganic Complexes

II.10a. Sigma Bonding in Octahedral ML_6

Sigma bonding will usually occur via lone pair donation from the filled σ-SALC's of the ligands into empty metal orbitals. The ligand SALC's of appropriate symmetry to form these σ-bonds with the metal in an octahedral complex must therefore be determined.

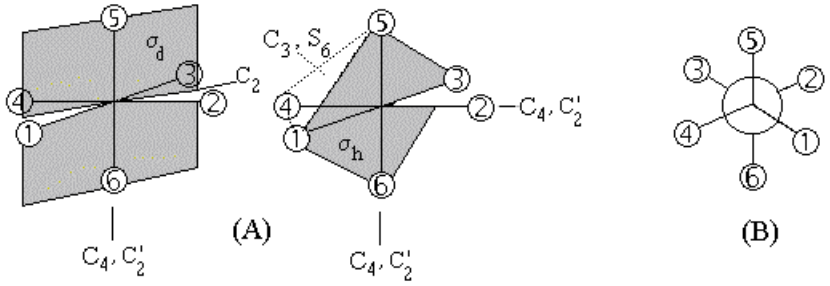

Figure II.18. (A) Numbering system and symmetry elements of octahedral ML_6. (B) View down the C_3 & S_6 axes.

The reducible representation of the ligand orbitals appropriate for σ-bonding is,

O_h	E	$8C_3$	$6C_2$	$6C_4$	$3C_2'$	i	$6S_4$	$8S_6$	$3\sigma_h$	$6\sigma_d$
Γ_σ	6	0	0	2	2	0	0	0	4	2

The reducible representation can be decomposed to yield the irreducible representations of the ligand SALC's: $a_{1g} + e_g + t_{1u}$. The symmetries of the metal orbitals are obtained from the character table to be: a_{1g} (s) + t_{1u} (p_x, p_y, p_z) + e_g (z^2, x^2-y^2) + t_{2g} (xz, yz,xy)

The a_{1g} ligand SALC is the easy one: $a_{1g} = \frac{1}{\sqrt{6}}(\sigma_1 + \sigma_2 + \sigma_3 + \sigma_4 + \sigma_5 + \sigma_6)$ and it has the correct symmetry to interact with the metal s-orbital. Figure II.19 is a representation of the bonding and antibonding combination. Since the ligand orbitals are expected to be much lower than the metal s-orbital, the bonding combination will be dominated by the ligand while the antibonding combination will be predominantly metal in character (see page 32).

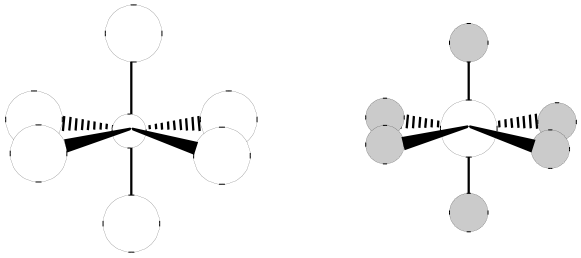

Figure II.19. Bonding and antibonding combination of a_{1g} ligand SALC and metal s-orbital.

The e_g and t_{1u} combinations would have to be constructed by using the complete projection operator (see section I.9) due to the ambiguity of appropriate operations to convert each of the ao's into one another, but in a group of order 48 this would be very tedious. Instead, one can

simply look at the metal orbitals and construct the appropriate SALC's by inspection. To construct the two e_g SALC's we need to consider the nature of the z^2 and x^2-y^2 orbitals. Remember that the amplitude of the z^2 torus in the xy plane is one-half that along the z-axis. Then the following two e_g bonding combinations can be constructed.

$$e_g(a) = \frac{1}{\sqrt{12}}\left(-\sigma_1 - \sigma_2 - \sigma_3 - \sigma_4 + 2\sigma_5 + 2\sigma_6\right) \qquad \& \qquad e_g(b) = \frac{1}{2}\left(-\sigma_2 - \sigma_4 + \sigma_5 + \sigma_6\right)$$

$e_g(a)+z^2$ $\qquad$ $e_g(b)+(x^2-y^2)$

Figure II.20. MO's formed from the e_g ligand SALC's and the d_{z2} and d_{x2-y2} metal orbitals. Again, the bonding combination is expected to be predominantly ligand in nature.

The three t_{1u} SALC's must combine with the metal p-orbitals. Since there are only two lobes on each of the p's, then only two ligand ao's will be involved in each.

$$t_{1u}(x) = \frac{1}{\sqrt{2}}\left(\sigma_2 - \sigma_4\right); \qquad t_{1u}(y) = \frac{1}{\sqrt{2}}\left(\sigma_5 - \sigma_6\right); \qquad t_{1u}(z) = \frac{1}{\sqrt{2}}\left(\sigma_1 - \sigma_3\right)$$

The x and y components are shown below.

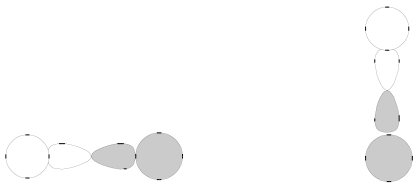

$t_{1u}(x)+p_x$ $\qquad$ $t_{1u}(y)+p_y$

Figure II.21. The x and y components of the t_{1u} mo's.

The energies of the σ-SALC's are expected to be quite low since they are derived from s and p-orbitals of relatively electronegative elements so their interaction will destabilize the metal orbitals with which they interact: $a_{1g}(s)$, t_{1u} (x,y,z), and e_g (z^2 and x^2-y^2). Since the e_g orbitals have the correct symmetry to interact with σ SALC's, they are referred to as the dσ orbitals, but since they are destabilized in the process, the e_g orbitals are also referred to as the dσ* orbitals. The t_{1g} orbitals are non-bonding with respect to σ-interactions. The approximate energy level diagram for σ-bonding in octahedral complexes is shown in figure II.22. Molecular orbital theory predicts the same picture as does crystal field theory. In crystal field theory, the e_g orbitals are forced to higher energy as the result of Coulombic repulsions with the ligand σ-orbitals while molecular orbital theory indicates that the higher energy e_g orbitals are of the correct symmetry to interact with the ligand σ-SALC's and are, therefore, destabilized.

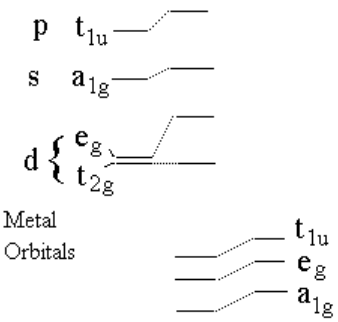

Figure II-22. Approximate mo diagrarm for σ mixing in octahedral field.

II.10b. Sigma bonding in tetrahedral ML_4

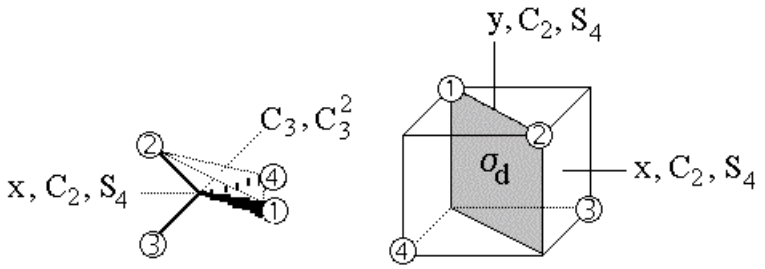

Figure II-23. Numbering, coordinate system and symmetry elements for T_d ML_4.

Reducible representation for the ligand sigma SALC's in tetrahedral ML_4.

Td	E	$8C_3$	$3C_2$	$6S_4$	$6\sigma_d$	
Γ_σ	4	1	0	0	2	$a_1 + t_2$

The σ SALC of a_1 symmetry is $\psi_1 = 1/2[\sigma_1 + \sigma_2 + \sigma_3 + \sigma_4]$ and the only metal orbital of that symmetry is the s-orbital. In the tetrahedral case, it is the t_2 orbitals that have the correct symmetry to interact with the low lying ligand sigma SALC's so they are destabilized relative to the e orbitals which are non-bonding. Again, the easiest way to construct the σ-SALC's is by matching their symmetries with that of the metal orbitals with which they interact, p or d. For illustrative purposes let us assume interaction with the p-orbitals and construct σ-SALC's which match the p-orbitals is both phase and amplitude.

$t_2(a) = 1/2[\sigma_1 - \sigma_2 + \sigma_3 - \sigma_4]$; $t_2(b) = 1/2[\sigma_1 + \sigma_2 - \sigma_3 - \sigma_4]$; $t_2(c) = 1/2[\sigma_1 - \sigma_2 - \sigma_3 + \sigma_4]$

$+ p_z$ $+ p_y$ $+ p_x$

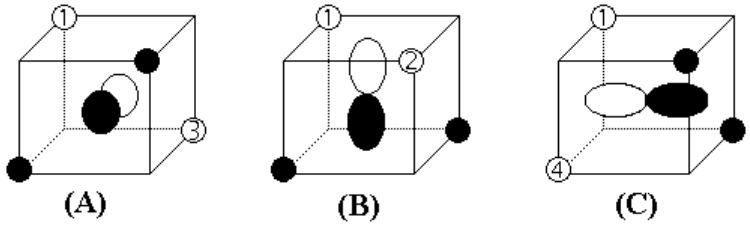

Figure II-24. Combinations of metal p-orbitals with the t_2 ligand σ-SALC's.

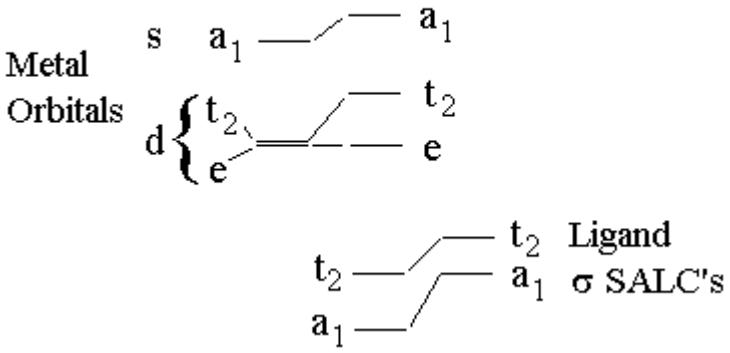

Figure II-25. Approximate mo diagram for σ mixing in T_d symmetry. Note the reversal of the d-orbitals relative to the octahedral case.

II.10c. π bonding in octahedral ML_6

π-bonding can also play an important role in the description of metal complexes. Indeed, the π-bonding effects in carbonyls, nitrosyls, cyanides, and some aromatics will be crucial to our understanding their spectra. We first define the set of vectors which will represent the ligand π-SALC's - the p_x and p_y orbitals on the ligands.

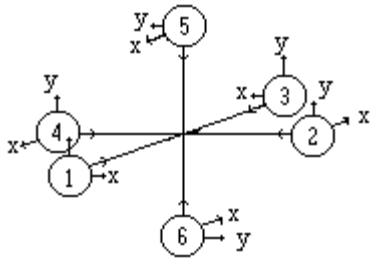

Figure II-26. The basis vectors for determining the reducible representation for the π-bonding in octahedral ML_6.

Since x ⇔ y for rotations about the bonds, the x and y vectors are degenerate and must therefore be treated as one set. The reducible representation for these vectors is:

O_h	E	$8C_3$	$6C_2$	$6C_4$	$3C_2'$	i	$6S_4$	$8S_6$	$3\sigma_h$	$6\sigma_d$
$\Gamma\pi$	12	0	0	0	-4	0	0	0	0	0

which can be decomposed to yield $\Gamma\pi = t_{1g} + t_{2g} + t_{1u} + t_{2u}$. From the character tables, the metal orbitals are seen to transform as $a_{1g}(s) + t_{1u}(x,y,z) + e_g(z^2, x^2-y^2) + t_{2g}(xy, xz, yz)$. Thus, the t_{1g} and t_{2u} π-SALC's are non-bonding with the metal, but the d_{xy}, d_{xz}, and d_{yz} have the correct symmetry as do the p-orbitals on the metal (see figure II.28).

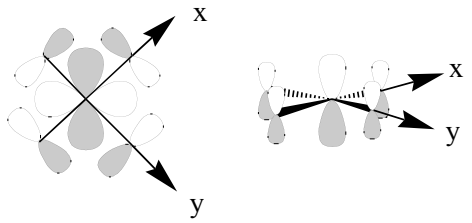

Figure II-28. Representation of one of the t_{2g} ligand SALC's with the d_{xy} and metal p_k with one of the t_{1u} SALC's. Simply changing the axes labels will yield the other members of these two triply degenerate representations.

The effect these interactions have on the metal orbitals is dictated by the nature of the ligand orbitals, *i.e.*, p, π or π*. If the ligand orbitals are filled (p or π) then they will lie lower than the unoccupied metal orbitals. In this case, the bonding mo's will be dominated by the ligand orbitals and the metal orbitals will be destabilized (mo description) or as electron density moves toward the metal from the ligand the metal orbitals are destabilized by the increased charge (CFT description). The extent to which the metal can accept electron density will depend upon the occupancy of the metal orbitals (the oxidation state of the metal). In many instances, the metal t_{2g}'s are occupied and interact with higher lying π* orbitals and are, therefore, stabilized and result in a bonding mo which is dominated by the metal. In CFT terms, electron density moves from the metal to the ligands stabilizing the t_{2g}'s - the metal behaves as an electron donor or base. Beacause they have the symmetry appropriate to π-bond, the t_{2g}'s are often referred to as the dπ's.

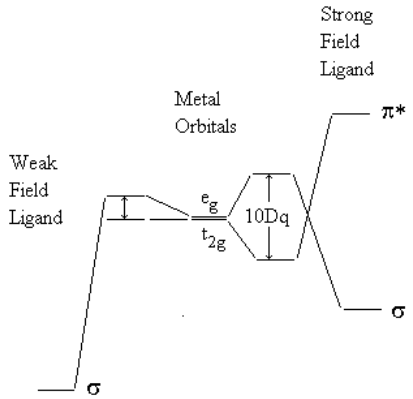

Figure II-28. Interaction of d-orbitals with strong field and weak field ligands in an octahedral field. A strong field is favored by high lying σ SALC's destabilizing the e_g and low lying π* stabilizing the t_{2g}.

The better the ligand σ-SALC's interact with the metal, the greater is the ligand field splitting as the e_g are pushed farther from the t_{2g}. Ligands which produce a large 10Dq are referred to as strong field ligands. If a ligand transfers electron density to the metal, the t_{2g} are also destabilized and thus 10Dq is reduced and the ligand is considered to have a reduced ligand field. However, ligands which accept electron density through low lying π* SALC's enhance their field strength due to the stabilization of the t_{2g}'s (see problem II.5). The **spectrochemical series** relates the relative field strengths of the ligands:

Spectrochemical Series

$$Br^- < S^{2-} < NCS^- < Cl^- < NO_3^- < F^- < OH^- < C_2O_4^{2-} < H_2O < SCN^- < CH_3CN < NH_3 < bpy < phen < NO_2^- < CN^- < CO$$

Problem II.10 Explain the following:

1. The field strengths of the halides are in the order $Br^- < Cl^- < F^-$.
2. Bipyridine has a greater field strength than ammonia.

II.10d. π-bonding in tetrahedral ML_4

The π-interactions in a tetrahedral molecule are difficult to draw so only a qualitative discussion will be given. The coordinate system is similar to the octahedral case in that the ligand z-axis is always the metal-ligand bond while the x & y axes are perpendicular to that bond. It is the p_x and p_y orbitals of the ligand that take part in π-bonding. Since one metal-ligand bond lies on each of the C_3 axes and the atoms lie on none of the other axes, only the C_3 and E characters are non-zero. The trace of the C_3 matrix in this 2-dimensional representation will be $2(\cos 2\pi/3) = -1$ and the dimension of the basis is 8.

Td	E	$8C_3$	$3C_2$	$6S_4$	$6\sigma_d$	
Γ_π	8	-1	0	0	0	$e + t_1 + t_2$

The t_1 SALC is non-bonding, but the e and t_2 SALC's have correct symmetry to interact. If the ligand is a relatively electronegative atom (Cl or O) then the following mo diagram might be expected.

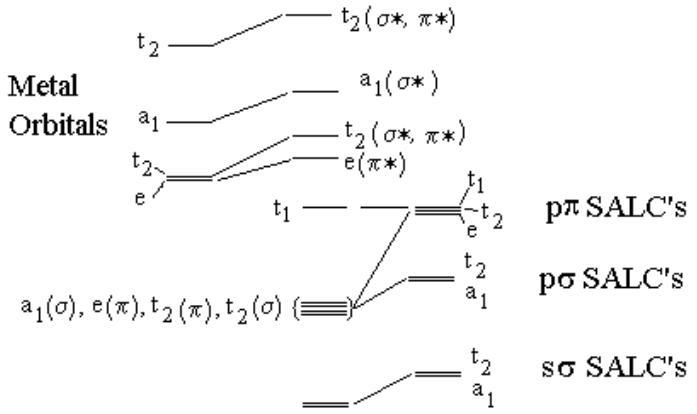

Figure II-29. Approximate mo bonding scheme for tetrahedral ML_4 where ligands have both σ and π interactions. In this figure it is assumed that the π interactions are through low lying p-orbitals rather than with high lying π* orbitals so there is no stabilization of the dπ's (t_2)

The same comments concerning field strengths of the ligands that were made in the ML_6 case apply in the ML_4 case.

Problem II.11 Draw approximate mo's (σ and π) for $SbBr_5$. For the σ bonds, use Br p-orbitals that "point" toward Sb. Make separate diagrams for σ and π bonding.

II.10e Ferrocene:

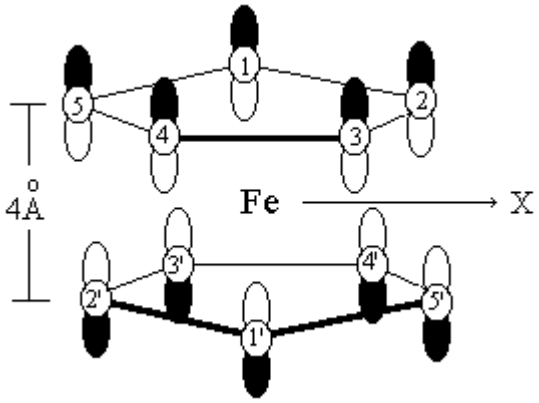

Figure II-30. Numbering and coordinate systems used in the treatment of ferrocene.

Ferrocene, $[(\xi^5\text{-}C_5H_5)_2Fe]$, has D_{5d} symmetry, although the eclipsed D_{5h} structure is very similar in energy. The bonding is between the π-system of the $C_5H_5^-$ rings and the metal orbitals. The ten p-orbitals on the rings form a symmetrically equivalent set since they can be interchanged by at least one of the operations of the group. However, a more intuitive way to think about the bonding is to consider the bonding to the cyclopentadienly SALC's which will combine in in-phase and out-of-phase combinations to form the ligand SALC's. The SALC's of the individual rings was determined in problem II.8 and are shown below. Since the two rings are 4Å apart, the in-phase and out-of-phase combinations are expected to have nearly the same energies.

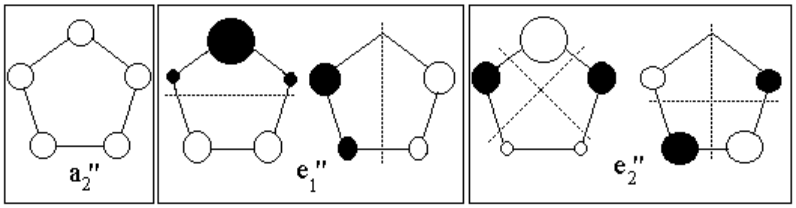

Figure II-31. Cyclopentadienyl SALC's. Shading indicates phase of p-orbitials and size represents the magnitude of the coefficient. Refer to problem II-8.

The reducible representation of the ten p orbitals in D_{5d} is

D_{5d}	E	C_5	C_5^2	C_2	i	S_{10}	S_{10}^3	σ_d
Γ_π	10	0	0	0	0	0	0	2

which can be decomposed to give $\Gamma_\pi = a_{1g} + a_{2u} + e_{1g} + e_{1u} + e_{2g} + e_{2u}$. The a_{1g} and a_{2u} mo's come from the in-phase and out-of-phase combinations of the a_2" SALC's, $\Psi(a_2") \pm \Psi'(a_2")$. The e_{1g} and e_{1u} mo's are derived from $\Psi'_{e1"} \pm \Psi'_{e1"}$ and the e_{2g} and e_{2u} orbitals are constructed from $\Psi_{e2"} \pm \Psi'_{e2"}$ linear combination. The in-phase (+) combinations are gerade while the out-of-phase (-) combinations are ungerade. The metal orbitals transform as a_{1g} (z^2, s) + a_{2u} (z) + e_{1u} (x, y) + e_{1g} (yz, xz) + e_{2g}(x^2-y^2, xy). With a careful examination of figure II-31 the appropriate combination of metal orbital and ligand SALC can be deduced: $a_{1g} + d_{z2}$; $a_{2u} + p_z$; ($e_{1u}(a) + p_y$ & $e_{1u}(b) + p_x$) ; ($e_{1g}(a) + d_{yz}$ & $e_{1g}(b) + d_{xz}$); ($e_{2g}(a) + d_{x2-y2}$ & $e_{2g}(b) + d_{xy}$) while the e_{2u} ligand SALC will be non-bonding.

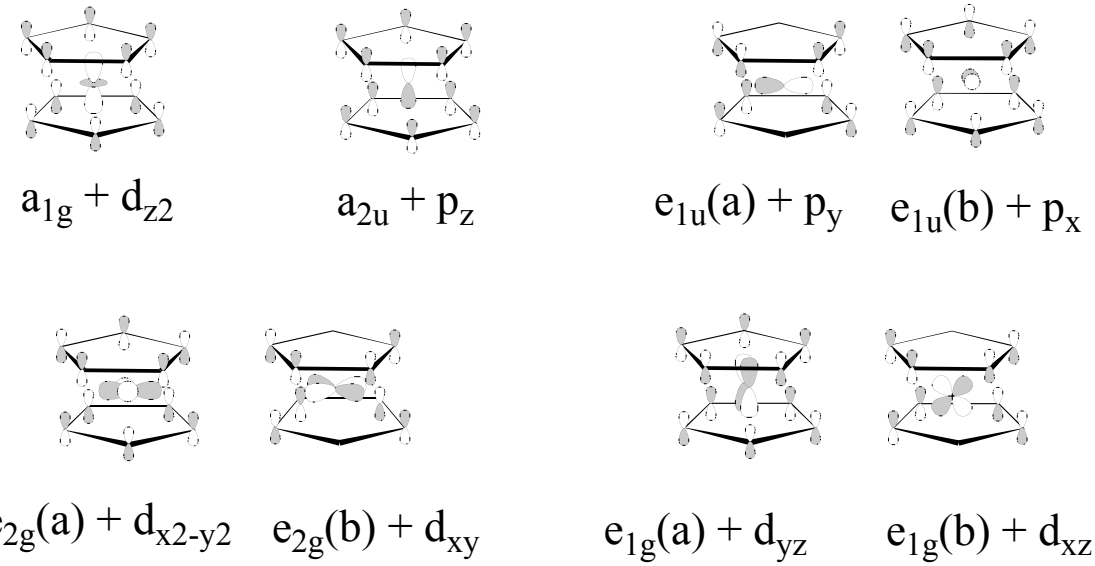

Figure II-32. Combinations of the cyclopentadienyl SALC's with the appropriate iron orbitals. Only the relative phases not the relative mixing coefficients of the orbitals are indicated.

The relative mo energies of ferrocene,

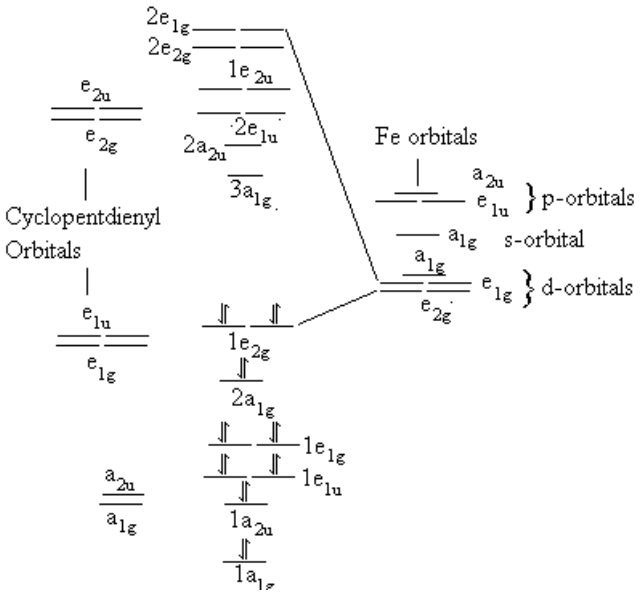

Figure II-33. MO diagram of ferrocene.

Since the e_{2g} orbitals on the iron (x^2-y^2, xy) have the same symmetry as higher lying π^* orbitals on the cyclopentadienyl ion they are stabilized while the e_{1g} iron orbitals (xz, yz), interact with a lower lying π-orbital and are therefore destabilized.

II.10f. Electron Deficient Bonds

We will now consider electron deficient bonds, more specifically we will derive the mo's for a three-center, two-electron bond in $(CO)_5W$-H-$W(CO)_5$. The three centers are the two tungsten atoms and the bridging hydride in a linear arrangement along the z-axis. The W-H-W moiety has $D_{\infty h}$ symmetry and the basis vectors will be the H 1s orbitals and the z^2 orbital on each tungsten.

$D_{\infty h}$	E	$2C_\infty^\phi$	$\infty\sigma_v$	i	$2S_\infty^\phi$	∞C_2	
H(1s)	1	1	1	1	1	1	σ_g^+
W	2	2	2	0	0	0	$\sigma_g^+ + \sigma_u^+$
σ_g^+	1	1	1	1	1	1	
σ_u^+	1	1	1	-1	-1	-1	

Thus the antisymmetric combination of W's (σ_u^+) is non-bonding. The resulting mo-diagram is given on the next page.

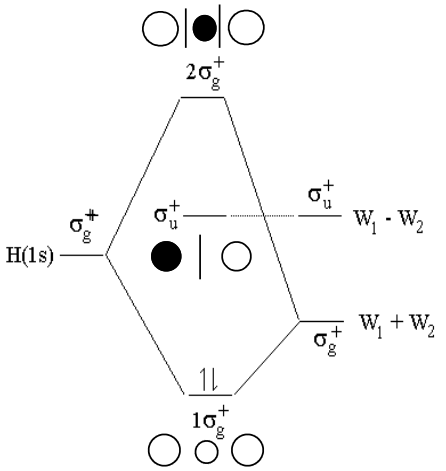

Figure II-34. MO diagram for the stable two-electron, three-center bond in $(CO)_5W\text{-}H\text{-}W(CO)_5$.

The z^2 is empty and there are only two electrons from the hydride. Thus there are only two electrons for this system but they enter a bonding orbital and a three-center, two-electron bond is formed.

Problem II.12 Use only the p_x and p_z orbitals on B and the 1s orbitals on H to construct an mo diagram for the bridge in diborane. Be sure to include the electrons.

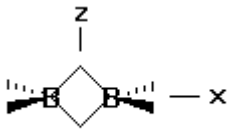

Figure II-35. The axis system to use for diborane (B_2H_6) in problem II.12.

Problem II.13 Steric crowding of the trimethyl phosphines forces the phosphines out of the XY plane ("ruffling") and results in D_{2d} symmetry for $[(Me_3P)_4WE_2]$ (E = O, S, Se, Te)- two trans phosphines up and the other two down as shown in the figure below. Construct the mo's (pictures) for the E=W=E moiety. What is the oxidation state and number of d-electrons on the tungsten? Use Appendix D, what you know of the crystal field splitting of tungsten (third row transition metal) and the relative field strengths of the chalcogens (see problem II.10) to determine the relative energies of the orbitals (ligand and metal) in the series. What is the nature of the HOMO and LUMO? What happens to the HOMO-LUMO separation in going from O to Te?

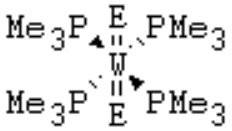

Figure II-36. The "ruffled" structure of $[(Me_3P)_4WE_2]$ (E = O, S, Se, Te).

Problem II.14 A combination of electrochemistry and spectroscopy indicate that the LUMO of the 2,2'-bipyridine ligand (bpy) in (bpy)MCl_2 (M=Pt and Pd) is at substantially lower energy than in $(bpy)_2MCl_2$ (M=Ru and Os). Suggest a mechanism for the stabilization of the bpy π* orbital in the square planar molecules relative to the octahedral molecules.

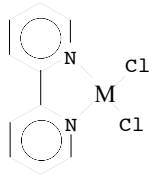

II.10g. Linear Chains

The most extensively studied inorganic one-dimensional compounds are those based on tetracyanoplatinate anions.[2,3,4] In these materials, the square-planar ions are stacked face-to-face to form linear chains of the platinum atoms which are well insulated from one another by the cyanide ligands, counterions and solvation. Bonding results from the interaction of the metal d_{z2} orbitals. The interaction will consist of both bonding and anti-bonding components,

Figure II-37. Bonding and antibonding mo's formed from the face-to-face interaction of the d_{z2} orbitals of $Pt(CN)_4^{2-}$

This process can be continued by adding another $Pt(CN)_4^{2-}$ unit to form a trimer. Now the three d_{z2} orbitals interactresulting in three mo's of a trimer. The lowest energy orbital will be lower than that of the dimer since there are two stabilizing interactions instead of only one. Similarly, the highest energy mo of the trimer, having an additional nodal plane, will be at a higher energy than the antibonding orbital of the dimer. Figure II-39 extends this argument to the tetramer. The result of these interactions is a linear chain of platinum atoms.

---

2. Miller, J.S.; Epstein, A.J., *Prog. Inorg. Chem*, **1976**, 20,1.
3. Krogmann, K., *Angew. Chem. Int. Ed*., **1969**, 8,35.
4. Tanner, D.B. in *Extended Linear Chain Compounds,* Miller J.S., Ed., Plenum: New York, 1982; Vol 2.

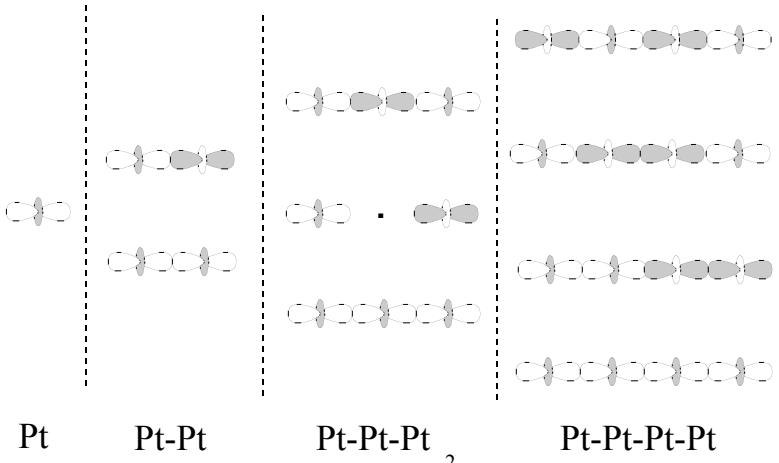

Figure II-38. The relative phases of the z^2 orbitals as the number of $Pt(CN)_4^{2-}$ units increases from 1 to 4.

As the chain lengthens, the most bonding orbital continues to stabilize while the most antibonding orbital continues to destabilize, but the individual levels still get closer together, *i.e.*, *both the energy width and the density of states of the mo's increase with increasing chain length*. In the limit of an infinite chain, the energy separation between adjacent levels is zero and the resulting structure is referred to as a **band**. Similar considerations can be made for the p_z orbitals which will also form a band. Perhaps the property most used to characterize the linear chains is the Pt-Pt distance which falls in the range of 3.1 to 3.7 Å for complexes of this type[5]. In the d^8 case, the z^2 orbitals are filled and so too is the resulting band. Since both the bonding and anti-bonding orbitals of the z^2 band are filled, no bond would be expected to form and the interaction should be quite weak. This conclusion is consistent with the fact that the ofbserved Pt-Pt distances are barely less than sum of the van der Waals radii for Pt (3.4 - 3.6 Å). The interaction between the members of the chain can be enhanced by a partial oxidation which results in the removal of electron density from the higher energy (anti-bonding) mo's at the top of the band. The result of a partial oxidation is twofold: first the Pt-Pt distances drop down to the range of 2.80 to 2.95 Å[6]; and second the band gap goes to zero since the occupied band is no longer full. Thus, $K_2[Pt(CN)_4]\cdot 3H_20$ forms a linear chain with a Pt-Pt separation of 3.48 Å and is an **insulator**[7] while the partially oxidized tetracyanoplatinate, $K_2[Pt(CN)_4]Br_{0.3}\cdot 3H_20$ is a **highly conducting** linear chain with a Pt-Pt separation of 2.89 Å.

---

[5]. Williams, J.M.; Schultz, A.J.; Underhill, A.E.; Carneiro, K.; in *Extended Linear Chain Compounds,* Miller J.S., Ed., Plenum: New York, 1982; Vol 1, Table 1, p. 76.

[6]. Williams, J.M.; Schultz, A.J.; Underhill, A.E.; Carneiro, K.; in *Extended Linear Chain Compounds,* Miller J.S., Ed., Plenum: New York, 1982; Vol 1, Table 5, p. 90-91.

[7]. Williams, J.M.; Schultz, A.J., in *Molecular Metals*, Hatfield, W.E., ed., Plenum Press., N.Y., 1979.

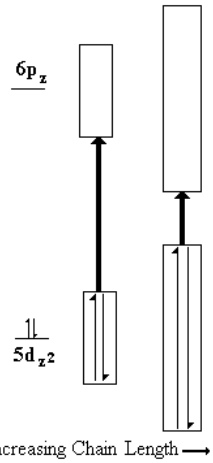

Figure II-39. The relative energies of the z^2 and z orbitals in platinum and the bands formed in the case of two chains of different length. The heavy black arrows represent the *band gap* and demonstrate how the electronic absorption shifts to lower energy as the chain length increases.

The relationship between color and the Pt-Pt distance has been recognized for some time.[8] Since the Pt-Pt interaction can perturb the absorption spectrum substantially (figure II-39), characterization of the linear chain can also be accomplished by electronic spectroscopy.[9] The electronic spectrum of a solution of $Pt(CN)_4^{2-}$ indicates no absorption below 35.8 kK (1kK = 1000 cm^{-1}) while a very strong, polarized absorption is observed at much lower energies for the chain compounds. Furthermore, the energy of the band decreases as the Pt-Pt distance decreases. Another indicator of the Pt-Pt separation is the emission maximum (band gap) which, for tetracyanoplatinates, is at 20 kK for Pt-Pt separations of about 3.3 Å but at 16 kK for a 3.1 Å separation.

Another type of interaction giving rise to stacked species is *π-stacking*. TTF-TCNQ, the first "organic metal",[10] exists in segregated stacks of TTF donors and TCNQ acceptors involved in a partial electron transfer. The conductivity in this system is dominated by the TCNQ stacks[11] in which overlap of the π-systems is optimized by a face to face orientation of the TCNQ molecules and results in one-dimensional bands along the stack axis. Thus, unlike the partially oxidized tetracyanoplatinates, conduction in this system is via a partially reduced "π-way". The $(bpy)_2Pt(CN)_2$ molecule is an example in which both modes of stacking are combined. The solid state structure of $(bpy)_2Pt(CN)_2$ was reported to consist of linear chains[12] with a 3.33 Å. The deep red color of the solid (solutions were colorless) was attributed to a $d\sigma \rightarrow p\sigma$ transition as shown in II-39. In electrochemical experiments,[13] however, evidence for chain growth on the electrode surface was apparent only after a partial reduction of the complex. This reduction involved an orbital which has some metal character

---

[8]. Yamada, S., *Bull. Chem. Soc., Japan*, **1951**, 24, 125.

[9]. Martin, D.S., in *Extended Interactions between Metal Ions*, Interrante, L.V., Ed.; A.C.S. Symposium Series 5; American Chemical Society; Washington, D.C., 1974.

[10] Ferrais, J.; Cowan, D.O.; Walatka, V.; Perlstein, J.H., *J. Am. Chem. Soc*., **1973**, 95, 948.

[11] (a) Tomkiewicz, Y.; Taranko, A.; *Phys. Rev. Lett*., **1976**, 36, 751. (b) Berlinsky, A.J.; Carolan, J.F.; Weiler, L., *Solid State Commun*., **1974**, 15, 795. (c) Soda, G.; Jerome, D.; Weger, M.; Alizon, J.; Gallice, J.; Robert, H.; Fabre, J.M.; Giral, L., *J. Physique*, **1977**, 38, 931.

[12] Che, C-M.; He, L-Y.; Poon, C-K.; Mak, T.C., *Inorg. Chem*., **1989**, 28, 3081.

[13] Cooper, J.B.; Rhodes, S.M.; Wertz, D.W., *J. Phys. Chem*., **1991**, 95, 4800.

but is *primarily* bipyridine π* (see problem II.14). Resonance Raman scattering (see section VI.6) indicated that the geometry change in the transition between the ground and excited state of the visible absorption was in the bipyridine. Based on these and other results, it was concluded that the interaction resulting in a linear chain at the electrode was due primarily to interactions between the bipyridines through their π-systems, and that the color of the sample was due to a "π→π*" transition found in the uv of the monomer. Unlike the partially oxidized $PtCN_4^{2-}$ discussed above, this is an example of chain growth initiated by a partial reduction similar to the TTF-TCNQ system.

Problem II.15 Discuss the π-stacking in the system shown below. Use the representations of the π and π* orbitals given below and assume that the stacking is of four monomers. Draw the mo's corresponding to each of the eight energy levels shown on the diagram below. Use arrows and a diagram similar to the one in figure II.39 to indicate the red shift of the π→π* transition with formation of the stacked tetramer. Describe the effects of a partial oxidation and reduction on the stack.

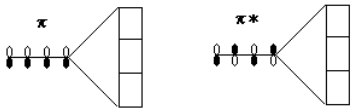

Problem II.16. Consider the bonding in $[OMoCl_4]^{2-}$.

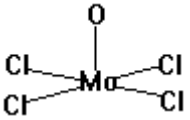

Assume that Cl interacts only in a σ fashion and that the $MoCl_4$ moiety is planar.

a. What are the irreducible representations of the Cl SALC's, the oxygen p-orbitals and the metal valence orbitals. How many d-electrons does the Mo contribute?
b. Construct (drawings & labels) the σ-SALC's for the Cl_4 fragment. Use Cl p-orbitals that "point" toward Mo.
c. **Use only the p-orbitals on O,** *i.e.*, assume the 2s orbital is buried and draw approximate mo's (***through the LUMO)***. Assume that each mo contains contributions from no more than two sources, *i.e.*, one metal orbital and/or either an O p-orbital or a Cl_4 SALC. Each metal orbital should be used only in that one SALC where it has optimum overlap. Give the symmetry label ($1a_1$, $2a_1$, 1e, etc.), and interaction type, *e.g.*, σ(Mo-O), for each.
c. Arrange the mo's in order of increasing energy - an energy level diagram. Clearly label each level with the same symmetry label as the mo. Add the electrons and clearly identify the HOMO and LUMO.
d. Show the relative energies of the **d-orbitals** (those that are predominately d in character) in the case where $MoCl_4$ is planar. Be certain to label each orbital. Next to this diagram show the relative energies of $MoCl_4$ if the Mo lies above the Cl_4 plane.
e. What is the Metal-oxo bond order? What would be the bond order for a d^6 metal?
f. Is the HOMO→LUMO transition dipole allowed? If so what is its polarization? What geometry changes might be expected during the transition?
g. Explain the effect of each of the following on the Mo-O bond length?
   i. one-electron reduction. ii. a one-electron oxidation.
   iii. changing Cl^- to NH_3. iv. changing Cl^- to CO.
   Which of these changes would have the greatest effect? Explain.

Chapter III. General Spectroscopic Considerations

III.1 Electromagnetic Radiation

Spectroscopy is the study of the interaction of electromagnetic radiation with matter. Electromagnetic radiation is an oscillating electric and magnetic field travelling through space at 2.998×10^8 m/s and as such is viewed as a wave which can be characterized by its wavelength (λ), its speed (c), and its frequency (ν - cycles/second or ω - radians/sec). The frequency and wavelength are related through the speed by $\mathbf{\nu\lambda = c}$ so that an electromagnetic wave with wavelength 600 nm would have a frequency of $2.998 \times 10^8 / 600 \times 10^{-9} = 5.00 \times 10^{14}\ s^{-1} = 0.50\ fs^{-1}$.

In this course we will be interested in the electric field, $\varepsilon = \varepsilon^o \cos[(2\pi/\lambda)x + \phi] = \varepsilon^o \cos[\omega t + \phi]$. Figure III.1 shows two representations of two different wavelengths of light, one of 600 nm with $\mathcal{E}^o = 5$ and one of 300 nm with $\tilde{o}^o = 8$. Figure III.1(a) is a snapshot of the disturbance in space over a distance of 2000 nm and clearly demonstrates the two wavelengths - one wavelength is twice the other. Figure III.1(b) shows the time dependence of the field at one point in space and demonstrates the frequency - there are twice as many of the shorter wavelength waves/unit time. However, the same statement pertaining to the frequency of waves can be made about the number of waves/unit length in the figure III.1(a) - there are (1/600) waves/nm and (1/300) waves/nm so there are twice as many wavelengths/nm of the higher frequency (longer wavelength) radiation. The number of waves/unit length is called the wavenumber ($\bar{\nu} = 1/\lambda$), a very important unit in spectroscopy with units of cm^{-1}. In electronic spectra, energies are in the tens of thousands of cm^{-1} so the **kiloKaiser (1kK = 1000 cm^{-1})** is often used. We will use the kK extensively in the electronic spectroscopy portion of this course, but, since it is not an SI unit, many journals will not accept it.

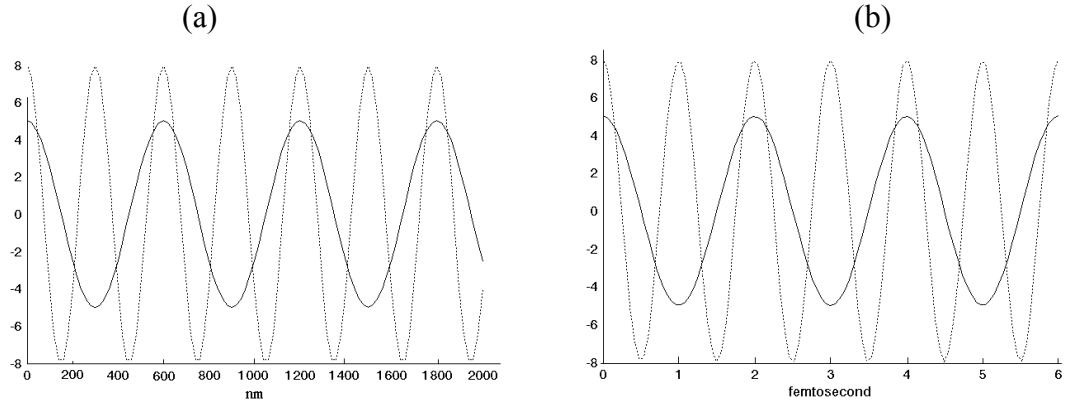

Figure III.1. The magnitude of the electric field vs position (a) and time (b) for two different electromagnetic waves:

(a) $\varepsilon = 5.0\cos(2\pi/600)x$ and $\varepsilon = 8.0\cos(2\pi/300)x$
(b) $\varepsilon = 5.0\cos[2\pi(5.00 \times 10^{14})t]$ and $\varepsilon = 8.0\cos[2\pi(1.00 \times 10^{15})t]$

The regions of the electromagnetic spectrum are given below:

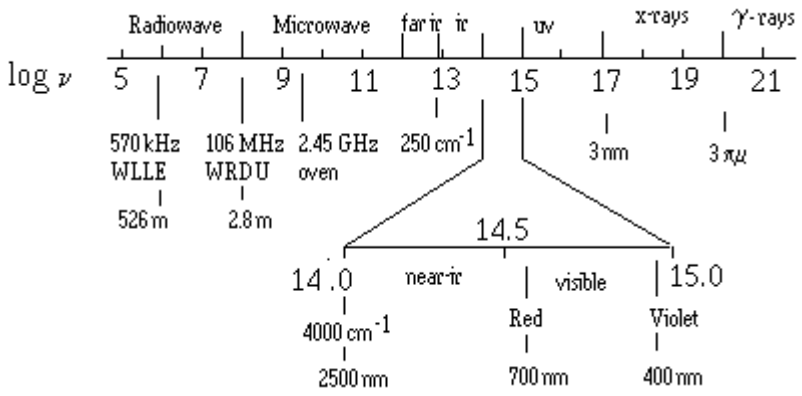

This course deals with vibrational and electronic spectroscopy. Vibrational spectra are observed in the infrared and the far-infrared while most electronic spectra are investigated in the visible and ultraviolet (uv) regions with a lesser contribution from the near ir. Historically, wavelength was the preferred unit of measure of light due to the fact that grating instruments are based on the Bragg equation: $n\lambda = 2d\sin\theta$. Thus most instruments present the spectra as linear in wavelength. However, as Planck (black-body radiation) and Einstein (photoelectric effect) showed, light also has properties of particles, called photons, which have discreet energies given by **$E = h\nu$ - energy is linear in frequency not wavelength**. Although giving the wavelength of a photon of light as 680 nm does indeed indicate that the photon is in the visible region, the use of ν (c/λ) or $\bar{\nu}$ ($1/\lambda$) is much preferred because of their linear relationship to energy - especially if one is referring to bandwidths, shifts or separations. For example, consider the spectrum shown in Figure III-2, which shows four peaks a, b, c, and d plotted versus wavenumber and wavelength. Two characteristics of these spectra should be noted:

1. $\bar{\nu}_a - \bar{\nu}_b = \bar{\nu}_c - \bar{\nu}_d = 3000$ cm^{-1} while $\lambda_b - \lambda_a = 111.1$ nm and $\lambda_d - \lambda_c = 15.9$ nm, *i.e.*, the separations between peaks can be distorted.
2. The bandwidth of all four peaks is 1200 cm^{-1}. However, the wavelength view severely distorts the spectra making the long wavelength peak appear to be much broader.

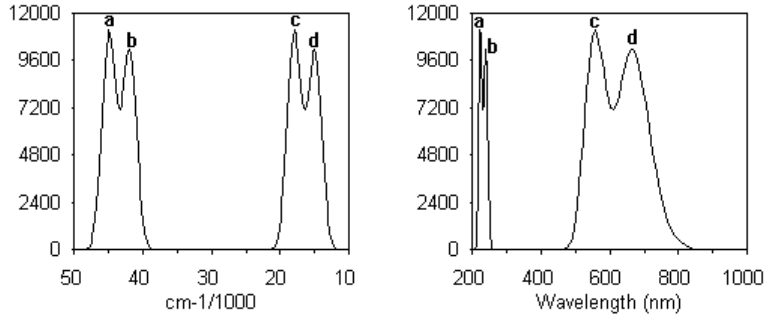

Figure III-2. Wavenumber *versus* wavelength display of spectra. The spectrum indicates two pairs of peaks with identical bandwidths and peak separations when displayed *vs*. wavenumbers. The peak separations and bandwidths of the two pairs of peaks appear very distorted when plotted on the wavelength scale.

Comparisons of the shifts, bandwidths or separations between peaks in wavelength should be avoided.

III.2 Experimental

There are as many optical designs as there are manufacturers, but there are basically three different types: scanning, array and FT. We give here a very brief description of each.

Scanning Double Beam Spectrometer. This type of spectrometer is used in the CARY-14 UV/Vis, and several of the older infrared spectrometers in the Department. A schematic representation is shown in figure III.3. The grating instrument consists of a source compartment "**S**", a sample compartment, a monochrometer and a detector. The radiation from the source is divided into two beams (reference, I_o and sample, I) which both impinge on a chopper, "**C**". The chopper is essentially a rotating semi-circular mirror - when the mirror is in the beam, the sample radiation is reflected into the monochrometer through the entrance slit, "**S1**", but when the mirror is out of the beam, the reference beam passes into the slit. Thus, after the chopper, both beams have the same path, but the radiation is alternating sample/reference (I/I_o) with the frequency of the chopper. The beam is reflected off a mirror onto the grating, "**G**" which disperses the radiation according to Bragg's Law: $n\lambda = 2d\sin\theta$ (n is the order of the grating, d is the groove spacing on the grating and θ is the angle of incidence). The radiation is reflected off of two more mirrors then through an exit slit, "**S2**", a filter to get rid of radiation of the wrong order, *i.e.*, wrong value of n in the Bragg Equation, and onto the detector. The entire spectrum is dispersed onto the plane of the exit slit and is passed across this slit by changing the angle of the grating. At any given moment in the scan, the detector will sample only a small portion of the spectrum, $\lambda \pm \Delta\lambda$, where $\Delta\lambda$ is the resolution which is dictated experimentally by the slit width. Since each wavelength must be sampled individually, long acquisition times are common.

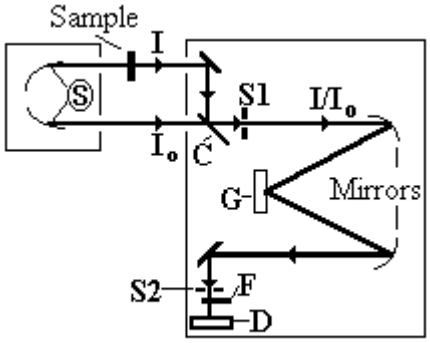

Figure III.3. Schematic representation of a scanning spectrometer.

Diode Array spectrometer: Routine UV/Vis spectra are typically obtained with this type of instrument since the long acquisition time of the the scanning spectrometer is not required. Figure III.4 is a schematic representation of HP 8452A optical system. Since this is a single beam instrument, separate sample and reference spectra must be obtained. Radiation from the source is gathered into a lens "L1" and onto a shutter "Sh". When the shutter opens, the light is passed through the sample, a second lens, "L2" and the slit, "S1". The beam is dispersed as in the grating instrument by the grating, "G". Instead of scanning the spectrum across a "point" detector as above, the entire spectral range is sampled simultaneously by an array of detectors - diodes. Resolution then is a function of the dispersive power of the grating and the size of the diodes. The HP 8452A uses 328 individual photodiodes and circuits etched onto a semiconductor chip 2mm x 18 mm in size. In this instrument, each diode samples a bandwidth of

about 2 nm for a spectral range of about 650 nm (190 to 820 nm in practice). Good quality spectra can be obtained with well under a minute of exposure time with these instruments.

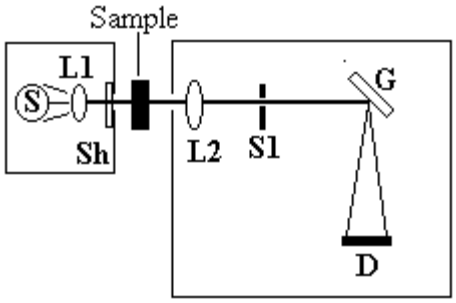

Figure III.4. Schematic representation of a diode array spectrometer.

FTIR: Rapid data acquisition in the infrared region is obtained by FTIR (Fourier Transform InfraRed). Figure III.5 shows a schematic representation of the optical system of a typical FTIR. The beam size leaving the source is dictated by an iris, "**I**". Small beam sizes yield more reliable spectra, but they also reduce the energy. The beam passes through a beam splitter, "**BS**" which reflects half of the beam to a fixed mirror, "**FM**", and transmits half of the beam to a moving mirror, "**MM**". Both beams are reflected back to the beam splitter where they are combined. The beams interfere with one another when they are recombined and are then partially transmitted and reflected once again. If the distance to **FM** is d_f and the distance to **MM** is d_m then the two beams will have travelled $2d_f$ and $2d_m$. The beams will interfere constructively only when $|2d_f-2d_m|$ is an integral number of wavelengths. The variation in the intensity of the beams passing to the detector as a function of this path difference yields the spectral information in the Fourier transform spectrometer. Since the mirror is moving with a constant speed, the variation can be treated with respect to time rather than distance. Thus, the spectrum is obtained in the *time domain* and Fourier transformed into the *frequency domain*. As in the array instruments, it is the entire spectrum which is sampled and spectra are typically collected in a few minutes. Almost all infrared instruments are now FTIR's.

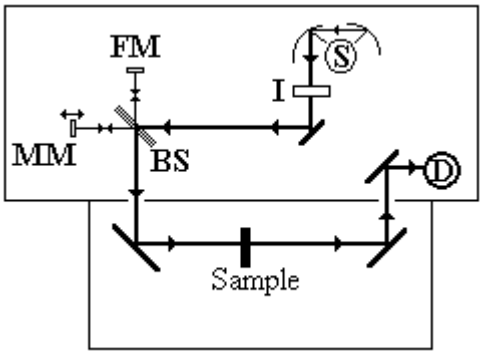

Figure III.5. Schematic representation of an FTIR.

III.3 Time Dependent States

The Schrödinger equation is usually written as $H\psi_j=E_j\psi_j$, but this applies to stationary states, *i.e.*, states whose energy is not changing. When the system's energy does change with time, the time dependent Schrödinger equation must be used:

$$H_0 \Psi_{(x,t)} = i\hbar \frac{\partial \Psi_{(x,t)}}{\partial t}$$

$$\Psi_{(x,t)} = \sum_{j=0}^{\infty} a_j \psi_j, \qquad E = \sum_{j=0}^{\infty} a_j^* a_j \varepsilon_j, \qquad \psi_j = |j\rangle \exp\left(\frac{-i\varepsilon_j t}{\hbar}\right)$$

where $a_j^* a_j$ represents the probability that the system has an energy ε_j and ψ_j is the time evolution of the j^{th} stationary state. We assume that initially, the system is in the ground state, i.e., $a_0 = 1$ and $a_j = 0$ for $j > 0$. We now perturb the system with an H'.

$$H_0 \sum_{j=0}^{\infty} a_j \psi_j + H' \sum_{j=0}^{\infty} a_j \psi_j = i\hbar \frac{\partial}{\partial t} \sum_{j=0}^{\infty} a_j \psi_j = i\hbar \sum_{j=0}^{\infty} [\dot{a}_j \psi_j + a_j \dot{\psi}_j]$$

$$\text{but,} \quad H_0 \sum_{j=0}^{\infty} a_j \psi_j = i\hbar \sum_{j=0}^{\infty} a_j \dot{\psi}_j$$

$$\text{so,} \quad H' \sum_{j=0}^{\infty} a_j \exp\left(\frac{-i\varepsilon_j t}{\hbar}\right)|j\rangle = i\hbar \sum_{j=0}^{\infty} \dot{a}_j \exp\left(\frac{-i\varepsilon_j t}{\hbar}\right)|j\rangle$$

Premultiplying by ψ_l^* and integrating, *i.e.*, taking the dot product of each term with $\exp\left(\frac{+i\varepsilon_l t}{\hbar}\right)\langle l|$ and using the orthonormality of the wavefunctions, $\langle j | l \rangle = \delta_{jl}$, we arrive at the following.

$$\sum_{j=0}^{\infty} a_j \exp\left(\frac{-i(\varepsilon_j - \varepsilon_l)t}{\hbar}\right)\langle l|H'|j\rangle = i\hbar \dot{a}_l$$

At t=0, $a_j = 0$ for $j > 0$ and $a_0 = 1$. Thus at t=0 (assuming $\varepsilon_o = 0$),

$$\dot{a}_l = -\frac{i}{\hbar} \exp\left(\frac{i\varepsilon_l t}{\hbar}\right)\langle l|H'|0\rangle$$

We are interested in the interaction of the electric field of the electromagnetic radiation with the dipole of the molecule so the perturbation is $H' = \varepsilon \cdot \mu$ or,

$$H' = \varepsilon_x \cdot \mu_x + \varepsilon_y \cdot \mu_y + \varepsilon_z \cdot \mu_z, \qquad \varepsilon_x = \varepsilon_x^0 (e^{2\pi i \nu t} + e^{-2\pi i \nu t})$$

$$so, \quad \langle l|H'|0\rangle = (e^{2\pi i \nu t} + e^{-2\pi i \nu t})(\varepsilon_x^0 \langle l|\mu_x|0\rangle + \varepsilon_y^0 \langle l|\mu_y|0\rangle + \varepsilon_z^0 \langle l|\mu_z|0\rangle)$$

The integral $\langle l | \mu | j \rangle = \langle \mu \rangle_{jl}$ is called the **transition moment** for the j→l transition. Upon integrating the expression for da_l/dt above, we arrive at the value of a_l,

$$a_l = \varepsilon^o \langle \mu \rangle_{0l} \left[\frac{1 - \exp\{\frac{i(\varepsilon_l - \varepsilon_0 + h\nu)}{\hbar}\}}{\varepsilon_l - \varepsilon_0 + h\nu} + \frac{1 - \exp\{\frac{i(\varepsilon_l - \varepsilon_0 - h\nu)}{\hbar}\}}{\varepsilon_l - \varepsilon_0 - h\nu} \right]$$

The importance of the l^{th} state in the description of the system is $a_l^* a_l$, which can be simplified to,

$$a_l^* a_l = 4\langle\mu\rangle_{0l}^2 (\varepsilon^o)^2 \left[\frac{\sin^2\left(\frac{\pi(\varepsilon_l - \varepsilon_0 - h\upsilon)t}{h}\right)}{(\varepsilon_l - \varepsilon_0 - h\upsilon)^2} \right]$$

This expression represents the effect of the interaction of a given frequency, ν. Integrating over all frequencies (ε^o assumed constant over the range of importance) we obtain,

$$a_l^* a_l = \frac{\langle\mu\rangle_{0l}^2 (\varepsilon^0)^2}{\hbar^2} t$$

The energy density is the energy per unit volume of the radiation: $\rho = 1/2(\varepsilon^o)^2 \in_o$ where $\in_o$ is the dielectric constant of free space. Substituting it for ε^o and differentiating, we arrive at the rate of change of the importance of the l^{th} state in the description of the system,

$$\frac{d}{dt}(a_l^* a_l) = \frac{2\langle\mu\rangle_{0l}^2}{\in_0 \hbar^2} \rho = B_{0l}\rho$$

where B_{0l} is Einstein's coefficient of induced absorption.

It can be seen that several factors dictate the importance of the l^{th} state in the description of the system:

1. ρ, the energy density of the radiation
2. The magnitude of the transition moment which is a measure of how much the interaction mixes the 0^{th} and l^{th} states. It is this term which will lead to the **selection rules.**
3. The effect of a photon of a given frequency, depends on how close to resonance the photon energy is. The resonance condition is $h\nu = \varepsilon_0 - \varepsilon_l$ or $h\nu = \varepsilon_l - \varepsilon_0$ depending on whether $\varepsilon_0 > \varepsilon_l$ (emission) or $\varepsilon_0 < \varepsilon_l$ (absoroption). As the photon approaches resonance, one of the denominators will approach zero (there is actually a damping term in the denominator to assure it never equals zero) and a_l will get large if the transition moment is large.

III.4 Experimental Quantities

The intensity, I, of an electromagnetic wave is the energy per unit time crossing a unit square surface and is therefore the energy density times the speed of the wave, c.

$$I = \rho c\ [(j\text{-}m^{-3}) \times (m\text{-}s^{-1}) = j\text{-}m^{-2}\text{-}s^{-1}] = 1/2(\varepsilon^o)^2 \in_o c.$$

The change in intensity of the radiation as it passes through a thickness, $d\ell$, of a sample with molar concentration, C, is given by Beer's law to be

$$-dI = \alpha(\nu) I C d\ell$$

where $\alpha(\nu)$, the **molar absorption coefficient**, is frequency dependent and has units of $M^{-1}\text{-}cm^{-1}$. Integrating over the entire pathlength of the cell, we arrive at the integrated form of Beer's law,

$$A = \log(I_o/I) = \in(\nu) C \ell$$

where $\in(\nu) = \alpha(\nu)/2.303$ is the **molar extinction coefficient** and I_o/I is the ratio of incoming to transmitted intensities or reference to sample intensities. The integrated absorption, A is

$$A = \int_0^\infty \in(\nu)d\nu \quad or \quad \bar{A} = \int_0^\infty \in(\bar{\nu})d\bar{\nu} = \frac{A}{c}$$

and $A \propto \langle\mu\rangle_{0l}^2$.

Occasionally, the strength of a band is given in terms of its oscillator strength, f, which is a dimensionless quantity which relates the strength of a transition to that of a single electron in a 3D-harmonic potential well.

$$f = \tilde{A}_{obs}/\tilde{A}_{theor} = 4.33x10^{-9}\tilde{A}_{obs}$$

Selection Rules: The strength of a transition from state l to state m is proportional to $\langle\mu\rangle_{lm}^2$ thus it is allowed ($A \neq 0$) only if $\langle l|\mu|m\rangle \neq 0$. As was mentioned in Chapter I, this matrix element can be non-vanishing only if the direct product of $\langle l|\otimes\mu\otimes|m\rangle$ contains the totally symmetric representation. The dipole moment consists of three terms, μ_x, μ_y, and μ_z, so the operator transforms as x, y and z - the same as the p-orbitals. The direct product of two non-degenerate irreducible representations will contain the totally symmetric representation if and only if the two irreps are of the same symmetry. Thus $\langle l|\mu|m\rangle \neq 0$ if $\langle l|\otimes|m\rangle$ transforms as x, y, or z. If it is the x-component that makes the transition allowed, then it is the x-component of the radiation which will mix the two states, and the transition is said to be x-**polarized** and only that component of light polarized in the x-direction can be absorbed.

III.5 Band Shapes

Two common idealized band shapes are the Lorentzian and Gaussian,

$$\varepsilon = \varepsilon_{max}\left\{\frac{\Gamma^2}{\Gamma^2 + (\bar{\nu} - \bar{\nu}_{max})^2}\right\}; \text{Lorentzian line shape}$$

$$\varepsilon = \varepsilon_{max}\exp\left\{\frac{(\ln 2)(\bar{\nu} - \bar{\nu}_{max})^2}{\Gamma^2}\right\}; \text{ Gaussian line shape}$$

where $\in_{max}$ is the extinction coefficient at the peak maximum and Γ is the half-width at half-maximum (HWHM) or $1/2\ \Delta\bar{\nu}_{1/2}$ (1/2 the FWHM). These terms are described in the following figure which compares the two band shapes with the same set of parameters.

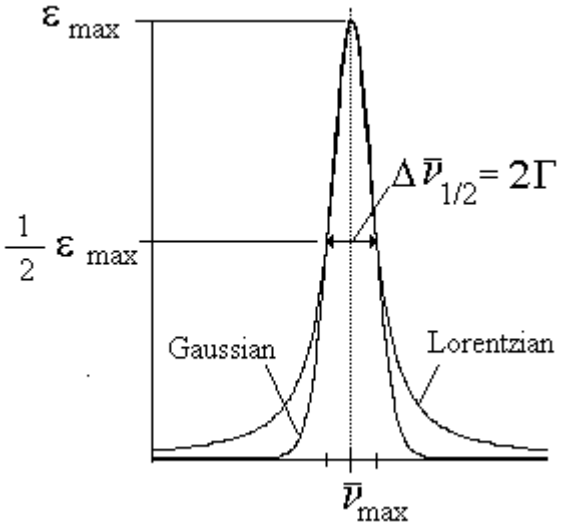

Figure III.6. Gaussian and Lorentzian line shapes with the same parameters.

Far and away the most often used term to describe the strength of a band is the molar extinction coefficient ($\in$=A/ℓC) which has units of M^{-1} cm^{-1}. Giving absorbance units really indicates nothing of the strength of the band unless the concentration and pathlength are also given. Figure III-2 was generated by using the following set of parameters and a Gaussian line shape:

$\bar{\nu}$ (cm^{-1})	ε	Γ(cm^{-1})
15,000	10,000	1200
18,000	11,000	1200
42,000	10,000	1200
45,000	11,000	1200

The type of line shape that characterizes a spectroscopic transition depends in part on the mechanisms that contribute to "relaxation" following the transition (see Chapter 6). For example, relaxation mechanisms in magnetic resonance are often modeled using a Lorentzian line shape (*e.g.* for T_2 in NMR), while electronic absorption bands are modeled using a Gaussian line shape (best when the sample is a statistical distribution, like a fluid solution). Often, because of the large number of different relaxation mechanisms, a combination of the two line shapes is used.

Chapter IV. Vibrational Spectroscopy
Part I. Theory

When bonds break or molecular geometries change, vibrational degrees of freedom are involved. Since the vibrations are governed by the restoring forces in the bonds, vibrational spectra can serve as sensitive probes of bonding or changing electron density. The problem presented by vibrational spectroscopy, however, is that there is so much information that it can be overwhelming to the point that no information can be extracted. This wealth of information results from the fact that a molecule composed of N atoms will have 3N-6 vibrational degrees of freedom - there are just too many spectral peaks. In addition, the atomic displacements during any one vibration are usually complicated so that during a "metal-chlorine stretch", other bonds will be changing as well. However, information on the nature of the actual motions of the atoms is important if we hope to unravel the information on geometry or bonding changes that is available in a vibrational spectrum. In this chapter we present enough theory on the nature of vibrations to give the student an appreciation of the complexities and a vocabulary sufficient to read the literature on the subject.

IV.1 The Harmonic Oscillator - a classical view

The separation of two masses attached to a spring at rest is r_e, the equilibrium separation. If that separation is changed to r and the spring obeys Hooke's Law, a restoring force back toward the equilibrium separation, $F = -k(r-r_e)$, is developed where k is the spring force constant.

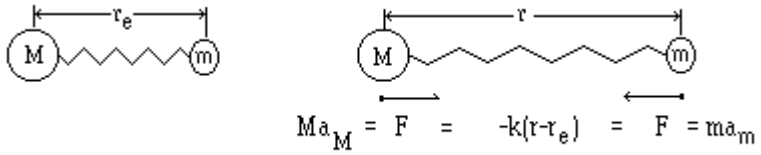

It is more convenient to discuss the motion in terms of the internal coordinate, Q,

$$Q = (r-r_e). \qquad \text{Eq iv-1}$$

The restoring force can then be written as

$$F = -kQ. \qquad \text{Eq. iv-2}$$

Force is the gradient of the potential,

$$F = -dV/dQ = -kQ \text{ or } dV = kQdQ \Rightarrow \int dV = k\int QdQ \text{ or}$$

$$V = 1/2kQ^2 \qquad \text{Eq. iv-3}$$

Eq iv-3 defines the potential energy of the spring as a parabola. The force constant then is the curvature of the potential energy,

$$k = d^2V/dQ^2 \qquad \text{Eq. iv-4}$$

Figure IV-1 shows the potential energy as a function of Q for two springs with force constants differing by a factor of 2. The heavy line has the steeper curvature and represents the case of the larger force constant. These curves indicate that, *at the same energy*, the amplitude of vibration is greater for the spring with the smaller force constant.

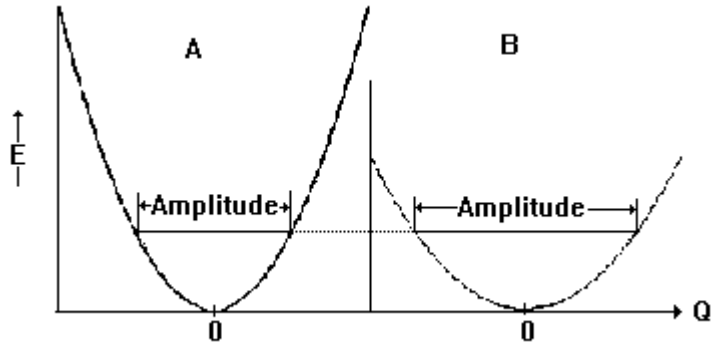

Figure IV-1 The potential energy of two different springs A & B where $k_A = 2k_B$. The steeper curve has twice the curvature of the more shallow curve. The amplitude of vibrations of the low force constant spring is much greater than that of the high force constant spring at the same energy.

Both masses will experience the same restoring force, but according to Newton's second law, the force experienced by an object is the product of its mass and its acceleration, F=ma. The smaller mass will have a greater acceleration and thus will be moving faster during most of the motion. When dealing with systems involving the motion of particles relative to one another, the reduced mass, μ, of the system is used rather than the individual masses of the particles. For a two particle system,

$$1/\mu = 1/m + 1/M \text{ or } \mu = mM/(m+M). \qquad \text{Eq. iv-5}$$

The value of the reduced mass is indicative of the relative motions of the two particles. If M>>m, then $m + M \approx M$ and $\mu \approx mM/M = m$, which indicates that only the small mass is moving.

The solution to the equations of motion for this system is an expression for Q as a function of time,

$$Q = A\cos(\omega t + \phi) \qquad \text{Eq. iv-6}$$

which can be thought of in terms of a vector of length A rotating in the xy plane with an angular frequency of ω and a phase of ϕ, (at t=0 the vector makes an angle of ϕ with the x-axis). Q is then the projection of A on the x-axis. The definition of the angular frequency of vibration is given in figure IV-2. At t=0, $Q=A\cos\phi$ which simply means that if $\phi \neq 0$, then the separation between particles was not at the maximum. After t seconds, the angle will change to $\phi+\omega t$ with Q changing to $A\cos(\omega t+\phi)$. Thus the system undergoes simple harmonic oscillation reaching maxima and minima at +A and -A.

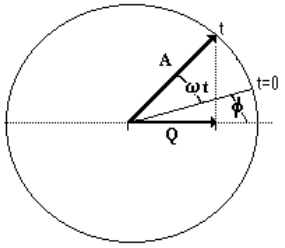

Figure IV-2 The variation of Q with time.

It is easier to visualize the frequency of oscillation in cycles per second (ν) than in radians per second. Since one cycle is 2π radians, $\nu = \omega/2\pi$. The frequency of vibration is related to the force constant,

$$\nu = \frac{1}{2\pi}\sqrt{\frac{k}{\mu}} \quad s^{-1} \qquad \text{Eq. iv-7}$$

The most convenient unit for spectroscopic studies is the wavenumber, cm^{-1}. The frequency of vibration in wavenumbers, $\bar{\nu}$, is ν/c^* where c^* is the speed of light in cm/s.

$$\bar{\nu} = \frac{1}{2\pi c^*}\sqrt{\frac{k}{\mu}} \quad cm^{-1} \qquad \text{Eq.iv-8}$$

For molecular vibrations, μ is the molecular mass in kg and k is in N/m. If the reduced mass is in amu rather than kg, eq iv-8 can be rewritten as

$$\bar{\nu} = 130.3\sqrt{\frac{k}{\mu}}\ cm^{-1};\ \mu \text{ in amu} \qquad \text{Eq.iv-9}$$

where $130.3 = (N_A x 10^3)^{1/2}/(2\pi c^*)$. Finally equation iv.9 can be solved for the force constant to give,

$$k = \left(\frac{\bar{\nu}}{130.3}\right)^2 \mu \ \text{N/m} \qquad \text{Eq.iv-10}$$

N_2 has a high bond order (BO=3) and is therefore be expected to have a high force constant while Na_2 has a very weak bond and consequently a low force constant is predicted. For the N≡N stretch,

$$\bar{\nu} = 2331 cm^{-1}; \text{ and } \mu = \frac{1}{2}(14.0) = 7.00 \text{ amu so } k = 7.00\left(\frac{2331}{130.3}\right)^2 = 2240 \text{ N/m}$$

while, for the Na-Na stretch,

$$\bar{\nu} = 157.8 cm^{-1} \text{ and } \mu = \frac{1}{2}(23.0) = 11.5 \text{ amu so } k = 11.5\left(\frac{157.8}{130.3}\right)^2 = 16.9 \text{ N/m}$$

Considering these two examples as representative of the extremes, we can conclude that molecular *stretching* force constants are expected in the range of 1- 2500 N/m.

Problem IV.1 The ^{79}Br-^{79}Br stretch is observed at 325.4 cm^{-1}. What is the Br-Br force constant? Where would the ^{79}Br-^{81}Br and ^{81}Br-^{81}Br stretches be observed?

IV.2 Quantum Mechanical Description of the Harmonic Oscillator

Solving the Schrödinger equation ($H\Psi_v = E_v\Psi_v$) for the Harmonic oscillator yields quantized expressions for the energy,

$$E_v = (v+1/2)h\nu \text{ joules} = (v+1/2)\ \bar{\nu}\ cm^{-1}, \quad v= 0,1,2,3,... \qquad \text{Eq.iv.11}$$

where ν and $\bar{\nu}$ are the classical frequencies as defined above. Note that there is a zero point energy of $1/2\bar{\nu}$ so that the ground vibrational level for N_2 is at 1/2(2331) = 1166 cm^{-1} above the minimum in the potential. The v=7 level is at (7+1/2)(2331) = 17483 cm^{-1} = 2.167 eV.

Problem IV.2 The equilibrium bond length in Br_2 is 228.4 pm. What would be the maximum ^{79}Br-^{79}Br distance in the v=7 vibrational state? Would it be the same in the other isotopes? Refer to Problem IV.1.

The squares of the harmonic oscillator wavefunctions are shown in figure IV-3.There are four important features of these wavefunctions that imply non-classical behavior:

- There are v nodal planes in the vth level. This implies that in the v=1 level, the nuclei never achieve the equilibrium separation since there is a nodal plane at Q=0.
- Ψ^2 exceeds the classical limits. The nuclei have a finite probability of being closer together or farther apart than their energy warrants.
- In the ground vibrational state, the most probable postion for the nuclei is the equilibrium position - Ψ^2 has a maximum at Q=0 in the v=0 level. Classically,

the nuclei are moving the fastest when at the equilibrium position and slow to a stop at the extrema so that the most probable postion for the classical particles would be at the extrema.

- The most probable position approaches the classical limit at high values of v. This is already apparent in the v=2,3 and 7 levels where the maximum amplitude in ψ^2 is reached near the extreme value of Q. This will be an important consideration in our discussion of Franck-Condon factors in electronic spectroscopy.

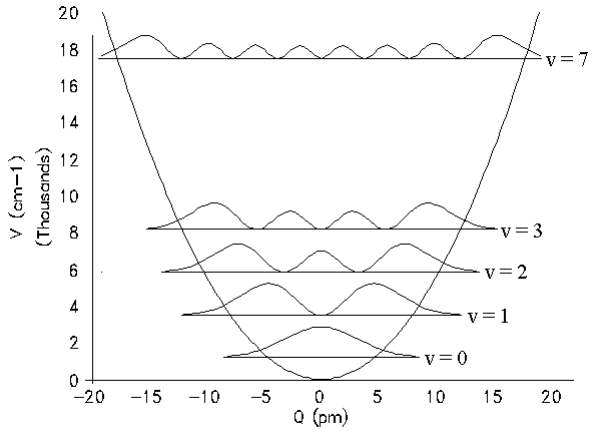

Figure IV.3. Potential function for N_2 showing the v=0, 1, 2, 3, and 7 energy levels and ψ^2 for each level. All wavefunctions are normalized.

IV.3 Selection rules for the harmonic oscillator

As discussed in chapter III, the selection rules are based on the transition moment which, for the harmonic oscillator transition v→v' would be <v'|μ|v>. The dipole moment is expanded as a Taylor series in terms of Q.

$$\mu = \mu_o + \left(\frac{d\mu}{dQ}\right)_{Q=0} Q + \frac{1}{2}\left(\frac{d^2\mu}{dQ^2}\right)_{Q=0} Q^2 + \frac{1}{6}\left(\frac{d^3\mu}{dQ^3}\right)_{Q=0} Q^3 + \ldots \quad \text{so}$$

$$\langle v'|\mu|v\rangle = \langle v'|v\rangle\mu_0 + \langle v'|Q|v\rangle\left(\frac{d\mu}{dQ}\right)_{Q=0} + \langle v'|Q^2|v\rangle\left(\frac{d^2\mu}{dQ^2}\right)_{Q=0} + \ldots$$

The first term vanishes for n ≠ n' since the eigenfunctions form an orthonormal basis, and <v'|Q|v> in the second term gives rise to the important selection rule for the harmonic oscillator, and is usually given as $\mathbf{\Delta v = \pm 1}$. The origin of this selection rule lies in the form of the vibrational eigenfunctions which are Hermite polynomials. In addition to the $\mathbf{\Delta v = \pm 1}$ selction rule, $\left(\frac{\partial\mu}{\partial Q}\right)_{Q=0}$ indicates that the bond dipole must change during the vibration. Quite often, the higher-order terms are non-zero and are called overtones. The resonance condition for the harmonic oscillator is $\Delta E = E_{v+1} - E_v = (v + 3/2)\bar{\nu} - (v + 1/2)\bar{\nu} = \bar{\nu}$ so that all of the Δv = 1 transitions would occur at the same energy, the classical frequency, and the overtones would occur at $2\bar{\nu}$ for the first overtone and at $3\bar{\nu}$ for the second overtone.

The N≡N stretch in N_2 is not IR active (no dipole change) but it is observed in the Raman (see section IV.10) at 2331 cm^{-1}. What is the vibrational period of the N≡N stretch? Since the observed energy is the classical frequency, $\nu = c^* = (2331)(2.998\text{x}10^{10}) =$

6.988×10^{13} s^{-1}. The reciprocal of the oscillation frequency is the **vibrational period, $\tau = 1/\nu$** $= 1.431 \times 10^{-14}$ s = 14.31 fs. The N≡N bond undergoes one complete vibration every 14.31 fs.

Problem IV.3 How many vibrations does a Li-Li molecule undergo during 1 ps? ($\bar{\nu}$ = 351.4 cm^{-1})

IV.4 The anharmonic oscillator

The harmonic oscillator expression, $V=1/2kQ^2$, is only an approximation for the dependence of the potential energy on internuclear separation. The actual picture is better described by that shown in figure II-3 which shows the energy of the σ orbital of H_2^+ as a function of the H-H distance. The force constant is actually a function of the internuclear separation getting smaller as the distance gets larger due to reduced overlap while getting larger at short separations due to internuclear repulsion. The result is that, in order to realize all of the energy of vibration into potential energy at the extrema, the bond will lengthen past the harmonic maximum but will not compress to the harmonic minimum. A common approximation to this behavior is the Morse potential,

$$V = D_e(1-e^{-aQ})^2 \qquad \text{Eq iv-13}$$

where $\mathbf{D_e}$ is the *spectroscopic bond dissociation energy* and **a** is a parameter which depends on the system. It should be noted that the spectroscopic dissociation energy is not the same as the bond energy, the thermodynamic dissociation energy, D_o. Thermodynamics measures the difference in energy between the bound and dissociated atoms, but the bound atoms are at the zero point energy, E_o, not at the minimum of the well, *i.e.*, $D_o = D_e - E_o$.

The anharmonic potential does not have a constant curvature so **the force constant is defined as the curvature of the well at its minimum.** Figure IV-4 compares a Morse potential and a harmonic potential with the same curvature at the minima (force constants) and differentiates between the spectroscopic dissociation energy (D_e) and the thermodynamic dissociaton energy (D_o). The energy levels for an anharmonic potential are obtained by a perturbation treatment and are given as,

$$E_v = (v+1/2)\bar{\nu}_e - (v+1/2)^2\bar{\nu}_e\chi_e \qquad \text{Eq iv-14}$$

where $\bar{\nu}_e$ is the frequency of the harmonic oscillator with the same force constant and $\bar{\nu}_e\chi_e$ **is the anharmonicity constant**. The force constant can be calculated using $\bar{\nu}_e$ in equation iv-10. Values for $\mathbf{D_e}$ and **a** in equation iv-13 can be derived to be

$$D_e = \frac{\bar{\nu}_e}{4\chi_e} \qquad \text{Eq. iv-15} \qquad \text{and} \qquad a = \sqrt{\frac{k}{2D_e}} \qquad \text{Eq. iv-16}$$

From Eq iv-14, it can be seen that the energy levels get closer together as v increases, reaching a near continuum at the dissociation energy. It is for this reason that overtones are usually observed at wavenumbers lower than the calculated value of $n\bar{\nu}_e$.

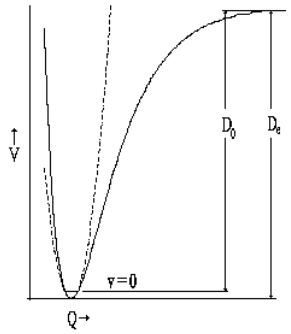

Figure IV-4 A Morse potential (solid) and a harmonic potential with the same force constant.

It is often stated that a high force constant is indicative of a strong bond. Certainly a large curvature of the well at the minimum would be expected to lead to a strong bond, but the anharmonicity is also a factor ($D_e = \frac{\bar{\nu}_e}{4\chi_e} = \frac{\sqrt{k/\mu}}{8\pi c * \chi_e}$) . A nearly harmonic oscillator with a low force constant has a large dissociation energy simply because χ_e is extremely small. Thus D_e increases with the force constant (as measured by $\bar{\nu}$) but decreases with increasing anharmonicity. As mentioned earlier, the bond energy, $D_o = D_e - E_o$, but $E_o = ½\ \bar{\nu}_e - ¼\ \bar{\nu}_e\chi_e$. The bond energy then becomes,

$$D_0 = \frac{\bar{\nu}_e}{4\chi_e} - 1/2\ \bar{\nu}_e + 1/4\ \bar{\nu}_e\chi_e \qquad \text{Eq iv-17}$$

Electronic spectra (absorption and emission) and resonance Raman scattering often contain long series of vibrational peaks (figure IV-5). These transitions, which are all of the type $0 \rightarrow v$, are labelled $\bar{\nu}(v)$ and each has an energy equal to $E_v - E_0$ which can be determined by application of eq iv-14 to be

$$\bar{\nu}(v) = E_v - E_o = v\bar{\nu}_e - v(v+1)\bar{\nu}_e\chi_e. \qquad \text{Eq. iv-18}$$

A plot of $\bar{\nu}(v)/v$ *vs*. (v+1) should be linear with an intercept of ϖ_e and a slope of $-\bar{\nu}_e\chi_e$. The bond energy can then be estimated by eq iv-17.

Problem IV.4 Figure IV-5 shows the resonance Raman spectrum of $Cs_4Mo_2Cl_8$. The long progression of lines has been assigned to the fundamental and overtones of the Mo-Mo stretch. From the frequencies of these lines, deduce the Mo-Mo force constant (N/m) and bond energy (kJ/mol). Observed bands: 340, 680, 1018, 1356, 1691, 2025, 2358, 2688, 3020, 3350, and 3675 cm^{-1}. Include a plot of the **observed (points)** and **calculated (line) wavenumbers**. The Mo-Mo bond in the compound is a quadruple bond (see Problem II.2). This problem is ideal for a spreadsheet.

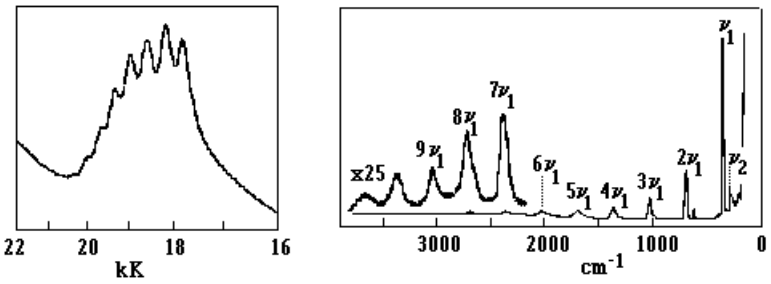

Figure IV-5. Visible absorption spectrum (left) and resonance Raman spectrum (right) of $Cs_4Mo_2Cl_8$. Modified from that given by Clark, R.J.H.; Franks, M.L., *J. Am. Chem. Soc*., **1975**, 97, 2691

IV.5 The Wilson FG-Matrix formulation of Molecular Vibrations

There are 3N degrees of freedom for a molecule with N atoms. For a non-linear molecule, six are external degrees (translations and rotations) leaving 3N-6 internal degrees (vibrations). For linear molecules, one of the degrees of rotational freedom is lost since there can be no rotational energy for a rotation about the bond axis. Consider the difference between CO_2 and SO_2.

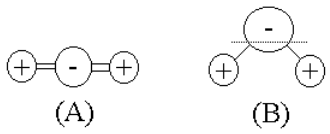

Figure IV-6. (A) Out of plane bending mode of linear molecule is an internal degree of freedom - a genuine vibration. (B) Out-of-plane motion of a non-linear molecule is an external degree of freedom - rotation about dotted line.

In the following, a non-linear molecule is assumed.

There are many ways to treat the vibrational motions of a molecule. The main difference between them is the choice of basis sets. One possibility is to use the set of 3N cartesian displacement vectors, $\{x_i \mid i = 1, 2, 3, ..., 3N\}$ where x_1, x_2 and x_3 correspond to the x, y and z Cartesian vectors on atom 1. The potential energy expressed in this basis is $V = \frac{1}{2}\sum_i \sum_j b_{ij} x_i x_j$, where the elements of the matrix, b_{ij} represent the restoring force experienced along x_i when x_j is changed - the Cartesian force constants. This choice of basis suffers since there is no chemical intuition involved and the force contstants derived have no clear physical meaning - the restoring force of atom 1 in the x direction when atom 5 is displaced in the y direction is $b_{1,14}$ but it tells us nothing about the bonding.

The most commonly used method is the Wilson FG-matrix method which uses four different types of **internal coordinates** (figure IV-7):

- bond stretchings (ν)
- in-plane angle bendings (δ)
- out-of-plane angle bendings (π)
- torsions (τ)

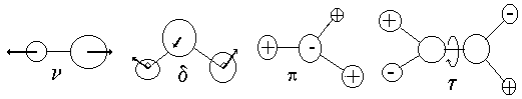

Figure IV-7. The four types of internal coordinates. $\nu \equiv$ bond stretch; $\delta \equiv$ in-plane angle bend; $\pi \equiv$ out-of-plane angle bend and $\tau \equiv$ torsion about a bond. The motions of the atoms preserve the center of mass.

Each internal coordinate is a linear combination of atomic displacements, but each atomic displacement is a linear combination of Cartesian diplacements. The i^{th} internal coordinate can thus be defined as $R_i = \Sigma c_{ij} x_j$. More conveniently, all of the internal coordinates ($\geq$3N-6) can be represented as a vector, **R**, then all of the R_i's can be defined with one matrix expression,

$$\mathbf{R} = \mathbf{CX} \qquad \text{Eq iv-19}$$

where **C** is a matrix with 3N columns and a number of rows equal to the number of internal coordinates.

The potential energy then becomes

$$V = 1/2\mathbf{R}^t\mathbf{FR} \qquad \text{Eq iv-20}$$

where **F** is the force field, *i.e.*, it is the matrix of force constants for the internal coordinates and the interactions between them, and $\mathbf{R}^t$ is the transpose of **R**. The kinetic energy is

$$T = 1/2\,\dot{\mathbf{R}}^{t}\mathbf{G}\,\dot{\mathbf{R}} \qquad \text{Eq iv-21}$$

where the **G**-matrix,

$$\mathbf{G} = \mathbf{C}\mathbf{M}^{-1}\mathbf{C}^{t} \qquad \text{Eq iv-22}$$

is the reduced mass matrix for the internal coordinates and $\mathbf{M}^{-1}$ is a diagonalized matrix with elements $1/m_i$ ($m_1 = m_2 = m_3$ and $m_4 = m_5 = m_6$, *etc.*). The equations of motion then become

$$(\mathbf{FG} - \lambda\mathbf{E})\mathbf{Q} = 0 \qquad \text{Eq iv-23}$$

(**E** is the identity matrix) and the secular equation for vibrations is

$$|\mathbf{FG} - \lambda\mathbf{E}| = 0 \qquad \text{Eq iv-24}$$

where the λ's are the vibrational eigenvalues,

$$\bar{\nu} = 130.3\sqrt{\lambda} \qquad \text{Eq iv-25}$$

Essentially, we "diagonalize" the FG matrix - it's not quite that simple since the FG matrix is often not a square matrix- and the results are the eigenvalues (**λ**) and the eigenvectors ("normal coordinates," **Q)**.

The problem then is to associate a normal coordinate with every vibrational frequency, *i.e.*, to **assign the spectrum**. Presumably all of the $\bar{\nu}$'s and therefore λ's can be determined experimentally. The G-matrix depends only on the atomic masses, molecular structure and choice of internal coordinates - it is, therefore, known. A force field calculation then involves iterating the force constants (F-matrix) until solving eq iv-24 yields a set of λ's which nearly reproduce the experimental set. Typically, the researcher will have many more force constants, f_{ij}'s, than frequencies, $\bar{\nu}_k$'s, so solutions are usually not unique. Fortunately, however, force fields are relatively transferable - the force constant for a Pt-Cl stretch will have **similar** values in all compounds. In addition, it is assumed that isotopic substitution will not affect the force field thus the Pt-^{35}Cl and Pt-^{37}Cl stretches will have different $\bar{\nu}$'s due to changes in mass not in force constants so it is possible to increase the size of the data set without increasing the number of force constants to be fitted. The problem for large molecules, however is formidable and the results should be treated with care.

IV.6 Symmetry Coordinates

The results of these calculations are the eigenvectors or the **normal coordinates** - the relative motion of the atoms during a vibration given as linear combinations of the internal coordinates used to generate the **F**- and **G**-matrices. The closer our choice of basis vectors is to the actual normal coordinates, the fewer and smaller will be the off-diagonal elements. Each normal coordinate forms the basis for one of the irreps of the molecular point group so one improvement in the basis set would be to use one that formed the basis for the irreps of the molecular point group. Such a set of internal coordinates is called the **symmetry coordinates**, **S**, which can be written as a linear combination of the internal coordinates,

$$\mathbf{S} = \mathbf{U}\mathbf{R} \qquad \text{Eq iv-26}$$

Symmetry coordinates represent a much better description of the motion. Consider two members of this set, S_i and S_j which belong to different irreps. Since they form the basis of different irreps, the direct product $S_i \otimes S_j$ must change sign for at least one operation of the group, but the potential energy,

$$V = 1/2\Sigma\Sigma f_{ij}S_iS_j \qquad \text{Eq iv-27}$$

must remain invariant under all operations. Therefore $f_{ij} = 0$ if S_i and S_j belong to different irreps - the **F-matrix is block diagonalized when symmetry coordinates are used**. The **F**- and **G**-matrices are still set up in terms of internal coordinates but are then **symmetrized** (block diagonalized) by a similarity transformation,

$$\mathbf{G}_{sym} = \mathbf{U}\mathbf{G}\mathbf{U}^{t} \text{ and } \mathbf{F}_{sym} = \mathbf{U}\mathbf{F}\mathbf{U}^{t} \qquad \text{Eq iv-28}$$

Each block of the resulting $\mathbf{F}_{sym}\mathbf{G}_{sym}$ matrix is then treated as a separate problem.

The convention for numbering the normal modes is from the highest frequency to lowest within an irrep and the irreps are given from top to bottom in the character table with degenerate modes last. Thus for a C_{2v} molecule, $\bar{\nu}_1$ will always be the highest frequency mode of a_1 symmetry while $\bar{\nu}_{3N-6}$ will the lowest frequency mode of b_2 symmetry (if there are b_2 modes).

To generate symmetry coordinates

1. Determine the reducible representation of the 3N Cartesian displacement vectors and decompose it into irreps.
2. Subtract out the external degrees of freedom (x, y, z, R_x, R_y, and R_z).
3. Decide on a set of internal coordinates and determine the reducible representations of the symmetrically equivalent sets and decompose each.
4. Construct the symmetry coordinates of each irrep as linear combinations of the appropriate internal coordinates as determined in number 3.

The water molecule belongs to the C_{2v} point group.

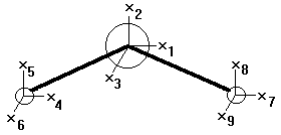

Figure IV-8. The 3N Cartesian vectors for water.

Remember that in order to determine the reducible representation for these vectors, we first determine the number of atoms (N) that lie on each symmetry element since the vectors on other atoms cannot contribute to the trace. To determine the character of an operation in the reducible representation, the number of unshifted atoms for the operation is multiplied by the contribution of the operation, *i.e.*, by the trace of the 3x3 matrix corresponding to the operation.

Operation	**Contribution per unshifted atom**
E	+3
i	-3
σ	+1
C_n	$+1 + 2\cos(2\pi/n)$
S_n	$-1 + 2\cos(2\pi/n)$

For water then,

C_{2v}	E	C_2	σ_v	σ_v'
N	3	1	3	1
Contribution	3	-1	1	1
Γ_{tot}	9	-1	3	1

Upon decomposition, $\Gamma_{tot} = 3a_1 + a_2 + 3b_1 + 2b_2$. From the character table, $\Gamma_{trans} = a_1 + b_1 + b_2$ and $\Gamma_{rot} = a_2 + b_1 + b_2$ therefore, $\Gamma_{vib} = 2a_1 + b_1$. A set of internal coordinates must now be chosen. All bonds can change length, so there is one Δr for each bond. For water that leaves only one coordinate which must be the angle bending.

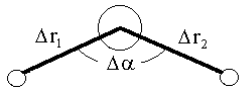

Figure IV-9. The internal coordinates of water

There are two symmetrically equivalent sets of internal coordinates for water: the Δr's and Δα.

C_{2v}	E	C_2	σ_v	σ_v'
Δα	1	1	1	1
Δr	2	0	2	0

Since the internal coordinates are individual vectors rather than sets of three vectors, there is no need to multiply by the contributions as we did above. $\Gamma(\Delta\alpha) = a_1$ and $\Gamma(\Delta r) = a_1 + b_1$. Thus, Δα is a symmetry coordinate, but we must determine the appropriate SALC's for the Δr. Since Δr_1 can be taken into Δr_2 by a C_2 operation, we need only consider the character of C_2 in the a_1 and b_1 irreps.

	E	C_2
a_1	1	1
b_1	1	-1

The appropriate SALC's are then $\Delta r_1 + \Delta r_2$ (a_1) and $\Delta r_1 - \Delta r_2$ (b_1). Ideally, the numbering of the symmetry coordinates will be in accord with convention. Stretches are typically higher than bendings so the a_1 stretch is S_1 the other a1 mode is S_2 The other stretch then becomes S_3.

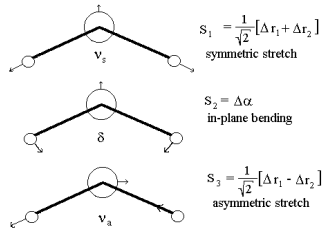

Figure IV-10. The symmetry coordinates of the water molecule. ν_S = symmetric stretch, ν_a = asymmetric stretch, δ = in-plane bending or deformation. Movement of the O atom is such as to preserve the center of mass.

The symmetry coordinate definitions in the form **S** = **UR**,

$$\begin{pmatrix} S_1 \\ S_2 \\ S_3 \end{pmatrix} = \begin{pmatrix} +0.707 & +0.707 & 0 \\ 0 & 0 & 1 \\ +0.707 & -0.707 & 0 \end{pmatrix} \begin{pmatrix} \Delta r_1 \\ \Delta r_2 \\ \Delta\alpha \end{pmatrix}$$

The **force field** for the internal coordinates is written as,

$$F = \begin{array}{c} \\ \Delta r_1 \\ \Delta r_2 \\ \Delta\alpha \end{array} \begin{array}{c} \begin{array}{ccc} \Delta r_1 & \Delta r_2 & \Delta\alpha \end{array} \\ \begin{pmatrix} f_{rr} & f_{rr'} & rf_{r\alpha} \\ f_{rr'} & f_{rr} & rf_{r\alpha} \\ rf_{r\alpha} & rf_{r\alpha} & r^2 f_{\alpha\alpha} \end{pmatrix} \end{array}$$

where the r and r^2 terms are used to maintain the same units for all force constants since angle bendings are unitless and have force constants in J not J/m^2 ($V = 1/2\Sigma\Sigma f_{ij}S_iS_j$).

IV.7 The X-Pt-Pt-X linear modes of $[Pt_2(pop)_4X_2]^{4-}$ - an example

The oxidized form of Platinum pop, $[Pt_2(pop)_4X_2]^{4-}$, pop = $[\mu\text{-}P_2O_5H_2]^{2-}$ is shown below.

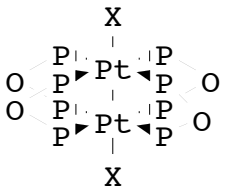

Figure IV-11. Structure of $[Pt_2(pop)_4X_2]^{4-}$, P ≡ O=P-(OH).

Its very unusual and reactive excited state has resulted in a considerable amount of research, and an important aspect of the research has been the nature of the Pt-Pt interaction in the ground and excited states. The following Raman data and assignments have been reported.[1]

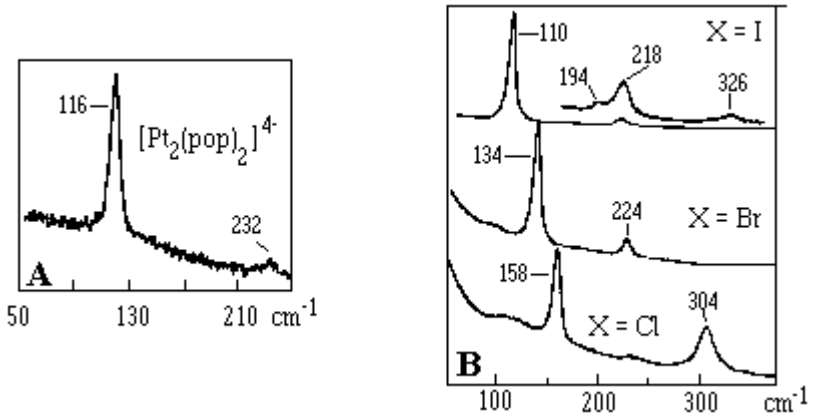

Figure IV-12. (A) The resonance Raman spectra of $[Pt_2(pop)_4]^2$. (B) resonance Raman of $[Pt_2(pop)_4X_2]^{4-}$ (X= Cl^-, Br^- and I^-)

X =	None	Cl	Br	I
ν(Pt-Pt)	116	158	134	110
ν_s(Pt-X)	-	304	224	194
ν_a(Pt-X)	-	285	201	178

It is tempting to look at the Raman spectra and infer that since ν(Pt-Pt) increases in going from I to Br to Cl the Pt-Pt interaction must also be increasing presumably with increasing electronegativites of the terminal halide, but is "ν(Pt-Pt)" truely a Pt-Pt stretch? A simple normal coordinate analysis will answer that question. The molecule has D_{4h} symmetry. To simplify the force field calculations, it is assumed that the stretching vibrations of the linear X-Pt-Pt-X moiety can be isolated from the rest of the modes.

These calculations are simple yet very informative.[2] The stretches all lie along the z-axis so this is a 1-D problem. The Cartesian vectors and internal coordinate therefore are,

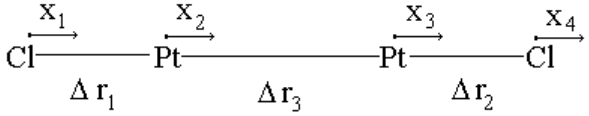

Figure IV-13. Cartesian displacments and internal coordinates for stretching modes of linear portion of $[Pt_2(pop)_4X_2]^{4-}$.

[1] Stein, P.; Dickson, M.K.; Roundhill, D.M., *J. Am. Chem. Soc.*, **1983**, 105, 3489

[2] Note that there is an error in the calculations presented by Roundhill *et al* which has been corrected in what follows.

First, the internal coordinates must be defined , *i.e.*, **C** in **R=CX** must be determined.

$$\begin{pmatrix} \Delta r_1 \\ \Delta r_2 \\ \Delta r_3 \end{pmatrix} = \begin{pmatrix} -1 & +1 & 0 & 0 \\ 0 & 0 & -1 & +1 \\ 0 & -1 & +1 & 0 \end{pmatrix} \begin{pmatrix} x_1 \\ x_2 \\ x_3 \\ x_4 \end{pmatrix}$$

Notice that with these definitions, each *Δr is an elongation of the bond.* Since the motion is only one dimensional, each mass enters the $\mathbf{M}^{-1}$ matrix only once, so

$$M^{-1} = \begin{pmatrix} 35.5^{-1} & 0 & 0 & 0 \\ 0 & 195.1^{-1} & 0 & 0 \\ 0 & 0 & 195.1^{-1} & 0 \\ 0 & 0 & 0 & 35.5^{-1} \end{pmatrix} = \begin{pmatrix} 0.0282 & 0 & 0 & 0 \\ 0 & 0.0051 & 0 & 0 \\ 0 & 0 & 0.0051 & 0 \\ 0 & 0 & 0 & 0.0282 \end{pmatrix}$$

The G-matrix is now determined from Eq iv-22, **G = CM^{-1}C^t - it is known if the structure of the molecule is knowm**,

$$G = \begin{pmatrix} -1 & 1 & 0 & 0 \\ 0 & 0 & -1 & 1 \\ 0 & -1 & 1 & 0 \end{pmatrix} \begin{pmatrix} 0.028 & 0 & 0 & 0 \\ 0 & 0.0051 & 0 & 0 \\ 0 & 0 & 0.0051 & 0 \\ 0 & 0 & 0 & 0.028 \end{pmatrix} \begin{pmatrix} -1 & 0 & 0 \\ 1 & 0 & -1 \\ 0 & -1 & 1 \\ 0 & 1 & 0 \end{pmatrix} = \begin{pmatrix} 0.033 & 0 & -0.005 \\ 0 & 0.033 & -0.005 \\ -0.005 & -0.005 & 0.0103 \end{pmatrix}$$

The complete force field would require four force constants: a Pt-Pt stretching, f(Pt-Pt), a Pt-Cl stretching, f(Pt-Cl), an interaction between the Pt-Pt and Pt-Cl stretches, I(Pt-Pt, Pt-Cl) and an interaction between the two Pt-Cl stretches, I(Pt-Cl,Pt-Cl'). There are, however, only three observed frequencies so a unique force field is not determined. Roundhill, *et al* chose to set the Pt-Cl, Pt-Cl' interaction force constant to zero and then calculate the remaining three force constants. The results of their calculations are: f(Pt-Pt) = 170 N/m, f(Pt-Cl) = 165 N/m, and I(Pt-Pt, Pt-Cl) = 16 N/m. For reasons discussed later, this force field calculates the same frequencies for the symmetric and antisymmetric Pt-Cl stretches so the following force constants will be used in our discussion: f(Pt-Cl) = 150 N/m and f(Pt-Pt) = 170 N/m, I(Pt-Pt,Pt-Cl) = 8 N/m, I(Pt-Cl,Pt-Cl') = 7 N/m.

The F-matrix can then be written as,

$$F = \begin{array}{c} \begin{matrix} \Delta r_1 & \Delta r_2 & \Delta r_3 \end{matrix} \\ \begin{pmatrix} 150 & 7 & 8 \\ 7 & 150 & 8 \\ 8 & 8 & 170 \end{pmatrix} \begin{matrix} \Delta r_1 \\ \Delta r_2 \\ \Delta r_3 \end{matrix} \end{array}$$

Since we are using four force constants to fit only three frequencies, we expect an excellent fit of the data, but the solutions are not unique. Arguments about the transferrability of this force field to the Br and I complexes do add some credence to its validity, however.

Construction of the symmetry coordinates can be done without a character table since the three coordinates are obiviously two linear combinations of the symmetrically equivalent Pt-Cl stretches, $\Delta r_1 \pm \Delta r_2$, and the Pt-Pt stretch, Δr_3. The Pt-Pt bond transforms as a_{1g} in D_{4h} while the two Pt-Cl bonds are $a_{1g} + a_{2u}$. The normalized symmetry coordinates (**S = UR**) can be written as,

$$\begin{pmatrix} S_1 \\ S_2 \\ S_3 \end{pmatrix} = \begin{pmatrix} 0.707 & 0.707 & 0 \\ 0 & 0 & 1 \\ 0.707 & -0.707 & 0 \end{pmatrix} \begin{pmatrix} \Delta R_1 \\ \Delta R_2 \\ \Delta R_3 \end{pmatrix},$$

where $S_1 = \nu_s$(Pt-Cl); $S_2 = \nu$(Pt-Pt); $S_3 = \nu_a$(Pt-Cl).
The symmetrized G-matrix is $\mathbf{G}_{sym} = \mathbf{UGU}^t$ (Eq iv-28),

$$G_{sym} = \begin{pmatrix} 0.0333 & -0.007 & 0 \\ -0.007 & 0.0103 & 0 \\ 0 & 0 & 0.0333 \end{pmatrix}$$

while the symmetrized F-matrix becomes,

$$F_{sym} = \begin{pmatrix} 157 & 11.3 & 0 \\ 11.3 & 170 & 0 \\ 0 & 0 & 143 \end{pmatrix}$$

Note that both matrices are block diagonalized into a 2x2 a_{1g} block and a 1x1 a_{2u} block. This means that S_1 and S_2 can "couple" to form the normal coordinates and indeed they do since the interaction term is not zero. The implication then is that there is no "pure" Pt-Pt stretch. The asymmetric Pt-Cl mode, however, is a normal coordinate and represents the actual motion of the atoms since it is "not connected" to another symmetry coordinate.

The result of the similarity transformation is that for the Pt-Cl stretches, F_{sym} = f(Pt-Cl) + I(Pt-Cl,Pt-Cl) and F_{asym} = f(Pt-Cl) - I(Pt-Cl,Pt-Cl) or 150+7 and 150-7. The only reason there are two different Pt-Cl stretches is that they interact, I(Pt-Cl,Pt-Cl) ≠ 0. In the force field used by Roundhill *et. al*, this interaction was assumed to be zero and both modes were calculated to be at 304 cm^{-1}. The interaction term can be positive or negative so the symmetric stretch can be either higher or lower in energy than the asymmetric stretch, but if the interaction term is zero, only one stretch will be observed. As the two bonds get farther away from one another, this interaction will get smaller and the two stretches get closer together. Thus, **group theory predicts only the maximum number of observed peaks, the actual number may well be less, especially for large molecules where two symmetrically equivalent coordinates are far from one another.**

The eigenvalues can be determined from Eq iv-24. For the a_{2u} mode, $\lambda_3 = F_{33}G_{33}$ = 143x0.033 = 4.7 so $\bar{\nu}_3 = 130.3(4.7)^{½}$ = 280 cm^{-1} and the normal coordinate $Q_3 = S_3 = 0.707(\Delta r_1 - \Delta r_2) = 0.707(-x_1 + x_2 - x_3 + x_4)$.

Determining the other eigenvalues and eigenvectors is a little more complicated, but still relatively simple - we need only solve the 2x2 determinant $|\mathbf{FG}-\lambda\mathbf{E}|=0$. For the a_{1g} block we can write

$$\begin{vmatrix} 5.15 - \lambda & -1.02 \\ -0.856 & 1.66 - \lambda \end{vmatrix} = 0$$

which is expanded to (5.15-λ)(1.66-λ) - (-1.02)(-0.856) = 0. The resulting quadratic has two roots: λ_1 = 5.38 ($\bar{\nu}_1$ = 302 cm^{-1}) and λ_2 = 1.43 ($\bar{\nu}_2$ = 156 cm^{-1}). The force field has reproduced the observed frequencies to within ±3 cm^{-1} - the best fit. Now to deduce the assignment, *i.e*, the normal modes.

The Q_i are the relative motions and are defined as $Q_i = \Sigma a_{ij}R_j$. The elements of the matrix **Q** are the a_{ij}. Only the relative values of a_{ij} can be determined not the absolute

distances moved. **Q** is determined from the equations of motion as given by Eq iv-23, (**FG** - λ**E**)**Q** = 0. For Q_1, λ = 5.38.

$$(FG - \lambda_1 E)Q = \begin{pmatrix} 5.15 - 5.38 & -1.02 \\ -0.856 & 1.66 - 5.38 \end{pmatrix}\begin{pmatrix} a_{11} \\ a_{12} \end{pmatrix} = \begin{pmatrix} -0.23 & -1.02 \\ -0.856 & -3.72 \end{pmatrix}\begin{pmatrix} a_{11} \\ a_{12} \end{pmatrix} = 0$$

which yields two equations: $-0.23a_{11} - 1.02a_{12} = 0$ and $-0.856a_{11} - 3.72a_{12} = 0$. Either equation yields the same ratio of coeficients: $a_{11} = -(3.72/0.856)\, a_{12} = -4.4\, a_{12}$. Thus, the first normal coordinate involves 4.4 times more motion along S_1 than S_2 and as one bond elongates, the other compresses, *i.e.*, $Q_1 = \begin{pmatrix} 4.4N \\ -N \end{pmatrix}\begin{pmatrix} S_1 \\ S_2 \end{pmatrix}$ where N is chosen to yield a normalized vector. Normalizing ($N^2 + (4.4N)^2 = 1$) yields a normalization constant of N = 0.22 so the normalized normal mode is $Q_1 = \begin{pmatrix} 0.97 \\ -0.22 \end{pmatrix}\begin{pmatrix} S_1 \\ S_2 \end{pmatrix}$. In a similar manner, one arrives at $Q_2 = \begin{pmatrix} 0.27 \\ 0.96 \end{pmatrix}\begin{pmatrix} S_1 \\ S_2 \end{pmatrix}$. So, $Q_1 = 0.97\, S_1 - 0.22S_2$ and $Q_2 = 0.27S_1 + 0.96S_2$. However, $S_1 = 0.707[\Delta r_1 + \Delta r_2] = 0.707[(-x_1+x_2) + (-x_3+x_4)]$ and $S_2 = \Delta r_3 = -x_2+x_3$. Thus,

$$\begin{aligned} Q_1 &= 0.97(-0.7x_1 + 0.7x_2 - 0.7x_3 + 0.7x_4) - 0.22(-x_2 + x_3) \\ &= -0.68x_1 + 0.46x_2 - 0.46x_3 + 0.68x_4 \end{aligned}$$

and

$$\begin{aligned} Q_2 &= 0.27(-0.7x_1 + 0.7x_2 - 0.7x_3 + 0.7x_4) + 0.96(-x_2 + x_3) \\ &= -0.19x_1 - 0.78x_2 + 0.78x_3 + 0.19x_4 \end{aligned}$$

The above represent the relative Cartesian displacements during Q_1 and Q_2. These displacements are depicted pictorially in figure IV-14.

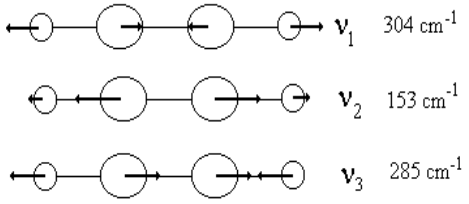

Figure IV-14. The normal modes and normal frequencies of vibrations of $[Pt(pop)_4Cl_2]^{4-}$

Examination of figure IV-14 shows that the Pt-Pt bond length changes in both ν_1 and ν_2 while the Pt-Cl bond lengths change in all three modes. This means that the mass of the halide plays a role in the frequency of the vibration and one must compare force constants to determine if the Pt-Pt bond is changing in this series.

Pt-Pt stretching force constants for the series $[Pt(pop)_4X_2]^{4-}$

X =	None	Cl	Br	I
f(Pt-Pt)	30	170	170	170
f(Pt-X)	-	150	140	100

Thus, the Pt-Pt stretching force constant does not change in the series so the entire shift from 153 cm^{-1} in the chloride down to 110 cm^{-1} in the iodide can be attributed to mass effects resulting from the mixing of the Pt-Pt and Pt-X stretches.

IV.8. The Potential Energy Distribution

The eigenvectors do not always give the best picture of what is happening due to the different masses of the atoms and the fact that bendings have different units than do

stretches. As a result, the contribution of the internal coordinates to the normal coordinates is given by the **Potential Energy Distribution (PED)**. The potential energy of the n^{th} normal mode can be written as, $V(Q_n) = 1/2Q_n^2\Sigma f_{ii}a_{in}^2$, where the f_{ij} terms have been dropped because off-diagonal (interaction) force constants are usually very small compared to the diagonal constants. The $\Sigma f_{ii}a_{in}^2$ is usually normalized to 100 so that each term represents a percentage of the potential energy. For Q_1 of the chloride, $150(0.97)^2 + 170x(0.22)^2 = 150 + 8.5 = 160$ which yields 150/160= 0.94 for S_1 and 8.5/160 = 0.053 for S_2.

PED for Cl-Pt-Pt-Cl

	Q_1	Q_2	Q_3
S_1	94	7	0
S_2	5	93	0
S_3	0	0	100

Thus the peak at 304 cm^{-1} is 94% symmetric Pt-Cl stretch, the peak at 158 cm^{-1} is 93% Pt-Pt stretch and the peak at 285 cm^{-1} is purely an asymmetric Pt-Cl stretch.

Problem IV.5 In the detailed treatment of symmetrical metal carbonyls,[3] the force constants for the C≡O bond were found to be about 1700 N/m while those of the M-C bond were found to be about 200 N/m. Interaction force constants were found to be about 70 N/m. Assume a mass of 60 amu for the metal. Since none of the internal coordinates are symmetrically equivalent, there is no need to construct symmetry coordinates.

(a) Use the FG-matrix method to do the normal coordinate calculations.

- Define the two internal coordinates as linear combinations of the three cartesian displacements, **R** = **CX, C** should be a 2x3matrix.
- Determine the **M**-matrix, 3x3 and the 2x2 **G**-matrix, $\mathbf{G} = \mathbf{CM}^{-1}\mathbf{C}^t$
- Write down the 2x2 **F**-matrix and determine the **F**x**G** product
- Expand the $|\mathbf{FG} - \lambda\mathbf{E}|$ determinant and get the two roots (λ_1 & λ_2)
- Use λ_1 in $(\mathbf{FG} - \lambda\mathbf{E})\mathbf{Q} = 0$ to determine Q_1. Use λ_2 to get Q_2
- Represent Q_1 and Q_2 with arrows showing the motions of the atoms in the normal modes
- Use the squares of the numbers in Q along with the appropriate f_{ii}'s to generate the PED.

(b) What would the vibrational wavenumbers be if ^{18}O had been used? A G-matrix effect.

(c) Many times, researchers will assume that the two modes are those of two isolated diatomic molecules. Use your calculated frequencies to determine the isolated force constants. Is this a good approximation? Explain.

Problem IV.6 The spectrum of NNO can be fitted with the following force constants: N=N stretch = 1788 N/m; N=O stretch = 1139 N/m; interaction term = 136 N/m. Explain why the interaction term in NNO is so much larger than it is in M-C≡O. Why is the Pt-Cl, Pt-Cl' interaction in $[Pt_2(pop)_4X_2]^{4-}$ expected to be the smallest of the three?

IV.9 Overtones and combinations:

[3] Jones,L.H..; McDowell,R.S.; Goldblatt, M., *Inorg. Chem.*, **1969**, 8, 2349.

In order to completely specify a vibrational level in the linear Cl-Pt-Pt-Cl system, one must supply three quantum numbers, v_1, v_2 and v_3, the number of vibrational quanta in the symmetric Pt-Cl stretching, the Pt-Pt stretching and the asymmetric Pt-Cl stretching. The energy level diagram shown in figure IV-15 was constructed for the Cl-Pt-Pt-Cl system by using the observed wavenumbers of the three fundamentals ($\bar{\nu}_1$ = 304, $\bar{\nu}_2$ = 158, and $\bar{\nu}_3$ = 285 cm^{-1}) which were assumed to be harmonic.

Fundamental transitions are those originating in the ground state and involving only one quantum of vibrational energy. There are only three fundamentals in Cl-Pt-Pt-Cl. There are two types of transitions involving more than one vibrational quanta: **overtones** in which all quanta are in the same vibration and **combinations** where at least two different vibrations are excited. Any transition originating from an excited level is referred to as a **difference band** or "hot-band" because of the temperature dependence of its intensity. Figure IV-15 shows some of the possible levels as well as their energies which are merely the sum of the vibrational quanta involved. It should be noted that overtones and combinations often lie at energies less than calculated from the sum of quanta due to anharmonicity, but it is very unusual to make an assignment of one of these transitions to an energy higher than predicted.

The **symmetry of a vibrational level** is the direct product of the symmetries of all of the contributing modes - vibrational ground states are always totally symmetric. Since the direct product of any non-degenerate irrep with itself is totally symmetric, **overtones involving an even number of quanta will be totally symmetric. Levels involving an odd number of quanta of a vibration will have the symmetry of the mode.** The symmetries of overtone levels of degenerate vibrations are not so easily ascertained and will not be discussed here. However, an excellent discussion is available.[4]

Vibrations of the same energy which are very close in energy can mix in a manner analagous to mo's, *i.e.*, the two resulting levels are "repelled" in energy and gain the character of both modes. This can result in substantial "intensity borrowing" so that if a weak overtone is close in energy to a very strong, totally symmetric mode, the result *can be* two relatively strong peaks which are not as close in energy. This phenomenon is called **Fermi resonance**. The classical example of Fermi resonance is CO_2 where two moderately strong Raman bands are observed at 1388 and 1286 cm^{-1}, one of which is due to the overtone of the ir-active out-of-plane bending mode (π_u) at 667 cm^{-1} while the other is the symmetric stretch (σ_g^+). Presumably, the two peaks would be observed as one very weak band at 2x667= 1334 cm^{-1} and one very strong band close to that energy in the absence of Fermi resonance. After mixing, however, the overtone gains some of the character of the stretch and thus gains intensity while the stretch gains overtone character and loses intensity. Assignment of one peak to the overtone and the other to the stretch is unwarranted. In the Cl-Pt-Pt-Cl example, a prime situation for Fermi resonance would be between $2\bar{\nu}_2$ (≤ 316) and $\bar{\nu}_1$ (304) as they are both totally symmetric and lie within 12 cm^{-1} of one another. There is no way, however, to predict if the two levels will mix.

[4] Wilson, E.B.; Decius, J.C.; Cross, P.C., *Molecular Vibrations: The Theory of Infrared and Raman Vibrational Spectra*, McGraw-Hill, 1955, pp 151-155.

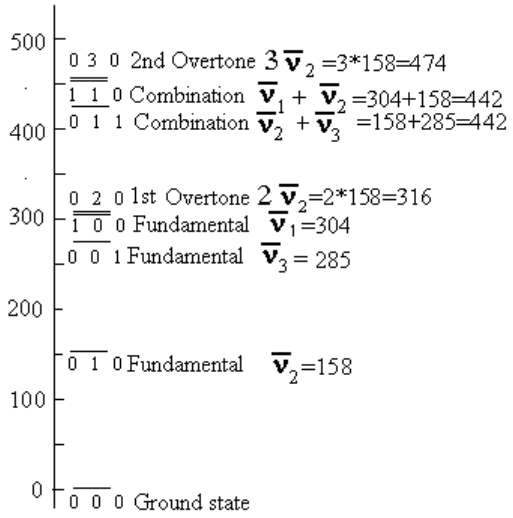

Figure IV-15. An energy level depicting the fundamental and some of the overtone and combination levels for linear Cl-Pt-Pt-Cl. The quantum numbers for each level are in the order: v_1 v_2 v_3.

You should now have a working vocabulary and at least a small appreciation for the mechanics of normal vibrations and the FG-matrix method. We want to turn to the generation of symmetry coordinates for larger molecules and then to the assignment of these symmetry coordinates to the observed spectra. However, before we can do that we must first consider Raman scattering which plays an important role in vibrational assignments.

IV.10 Raman scattering

As a photon with a wavenumber $\bar{\nu}_o$ traverses a molecule, it manifests itself in the induced oscillation of the electrons in the molecule. Ordinarily, the photon's energy is unchanged by the process and the scattering event is elastic. This type of scattering is called Rayleigh scattering. However, occasionally, the oscillation of the electrons can induce vibrations in the molecule and thus the scattered photon's wavenumber $\bar{\nu}$ will be decreased by the energy of the vibration, *i.e.*, $\bar{\nu}_o - \bar{\nu} = \Delta\bar{\nu} = \bar{\nu}_{vib}$ This latter type of scattering is called Raman scattering and is inelastic (photon's energy is not conserved). In Raman scattering, an incoming photon can also encounter a vibrationally excited molecule which can add the vibrational energy to the photon. The two different types of Raman scattering are called Stokes ($\bar{\nu} < \bar{\nu}_o$) and anti-Stokes ($\bar{\nu} > \bar{\nu}_o$) - see figure IV-16. Due to the Boltzmann distribution of molecules among vibrational levels, the anti-Stokes events get very rare as the vibrational energy increases. Raman spectra are usually reported versus $\Delta\bar{\nu}$ rather than $\bar{\nu}$ since it is the vibrational energies that are important.

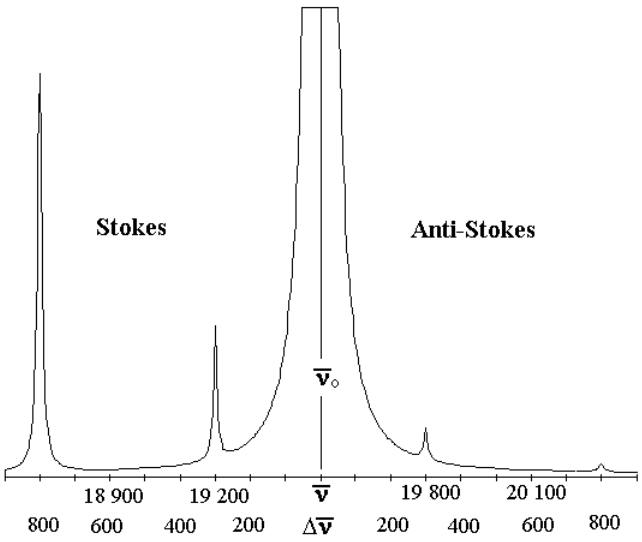

Figure IV-16. The Raman spectrum of a compound with vibrational modes at 300 and 800 cm^{-1} observed with a 19,500 cm^{-1} exciting line at 300K. The very strong line at $\bar{\nu}_0$ is due to Rayleigh scattering. The anti-Stokes component of the Raman scattering is weaker than the Stokes component by $\exp(-E_{vib}/kT)$.

In normal Raman, the scattering is not from a stationary state but from a virtual state (figure IV-17). Virtual states can be considered as stationary states that have been spread out by the uncertainty principle, $\Delta E\, \Delta t \approx h$ where ΔE is the amount by which the photon's energy fails to be in resonance with the closest lying excited state and Δt is the time the system can spend in this state. Thus $\Delta t \approx (\bar{\nu} c^*)^{-1}$ so if the exciting line, $\bar{\nu}_0$ is in the visible at 20 kK and the lowest excited state is 30 kK then $\Delta E = 1x10^4$ cm^{-1} and $\Delta t \approx (1x10^4 x3x10^{10})^{-1} \approx 3$ fs or about a vibrational period - normal Raman scattering is a very fast process.

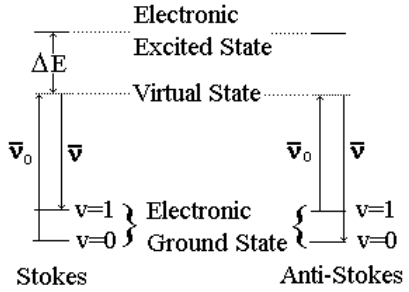

Figure IV-17. The two types of normal Raman scattering.

What fraction of the molecules will undergo scattering will depend upon how the electrons are affected by the field, *i.e.*, on the molecule's **polarizability** (α). One can view the process as the photon initiating an oscillating dipole (μ) in the molecule as the electrons oscillate with the electric field; it is then the oscillating dipole that radiates the scattered photon (much like a radio transmitter). The strength of this induced dipole is proportional to the electric field of the photon. The proportionality constant is the molecular polarizability. Since the dipole and the electric field are actually vectors, the polarizability is a tensor.

$$\boldsymbol{\mu} = \boldsymbol{\alpha}\boldsymbol{\varepsilon} \qquad \text{eq iv-29}$$

or $\begin{pmatrix}\mu_x\\ \mu_y\\ \mu_z\end{pmatrix} = \begin{pmatrix}\alpha_{xx} & \alpha_{xy} & \alpha_{xz}\\ \alpha_{yx} & \alpha_{yy} & \alpha_{yz}\\ \alpha_{zx} & \alpha_{zy} & \alpha_{zz}\end{pmatrix}\begin{pmatrix}\varepsilon_x\\ \varepsilon_y\\ \varepsilon_z\end{pmatrix}$ where α_{xz} is a measure of how easily the z-component of the electric field (z-polarization) induces a dipole in the x-direction - this would imply that the vibration interacts in such a way as to rotate the polarization. Indeed, one of the important pieces of information available from Raman scattering is the polarization change that the incoming photon undergoes.

The exciting lines in the modern Raman experiment are from lasers and the output from most lasers is polarized because of the use of Brewster angle windows. The polarization, however, can be rotated with a quarter wave plate so any orientation of polarization is possible so long as the polarization is perpendicular to the direction of propagation of the light. A polarizer after the sample will allow light only of a given polarization to pass. The experimental setup is shown in figure IV-18.

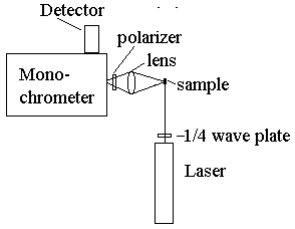

Figure IV-18.Typical Raman experimental setup for 90^o scattering.

The intensity of scattered radiation which is polarized perpendicular to that of the incoming radiation is defined as $I_\perp$ and that of the radiation parallel to the incoming radiation as $I_\parallel$ then the **depolarization ratio, ρ** is defined as,

$$\rho = I_\perp/I_\parallel \qquad \text{eq iv-30}$$

In the case where the polarizability tensor is diagonal - the vibration does not rotate the electric vector - all of the intensity will remain parallel to the incoming radiation and $\rho = 0$. This is referred to as isotropic scattering. However, if any of the off-diagonal elements are non-zero, then there can be intensity in the perpendicular component and $\rho > 0$. In solutions or pure liquids (solids are excluded from the following discussion) which involve rotationally averaged, randomly oriented species, there are three irreducible tensors which remain invariant. They are

- the isotropy, $G^o = \alpha_{xx}^2 + \alpha_{yy}^2 + \alpha_{zz}^2 = 3\alpha_{avg}^2$, which transforms as the totally symmetric representation;
- the symmetric anisotropy, G^s, which transforms like the d-orbitals; and
- the anti-symmetric anisotropy, G_a, which transforms like the rotations.

The intensities of the two components can then be expressed as $I_\parallel \propto 10\,G^o + 4G^s$ and $I_\perp \propto 3G^s + 5G^a$. The total intensity of the scattered radiation is given as $I_{tot} = I_\parallel + I_\perp \propto 10G^o + 7G^s + 5G^a$. The depolarization ratio is then

$$\rho = \frac{3G^s + 5G^a}{10G^o + 4G^s} \qquad \text{Eq. iv-31a}$$

for normal Raman $G^a = 0$. So,

$$\rho = \frac{3G^s}{10G^o + 4G^s} \qquad \text{Eq. iv-31b}$$

For purely isotropic scattering, $G^s = 0$ so $\rho = 0$. For purely symmetric scattering, $G^o = 0$ so $\rho = 3/4$. Since G^o transforms as the totally symmetric representation, only totally symmetric modes can have $G^o \neq 0$ and thus only totally symmetric modes can have $\rho < 3/4$. Therefore, an important fact that will help in the assignment of normal modes is that for **non-totally symmetric modes, $\rho = 3/4$** but for **totally symmetric modes, $0 \leq \rho \leq 3/4$**. The actual value of ρ of a symmetric mode will depend on the relative contributions of G^o and G^s to the scattering tensor for that mode. It should be noted that **if $\rho < 0.75$ the peak is polarized and the vibration is totally symmetric,** but **if $\rho = 0.75$ one cannot conclude that the vibration is not totally symmetric** since totally symmetric modes can be active due to $G^s > 0$ - this is especially true in molecules of low symmetry. In resonance Raman (see section VI.8), it is possible for activity to result from G^a, in which case, there is no parallel intensity so $\rho \rightarrow \infty$. This is referred to as *anomalous polarization*.

Depolarization ratios of samples in solution can be measured in several different ways, but we will describe only the easiest here. The Raman spectrum of a solution, is recorded twice, once with the polarizer oriented so as to pass light polarized parallel to the incoming beam to measure $I_{\parallel}$ and then once with it rotated 90° to measure $I_{\perp}$.

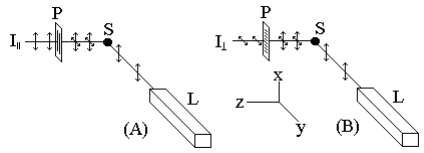

Figure IV-19. Measurement of depolarization ratio. Light leaves laser (L) polarized in the xy plane and is scattered from sample (S). If $G_s \neq 0$, the scattered radiation will have both xy and yz compnents. In experiment A, the polarizer (P) is adjusted to allow transmission of the xy component ($\parallel$ polarization) and the spectrum is recorded. In experiment B, the polarizer is turned to transmit the yz component ($\perp$ polarization) and a second spectrum is recorded. The depolarization ratio of a peak is the ratio of the second intensity to the first ($\rho = I_{\perp} / I_{\parallel}$).

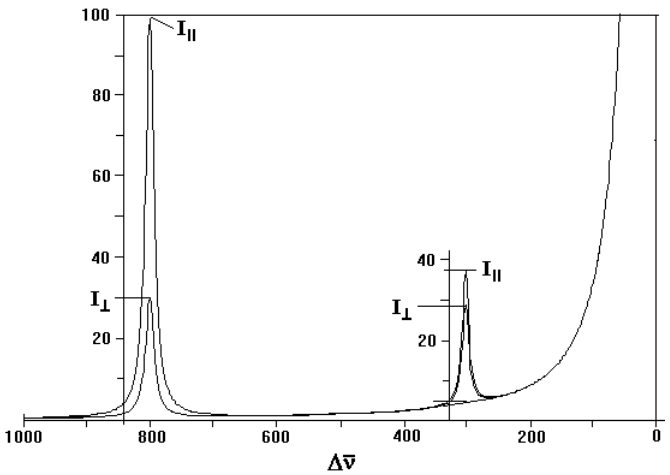

Figure IV-20. Raman spectra recorded in parallel and perpendicular polarizations. The peak at 800 cm^{-1} has a depolarization value of $\rho = I_{\perp} / I_{\parallel} = 30/100 = 0.3$ since $\rho < 0.75$ this peak is said to be polarized and must therefore be a totally symmetric mode. The peak at 300 cm^{-1} has a depolarization value of $\rho = (28-5)/(37-5) = 23/32 = 0.72$ which is sufficiently close to 0.75 that one would have to say that it is probably depolarized which means that it *might* be a non-totally symmetric mode.

IV.11 Raman Selection Rules

In normal Raman, activity is due to non-zero values for G^o and/or G^s. G^o is always totally symmetric so totally symmetric vibrations are always Raman active. G^s transforms like the d-orbitals so modes which have the same symmetry as one of the d-orbitals will also be Raman active. Furthermore, since only non-zero values of G^o can result in $\rho < 3/4$, only totally symmetric modes are polarized. As one example, consider the C_{2v} point group,

C_{2v}				
A_1	z	x^2, y^2, z^2	$G^o + G^s$	$0 \le \rho \le 0.75$
A_2	R_z	xy	$G^s + G^a$	$\rho = 0.75$
B_1	x, R_y	xz	$G^s + G^a$	$\rho = 0.75$
B_2	y, R_x	yz	$G^s + G^a$	$\rho = 0.75$

From the above, we can conclude that all vibrations are Raman active since the d-orbitals span all four irreps, but any a_2 modes would be IR silent. There are three contributions to the A_1 irrep in the third column; one of which must correspond to G^o the other two, therefore, correspond to G^s so in C_{2v} symmetry $0 \le \rho \le 0.75$ for a totally symmetric mode and values of zero should be rare. Since the other irreps all include a rotation and the d-orbital, they also contain G^a and G^s.

For the higher symmetry T_d point group,

T_d				
A_1		$x^2+y^2+z^2$	G^o	$\rho = 0$
A_2			-	Not Active
E		$(2z^2-x^2-y^2, x^2-y^2)$	G^s	$\rho = 3/4$
T_1	(R_x, R_y, R_z)		G^a	RRS only
T_2	(x, y, z)	(xy, xz,yz)	G^s	$\rho = 3/4$

From the T_d table we can conclude that only t_2 modes are IR active while $a_1 + e + t_2$ modes are Raman active. Since only one term is listed for A_1 in the "d-orbital column", it must arise from G^o therefore there are no contributions to a_1 Raman active modes from G^s and they are purely isotropic and thus $\rho = 0$ for totally symmetric modes. The e and t_2 modes are active due to G^s terms and will have $\rho = 0.75$. The t_1 irrep contains the rotations and therefore G^a so t_1 modes are not active in normal Raman but can be active in resonance Raman (RRS) experiments where they are expected to show anamalous polarization.

IV.12 Infrared and Raman Intensities

Infrared absorption is due to the interaction of the electric field of the light with the dipole of the molecule and the intensity of an IR band depends upon $(\mu/\Delta Q)$, the change in dipole during the vibration. Raman activity, however, is due to the interaction of the electric field with the electrons and depends upon the polarizability of the electron cloud. Expansion of the polarizability in terms of the normal coordinates yields the result that the intensity of a Raman band depends upon (α/Q), the change in polarizabilty during the vibration. Thus, two general rules of intensities are:

- **Infrared bands** are generally strong for asymmetric modes involving electronegative atoms. This combination results in a large $(\partial\mu/\partial Q)$.

$$\left(\frac{\partial \mu}{\partial Q}\right)_{Q=0} = 0 \qquad \left(\frac{\partial \mu}{\partial Q}\right)_{Q=0} \neq 0$$

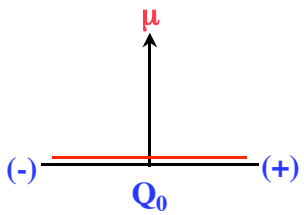

e.g., $\nu_{\square\square\square}$ ($R_2C{=}CR_2$)

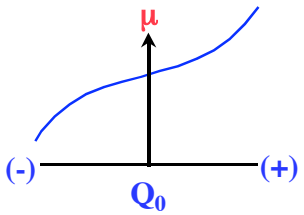

e.g., $\nu_{\square\square O}$ ($R_2C{=}O$)

- **Raman bands** are generally strong for symmetric modes involving large atoms resulting in a large change in the size of the molecule. This combination results in a large (α/Q).

$$\left(\frac{\partial\alpha}{\partial Q}\right)_{Q=0} = 0$$

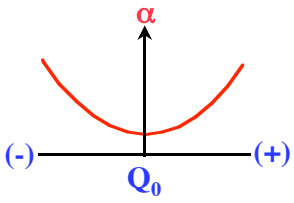

e.g., ν_a (O=C=O)

$$\left(\frac{\partial\alpha}{\partial Q}\right)_{Q=0} \neq 0$$

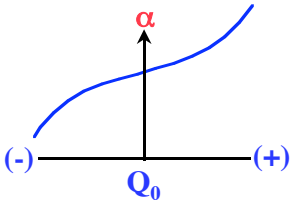

e.g., ν_s (O=C=O)

These rules are "rough rules of thumb" but can often be helpful in vibrational assignments when there is little else to use as guidance.

IV.13 A complete vibrational assignment, $SbCl_5$

A *vibrational assignment* consists of associating a symmetry coordinate to each of the observed peaks in the IR and Raman spectra. Group theory and selection rules are invaluable tools in this process. As an example, the vibrational spectrum of $SbCl_5$, given below, will be assigned.

cm^{-1}	IR	Raman	Polarized
395	x	x	
371	x		
356		x	x
307		x	x
172	x	x	
165		x	
154	x		
72	x	x	

First a set of internal coordinates for the D_{3h} molecule must be defined.

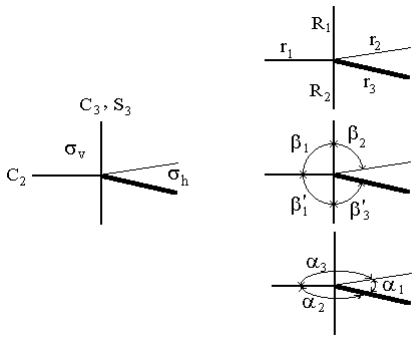

Figure IV-21. The symmetry elements and internal coordinates for $SbCl_5$.

The D_{3h} character table is given below along with the number of unshifted atoms (N) and the contribution per unshifted atom for each character. Γ_{tot} then is the product of these two and represents the reducible representation for all degrees of freedom for the molecule. Note that under E the character is 18 - the dimension of the representation. Figure IV-21 also gives the internal coordinate descriptions. Note there are 14 (5 stretches + 9 bendings) while 3N-6 = 12. Each of the bonds must stretch, so 5 stretches is correct, but that leaves only seven bends. The additional two bends are called **redundancies** and will be removed when we construct the symmetry coordinates.

D_{3h}	E	$2C_3$	$3C_2$	σ_h	$2S_3$	$3\sigma_v$		
A_1'	1	1	1	1	1	1		$x^2 + y^2, z^2$
A_2'	1	1	-1	1	1	-1	R_z	
E'	2	-1	0	2	-1	0	(x,y)	(x^2-y^2, xy)
A_1''	1	1	1	-1	-1	-1		
A_2''	1	1	-1	-1	-1	1	z	
E"	2	-1	0	-2	1	0	(R_x, R_y)	(xz, yz)
N	6	3	2	4	1	4		
cont	3	0	-1	1	-2	1		
Γ_{tot}	18	0	-2	4	-2	4		

Γ_{tot} can be decomposed to give,

$\Gamma_{tot} = 2a_1' + a_2' + 4e' + 3a_2'' + 2e''$.

The character table indicates that the external degrees of freedom transform as

$\Gamma_{ext} = \quad a_2' + e' + \quad a_2'' \; + \; e''$

Subtracting the external degrees from the total gives the internal degrees

$\Gamma_{vib} = 2a_1' \quad + \quad 3e' \quad + 2a_2'' \; + \; e''$

The following can be deduced from the character table:

$2a_1'$ modes are Raman-only active and polarized. They can thus be assigned to the two polarized Raman only bands as $\bar{\nu}_1 = 356$ cm^{-1} and $\bar{\nu}_2 = 307$ cm^{-1}.

$2a_2''$ modes are IR-only active. There are only two peaks that are observed only in the IR so $\bar{\nu}_3 = 371$ cm^{-1} and $\bar{\nu}_4 = 154$ cm^{-1}.

3e' modes are IR and Raman active which is consistent with three observed IR and Raman active modes at $\bar{\nu}_5 = 395$ cm^{-1}, $\bar{\nu}_6 = 172$ cm^{-1} and $\bar{\nu}_7 = 72$ cm^{-1}.

e" vibration is Raman-only active but not polarized consistent with $\bar{\nu}_8 = 165$ cm^{-1}.

The symmetry coordinates are now constructed. The symmetrically equivalent sets of internal coordinates transform in the following way,

D_{3h}	E	$2C_3$	$3C_2$	σ_h	$2S_3$	$3\sigma_v$	
R	2	2	0	0	0	2	$a_1' + a_2''$
r	3	0	1	3	0	1	$a_1' + e'$
α	3	0	1	3	0	1	$a_1' + e'$
β	6	0	0	0	0	2	$a_1' + a_2'' + e' + e''$

The sum of the irreducible representations of the internal coordinates is the same as Γ_{vib} except that there are $4a_1'$ coordinates but only $2a_1'$ modes. The two redundancies are both a_1' and they must come one from α and one from β. Since all of the characters of the a_1' irrep are positive, these two redundancies would correspond to all of the α's and all of the β's increasing which

is impossible. Thus the redundancies are easily eliminated and the 3N-6 symmetry coordinates can now be constructed in the same order as the $\bar{\nu}_i$, from high $\bar{\nu}$ to low $\bar{\nu}$ in each irrep.

Determination of the vibrational SALC's. The operation used to transform the reference vector into one of the members of the symmetrically equivalent set in the generation of the SALC's should perform this operation uniquely. For example, C_2 is a poor choice for $\Delta\beta_1 \Rightarrow \Delta\beta_2'$ as there are three C_2 operations and they all have different effects on $\Delta\beta_1$. However, C_2 is an acceptable operation to convert ΔR_1 into ΔR_2 since all three of the C_2 rotations have the same effect. The following choice of operations are unique in this respect.

$\Delta R_1 =$	ΔR_1 E	ΔR_2 C_2
a_1'	+1	+1
a_2''	+1	-1

$\Delta r_1 =$	Δr_1 E	Δr_2 C_3	Δr_3 C_3
a_1'	+1	+1	+1
e'	+2	-1	-1

$\Delta\alpha_1 =$	$\Delta\alpha_1$ E	$\Delta\alpha_2$ C_3	$\Delta\alpha_3$ C_3
e'	+2	-1	-1

$\Delta\beta_1 =$	$\Delta\beta_1$ E	$\Delta\beta_2$ C_3	$\Delta\beta_3$ C_3	$\Delta\beta_1'$ σ_h	$\Delta\beta_2'$ S_3	$\Delta\beta_3'$ S_3
a_2''	+1	+1	+1	-1	-1	-1
e'	+2	-1	-1	+2	-1	-1
e"	+2	-1	-1	-2	+1	+1

The numbers in the above tables are the coefficients (not normalized) of the internal coordinates in each of the symmetry coordinates.

The $2a_1'$ modes, ΔR and Δr, are the axial and equatorial stretches. X-ray data indicate that the axial bond is longer than the equatorial so we will assume that the equatorial modes are at higher energy.

Figure IV-22. The a_1' modes of $SbCl_5$

One of the a_2'' modes is the antisymmetric axial stretch, ΔR, while the other is a $\Delta\beta$, an out-of-plane motion of the equatorial Cl's, *i.e.*, $\pi(SbCl_3)$. Since stretching force constants are almost always higher than bending force constants, the higher energy mode is assigned to the stretch. This assignment is also consistent with the assignments of the a_1' stretches to above 300 cm^{-1}.

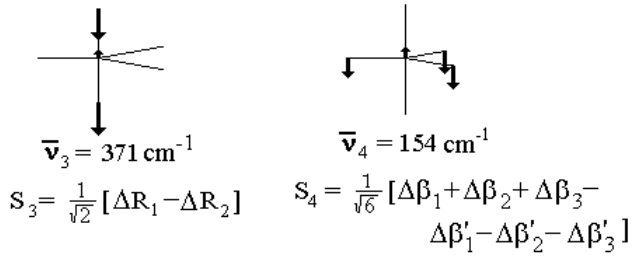

Figure IV-23. The a_2'' modes of $SbCl_5$.

The three e' modes consist of a stretch, Δr, and two bends, Δα and Δβ. Consistent with the assignments of the previous stretches, $\bar{\nu}_5$ is assigned to the stretch. There is no clear way to distinguish between the two bending modes. However, normal coordinate analysis has confirmed that the Δβ mode is the lower of the two. There is only one coordinate of e" symmetry so $\bar{\nu}_8$ is clearly due to S_8, a bending mode.

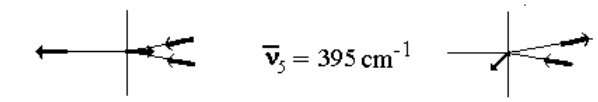

$\bar{\nu}_5 = 395\ cm^{-1}$

$$S_{5a} = \frac{1}{\sqrt{6}}[2\Delta r_1 - \Delta r_2 - \Delta r_3] \qquad S_{5b} = \frac{1}{\sqrt{2}}[\Delta r_2 - \Delta r_3]$$

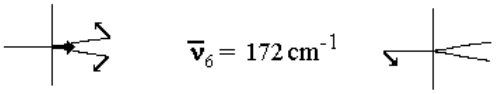

$\bar{\nu}_6 = 172\ cm^{-1}$

$$S_{6a} = \frac{1}{\sqrt{6}}[2\Delta\alpha_1 - \Delta\alpha_2 - \Delta\alpha_3] \qquad S_{6b} = \frac{1}{\sqrt{2}}[\Delta\alpha_2 - \Delta\alpha_3]$$

Figure IV-24. Two of the e' modes of $SbCl_5$. The third component is shown in figure IV-25.

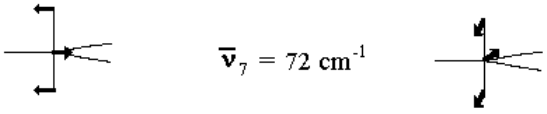

$\bar{\nu}_7 = 72\ cm^{-1}$

$$S_{7a} = \frac{1}{\sqrt{12}}[2\Delta\beta_1 - \Delta\beta_2 - \Delta\beta_3 + 2\Delta\beta_1' - \Delta\beta_2' - \Delta\beta_3'] \qquad S_{7b} = \frac{1}{2}[\Delta\beta_2 - \Delta\beta_3 + \Delta\beta_2' - \Delta\beta_3']$$

Figure IV-25. The two bendings of t equatorial Sb-Cl bonds.

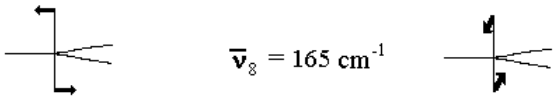

$\bar{\nu}_8 = 165\ cm^{-1}$

$$S_{8a} = \frac{1}{\sqrt{12}}[2\Delta\beta_1 - \Delta\beta_2 - \Delta\beta_3 - 2\Delta\beta_1' + \Delta\beta_2' + \Delta\beta_3'] \qquad S_{8b} = \frac{1}{2}[\Delta\beta_2 - \Delta\beta_3 - \Delta\beta_2' + \Delta\beta_3']$$

The vibrational assignment in complete, but before leaving this example, there are two aspects of the motion which are worthy of further discussion.

Degenerate vibrations are two dimensional, *i.e.*, they are not restricted to the one dimensional coordinates S_{7a} and S_{7b} but rather to the plane defined by the two basis vectors. The actual motion is better described as a circular motion in the plane described by S_{7a} and S_{7b} so $\bar{\nu}_7$ and $\bar{\nu}_8$ are better described as in-phase and out-of-phase rotations of the equatorial Cl's as shown in Figure IV-26.[5]

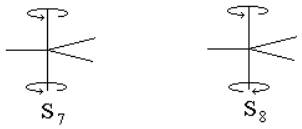

Figure IV-26. Representation of the two degenerate vibrations S_7 and S_8

All of the symmetry coordinates of a given irrep can "couple" and the normal modes are linear combinations of them. Thus, the actual motions of Q_1 and Q_2 could be in-phase and out-of-

[5]The bending mode of CO_2 describes a similar motion so that the molecule never goes through the linear form.

phase combinations of the symmetric equatorial and symmetric axial stretches. S_8, on the other hand, is a normal coordinate since there is only one e" mode - no other coordinate of e" symmetry can be constructed! Normal coordinate calculations indicate that $Q_7 = 0.01S_5 + 0.08S_6 + 1.0\ S_7$. Which means that during this vibration, two equatorial bond lengths increase as does the bond angle between them while at the same time the angle between the axial bonds is decreasing. Refer to figure IV-27.

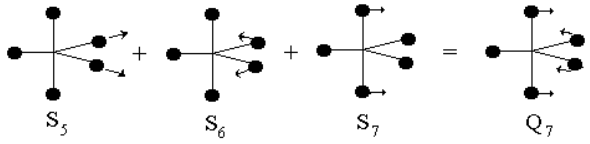

Figure IV-27. A representation of the normal coordinate Q_7 derived from a linear combination of the three e' symmetry coordinates.

IV.14. Pseudorotation in a trigonal bipyramid

Q_7 is a very low frequency mode ($\bar{\nu}_7$ = 72 cm^{-1}) so it is expected to have a large amplitude of vibration (see figure VI-1). The following discussion relates to figure IV-28. We will begin with the molecule in the equilibrium trigonal bipyramid at "A". As it moves along the Q_7 normal coordinate, the 2-3 bond angle opens up from 120°, the 4-5 angle starts to reduce from 180°, and the 2 and 3 bonds lengthen, approaching the 4 and 5 bond lengths. As this happens, the potential energy of the molecule is increasing. At point "B", the molecule has C_{4v} symmetry, *i.e.*, the 2, 3, 4 and 5 bonds are the same length and the bond angles have reached those of a square pyramid, and it has reached a maximum in energy. As the molecule passes through the square pyramid, it again approaches D_{3h} symmetry and the energy drops until at "C" a new equilibrium trigonal bipyramid is achieved. In going from "A" to "C", however, atoms 4 and 5 have gone from axial to equatorial while atom 2 and 3 have done the reverse - the molecule has undergone an axial-equatorial interconversion. This process then continues as shown and beyond. If one considers only the D_{3h} molecules in the figure and removes the labels, it appears that the molecule is simply rotating in space. This motion, therefore, is called **pseudorotation**, and the energy difference between the trigonal-bipyramid and the square pyramid is called the barrier to pseudorotation which has been determined to be 8.9 kcal/mol or about $3x10^3$ cm^{-1} in $SbCl_5$.[6]

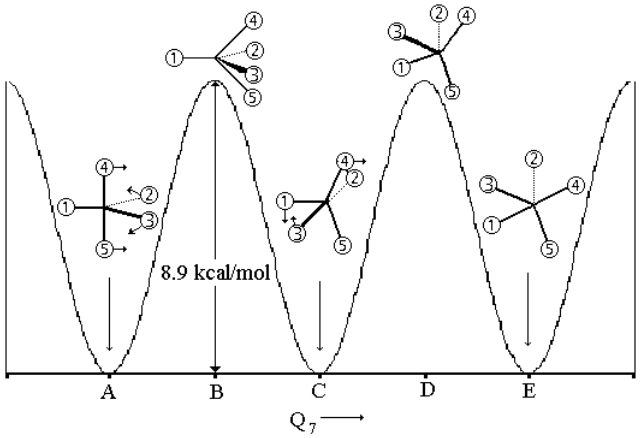

Figure IV-28. Pseudorotation of the trigonal bipyramid $SbCl_5$

[6] Holmes, Dieter and Golen, Inorg. Chem., **1969**, 8, 2612.

Problem IV.7 Three bands are observed in the infrared spectrum of $PtBr_4^{2-}$ (105, 112 and 227 cm^{-1}) and in the Raman (106, 194, 208 cm^{-1}). Only the 208cm^{-1} Raman line is polarized in solution spectra, and single crystal IR indicates that the modes at 227 and 112 cm^{-1} have the same polarization. Draw a set of symmetry coordinates describing each as ν, δ or π. Give only one component of the degenerate modes. Be certain to include the Pt motion. Assign each of the observed bands to the correct symmetry coordinate. The symmetry coordinates should be numbered consistent with convention.

IV.15 Multi-minima potential functions

The potential function which is approximated in figure IV-28 is obviously not harmonic, but neither is it Morse like. It is a multi-minimum potential function - functions like this are very important to the understanding of the molecular structure of many compounds. There are two types of multiminima potentials. Periodic minima continue in a cyclic manner (psuedorotation potential shown in figure IV-27) and potentials which have only a few minima (almost always two) before rising rapidly. We will discuss one example of each; hindered internal rotation and inversion.

The classic example of hindered rotation is that of a methyl group which is often said to be a "free rotation", but how free the rotation is depends primarily on the method used to measure it. The normal coordinate in ethane is the C-C torsion which we will measure by the angle ϕ defined as the angle between C-H bonds on the different methyl groups.

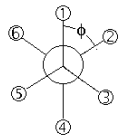

The potential energy reaches maxima whenever two bonds are eclipsed and will reach minima at the staggered conformation. The potential energy for this motion is identical in shape to that shown in figure IV-28 where $\phi = \pi/3$ at "A", $\phi = 2\pi/3$ at "B", $\phi = \pi$ at "C", etc. The barrier to internal rotation in ethane is 11.7 kJ/mol = 2.8 kcal/mol = 1.0×10^3 cm^{-1}.

The other case we want to consider is that of inversion. Inversion covers such things as a bent molecule inverting through the linear form, a pyramid going through planar and then back to a pyramid directed in the opposite direction, and an axial-equatorial conversion in a ring compound. In all of these cases, the molecule goes through a maximum energy conformation (*e.g.*, linear or planar) to reach a new minimum. The energy difference between the minimum and maximum is the **barrier to inversion**. The spectra of the vibrations which carry out these inversions are often rich[7] and informative. To understand why this is true, lets start out with a harmonic oscillator potential and place a barrier at the Q=0 position. The effect of the barrier is to increase the energy of all of the vibrational levels. The amount that these levels are increased by the barrier depends on the height and width of the barrier and the energy of the level (those at the bottom will be affected the most and those with energies well above the barrier not be affected at all). The amount of this energy change that is "felt" by a given level will also depend on the probability that the molecule can be found at Q=0. Figure IV-3, which shows the square of the vibrational wavefunctions,

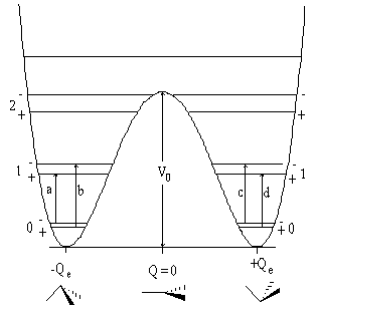

Figure IV-29. The double minimum potential function governing the inversion of NH_3. V_o is the barrier to inversion. Q_e is the equilibrium distance between the plane of the three hydrogens and the nitrogen. Lines a & b represent the ir-allowed transitions and lined c & d represent the Raman active

ergies, there is appreciable population of vibrationally excited states and a rved.

indicates that for odd values of v, there is a node at Q=0. Thus, the even levels are affected by the barrier more than are the odd levels. The eigenvalue spectrum for this system can get very irregular as v=0 approaches v=1 and v=2 approaches v=3 etc. If the barrier is "infinitely" high, these pairs of levels become degenerate and are labelled with the same value of v. To differentiate between them, a "+" or a "-" corresponding to the "+" and "-" linear combinations of two separated wells is used. As an example consider the inversion of ammonia, where the nitrogen "passes through" the plane of the three hydrogen atoms (figure IV-29).

The selection rules are + ↔ - for the IR and + ↔ + or - ↔ - for the Raman. The inversion fundamental is split in both the IR and the Raman. The IR frequencies are 931.6 and 968.1 cm^{-1} while the Raman peaks are at 934.0 and 964.3 cm^{-1}. The origin of the splitting is apparent in figure IV-29 as the IR bands correspond to a and b, respectively while the Raman bands are d and c, respectively.

The barrier to inversion is 2076 cm^{-1} (5.8 kcal/mol) in NH_3. The frequency of the $0^+ \rightarrow 0^-$ transition is called the tunnelling or inversion frequency and represents the frequency with which the two forms can interconvert without going over the barrier, *i.e.*, by tunnelling through the barrier - strictly a quantum mechanical consequence, but one that plays an important role in chemistry. For NH_3, the $0^+ \rightarrow 0^-$ transition is observed in the microwave at 0.793 cm^{-1} = 2.38×10^{10} s^{-1}. The period of inversion, $\tau = 1/\nu$ = 42 ps. Thus ammonia interconverts between the two forms on the average of once every 42 ps. It does this without going through the planar form! This frequency is very sensitive to the height of the barrier. For AsH_3, the barrier to inversion is 11,200 cm^{-1} and the period of inversion is 1.4 years.

IV.16 The use of IR and Raman spectra to deduce isomeric forms.

A combination of Γ_{vib} and the D_{3h} character table, allows us to deduce the following spectroscopic characteristics of $SbCl_5$.

Raman only	IR only	coincident	Raman polarized
3	2	3	2

If, on the other hand, $SbCl_5$ had been square pyramidal, C_{4v}, we would find that

Raman only	IR only	coincident	Raman polarized
3	0	6	3

Can we conclude that $SbCl_5$ is indeed trigonal bipyramidal based on the IR and Raman data presented earlier. When answering this question, one must be careful not to overinterpret negative results. For example, can we rule out C_{4v} since we observed only two polarized peaks where C_{4v} calls for 3? No! Remember that a totally symmetric peak may have $\rho = 3/4$. Group theoretical considerations simply indicate the number of modes that are possible not the intensities or the splittings. If two Sb-Cl bonds do not couple (not the case here) than we would see only one Sb-Cl stretch instead of the two predicted. If a KBr pellet is used, solid state effects might cause bands to split resulting in the observation of more bands than predicted. It is possible that the polarizibility or dipole change is just so small for a vibration that even though group theoretical considerations predict a non-zero dipole or polarizability matrix element, the mode may be so weak that it is not observed in either the IR or the Raman. So extreme care must be used for structural determinations with IR and Raman alone.

Care must also be taken that overtones and combinations are not counted as fundamentals. Positive evidence, however, like observing too many Raman polarized bands (no overtones) or too many coincident bands, etc. is strong support for lower symmetry forms. Thus, we can not definitely rule out the square pyramid based on these results, but we could certainly say the results were consistent with and strongly supported a D_{3h} geometry. If, on the other hand, we obtained the C_{4v} results, we could definitely rule out the D_{3h} structure. So, be careful!

As our next example, we will attempt to distinguish between the *fac*- and *mer*-isomers of $ML_3(CO)_3$ based on the CO vibrations. CO's are excellent ligands for vibrational studies since their frequencies of around 2000 cm^{-1} are removed from other fundamentals. If L=pyridine, there will be a rich IR spectrum of the pyridine ligand (just one not three since they do not couple - I(py-py) =0) and these peaks can obscure other important pieces of information and make interpretation difficult. Thus, the CO stretches are a common probe of the structure of carbonyl complexes.

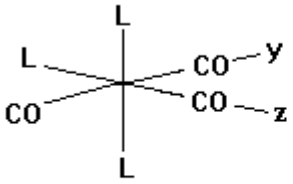

mer-

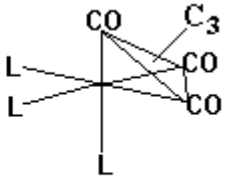

fac-

The meridial isomer has C_{2v} symmetry while the facial isomer is C_{3v}. The Γ_{vib} for the C≡O stretches is the same as Γ_{bond}

C_{2v}	E	C_2	xz	yz
Γ_{CO}	3	1	1	3

$\Gamma_{vib} = 2a_1 + b_2$
all IR and Raman active
2 Raman polarized

C_{3v}	E	$2C_3$	$3\sigma v$
Γ_{CO}	3	0	1

$\Gamma_{vib} = a_1 + e$
both IR and Raman active
1 Raman polarized

solutions

If three bands are observed in the IR and/or Raman in the 2000 cm^{-1} region, then the sample is probably the *mer*-form. However beware of:

- overtones and combinations
- very weak or missing modes that are predicted to be active
- solid state effects could split the e modes (see last section this chapter)

Consider the three isomers of SbX_2Y_3.

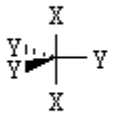

aa

D_{3h}

D_{3h}	E	C_3	C_2	σ_h	S_3	σ_v
N	6	3	2	4	1	4
Γ	18	0	-2	4	-2	4

$\Gamma_{vib} = 2a_1' + 3e' + 2a_2'' + e''$

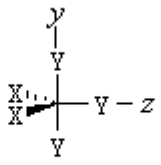

ee

C_{2v}

C_{2v}	E	C_2	yz	xz
N	6	2	4	4
Γ	18	-2	4	4

$\Gamma_{vib} = 5a_1 + a_2 + 3b_1 + 3b_2$

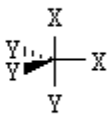

ae

C_s

C_s	E	σ
N	6	4
Γ	18	4

$\Gamma_{vib} = 8a' + 4a''$

	coinciden t	IR-only	Raman-only	polarized
D_{3h}	3	2	3	2
C_{2v}	11	0	1	5
C_s	12	0	0	8

Because the differences between the D_{3h} isomer and the other two are so great, it should be easy to identify or rule-out the D_{3h}. The C_s character table has only two irreps so there will be a large contribution to the Raman activity of totally symmetric modes from the symmetric anisotropy resulting in depolarization ratios of near 0.75. In this case, differentiation between C_{2v} and C_s would be very difficult unless more than five bands have $\rho<0.75$. Thus we could be firm in our assignment to C_s, but there is no clear way to confidently state a case for C_{2v}. If the C_{2v} results are obtained, you can only state they are consistent with C_{2v} but do not rule out C_s.

In this section, you should have learned that care is necessary in the deduction of structure from IR and Raman data and all one can usually say is that the spectra are consistent with a structure.

Problem IV.8 For each of the following, determine molecular symmetry, the number of IR & Raman active modes and the number Raman polarized lines to be expected: *cis*- and *trans*-Cl_2PtBr_2, $(N)Os(O)_3^-$ (pyramidal).

Problem IV.9 For each of the following give the symmetry or isomer of the molecule based on the information contained in the IR and Raman spectra. Be certain to indicate the degree of confidence with which you make the assignment.

a. Two A-X stretches are observed in each the IR and Raman spectra of AX_3.

b. One M-X stretch is observed at nearly the same frequency in both the IR and Raman for the trigonal bipyramidal MX_2Y_3.

c. Two C≡O stretches of $M(CO)_3L_3$ are observed in both the IR and the Raman (one polarized).

IV.17 The Vibrational Spectra of Solids.

Since such a large fraction of inorganic substances are solids it is important to have an understanding of how the spectra of solids differ from those of solutions. The most encountered effect of the intermolecular forces in the solid state is a lowering of symmetry which can lead to splitting of degenerate vibrations or giving activity to previously silent modes in the IR and Raman. Those degrees of freedom which we characterized as external degrees become **lattice modes** - the translation or rotation of one molecule in the solid becomes a vibration where the entire molecule oscillates in the crystal site. These modes are usually very low in energy depending on the mass of molecule, but combination bands of the fundamentals and these lattice modes can be observed adding complexity to the spectra.

The Bravais cell is the smallest unit in which no atom can be translated into an identical atom. It is used by the spectroscopist to determine the irreps for the lattice vibrations. It may be the same as the crystalographic unit cell, but it is only a fraction (1/R) of the crystalographic unit cell for some crystal structures. See the table of R values of space groups on the following page.

The number of molecules in the Bravais cell = the number of molecules in the crystalographic unit cell /R, i.e., $Z^B = Z/R$. Each Bravais cell contains a number of sites, each with its own site symmetry which is a subgroup of both the space group and the molecular point group.

When dealing with solids then, one needs to be concerned with three groups: the molecular point group, the space group (crystallographic symmetry) and the site groups. The space group is determined by X-ray while the site group is determined from tables of possible site symmetries and numbers of equivalent sites:

1. Halford, R.S., *J. Chem. Phys*., **1946**, 14, 8.
2. Fateley, W.G., et al., *Infrared and Raman Selection Rules for Molecular and Lattice Vibrations: the Correlation Method*, Wiley (1972).

and the two conditions:

- Site group must be a subgroup of the space group and the molecular point group.
- The number of equivalent sites must be equal to the number of ions or molecules of a given type that occupy those sites.

Table of R values of space groups.

Crystal Structure	R
A	2
B	2
C	2
F	4
I	2
P	1
R	3 or 1*

* 1 unless the number of molecules in the unit cell is divisible by 3

Cu_2O belongs to the Pn3m (O_h^4) space group and has two molecules/unit cell. The Pn3m space group in the second of the two tables referenced above contains the following entry:

	Space Group	Site Symmetries
223	Pn3m, O_h^4	$T_d(2)$; $2D_{3d}(4)$; $D_{2d}(6)$; $C_{3v}(8)$; $D_2(12)$; $C_{2v}(12)$; $3C_2(24)$; $C_s(24)$

The entry $2D_{3d}(4)$ means there are two different kinds of sites with D_{3d} site symmetry and there are four equivalent atoms or ions accomodated on these sites.

For P structures, the table above indicates that R=1 so $Z^B = 2/1 = 2$. Thus, in the Bravais cell, there are two Cu_2O molecules so there are four copper atoms and two oxygen atoms. The copper atoms must lie on one of the D_{3d} sites while two oxygen atoms must lie on T_d sites.

According to Halford, the molecular vibrations in the crystal are determined from the site group. The site group analysis on the two forms of $CaCO_3$ follows:

Calcite (marble, chalk, limestone - cold weather)
Aragonite (coral, sea shells, pearls - warm weather)

Calcite x-ray data: Space group = $\bar{R}3c = D_{3d}^6$ & Z=2.

From the table of R values, R = 1 (Z/3 is not an integer) so $Z^B = 2/1 = 2$. There are two Ca^{2+} and two CO_3^{2-} sites. From site symmetry tables in reference 2 we obtain the following sites: $D_3(2)$; $C_{3i}(2)$; $C_3(4)$; $C_i(6)$; $C_2(6)$; $C_i(12)$. The only site available to accomodate two ions are the D_3 and the C_{3i}. However the C_{3i} sites can be ruled out since they contain inversions while the molecular point group (D_{3h}) does not, *i.e.*, C_{3i} is not a subgroup of D_{3h}. Therefore, the carbonate ions lie on D_3 sites in calcite.

Aragonite x-ray data: Space group = Pnma = D_{2h}^{16} & Z = 4.

Again, R=1 so $Z^B = 4$ and there are 4 carbonates in the Bravais cell. The available sites from the reference 2 are $2C_i(4)$ and $C_s(4)$, C_i is not a subgroup of D_{3h} so the carbonates lie on the C_s sites.

The normal modes of the carbonate ion are:

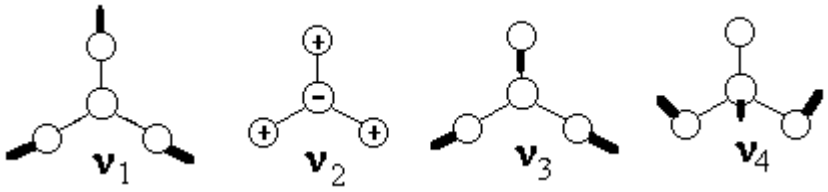

D_{3h}	a_1' (R)	a_2'' (IR)	e' (IR & R)	e'(IR & R)
D_3	a_1(R)	a_2 (IR)	e (IR & R)	e (IR & R)
C_s	a' (IR & R)	a'' (IR & R)	a' + a'' (IR & R)	a' + a'' (IR & R)

Thus lowering the symmetry down to D_3 has no effect on the spectra of the carbonate ion, and the spectrum of the calcite powder would have the same appearance as a solution of carbonate. The interactions in the aragonite powder, however, have extensive effects on the spectra as ν_1 is observed in the IR and ν_2 is also observed in the R while ν_3 and ν_4 are each split. Based on the IR and Raman spectra without the considerations of site symmetry, one would conclude that the carbon oxygen bonds of the carbonate ion in aragonite were not equivalent. Therefore, care must be taken in the interpretation of the spectra of solid samples! When dealing with oriented single crystals, one must use the factor group to deduce the lattice modes. Although this procedure is not difficult, it is somewhat tedious and will not be discussed here (refer to Fateley *et. al* reference above for the most straightforward treatment). However, there is a great deal of information contained in single crystal spectra - both IR and Raman. From polarization studies in the IR, one can determine which modes are x-allowed, y-allowed and z-allowed, i.e., the symmetries of the vibrations can be determined. Similarly, by varying the crystal orientation, the polarization of the laser, and the polarization of the light entering the monochrometer, one can determine which of the polarizability tensor elements responsible for the Raman activity of each mode. The experiments can be very difficult to do correctly, but they contain a wealth of information.

Chapter V. Vibrational Spectroscopy Part II. Examples

In this chapter, the vibrational frequencies of a number of metal-ligand modes are presented, and the effects of mass, oxidation state, and mode of bonding on them is discussed. The utility of vibrational frequencies in the elucidation of metal-ligand bonding chararacteristics are examined.

V.1 The effect of mass

Vibrational wavenumbers are frequently used in the elucidation of the relative strength of interaction between the metal and a ligand, but care must be used not to neglect the effects of mass - remember how ν(Pt-Pt) in shifted with X in X-Pt-Pt-X. Consider the following data recorded in the solid state for two linear halides:

ion	ν_s (Cl-M-Cl)	π (Cl-M-Cl)	ν_a (Cl-M-Cl)	References
$CuCl_2^-$	300	109	405	1
$AuCl_2^-$	329	120,112[(a)]	350	2

(a) The degeneracy lifted by solid state effects. See section IV.14.

In going from Cu(I) to Au(I), the symmetric stretch **increases** by 29 cm^{-1}, the bending changes only slightly and the asymmetric stretch **decreases** by 55 cm^{-1} . Which shift in frequency is indicative of the relative bonding strengths? Let's look more carefully at the three modes,

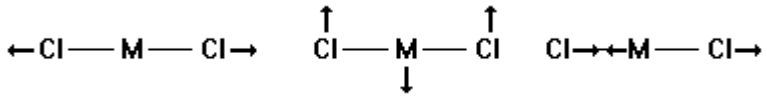

It should be apparent that both the bending and the asymmetric stretch involve motion of the metal and since the mass of gold is three times the mass of copper, a large amount of the frequency decrease in the asymmetric stretch can be attributed to a mass effect. As a result, the relative frequencies are not functions of the force constants alone. In the symmetric stretch, however, only the chlorines move so the reduced mass of the vibration (μ = m(Cl) = 35.5 amu) is the same in both ions. We can state, therefore, that the Cl-M-Cl symmetric stretching force constant in the gold complex is higher than in the copper complex. Since there is no metal movement we can write, $\nu_{Au}/\nu_{Cu} = [k_{Au}/k_{Cu}]^{½} \Rightarrow [k_{Au}/k_{Cu}] = \{329/300\}^2 = 1.2$ or the AuCl force constant is 20% higher than the CuCl force constant . In general, the **totally symmetric modes of symmetric compounds will not involve the mass of the metal atom, but care must be taken when the compound is not symmetrical or a non-totally symmetric mode is being used**.

Problem V.1 Given the symmetric stretching frequencies of the following tetrahedral complexes, indicate order of increasing force constants. $PbCl_4$ (331 cm^{-1}); $HgCl_4^{2-}$ (267 cm^{-1}) and $SnBr_4$(222 cm^{-1}).

V.2 The effect of the oxidation state of the metal

Crystal field theory predicts that as the metal becomes more positive, it attracts the electron rich ligand more tightly and thus the frequency of the M-L stretch increases. Molecular orbital theory comes to the same conclusion because either the electron that is removed is an antibonding (dσ*) and/or the d-orbitals become more energetically compatible with the σ-SALC's on the ligands as their energies drop due to the removal of electron

density. Either way, **as the oxidation state of the metal goes up, so does the M-L stretching frequency**. Consider the following table of data (cm^{-1}) for some tetrahedral species.

	$\nu_1(a_1)$ $\nu_s(MX)$	$\nu_2(e)$ $\delta_d(XMX)$	$\nu_3(t_2)$ $\nu_d(MX)$	$\nu_4(t_2)$ $\delta_d(XMX)$	Reference
$[FeCl_4]^-$	330	114	378	136	[1]
$[FeCl_4]^{2-}$	266	82	286	119	"
$[FeBr_4]^-$	200	-	290	95	"
$[FeBr_4]^{2-}$	162	-	219	84	"
$[VO_4]^{3-}$	826	336	804	-	[2]
$[VO_4]^{4-}$	818	319	780	368	[3]
$[MnO_4]^-$	834	346	902	386	[4]
$[MnO_4]^{2-}$	812	325	820	332	5
$[MnO_4]^{3-}$	789	308	778	332	[5]

V.3 Amines

The wavenumbers of the amine modes in free ammonia and several metal complexes are given below.

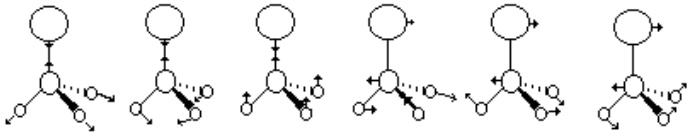

	$\nu_s(NH_3)$	$\delta_s(NH_3)$	ν(M-N)	$\nu_a(NH_3)$	$\delta_d(NH_3)$	$\rho_r(NH_3)$	Reference
$NH_3(s)$	3223	1060		3378	1646		[6]
$[Ru(NH_3)_6]Cl_2$	3210	1220	409	3315	1612	763	[7]
$[Ru(NH_3)_6]Cl_3$	3077	1368	463	3077	1618	788	[8]
$[Co(NH_3)_6]Cl_2$	3250	1163	325	3330	1602	654	[9]
$[Co(NH_3)_6]Cl_3$	3160	1329	498	3240	1619	831	[10]
$[Co(ND_3)_6]Cl_3$	2300	1020	462	2440	1165	667	[11]
$[Pt(NH_3)_4]Cl_2$	3156	1325	510	3236	1563	842	14
$[Pt(NH_3)_6]Cl_4$	3050	1370	530	3150	1565	950	[12]

Note: In octahedral amines, there are six M-N stretches ($a_{1g}+e_g+t_{1u}$). Only the IR active t_{1u} is given. $\rho_r(NH_3)$ = NH_3 rocking

As electron density is drawn into the M-N bond, it depletes the electron density in the N-H bond and weakens it. As the M-N bond strengthens due to a higher oxidation number on the metal, the N-H stretch drops even more. Thus the lower is the N-H stretch, the higher will be the M-N stretch. In addition, some of the decreases in the above table are due to hydrogen bonding to the chloride counterion.

Problem V.2 Based on the data in the previous table, which bonds more strongly to NH_3, Ru^{II} or Co^{II}. Use at least two frequencies in your discussion.

V.4 Nitro and Nitrito Complexes

Nitro complexes which are nitrogen bound to the metal and nitrito complexes which are bound through an oxygen can be distinguished by the frequencies of the NO_2 stretches. The antisymmetric NO_2 stretch in free NO_2^- ion occurs at 1250 while the symmetric stretch is found at 1355 cm^{-1}. The antisymmetric mode is only slightly higher in the nitrito complexes, but since the range in which this mode is expected badly overlaps in the two complexes, it is not very informative. The symmetric NO_2 stretch, however, is ~200 cm^{-1} lower in the nitrito. Nitro complexes can also chelate (both oxygens are bound to the metal) in which case both modes shift to lower energy.

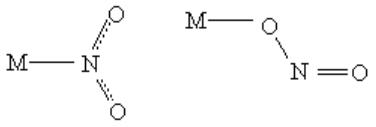

Nitro Complex	Nitrito Complex
$1470 > \nu_a > 1350$	$1485 > \nu_a > 1350$
$1340 > \nu_s > 1320$	$1110 > \nu_s > 1050$

Figure V.1. Nitro vs. nitrito linkages and expected NO stetching frequencies.

Problem V.3 Four peaks in the spectrum of $K_4[Ni(NO_2)_2(ONO)_2]$ have been assigned to NO stretching frequencies: 1387, 1347, 1325, 1206 cm^{-1}. Assign each mode.

V.5 Carbonyl Complexes

The bonding of carbonyls to metals consists of two parts:

- **Sigma bond**: The filled 5σ orbital on the CO interacts with the metal dσ orbitals stabilizing the 5σ. As mentioned in section II.5, the 5σ orbital is somewhat antibonding in character and the removal of electron density from this orbital will increase the C≡O stretching frequency slightly.
- **Pi bond**: The empty C≡O π* mixes with the metal dπ orbitals stabilizing them (back π-bonding). The mixing moves electron density from the dπ's into the C≡O π* thus reducing the C≡O order and stretching frequency.

Free CO absorbs at 2155 cm^{-1} while ν(C≡O) is found between 1800 and 2100 cm^{-1} in most metal carbonyls. The complexed frequency is *usually* less than that of free CO indicating that the CO is a good π-acid. In some instances, however, ν(C≡O) is at a higher frequency so it can also behave as a σ-donor. What then does a C≡O stretch close to 2100 cm^{-1} mean - a weak interaction or one in which the σ- and π-effects are balancing one another? The answer lies in the M-C stretching frequency since ν(M-C) will increase with either interaction. Thus the strength of the interaction is determined from ν(M-C) while the relative extent of σ *vs.* π contributions is found from ν(C≡O).

In hexacarbonyls of O_h symmetry, both the CO stretches and the M-C modes transform as $a_{1g} + e_g + t_{iu}$.

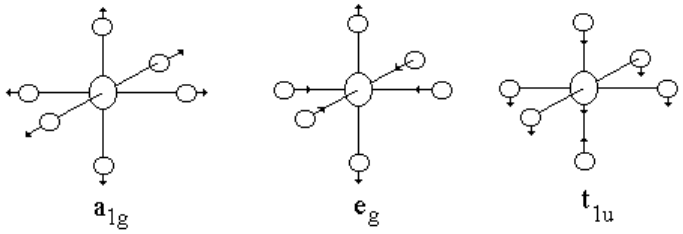

Figure V.2. The M-C stretching modes in hexacarbonyls. Only one component of each degenerate set is shown. The arrows can also can be viewed as the phases of the C≡O stretches so for the C≡O stretch of e_g symmetry, two C≡O bonds are elongating as the other four are compressing.

As can be seen in the following table, ν(C≡O) increases in the order V < Cr < Mn for all three modes (from 9 to 13% depending on the mode) indicating that either the σ-interaction is increasing and/or that the π-interaction is decreasing. The M-C modes, however, change only very slightly in the a_{1g} and e_g modes, but drop in the t_{1u} mode. Since the t_{1u} mode involves motion of the metal (figure V.2), its frequency will also reflect mass differences and thus it cannot be used directly. Our conclusion then is that the total strength of the total interaction is

	$\bar{\nu}$ (C≡O)			$\bar{\nu}$ (M-C)			
	a_{1g}	e_g	t_{1u}	a_{1g}	e_g	t_{1u}	Refs.
$[V(CO)_6]^-$	2020	1894	1858	374	393	460	13
$Cr(CO)_6$	2119	2027	2000	379	391	440	14
$[Mn(CO)_6]^+$	2192	2125	2095	384	390	412	15

about the same since ν(M-C) is essentially unchanged in the series, but the π-interaction is decreasing by about the same amount that the σ-interaction is increasing in going from V to Mn since ν(C≡O) is increasing in this series. These changes can be rationalized in terms of the change in oxidation states in the series {V(-1), Cr(0) and Mn(+1)}. The higher the oxidation state on the metal, the better it will attract σ electrons and the less likely it is to donate π electrons. In the Mn(+1) complex, the frequency actually exceeds that of free carbon monoxide and is certainly indicative of very little π-interaction.

Problem V.4 The CO stretching wavenumbers for $L_3Mo(CO)_3$ are:

L	$\bar{\nu}$ (cm^{-1})
PCl_3	1989, 2041
pyridine	1746, 1888

(a) What are the relative π-accepting abilities of CO, pyridine and phophorous trichloride in $L_3Mo(CO)_3$?

(b) Would the CO stretches in $Mo(CO)_6$ be expected above 2000 cm^{-1}, in the 1800 to 2000 cm^{-1} range or below 1900 cm^{-1}?

(c) Which would have a higher CO stretching frequency $Ni(CO)_4$ or $[Fe(CO)_4]^{2-}$?

V.6 Cyano complexes

The bonding in cyano complexes is analagous to that in carbonyls. The C≡N and M-C stretches again serve as indicators of relative σ- / π-bonding and total interaction, respectively. The C≡N stretch in free cyanide is at 2080 cm^{-1}. In general, C≡N is a better σ-

donor and poorer π-acceptor than CO, thus, unlike the carbonyls, the cyano complexes *usually* involve shifts in ν(C≡N) to higher energy upon complexation with the result that the C≡N stretching frequency is generally in the range of 2000 to 2200 cm^{-1}. Both carbonyls and cyanides are excellent compounds to study vibrationally because their frequencies are isolated from the spectrum of the rest of the rest of the compound. This isolation also implies that they do not couple with other modes (coupling of modes depends on the modes being relatively close in energy) so we can, to a good approximation, calculate the C≡N force constant from $k = (\bar{\nu}/130.3)^2\mu = (\bar{\nu}/130.3)^2(6.46)$. For example,

	$Ni(CN)_4^{2-}$	$Pd(CN)_4^{2-}$	$Pt(CN)_4^{2-}$	KCN	
ν(C≡N)	2128	2143	2150	2080	cm^{-1}
k	1723	1747	1759	1646	N/m

In the above series, all frequencies are higher than free cyanide and therefore represent a predominatly σ-effect with the effect being the greatest in platinum. Thus, in terms of σ-acceptor abilities, Pt(II) > Pd(II) > Ni(II), the same order as their electronegativities, *i.e.*, the more electronegative the metal, the higher will be the C≡N stretching frequency.

Problem V.5 Given the following force constants, arrange Fe^{III}, Fe^{II}, Ru^{II} and Os^{II} in order of increasing strengths as a σ-acceptors and as π-donors.

	$K_3Fe(CN)_6$	$K_4Fe(CN)_6$	$K_4Ru(CN)_6$	$K_4Os(CN)_6$	
k(C≡N)	1700	1510	1530	1490	N/m
k(M-C)	170	240	280	330	N/m

Problem V.6 Account for the following trend.

.	$Ag(CN)_4^{3-}$	$Ag(CN)_3^{2-}$	$Ag(CN)_2^{-}$
ν(C≡N)	2092	2105	2135

Problem V.7 The M-N stretching frequencies of high spin $Mn(bpy)_3^{2+}$ (224 & 191 cm^{-1}) are over 150 cm^{-1} lower than those of low spin $Fe(bpy)_3^{2+}$ (386 & 376 cm^{-1}). Explain.

Problem V.8 Consider the bimetallic complex shown below.

a. What are the oxidation states on the tungstens at the A and B ends respectively?

b. Based on these oxidation states, which tungsten is predicted to be more electron rich?

c. $\bar{\nu}$(CN) in free 1,4-diisocyanobenzene is observed at 2128 cm^{-1}. $\bar{\nu}$(CN) is observed at 2141 cm^{-1} on the A side and at 2092 cm^{-1} on the B side[16] of the bimetallic complex. What conclusions can be drawn about the relative amount of electron density on the metals from the CN stretching frequencies?

d. Justify this experimental conclusion with the relative amounts of electron densities predicted from the oxidation states.

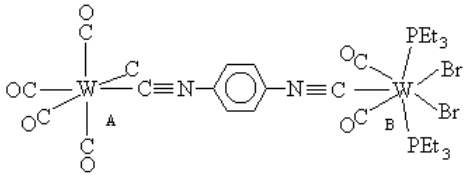

V.7. Nitrosyl complexes

NO has an unpaired electron in the 2pπ* orbital and the N≡O stretch is at 1876 cm^{-1}. Removal of the antibonding electron makes the much more stable nitrosonium ion (NO^+) with

an N≡O stretch near 2200 cm^{-1}. As in the two previous cases, it is both a σ-donor and a π-acceptor toward metals. As shown in figure V.3, these complexes can be either linear or bent,

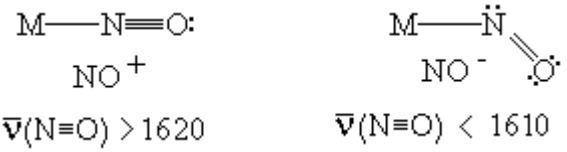

Figure V.3. NO^+ vs. NO^- bonding and expected NO frequencies.

In the linear form, the NO is a 10 electron ligand (M-N bonding electrons go to the N) which makes it NO^+ with a higher N≡O stretching frequency expected. In the bent form, it is a 12 electron ligand and thus NO^- since the additional electrons will be in π* orbitals, the NO bond order drops to two with a corresponding drop in the N=O stretching frequency. As a rough rule of thumb, **if the NO stretch is above 1620 cm^{-1} it is the linear form and if it is below 1610 cm^{-1} it is bent**.

Problem V.9 PbF_2 forms adducts with both NO and CO. In the case of the CO adduct, ν(PbF_2) decreases by 11 cm^{-1} while ν(CO) increases by 38 cm^{-1}. For the NO complex, ν(PbF_2) drops by 9 and while ν(NO) increases by 16 cm^{-1}. Discuss what these results imply about relative σ-donor and π-acceptor abilities of NO *vs.* CO.

Problem V.10 Predict the relative ease of reduction in a series of nitrosyls in which the N≡O stretching frequency is increasing. Use an energy level diagram in an explanation.

V.8 Monolefin Complexes

As the last example of the use of vibrational spectroscopy in the elucidation of σ- vs π-bonding we will look at the olefin complexes of platinum and palladium. In these complexes, the plane of the olefin is parallel to the XZ plane with the C=C bond perperdicular to the $PtCl_3$ plane. Zeise's anion, $[Cl_3Pt(C_2H_4)]^-$, the simplest of these complexes, is shown below. It should be noted that there are two different coordinate systems that can be used in cases like this: according to symmetry considerations, the principle axis of rotation should be the z-axis, but inorganic chemists prefer the z-axis to be perpendicular to the $PtCl_3$ plane. In order to avoid discussing x^2 and y^2-z^2 orbitals, we will follow the latter convention (figure V.4).

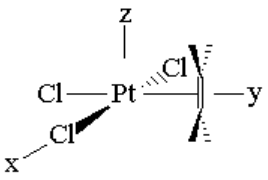

Figure V.4. Coordinate system used for Zeise' anion

As shown in figure V.5, the olefin can act as both a σ-donor (A) by donating electron density from its π-bonding orbital into the empty x^2-y^2 or dsp^2 orbital on the metal or as a π-acceptor (B), by accepting electron density from the filled metal yz into its empty π* orbital.

Both of these actions will lower the C=C bond order and therefore the C=C stretching frequency.

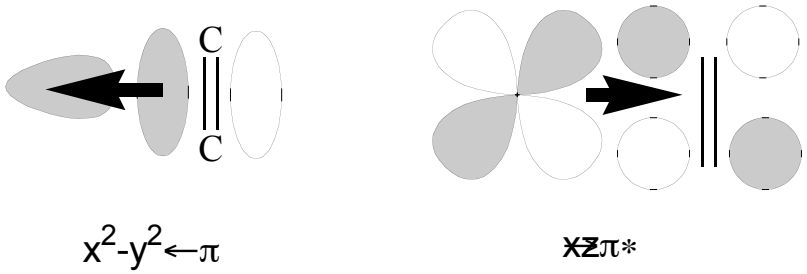

Figure V.5. Sigma and pi portions of the metal-olefin bond. Arrow indicates direction of electron density movement.

One assignment[17] of Zeise's salt put $\Delta\bar{\nu}$(C=C) at about -100 cm^{-1} upon complexation (from 1623 in free ethylene down to 1526 cm^{-1} in the salt). A major problem with the ethylene study is that the C=C stretch is strongly coupled to the CH_2 deformation and it is difficult to decouple the two effects. Also a shift of about 6.3% certainly indicates interaction, but it does little to elucidate the nature of the bonding (σ *vs.* π). Several years later, the vibrational spectra of the cyclopentene complexes of platinum and palladium[18] were reported. In this study, the σ- and π-interactions were distinguished based on other modes that proved to be sensitive to electron density in the π-component of the bond (figure V.6). These modes consisted of the out-of-plane motions of the olefinic C-H's and the motions of the olefin relative to the metal.

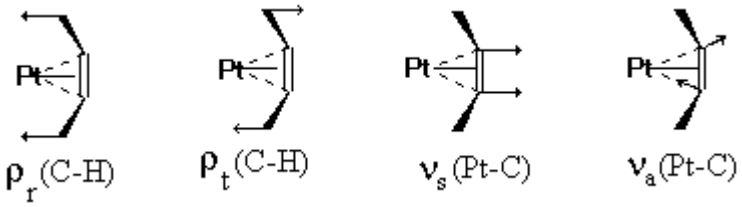

Figure V.6. Modes of the olefin expected to be sensitive to π electron density.

Palladium does not form a monomeric analog to Zeise's salt but does form a chlorine bridged dimer. So that comparisons of the two metals can be made, the data for the dimer is given for both Pt and Pd. The ir spectra of $[M(C_5H_8)X_2]_2$ (M=Pt, Pd; X=Cl,Br) are shown in figure V.7.

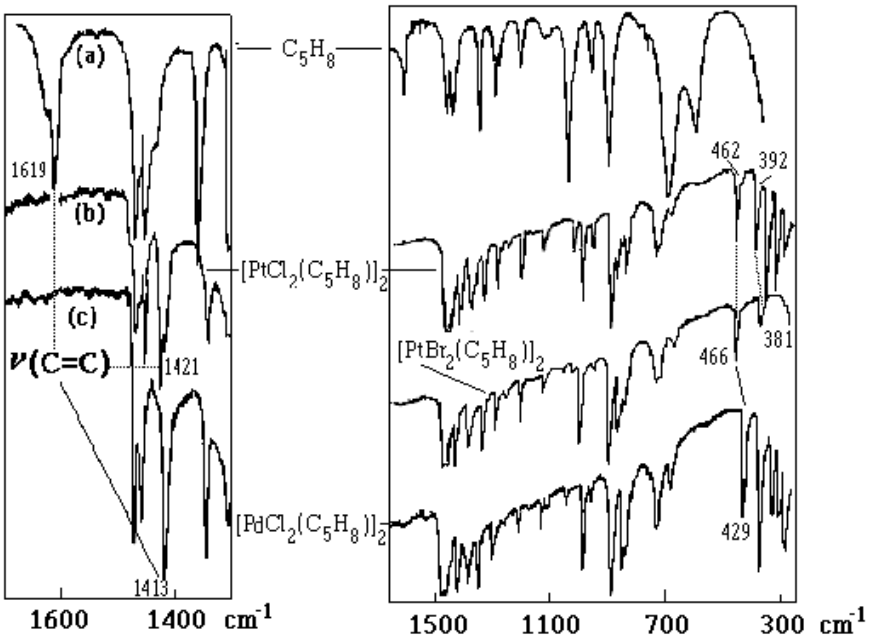

Figure V-7. The ir spectra of cyclopentene and several cyclopentene complexes of Pt(II) and Pd(II).

The frequencies pertinent to the nature of the bond.

mode	C_5H_8	$[Pt(C_5H_8)Cl_2]_2$	$[Pd(C_5H_8)Cl_2]_2$
ν(C=C)	1619	1421	1413
ρ_r(CH)	858	872	838
ρ_t(CH)	698	737	728
ν_a(M-C)		462	
ν_s(M-C)		392	429

The shift in the C=C stretch is almost doubled from what it was in the ethylene complex due to a combination of a very strong interaction with the metal and to less coupling with the CH deformation which hardly shifts upon complexation. The shift is somewhat greater for the palladium complex. Indeed, most of the cycolpentene *peaks which shift to lower energy shift farther in palladium* while those *peaks which shift to higher energy shift farther in platinum.* The peaks shifting to lower energy are indicative of loss of the double bond character in the cyclopentene, while those modes shifting to higher energy involve moving olefinic hydrogens into the region of π density between the metal and olefin. For the CH rocking, the shift is +14 for Pt and -20 cm^{-1} for Pd. The implication then is that there is more π-density in the Pt analog which serves as a barrier to the motion of the H into this region thus increasing the frequency. The most telling information, however, is in the low energy region. The mode labelled ν_a in figure V.6 would indeed be an asymmetric stretch in the case of extensive π-interaction and would therefore be expected in the region of the other Pt-C stretch, ν_s. If, on the other hand, there is little or no π density, then this mode would be a very low energy twist. The fact that two modes are observed in the Pt-C stretching region while only one is observed in the Pd-C stretching region certainly argues in favor of much more π-interaction in the Pt complex. It was therefore concluded that in Pt and Pd the total interaction was comparable since $\Delta\bar{\nu}$(C=C) is the same, but the π interaction in Pt was far greater than in Pd. Thus, $Pt_\pi > Pd_\pi$ but $Pd_\sigma > Pt_\sigma$.

V.9 Metal Ligand Multiple Bonds

The oxo and nitrido ligands are both closed shell and very electronegative. Thus multiple bond formation requires empty d-orbitals which are low in energy, *i.e.*, metals in high oxidation states. Thus, the vast majority of these complexes are with d^0, d^1 and d^2 metals. The bond is between a highly positive metal and a very negative ion so that the metal-oxo and metal-nitrido stretch will involve large changes in dipole moment and result in strong IR absorption. Characterization of the complexes therefore is often done with infrared. In addition, their motions are not usually coupled to the motions of the other atoms and may be treated as diatomic vibrators to good approximation. As a result, isotopic substitution of ^{18}O and ^{15}N have predictable effects on the stretching frequencies which aids in their assignment. The following ranges are found to be generally reliable

- M=O stretches[19] lie in the range of 900 to 1100 cm^{-1}
- M-O-M stretches[21] are found between 800 and 900 cm^{-1}
- M≡N stretches[20] lie between 1020 and 1150 cm^{-1}

Some examples are given in the following tables.

M=O stetching frequencies (cm^{-1}) in monoxo metal complexes

Complex	$\nu(^{16}O)$	$\nu(^{18}O)$	Reference
Cr(O)Cl(tpp)	1026	982	[21]
Mn(O)(tpp)	1060	1000	[22]
Fe(O)(tpp)	852	818	[23]
$[Ru(O)(bpy)_2(py)](ClO_4)_2$	792	752	[24]

M≡N stretching frequencies (cm^{-1}) in some metal nitrido complexes

Complex	$\nu(^{14}N)$	$\nu(^{15}N)$	Reference
Cr(N)(tpp)	1017	991	[25]
Mn(N)(tpp)	1036	1008	[26]
$K[Os(N)O_3]$	1026	995	[27]
$Ph_4As[Os(N)Cl_4]$	1123	1087	[28]
$Cs_2[Os(N)Cl_5]$	1073	1040	[29]
$Cs_2[Os(N)Br_5]$	1073	1040	"

tpp = the tetraphenyl porphyrin dianion

The reduced mass of the $Mn=^{16}O$ stretch is 12.4 amu while that of the $Mn=^{18}O$ stretch is 13.6 amu thus in the diatomic limit, $\nu(Mn=^{16}O)/\nu(Mn=^{18}O) = [13.6/12.4]^{½} = 1.05$ in good agreement with the 1.06 observed in Mn(O)tpp. For the Ru=O stretch, the reduced masses are 13.8 and 15.3 so that $\nu(Ru=^{16}O)/\nu(Ru=^{18}O) = 1.05$ which is also the observed value. So the use of isotopic substitution can be a vaulable tool in the assignment of these modes, but care must be taken with imido complexes (M=N-R) where the M=N stretch often couples with the N-R stretch and with some of the skeletal modes of R .

Addition of a second oxo to the complex reduces the frequency of ν(M=O) as both oxygens compete for the dπ electrons. This effect is much greater when the oxygens are *trans*. Thus, ν(M=O) lies in the range of 768-895 cm^{-1} for the *trans* dioxo complexes and in the range of 862-1025 cm^{-1} for the other dioxo complexes. In the *trans*-complexes, the O=M=O unit is linear with a center of inversion so the symmetric stretch will be independent of the metal mass and will be observed only in the Raman while the asymmetric stretch will be dependent on the mass of the metal and will be observed only in the ir.

V.10 Metal-Metal bonds

Due to the large masses and relatively weak interactions involved in M-M bonding, the ν(M-M) is generally quite low (100-250 cm^{-1}). Due to the symmetric nature of the bond the metal-metal stretching vibrations are usually quite weak in the ir but very strong in the Raman.

Compound	$\bar{\nu}$ (M-M)	Reference
$Mn_2(CO)_{10}$	160	[30]
$Tc_2(CO)_{10}$	148	"
$Re_2(CO)_{10}$	122	"
$(CO)_5Re\text{-}Mn(CO)_5$	157	"
$[Mo_2Cl_8]^{4-}$	345	[31]
$[Re_2Cl_8]^{2-}$	272	[32]

Many of the interesting features of metal-metal multiple bonds involve electronic and resonance Raman results so further discussion of these species will be postponed until later.

Problem V.11 What are the Re-Re force constants in $Re_2(CO)_{10}$ and $[Re_2Cl_8]^{2-}$? Assume that the Re-Re stretching vibration is isolated from the other modes (probably not a very good assumption for $[Re_2Cl_8]^{2-}$). Discuss the bonding in the two complexes based on these results. Be thorough!

References

[1] Avery, J.S.; Burbridge, C.D.; Goodgame, D.M.L., Spectrochim. Acta, 1968, 24A, 1721.
[2] Weinstock, M.; Schulze, H.; Müller, A., J. Chem. Phys., 1973, 59, 5063.
[3] Gonzalez-Vilchez, F.; Griffith, W.P., J. Chem. Soc., Dalton Trans., 1972, 1416.
[4] Homborg, H.; Preetz, W., Spectrochim Acta, 1976, 32A, 709.
[5] Baran, E.J.; Manca, S.G., Spectrosc. Lett., 1982, 15, 455.
[6] Reding, F.P.; Hornig, D.F., J. Chem. Phys., 1951, 19, 594. & 1954, 22, 1926.
[7] Deak, A.; Templeton, J.L., Inorg. Chem., 1980, 19, 1075.
[8] Griffith, W.P., J. Chem. Soc. A, 1966, 899.
[9] Shimanouchi, T.; Nakagawa, I., Inorg. Chem., 1964, 3, 1805.
[10] Long, T.V.; Herlinger, A.W.;Epstein, E.F.; Bernal, I., Inorg. Chem., 1970, 9, 459.
[11] Schmidt, K.H.; Müller, A., J. Mol. Struct, 1974, 22, 343.
[12] Hiraishi, J.; Nakagawa, I.; Shimanouchi, T., Spectrochim. Acta, 1968, 24A, 819.
[13] Abel, E.; McLean, R.; Tyfield, S.; Braterman, P.; Walker, A.; Hendra, P., J. Mol. Spectrosc., 1969, 30, 29.
[14] Jones, L.H.; McDowell, R.S.; Goldblatt, M., Inorg. Chem. 1969, 8, 2349.
[15] McLean, R.A.N., Can. J. Chem., 1974, 52, 213.
[16] Grubish, D.S.; Rommel, J.S.; Lane, T.M.; Tysoe, W.T.; Bennett, D.W. *Inorg. Chem*., **1992**, 31, 5022.
[17] Grogan, M.J.; Nakamoto, K., J. Am. Chem. Soc., 1966, 88, 5454.
[18] Wertz, D.W.; Bocian, D.F.; Hazouri, M.J., Spectrochim. Acta, 1973, 29A, 1439.
[19] Barraclough, C.G.; Lewis, J.; Nyholm, R.S., J. Chem. Soc., 1959, 3552.
[20] Griffith, W.P., Coord. Chem. Rev., 1972, 8, 369.
[21] Groves, T.J.; Kruper, W.J., J. Am. Chem. Soc., 1979,18,984.
[22] Willner, I.; Otvos, J.W.; Calvin, M., J. Chem. Soc. , Chem Comm., 1980, 964.
[23] Bajdor, K.; Nakamot, K., J. Am. Chem. Soc., 1984, 106,3045.
[24] Moyer, B.A.; Meyer, T.J., Inorg. Chem, 1981, 20, 436.
[25] Groves, T.J.; Takahashi, T.; Butler, W.M., Inorg. Chem., 1983, 22, 884.
[26] Hill, C.L.; Hollander, F.J., J. Am. Chem. Soc., 1982, 104, 7318.
[27] Schmidt, K.H.; Flemming, V.; Müller, A., Spectrochim. Acta, Part A, 1975, 31, 1913.
[28] Collin, R.J.; Griffith, W.P., Pawson, D., J. Mol. Struct., 1973, 19, 531.
[29] Griffith, W.P.; Pawson, D.J., J. Chem. Soc., Dalton Trans., 1973, 1315.
[30] Quicksall, C.O.; Spiro, T.G., Inorg. Chem., 1969, 8, 2363.
[31] Angell, C.L.; Cotton, F.A.; Frenz, B.A.; Webb, T.R., Chem. Commun., 1973, 399.
[32] Clark, R.J.H.; Franks, M.L., J. Am. Chem. Soc., 1976, 98, 2763.

Chapter VI. Electronic Spectroscopy
Part I. Theory

The wavefunctions pertinent to the study of electronic spectroscopy depend on the occupied electronic orbitals, the nuclear coordinates and the electron spin. To a zero order approximation, these three contributions are separable, $\Psi = \psi_{mo}\psi_{vib}\psi_{spin} = |n\rangle|v\rangle|s\rangle$. $\psi_{mo} = \Pi\phi_{mo}$ where ϕ_{mo} is the wavefunction for a single electron molecular orbital, *i.e.*, the overall orbital wavefunction is the product of the occupied one electron wavefunctions. There are many instances where such zero order approximations fail to account for the observed spectral properties of the system and spin-orbit coupling and/or vibronic coupling are invoked as perturbations to the zero-order approximation.

Electronic transitions involve changes in molecular orbitals but, due to possible changes in the spin and/or vibrational levels, they are not simply orbital transitions. Spectroscopically, we measure ΔE, the energy difference between two *states* and the state of a molecule is not given by its orbital occupancy alone - the vibrational and spin states are also required to define the states involved in a typical electronic transition.[1] The $\phi_a \rightarrow \phi_b$ orbital transition can be viewed as the removal of an electron from ϕ_a followed by the addition of an electron to ϕ_b which, according to Koopman's theorem would be approximated as the ionization energy of ϕ_a minus the electron affinity of ϕ_b , *i.e.*, the orbital energy difference. However, this fails to take into account the fact that after the electron is removed, all orbitals will be stabilized and the orbital energy of ϕ_b will change.

Spectroscopic transitions involve changes in states not simply orbitals.

VI.1 Electron spin

The electron has a half-integral spin and as such is a Fermion which means that its wavefunction must be antisymmetric with respect to exchange of identical particles, but this wavefunction is a product of orbital and spin functions. In addition, since the particles are identical, the wavefunction cannot distinguish between them. Consider two electrons (1 & 2) in two mo's (a & b). The wavefunction $\phi_a(1)\phi_b(2)$ would be unacceptable because it is neither symmetric nor anti-symmetric with respect to exchange of identical particles, $\phi_a(1)\phi_b(2) \neq \pm \phi_a(2)\phi_b(1)$. Stated another way, the two electrons can be distinguished since electron 1 is the electron in orbital ϕ_a. Thus, *symmetrized* and *anti-symmetrized* wavefunctions are constructed:

$$\psi_s = \frac{1}{\sqrt{2}}\left(\phi_a(1)\phi_b(2) + \phi_a(2)\phi_b(1)\right) \quad \text{and} \quad \psi_a = \frac{1}{\sqrt{2}}\left(\phi_a(1)\phi_b(2) - \phi_a(2)\phi_b(1)\right)$$

The operation which exchanges two electrons i and j is called the permutation operator P_{ij}. Operating on the above two wavefunctions with P_{12} yields,

$$P_{12}\psi_s = \frac{1}{\sqrt{2}}\left(\phi_a(2)\phi_b(1) + \phi_a(1)\phi_b(2)\right) = \psi_s \quad \text{and} \quad P_{12}\psi_a = \frac{1}{\sqrt{2}}\left(\phi_a(2)\phi_b(1) - \phi_a(1)\phi_b(2)\right) = -\psi_a$$

or ψ_s is symmetric and ψ_a is antisymmetric with respect to exchange. But this is only half of the wavefunction, we still need to consider the electron spin. There are four possibilities for two electrons in two spin orbitals: $\alpha(1)\alpha(2)$, $\beta(1)\beta(2)$, $\alpha(1)\beta(2)$ and $\beta(1)\alpha(2)$. The first two

[1] Depending on the type of spectroscopy involved, other states (nuclear spin, rotational,etc.) might be required in the state designation.

are symmetric with respect to exchange, but the latter two are neither symmetric nor antisymmetric - they allow for distinction between the two electrons and are not acceptable spin functions. Linear combinations must again be taken for the latter two. The four acceptable spin functions and their symmetries with respect of exchange of identical particles are:

$$\alpha(1)\alpha(2); \quad \beta(1)\beta(2); \quad \frac{1}{\sqrt{2}}\left(\alpha(1)\beta(2)+\beta(1)\alpha(2)\right) \quad - \text{ symmetric}$$

$$\frac{1}{\sqrt{2}}\left(\alpha(1)\beta(2)-\beta(1)\alpha(2)\right) \quad - \text{ antisymmetric}$$

The *electronic wavefunction must be antisymmetric*, so the symmetric orbital wavefunction, ψ_s, must be combined with the antisymmetric spin function and since there is only one antisymmetric spin function, this combination is the "singlet" state. The antisymmetric orbital wavefunction, ψ_a, must be combined with the symmetric spin function. There are three symmetric spin functions, and the resulting three combinations are the components of the "triplet" state. Note that the product of the two functions (orbital x spin) is often referred to as an electronic **state**. One orbital transition can be responsible for several state transitions.

In general, the electron spin is determined as $S = \Sigma m_s$ where $m_s = \pm 1/2$ (α or β), but, since $\Sigma m_s = 1/2\text{-}1/2 = 0$ for all paired electrons, we need sum only over unpaired spins. The multiplicity (degeneracy) of a spin state is 2S+1 so five unpaired electrons gives rise to a multiplicity of 2(5/2)+1= 6, a sextet. For two unpaired electrons one has S=1 and 2S+1=3, the triplet discussed above. If all electrons are paired, S=0, a singlet.[2]

VI.2 States

VI.2a State Energies

Since the Hamiltonian is not a function of spin coordinates, the energies of the triplet and singlet states of the $\phi_a^1\ \phi_b^1$ configuration depend only on the space portions of the wavefunctions: $\psi = \phi_a(1)\phi_b(2) \pm \phi_b(1)\phi_a(2)$ ["+" for singlet and "-" for triplet] and are

$$E_1 = E(\phi_a) + E(\phi_b) + J + K \text{ and } E_3 = E(\phi_a) + E(\phi_b) + J - K$$

where $E(\phi_a)$ is the orbital energy of ϕ_a, J is the Coulomb integral and K is the exchange integral. Both J and K are positive. The only difference between these two expressions is the $\pm K$ which results due to "±" in the wavefunctions. Thus, the separation between the singlet and triplet states is $E_1 - E_3 = 2K$, *i.e.*, **the singlet is 2K higher in energy than the triplet**. Both J and K are matrix elements of the repulsion operator, e^2/r, where r is the electron-electron distance and e is the charge on the electron.

Coulomb integral: $J = \langle\phi_a(1)\phi_b(2)|\ e^2/r\ |\phi_a(1)\phi_b(2)\rangle$ shows electrons 1 & 2 as being in "charge clouds" described by $\phi_a^*\phi_a$ and $\phi_b^*\phi_b$ and represents the Coulombic repulsion of the two electrons.

Exchange integral: $K = \langle\phi_a(1)\phi_b(1)|\ e^2/r\ |\phi_a(2)\phi_b(2)\rangle$ shows each electron in both orbitals. There is no classical analog to the exchange integral, but it can be viewed as a quantum mechanical correction to the repulsion term which will depend on the overlap between ϕ_a and ϕ_b. Electrons in a triplet state avoid one another at small electron-electron distances, *i.e.*, $\lim_{r\to 0} \psi_a^2 = 0$ - this is referred to as a "Fermi hole". ψ_s^2, on the other hand, reaches a maximum at $r^2 = 0$ - a "Fermi heap". Thus, the electrons in a singlet spend

[2] Since 2S is the number of unpaired electrons, the easiest way to get the multiplicity is the number of unpaired elecrons + 1

appreciable time in close proximity while the electrons in the triplet avoid close proximity. As a result, the time averaged Coulombic repulsions are higher than J by an amount K in the singlet and reduced from J by an amount K in the triplet. The fact that the triplet lies lower than the singlet is summarized by **Hund's first rule**: the ground state is that state derived from the lowest energy orbital occupancy with the highest spin multiplicity. **Hund's second rule** states that any ambiguities that arise from application of the first rule are resolved by choosing the highest orbital angular momentum (L) state as the ground state. Finally, **Hund's third rule** states that if two states have the same S and L values, the state with the smallest total angular momentum (L+S) is lowest energy for subshells that are less than half-filled, and the state with the largest total angular momentum (L+S) is lowest energy for subshells that are more than half-filled.

In addition to the electron exchange interaction, there can also be a spin-spin (dipolar) interaction which can lift the 2S+1 degeneracy of a spin state. A charged particle with spin generates a magnetic field (the basis of ESR and NMR) in a direction which depends on the "sense of the spin" so that the magnetic fields generated by paired electrons (S=0) cancel. The magnetic fields of unpaired electrons, however, can interact so that the spin of one electron is affected by the spin of the other. The corrections to the electronic energy are given in terms of the **zero field splitting**, **D**, and another parameter, **E**, defined in figure VI-0. These *corrections* are given as:

$$E_x = D/3 - E \quad ; \quad E_y = D/3 + E \quad ; \quad E_z = -2D/3.$$

The resulting energy level pattern will depend on the molecular symmetry as shown in figure VI-0. These are small corrections (D is typically less than 10 cm^{-1}) and are not observed in the electronic spectrum, but emission of transition metal complexes is often from a high spin state and the effects of these multiple states is sometimes observed.

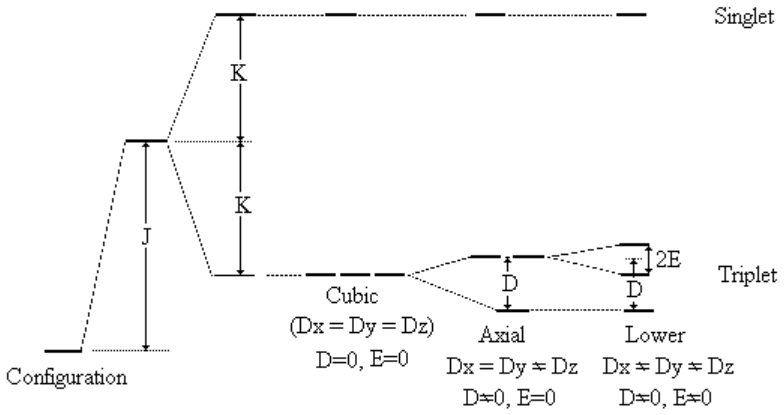

Figure VI-0. The energies of the singlet and tiplet states relative to that of the configuration. The zero-field splitting, D, resulting from interaction of the two spins in the triplet is also defined.

If different configurations give rise to states of the same symmetry the configurations can mix. This mixing is referred to as *configuration interaction* (CI). As with any mixing, the extent of configuration interaction will depend on the energy compatibility of the two states. This mechanism is sometimes used to give the ground state some properties of low lying excited states and is also invoked to explain the spectra of porphyrins (section VII.5).

VI.2b State Designations

An approximate orbital energy diagram for benzene is given in figure VI-1. Since benzene has six π electrons, the electron configuration for the ground state orbital occupancy is $(a_{2u})^2(e_{1g})^4$. In addition, Figure VI-1 also shows the four orbital transitions for this π-system. In this section, the states that are derived from each of these five orbital configurations will be determined. Remember that **capital letters are used for state designations**.

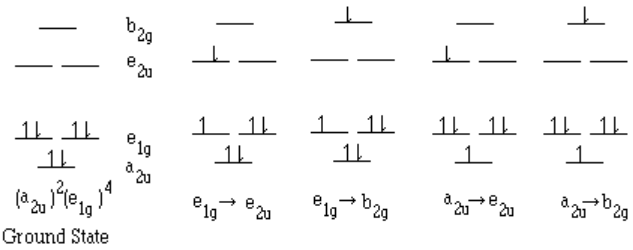

Figure VI-1. Orbital occupancies for the ground state and ππ* excited states of benzene.

The state symmetry is simply the product of all of the one-electron orbital symmetries, thus a filled orbital is totally symmetric ($\Gamma_i \otimes \Gamma_i = A_1$). Orbital configurations fall into four cases.

Case I. **All orbitals are filled**.

Since all orbitals are filled, there are no unpaired electrons so S=0 and the state is a singlet. The electron density in a completely filled orbital carries the full symmetry of the molecule, *i.e.*, it is totally symmetric. Thus, the ground state of benzene is $^1A_{1g}$ - singlet A_{1g}.

Case II. **A singly occupied orbital** with all others filled.

All filled orbitals are totally symmetric so the state symmetry will be that of the singly occupied orbital. Since there is only one unpaired electron, S=1/2 so the multiplicity is 2, a doublet. For example, if benzene were ionized to the $(a_{2u})^1(e_{1g})^4$ configuration, the resulting state would be $^2A_{2u}$.

Case III. **Two singly occupied orbitals excluding two orbitals which are degenerate.**

The state symmetry is the direct product of the two orbital symmetries. Two electrons implies both singlet and triplet states are possible. The orbital transition $a_{2u} \rightarrow b_{2g}$, results in an orbital occupancy of $(a_{2u})^1(e_{1g})^4(b_{2g})^1$ which gives rise to a state with the symmetry of the direct product of $a_{2u} \otimes b_{2g} = b_{1u}$ since the $(e_{1g})^4$ must be a_{1g}. Thus, two possible states can be derived from this orbital transition, $^3B_{1u}$ and $^1B_{1u}$ (triplet lower in energy).

The exclusion of two orbitals which are degenerate precludes only that case where the two electrons are in **the same degenerate orbital** (due to Pauli exclusion considerations - Case IV) but does not include two electrons in different degenerate orbitals. Since the direct product $e_{1g} \otimes e_{2u} = b_{1u} + b_{2u} + e_u$, six states are derived from the $e_{1g} \rightarrow e_{2u}$ transition ($^1B_{1u} + ^3B_{1u} + ^1B_{2u} + ^3B_{2u} + ^1E_u + ^3E_u$) with a total degeneracy of 16 = (1+3+1+3+2+6). This is consistent with the fact that there are 16 ways of representing this situation.

	e_{1g}		e_{2u}			e_{1g}		e_{2u}	
	a	b	a	b		a	b	a	b
1	∅ ↑	↓ ↑	↓		9	↓ ∅	↓ ↑	↓	
2	∅ ↑	↓ ↑		↓	10	↓ ∅	↓ ↑		↓
3	∅ ↑	↓ ↑	↑		11	↓ ∅	↓ ↑	↑	
4	∅ ↑	↓ ↑		↑	12	↓ ∅	↓ ↑		↑
5	↓ ↑	∅ ↑	↓		13	↓ ↑	↓ ∅	↓	
6	↓ ↑	∅ ↑		↓	14	↓ ↑	↓ ∅		↓

7	↓ ↑	∅ ↑	↑		15	↓ ↑	↓ ∅	↑	
8	↓ ↑	∅ ↑		↑	16	↓ ↑	↓ ∅		↑

Note that holes (∅ or h^+) can be treated like electrons so $(e_{1g})^3$ which has a single hole is the same as $(e_{1g})^1$. The above problem can be viewed as a one electron, one hole problem.

The above cases cover all of the possibilities for benzene and a state diagram can now be constructed. The lowest energy orbital transition is the $e_{1g} \rightarrow e_{2u}$, HOMO → LUMO, which gives rise to six states: three singlets and three triplets. The three lowest lying singlet states are therefore the B_{2u}, B_{1u} and E_{1u}, but we have no way to predict their order. However, spectroscopic assignments suggest the order given is that of increasing energy. The order of the states derived from the $a_{2u} \rightarrow e_{2u}$ and $e_{1g} \rightarrow b_{2g}$ is also unknown, but the highest energy state will derive from the $a_{2u} \rightarrow b_{2g}$ orbital transition. It should also be noted that the order of the triplet states does not have to be the same as that of the corresponding singlet states. Every singlet state (except the ground state) has a corresponding triplet state and transitions between singlets and triplets are "spin forbidden" so in order to simplify the diagram, the singlet and triplet states are usually placed in different columns. With these considerations in mind, the state diagram for benzene can be approximated (figure VI-2):

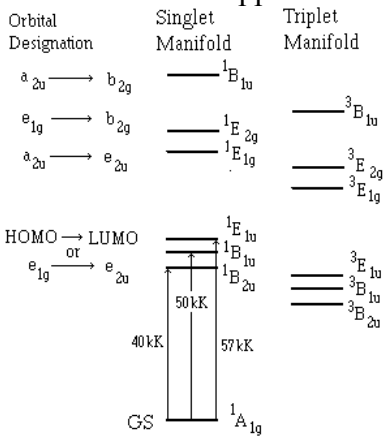

Figure VI-2. Approximate state diagram for benzene. The energies and ordering of the three lowest lying excited singlets are from uv spectra. Relative ordering of all other states is uncertain except that the highest energy state is certainly the $^1B_{1u}$.

All transitions originate from the $^1A_{1g}$ ground state irrespective of the orbital transition. The lowest energy, spin-allowed transition is the $^1A_{1g} \rightarrow {}^1B_{2u}$.

There is one more case. One that is not encountered in benzene.

Case IV. **Several electrons in a degenerate set of orbitals**.

Let us differentiate between $(e_{1g})^1(e_{1g})^1$ and $(e_{1g})^2$ configurations. The table for direct products under D_{6h} indicates that $e_1 \otimes e_1 = A_1 + [A_2] + E_2$ (g x g = g; the meaning of the square bracket will be explained shortly). If the two electrons are in different sets of e_{1g} orbitals then the derived states (Case III) are $^1A_{1g} + {}^1A_{2g} + {}^1E_{2g} + {}^3A_{1g} + {}^3A_{2g} + {}^3E_{2g}$ which yields the expected degeneracy of 16. If the electrons are in the same set of e_{1g} orbitals, $(e_{1g})^2$, the Pauli exclusion principle rules out many of these 16 possibilities. In this case there are only six possibilities.

	$e_{1g}(a)$	$e_{1g}(b)$
1	↑↓	
2		↑↓

3	↑	↑
4	↓	↓
5	↑	↓
6	↓	↑

To obey the Pauli Exclusion principle, the symmetric orbital must combine with the antisymmetric spin (singlet) and the antisymmetric orbital with the symmetric spin (triplet). We offer here without proof the characters of the symmetric (χ+) and antisymmetric (χ-) reducible representations for the two electron system:

Eq VI.1 - Two electrons in a degenerate set of orbitals

$$\chi+ = \chi(\text{singlet}) = 1/2\{[\chi(R)]^2 + \chi(R^2)\}$$
$$\chi- = \chi(\text{triplet}) = 1/2\{[\chi(R)]^2 - \chi(R^2)\}$$

As an example, consider the $(e)^2$ configuration in C_{3v}.

C_{3v}	E	$2C_3$	$3\sigma_v$
$\chi(R)$	2	-1	0
$[\chi(R)]^2$	4	1	0
R^2	E	C_3	E
$\chi(R^2)$	2	-1	2
χ(singlet)	3	0	1
χ(triplet)	1	1	-1

The irreducible representations for the singlet states are A_1 + E while the irreducible representation for the triplet is A_2. In the direct product table (Appendix B) under C_{3v}, e $\otimes$e = A_1 + [A_2] + E. Thus the two electron case is given in the direct product table and the **antisymmetric representation is given in square brackets**. The $(e)^2$ configuration in C_{3v} symmetry then results in the following states: $^1A_1 + {}^3A_2 + {}^1E$ with the expected degeneracy of six. Similarly, the $(e_{1g})^2$ configuration in D_{6h} symmetry results in $^1A_{1g} + {}^3A_{2g} + {}^1E_g$

For three electrons in a three-fold degenerate orbital, either a doublet or a quartet results, the reducible representations of which can be obtained as follows.

Eq VI-2. Three electrons in a degenerate set of orbitals

$$\chi(\text{doublet}) = 1/3\{[\chi(R)]^3 - \chi(R^3)\}$$
$$\chi(\text{quartet}) = 1/6\{[\chi(R)]^3 - 3\chi(R)\chi(R^2) + 2\chi(R^3)\}$$

These cases will handle any situation you will likely encounter. For more complicated systems, simply treat the combinations individually and then combine them. The most complicated system likely to be encountered is the high spin d^5 metal ion in octahedral symmetry, $(t_{2g})^3(e_g)^2$. First, the states derived from $(t_{2g})^3$ are determined then the states arising from $(e_g)^2$ are determined. Finally, the resulting states are combined.

$(t_{2g})^3$

O_h	E	$8C_3$	$6C_2$	$6C_4$	$3C_2'$	i	$6S_4$	$8S_6$	$3\sigma_h$	$6\sigma_d$
R^2	E	C_3	E	C_2'	E	E	C_2'	C_3	E	E
R^3	E	E	C_2	C_4	C_2'	i	S_4	i	σ_h	σ_d
$\chi(R)$	3	0	1	-1	-1	3	-1	0	-1	1

$\chi(R^2)$	3	0	3	-1	3	3	-1	0	3	3
$\chi(R^3)$	3	3	1	-1	-1	3	-1	3	-1	1
$\chi(R)^3$	27	0	1	-1	-1	27	-1	0	-1	1
χ(doublet)	8	-1	0	0	0	8	0	-1	0	0
χ(quartet)	1	1	-1	-1	1	1	-1	1	1	-1

Decomposing the reducible representations yields: $\Gamma(\text{doublet}) = E_g + T_{1g} + T_{2g}$ and $\Gamma(\text{quartet}) = A_{2g}$. Thus, the states derived from the $(t_{2g})^3$ configuration are: $^4A_{2g} + {}^2E_g + {}^2T_{1g} + {}^2T_{2g}$. The $(e_g)^2$ configuration can be determined from the direct product tables which show that for O, $e \otimes e = A_1 + [A_2] + E$ so the $(e_g)^2$ configuration results in $^3A_{2g} + {}^1A_{1g} + {}^1E_g$ states. The states of these two orbital occupancies are then combined, but first a word on combining spins. When spins are combined, the m_s values are added. The resulting spins are $|m_1 + m_2| \geq S \geq |m_1 - m_2|$ in increments of 1. For example, the possible spins resulting from the combination of a quartet (S=3/2) and a triplet (S'=1) are those for which $|1 + 3/2| \geq S \geq |1 - 3/2|$ or S = 5/2, 3/2, 1/2, *i.e.*, a doublet (1/2), a quartet (3/2) and a sextet (5/2). Multiplication tables are then used to determine the state symmetries.

The results are:

$$^3A_{2g} \otimes \begin{pmatrix} ^4A_{2g} \\ ^2E_g \\ ^2T_{1g} \\ ^2T_{2g} \end{pmatrix} = \begin{pmatrix} ^6A_{1g} + {}^4A_{1g} + {}^2A_{1g} \\ ^4E_g + {}^2E_g \\ ^4T_{2g} + {}^2T_{2g} \\ ^4T_{1g} + {}^2T_{1g} \end{pmatrix}; \; ^1A_{1g} \otimes \begin{pmatrix} ^4A_{2g} \\ ^2E_g \\ ^2T_{1g} \\ ^2T_{2g} \end{pmatrix} = \begin{pmatrix} ^4A_{2g} \\ ^2E_g \\ ^2T_{1g} \\ ^2T_{2g} \end{pmatrix}; \; ^1E_g \otimes \begin{pmatrix} ^4A_{2g} \\ ^2E_g \\ ^2T_{1g} \\ ^2T_{2g} \end{pmatrix} = \begin{pmatrix} ^4E_g \\ ^2A_{1g} + {}^2A_{2g} + {}^2E_g \\ ^2T_{1g} + {}^2T_{2g} \\ ^2T_{1g} + {}^2T_{2g} \end{pmatrix}$$

A total of 21 states are derived from a $(t_{2g})^3(e_g)^2$ configuration! The ground state can be determined by the application of Hund's first rule to be the $^6A_{1g}$.

Problem VI.1. What is the ground state of bromotris(2-dimethlyaminoethyl)-aminecobalt dication? The 2-dimethylaminoethyl)amine ligand is neutral. Assume the metal is low spin and in a C_{3v} environment.

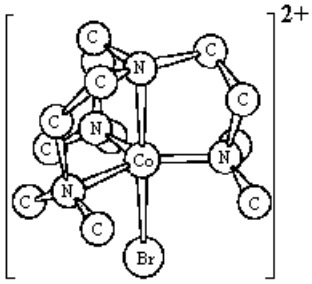

Problem VI.2 What are the ground states of a high spin and a low spin d^7 metal ion in an octahedral field?

Problem VI.3 (a) Deduce all of the states that can be derived from all **high spin** d^3 configurations in a tetrahedral field (e^2t^1, e^1t^2 & t^3). (b) Arrange the three states in a diagram in order of increasing energy with the ground state at the bottom.

VI.3 Selection Rules

The transition moment for a transition from the ground state (gs) to an excited state (es) is given as $\langle\mu\rangle = \langle gs|\mu|es\rangle$. To zero order, the state wavefunctions are products of orbital, spin, and vibrational wavefunctions. The excited state will be represented as $|nSv\rangle$ and the ground state as $|n'S'v'\rangle$. The dipole operator is a function of both the electronic and nuclear coordinates ($\mu = \mu_e + \mu_N$) but is independent of spin coordinates,

$$\langle\mu\rangle = \langle S'|S\rangle\langle n'v'|(\mu_e+\mu_N)|nv\rangle = \langle S'|S\rangle\{\langle n'v'|\mu_e|nv\rangle + \langle n'v'|\mu_N|nv\rangle\}.$$

The final result then is

$$\langle\mu\rangle = \langle S'|S\rangle\{\langle v'|v\rangle\langle n'|\mu_e|n\rangle + \langle n'|n\rangle\langle v'|\mu_N|v\rangle\} \qquad \text{Eq VI.3}$$

The term, $\langle n'|n\rangle\langle v'|\mu_N|v\rangle$, is for purely vibrational transitions: n' = n so $\langle n'|n\rangle = 1$ and $\langle v'|\mu_N|v\rangle$ leads to $\Delta v = \pm 1$. For electronic transitions, the initial vibrational state will *usually* be v'=0. The intensity of the transition is proportional to $\langle\mu\rangle^2$, so the following expression for the intensity of an electronic transition involving the S'→S, n'→n and v'→v transitions is obtained,

$$I \propto \langle\mu\rangle^2 = \langle S'|S\rangle^2\langle 0|v\rangle^2\langle n'|\mu_e|n\rangle^2 \qquad \text{Eq VI.4}$$

- $\langle S'|S\rangle$ dictates the **spin selection rule**. Since $\langle S'|S\rangle = \delta_{S'S}$, spin allowed transitions must be between states with the same spin, i.e., **$\Delta S=0$**. This is a fairly rigid selection rule and violations of it, *i.e.*, the observance of "spin forbidden" bands, occur due to spin-orbit coupling (section VI.7) which results in S no longer being a good quantum number (section VI.7).
- $\langle n'|\mu_e|n\rangle$ gives rise to the **orbital or symmetry selection rules**. A transition between two orbitals is orbitally allowed if $\Gamma(n') \otimes \Gamma(n)$ transforms the same as one of the components of the dipole operator, *i.e.*, like x, y or z. If the direct product $\Gamma(n') \otimes \Gamma(n)$ transforms as x, the electronic transition is said to be "x-polarized." Likewise if $\Gamma(n') \otimes \Gamma(n)$ transforms as y, the electronic transition is said to be "y-polarized," and if it transforms as z it is said to be "z-polarized."
- $\langle 0|v\rangle$ is the overlap of the vibrational wavefunctions in the ground (v'=0) and excited electronic states. The $\langle v'|v\rangle^2$ terms are referred to as the Franck-Condon factors and can modulate the intensity of the electronic transition.
- The intensity of a transition also depends on the **overlap of the ground and excited state wavefunctions**. Transitions between two orthogonal orbitals will have no intensity even if their direct product transforms as x, y, or z.

If, during the electronic transition, a quantum of an asymmetric vibration is also absorbed, the symmetry of the molecule will change and the group theoretical selection rules may be relaxed and a forbidden transition may become "vibronically allowed". Thus the electronic state has been coupled to the vibration through *weak vibronic coupling*. For these *vibronic* systems, electronic and vibrational components of Ψ are not separable. Thus,

$$\langle\mu\rangle = \langle S'|S\rangle\langle n',v'|\mu_e|n,v\rangle \qquad \text{Eq VI-5}$$

and it is the symmetry of the **vibronic states** given by the direct product of the orbital and vibrational irreducible representations that dictate the selection rules.

In centrosymmetric molecules, the d-orbitals are always gerade while the dipole operator is always ungerade and thus d-d transitions are orbitally forbidden $\langle g|u|g\rangle = 0$. g

→ g transitions are also said to be **Laporte forbidden**. These transitions, however, can be *vibronically allowed* through ungerade vibrations since in the v=1 vibrational level of an ungerade vibration, the molecule loses its center of symmetry and thus the selection rule is relaxed. In cases like this, the v' = 0 → v = 0 band (0-0 band) may not be observed and the peak maximum will be at an energy equal to the 0-0 plus one quantum of excited state vibrational energy. These peaks are referred to as "**false origins**". For example, consider ML_6, an octahedral d^6 compound with low spin, for which $\Gamma_{vib} = a_{1g} + e_g + t_{2g} + 2t_{1u} + t_{2u}$. The ground state is $^1A_{1g}$ (all orbitals are filled) and the lowest lying excited states are dd states arising from the $t_{2g} \rightarrow e_g$ orbital transition or $t_{2g} \otimes e_g = T_{1g} + T_{2g}$ states. The spin allowed transitions are $^1A_{1g} \rightarrow {}^1T_{1g}$ and $^1A_{1g} \rightarrow {}^1T_{2g}$. Both of these transitions are orbitally forbidden, but can be vibronically allowed. The dipole operator in O_h spans the t_{1u} irreducible representation so the modes which will make each transition vibronically allowed are the ones for which $\langle T_{1g} \otimes \Gamma_{vib} | t_{1u} | A_{1g} \rangle \neq 0$ or $\langle T_{2g} \otimes \Gamma_{vib} | t_{1u} | A_{1g} \rangle \neq 0$, *i.e.*, $T_{1g} \otimes \Gamma_{vib} \otimes t_{1u}$ or $T_{2g} \otimes \Gamma_{vib} \otimes t_{1u}$ must contain the A_{1g} irrep. The symmetries of the vibrations then must be $\Gamma_{vib} = T_{1g} \otimes t_{1u} = a_{1u} + e_u + t_{1u} + t_{2u}$ and $\Gamma_{vib} = T_{2g} \otimes t_{1u} = a_{2u} + e_u + t_{1u} + t_{2u}$. The only vibrations with the appropriate symmetry are the $2t_{1u}$ and t_{2u} modes so all three ungerade modes are vibronically active.

Problem VI.4. Which vibrations of the square planar $PtCl_4^{2-}$ ion are vibronically active in the lowest energy d-d band? Use the results of problem IV.7 for a description of the modes. Considering the vibronic coupling, draw and discuss the appearance of this absorption band.

It is possible to have vibronic bands on allowed transitions as well, for example, the $A_{1g} \rightarrow T_{2u}$ transition. In this case, $\Gamma_{vib} = T_{2u} \otimes t_{1u} = a_{2g} + e_g + t_{1g} + t_{2g}$ so either the e_g or t_{2g} modes have the correct symmetry.

Some selection rules are more rigid than others and the following table gives an indication of the strictness of the spin and orbital selection rules:

Spin	Orbital	log ε	Comments
Forbidden	Allowed	-5 to 0	spin-orbit coupling
Allowed	Forbidden	0 to 3	vibronically allowed
Allowed	Allowed	3 to 5	fully allowed

VI.4 Electronic Transitions

Figure VI-3 represents the types of electronic transitions typically encountered in inorganic spectroscopy. Transitions **A-D** originate in ligand orbitals but terminate in metal orbitals and thus involve a transfer of charge from the ligand to the metal. They are charge transfer (CT) transitions and due to the direction of the charge transfer are specifically called ligand to metal charge transfer (LMCT). Transition **E** and **F** are also CT transitions but they are metal to ligand charge transfer (MLCT). CT bands are quite intense with molar absorbtivities of around 10^4. Transition **G** is metal centered and is referred to as dd, ligand field or crystal field. These metal centered bands are forbidden in octahedral complexes as they are gerade → gerade and remain quite weak in lower symmetry molecules, ε ~ 1 to

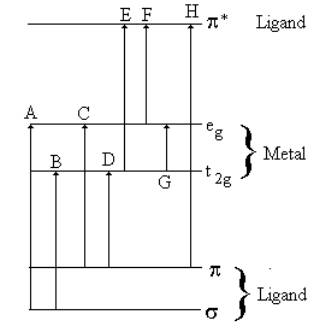

Figure VI-3. Transitions typically encountered in inorganic spectroscopy.

100. **H** is a ligand centered (LC) transition, specifically a $\pi \rightarrow \pi^*$ transition. These bands are very intense with molar absorbtivities of 10^5. Typically, LC bands other than $\pi \rightarrow \pi^*$ or an ocasional $n \rightarrow \pi^*$ are very high in energy.

Electronic transitions are governed by the **Franck-Condon principle,**

> Electron motion is so much faster than nuclear motion that electronic transitions can involve no change in either the positions or the momenta of the nuclei.

Transitions are usually represented on a diagram similar to that shown in figure VI-4 which shows the ground and excited state potential energies along one of the normal coordinates, Q. Since the nuclear displacements do not change during an electronic transition, the transitions are said to be "vertical". Essentially all of the molecules are originally in the vibrational ground state so the electronic transitions originate from v'=0 in which case the momentum is low. Also, it is *most probable* that the transition originates from the ground state equilibrium geometry (Q=0), and if the excited state equilibrium geometry is different, then a vertical transition to the v=0 level may be impossible, *i.e.*, the 0-0 transition may be very weak or missing. The larger the value of v, however, the greater will be the momentum at the middle of the well. Therefore, the strongest transitions other than 0-0 bands will occur when the transitions are to the extrema of the internuclear separations where the vibrational momentum is at a minimum.

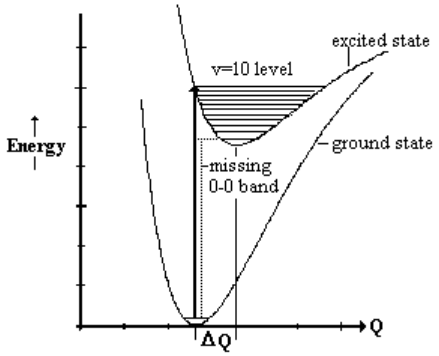

Figure VI-4. Vertical transition from ground state is to the v=10 level of the excited state. In a case this severe, the 0-0 band would be missing.

The same conclusion can be reached quantum mechanically by considering the Franck-Condon (FC) factors, $\langle 0|v\rangle^2$ in eq VI-4. These terms will be non-zero only if the upper surface is either distorted (different force constant) or displaced (different equilibrium geometry). If the upper surface is neither displaced nor distorted then the orthogonality of the vibrational wavefunctions is maintained and all FC terms are zero except for the 0-0 term which is unity. Remember that the maximum amplitude of the wavefunctions is at the extrema for large values of v but at the equilibrium position for v=0 (see figure IV.4), thus the maximum value of $\langle 0|v\rangle^2$ is expected at the v arrived at by making the vertical transition from the center of the lower surface to the edge of the upper surface - the same result one obtains when considering conservation of momentum.

As an example, consider the $^1\Sigma^+ \rightarrow {}^1\Pi$ transition in CO which is schematically represented in figure VI-5. The spectrum consists of a long progression starting at 64,703 cm^{-1} (0-0 band) and going to higher energy consistent with the absorption of more vibrational quanta as the transitions are of the form $0 \rightarrow v$ so the energy of each line would be $E_{0\text{-}0} + v'\bar{\nu}$ (assuming the vibration is harmonic). However, the spacings are consistent

with an anharmonic oscillator in which $\bar{\nu}_e$ = 1516 cm^{-1} and $\bar{\nu}_e\chi_e$ = 17.25 cm^{-1}. Long progressions in a vibration are indicative that the position of the potential minimum for the normal coordinate is changed in the excited state, *i.e.*, the equilibrium C-O bond length is different in the excited state than in the ground state. The fact that the vibrational frequency is much lower in the excited state indicates that the bond has elongated in the excited state.

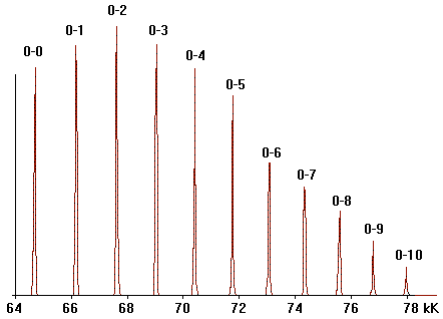

Figure VI-5. Schematic representation of the vibronic progression of the C≡O stretch on the $^1\Sigma^+ \rightarrow {}^1\Pi$ transition of carbon monoxide. The 0-0 band is at 64,793 cm^{-1}.

Analysis of the ground state and excited state vibrational progressions leads to the following parameters for CO in the two electronic states (bond lengths come from analysis of rotational spectra):

	$^1\Sigma^+$	$^1\Pi$	
$\bar{\nu}_e$	2169	1516	cm^{-1}
$\bar{\nu}_e\chi_e$	13.28	17.25	cm^{-1}
D_e	1060	398	kJ/mol
k_e	1900	928	N/m
r_e	1.13	1.24	Å

From these parameters the potential energy diagrams for the two states can be constructed (figure VI-6). Note that the upper surface is both *displaced* and *distorted* which leads to large FC factors. Also, the vertical transition from the middle of the lower surface intersects the upper surface at the v' = 2 level, in keeping with the 0→2 transition being the strongest.

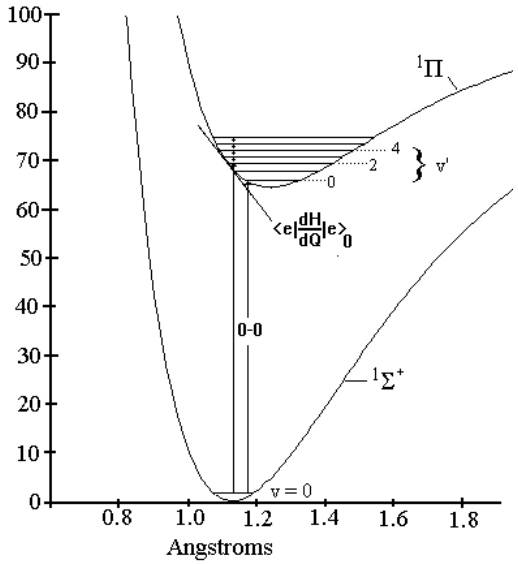

Figure VI-6. The Morse potential governing the C≡O stretch of carbon monoxide in the ground and lowest lying singlet excited state - the result of a π→π* (HOMO → LUMO) orbital transition. Vertical axis is Energy in kK. One-state vibronic coupling has shifted the upper surface to lower energy and to a longer C≡O bond length.

VI.5 Vibronic Coupling

The potential energy of each electronic state for a polyatomic molecule is a complicated 3N-5 dimensional surface which is ordinarily represented by a two dimensional drawing of potential energy along the normal coordinate of interest, *i.e.*, a slice of the potential surface. Upon electronic excitation, the molecule will still have the geometry of the ground state (FC principle) and if the excited state geometry is different from that of the ground state, the molecule will feel a restoring force pulling it toward the excited state equilibrium geometry. Force is $-\partial V/\partial Q$ or, in quantum mechanical terms, it is $\langle -\partial V/\partial Q \rangle = \langle -\partial H/\partial Q \rangle$ since ($H = T+V$). The restoring force is then $k\Delta Q_m = \langle e|\partial H/\partial Q_m|e\rangle_{Q=0}$ and is represented as the slope of a tangent on the excited surface at the ground state equilibrium value of Q_m, the m^{th} normal mode. This is referred to as a "one-state" vibronic coupling as it involves only the "e" state. The result is a shift of the minimum along Q_m by an amount ΔQ_m and a lowering of the minimum of the excited state by $\frac{1}{2}k\Delta Q_m^2$, *i.e.*, vibronic coupling stabilizes the excited state by deforming the molecule. See figure VI.5. The symmetry properties of $\partial H/\partial Q_m$ are the same as Q_m and $|e\rangle \otimes |e\rangle$, for non-degenerate excited states, is totally symmetric so $\langle e|\partial H/\partial Q_m|e\rangle \neq 0$ only if Q_m is a totally symmetric mode. In other words,

> Vibronic progressions will be observed only for totally symmetric modes since excited state potentials can be displaced only along totally symmetric normal modes.

Problem VI.5. MO's and spectra of MX_2 are given.

a. Draw the symmetry coordinates and assign the vibrational spectra given below. Note the Raman spectra were recorded in both parallel and perpendicular polarizations.

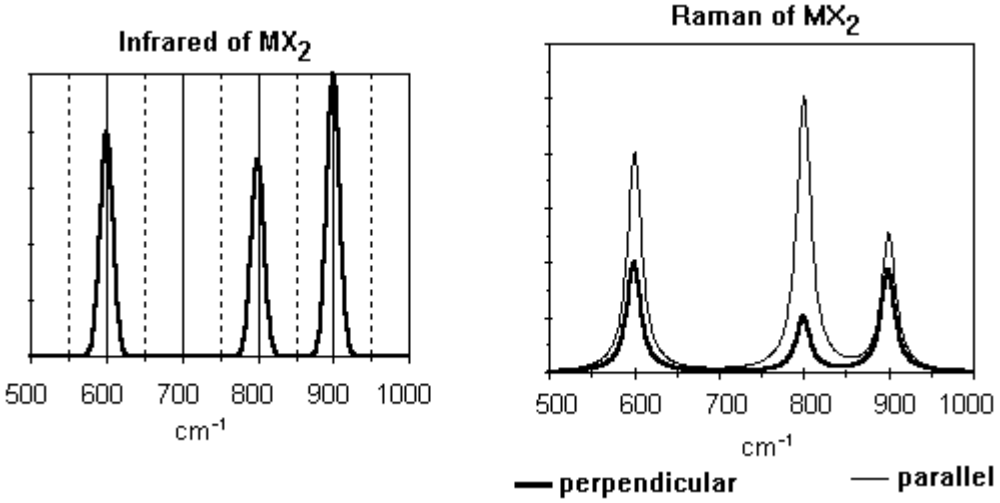

b. To what irreps do the SHOMO, HOMO and LUMO belong?

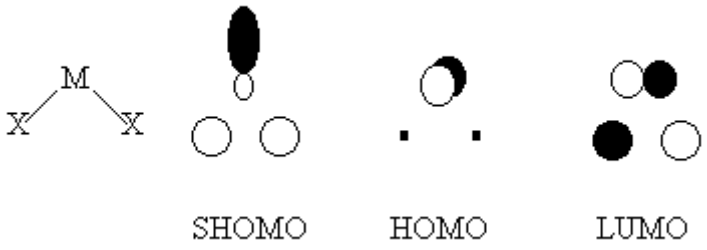

c. The electronic spectrum consists of two absorption regions - a weak system in the 25 to 29 kK range and a much stronger system in the 41 to 44 kK range. Assign the two systems

to state transitions and explain why the higher energy system is about 1000 times stronger. What is the 0-0 energy for each system?

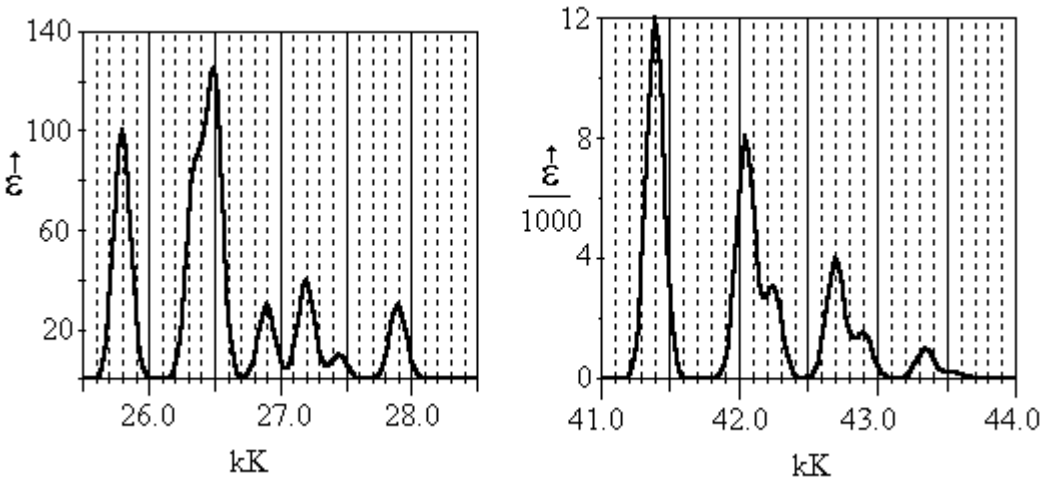

d. Assign **all** of the features in the 4K electronic spectra shown above and discuss differences in the excited state geometries. Use all of the data to formulate your conjecture. Begin by determining whether each electronic transition is electric dipole allowed or forbidden. Remember, forbidden transitions are typically vibronically allowed and will exhibit *false origins* (page 115).

VI.6 Jahn-Teller Distortions

It will be recalled from section II.8 that the energy levels of a metal ion in an O_h field will change as the ion undergoes a tetragonal distortion. Shown in figure VI.6 are the effects of a tetragonal compression (A) and an tetragonal elongation (B). In both cases the bonds along the x- and y-axes change in the opposite direction from those along the z-axis.

If the energy center is preserved, the magnitude of the energy change in the e_g is half that of the b_{2g} while the b_{1g} and a_{1g} changes are of the same magnitude. The splitting (δ_1, δ_2) is *typically* in the 200 to 2000 cm^{-1} range, *i.e.*, less than pairing energy. As a result a $(t_{2g})^1 = {}^2T_{2g}$ configuration will undergo a tetragonal compression to a ${}^2B_{2g}$ with a $(2/3)\delta_2$ stabilization while a $(t_{2g})^2 = {}^3T_{1g}$ is expected to tetragonally elongate to a ${}^3A_{2g}$ also with a $(2/3)\delta_2$ stabilization. A $(t_{2g})^3 = {}^4A_{2g}$ will result in equal occupancy of all three orbitals and result in no stabilization and thus there is no distortion. For over half-occupancy, the energy of the holes should be maximized thus $(t_{2g})^4 = {}^3T_{1g}$ tetragonally compresses while $(t_{2g})^5 = {}^2T_{2g}$ elongates along z. A $(t_{2g})^6$ will not distort. Similar energy considerations applied to the e_g filling predict that distortion should occur for $(e_g)^1 = {}^2E_g$ and $(e_g)^3 = {}^2E_g$, but not for the $(e_g)^2 = {}^3A_{2g}$ or $(e_g)^4 = {}^1A_{1g}$. In the latter case, however, no prediction regarding whether the distortion is an elongation or a compression can be made, but typically it is the tetragonal elongation which is observed. From the above considerations, it is clear that all of the *degenerate states* (degenerate orbital occupancy of one unpaired electron) and none of the non-degenerate states are expected to distort. This tendancy of degenerate electronic states to distort was summarized by Jahn and Teller in what has become known as the Jahn-Teller Theorem.

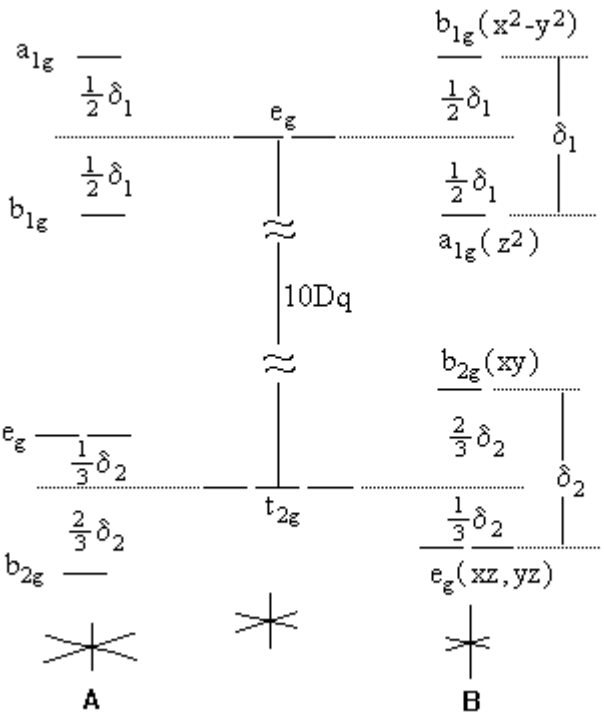

Figure VI-7. The effect of lowwering the symmetry of an octahedral field by a tetragonal distortion. (A) results from an axial compression and an equatorial elongation while (B) shows the effects of an axial elongation and an equatorial compression. $10Dq >> \delta_1 > \delta_2$.

Jahn-Teller Theorem: Non-linear molecules remove electronic degeneracies by undergoing a nuclear rearangement to lower symmetry.

Since the distortion is a nuclear rearrangement, it is carried out *via* the normal coordinates (Q) so Jahn-Teller distortion is another example of vibronic coupling. One state coupling in non-degenerate states must be along totally symmetric coordinates so there is **no symmetry breaking** - totally symmetric modes retain the symmetry of the molecule (as in vibronic progressions, page 118). However, if the state is orbitally degenerate, it is the symmetric part of $|e\rangle\otimes|e\rangle$ that is vibronically active, and vibronic coupling can lead to a lowering of symmetry, *i.e.*, lead to **a symmetry breaking**. For example, in O_h symmetry, $e_g\otimes e_g = a_{1g} + [a_{2g}] + e_g$ so a_{2g} modes are not vibronically active in E_g states, but e_g vibrations are active (a_{1g} modes are active but cannot lead to a symmetry change). Figure VI-8 shows both the e_g and t_{2g} vibrations of an octahedral ML_6 species. It is one of the phases of this e_g mode which results in the tetragonal distortion (the phase which is shown results in the tetragonal elongation). Note that **excited states can also undergo Jahn-Teller (JT) distortions**.

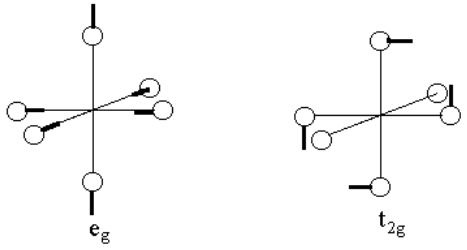

Figure VI-8. One component of each of the degenerate vibrations which are vibronically active in a t_{2g} electronic state. The e_g mode is also active in e_g states.

Octahedral $Ti(H_2O)_6^{3+}$ is predicted to have a $^2T_{2g}$ ground state, but the JT theorem predicts an instability in this state which leads to a lowering of the symmetry. $T_{2g}\otimes T_{2g} = a_{1g} + e_g + [t_{1g}] + t_{2g}$. Thus, the Jahn-Teller active modes are $e_g + t_{2g}$ (a_{1g} cannot lower the symmetry and t_{1g} is the antisymmetric part of the direct product). Again, it is the e_g mode which is almost always responsible for the distortion so the ion undergoes a tetragonal distortion to D_{4h} symmetry which results in a $^2B_{2g}$ ground state as it is the equatorial bonds that elongate.[3]

Jahn-Teller distortions of T states in O_h complexes are encountered far less frequently than for E states. This is because the t_{2g}'s are non-bonding so bond length changes will not affect them dramatically while the e_g's are antibonding and thus very sensitive to bond lengths, *i.e.*, $\delta_1 > \delta_2$. The distortion is so pronounced in Cu(II) complexes (d^9, ^2E_g ground state) that very few regular octahedral copper(II) complexes are known.

The **Jahn-Teller distortion can be either static or dynamic**. Dynamic Jahn-Teller is a weak coupling case (degenerate orbitals are non-bonding) in which the ion oscillates in a potential with three minima and appears, on the average, to be a regular octahedron. In static Jahn-Teller distortion, the coupling is strong enough to warp the potential surface and result in a permanent change in the bond lengths (degenerate orbitals are antibonding). In this latter case, an ion with unique axial and equatorial bonds results with lower symmetry - an example of *symmetry breaking*.

Two-state Vibronic Coupling - pseudo Jahn-Teller Effect

The Jahn-Teller effect can be viewed as an example of the coupling of two degenerate states, but coupling can occur even if the states are not degenerate. This coupling of two non-degenerate states is sometimes referred to as the *pseudo Jahn-Teller effect*. The two-state vibronic coupling operator is then given as $\langle e|\partial H/\partial Q_m|f\rangle_{Q=0}$ where $|e\rangle$ and $|f\rangle$ are two electronic states coupled by the normal coordinate Q. The symmetry of the coupling vibration must be the same as the direct product of $|e\rangle\otimes|f\rangle$ which is typically non-totally symmetric. As the vibronic coupling gets stronger, the upper surface narrows while the lower surface broadens (see figure VI-9). For non-totally symmetric modes, $\langle e|\partial H/\partial Q_m|e\rangle_{Q=0} = 0$ so the slope of both surfaces remains 0 at Q=0. However, in the strong coupling limit, Q=0 becomes a maximum in the lower surface which means that the equilibrium geometry is no longer at Q=0 and thus the molecular symmetry is different in this excited state, *i.e.*, there is *symmetry breaking* in this state.

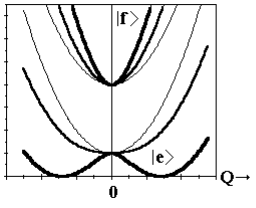

Figure VI-9. Effect of a two-state, $|e\rangle$ and $|f\rangle$, coupling through a non-totally symmetric mode, Q. The lightest line is the no coupling limit, the heaviest line is a strong coupling case and the intermediate line represents a weak coupling case.

An easily understood example of a two state coupling is the ethylene cation. The two lowest electronic states of the ethylene cation arise from removal of an electron from the two

[3] Most known examples involve a tetragonal elongation.

highest lying mo's of ethylene (see figure II-14). The resulting states, $^2B_{1u}$ and $^2B_{1g}$ are close in energy and are vibronically mixed. The symmetry of the coupling mode must be $B_{1u}\otimes B_{1g} = a_u$ - the C=C torsion. The coupling of these two states by the torsion results in a ground state which is twisted resulting in an ion with D_{2d} symmetry. The application of the vibronic coupling model can often lead to the prediction of excited state geometries.

VI.7 Spin Orbit Coupling

The spin-orbit operator, $\lambda L \bullet S$ (L is the orbital angular momentum operator and S is the spin angular momentum operator) transforms as the rotations (R_x,R_y,R_z) of the molecular point group. SOC exists in first- or second order if the direct product of a state term symbol(s) transform as the rotations: $a\otimes a' \Rightarrow R_x$, R_y, or R_z. The interaction is also proportional to the SOC constant, $\lambda = \pm\zeta/2S$, which in turn is proportional to atomic number and nuclear charge as shown in the table below.

Atomic spin-orbit coupling constants ζ (cm^{-1}). Values in parentheses are experimentally determined.

⇓Metal Oxidation State⇒	M(0)	M(I)	M(II)	M(III)	M(IV)	M(V)	M(VI)
Ti	70	90	120	155			
V	(95)	135	170	210	250		
Cr	(135)	(190)	230	275	325	380	
Mn	(190)	255	(300)	355	415	475	540
Fe	255	345	400	(460)	515	555	665
Co	390	455	515	(580)	(650)	715	790
Ni		605	630	(715)	(790)	(865)	950
Cu			830	(875)	(960)	(1030)	(1130)
Zr	270	340	425	500			
Nb	(365)	490	555	670	750		
Mo	(450)	(630)	(695)	820	950	1030	
Tc	(550)	740	(850)	(990)	(1150)	(1260)	1450
Ru	745	900	1000	(1180)	(1350)	(1500)	(1700)
Rh	940	1060	1220	(1360)	(1570)	(1730)	(1950)
Pd		1420	1460	(1640)	(1830)	(2000)	(2230)
Ag			1840	(1930)	(2100)	(2300)	(2500)

The spin-orbit coupling constant within a given Russell-Saunders multipley is $\lambda = \pm\zeta/2S$. "+" is for $1 \leq n \leq 4$ and "-" for $n > 4$.

Orbitals involved in the spin-orbit coupling must have angular momentum to exchange with the spin, but only those degenerate orbitals which can be carried into one another by rotation about an axis contain angular momentum. For example, an electron in degenerate xz and yz orbitals has angular momentum since rotation about the z-axis exchanges the two orbitals, but an electron in degenerate z^2 and x^2-y^2 has no angular momentum since a rotation will not exchange these orbitals. As a result, all E and T states will have angular momentum except for the E states of O_h and T_d. There must also be spin angular momentum so S>0, *i.e.*, singlet states cannot be split by SO coupling. The spin components of a non-dengenerate triplet will not be split by SO coupling since there is no orbital angular momentum, and the degenerate components of an ^1E state cannot be split by SO coupling because there is no spin angular momentum.

One effect of SOC is to relax the $\Delta S=0$ selection rule by mixing states of different spin multiplicity. In a simple, classical picture, an electron's acceleration near a large nuclear charge generates a magnetic field which is sufficient to interact with the spin magnetic moment and result in a "spin flip". However, since the angular momentum must be conserved, the momentum change associated with the change in spin is compensated for by a

change in orbital angular momentum. Thus, the orbital angular momentum and the spin angular momentum are coupled and neither is constant - only the resultant angular momentum, **J** = **L** + **S**, is conserved. In the case of strong spin-orbit coupling then, L and S are no longer good quantum numbers and the spin selection rule weakens. In a two electron case, the resulting states are no longer purely singlet and triplet in character as the spin-orbit coupling mixes singlet character into the triplet and *vice versa.* The more singlet character the triplet attains the stronger the "triplet" transition becomes as intensity is "borrowed" from the "singlet".

SOC can split a degenerate state into "J states" (J = |L+S|…|L-S|) when $a \otimes a \Rightarrow R_x,R_y,R_z$ and is comparable in magnitude to JT splitting (200 - 2,000 cm^{-1}). The energy splitting between the J states are in units of λ. Both JT and SOC splitting require a degenerate state so how does one determine which is operable (or if both are operable)? Generally JT distortions are greater in E states while SOC often dominates T states. This is explained by the fact that E states have electrons in $d\sigma^*$ orbitals, and these orbital energies are affected more by bond length changes that the weaker interacting $d\pi$ electrons of T states. Also, remember $a \otimes a \Rightarrow R_x,R_y,R_z$ for SOC to operate. For E_g states at O_h symmetry, $e_g \otimes e_g \Rightarrow a_{1g} + a_{2g} + e_g$. Since the R's transform as t_{1g}, SOC cannot remove the degeneracy and JT does the trick via the e_g mode(s). For T states at O_h symmetry, $t \otimes t \Rightarrow a_1 + e + t_1 + t_2$. Since the R's transform as t_{1g}, SOC can remove the degeneracy. In addition, the JT can contribute to the splitting via the e_g and t_{2g} modes. Thus, both types of splittings may be involved but to different degrees.

Finally, SOC plays an important role in magnetism and electron paramagnetic resonance by affecting the magnetic moment, altering the g-factor from the spin-only value, and creating large zero-field splittings. In fact, it is SOC that is responsible for *large* axial zero field splittings (5-50 cm^{-1}). To understand the effect of SOC on zero-field splittings, consider the three spin sublevels ($T_{\pm1}$ and T_0) of a spin triplet ground-state. In second-order SOC can mix these sublevels with those of an excited state, but mixes the $T_{\pm1}$ differently that it mixes the T_0. The result is an energy gap between the $T_{\pm1}$ and T_0 sublevels of the ground state. This energy gap is called zero-field splitting. The magnitude (and sign) is proportional to the SOC matrix elements, proportional to λ, and inversely proportional to the energy gap between ground and excited states.

Problem VI.6 In problem II.13 you constructed an energy level diagram for [$[(Me_3P)_4WE_2]$ (E=S, Se, Te) of D_{2d} symmetry. The spectra of the dd bands is given in A below.

- Assign them to orbital and state transitions of the D_{2d} molecule. In your discussion, you should argue that only one dd band is expected in this region.
- The two bands in each spectrum have been assigned to a JT splitting. What are the symmetries of the JT active modes? What is the probable nature of the distortion and the symmetry of the distorted molecule. Draw an orbital energy level diagram showing the orbitals involved in the transition in the D_{2d} molecule and the distorted molecule.
- Suggest why *trans*-$O_2Re(py)_4^+$ shows no such splitting.

Problem VI.7. The uv spectra of these compounds is given in B below. You may assume that all bands arise from transitions within the E=W=E moiety and into the LUMO.

- Assign the labelled peaks in a table. Include the state, orbital, and type (MLCT, dd, etc.) designation for each. Is there a relationship between the series comprised of the strongest peaks in the spectra and the series of bands at 18.2, 22.3 and 24.6 kK? Account for the apparent trend in intensities of the latter series.
- Evaluate the relative field strengths of S, Se and Te based on the spectra given below and the the dd spectra presented in the previous problem. Explain the observed trend.

- No band is observed in the spectra of the O=Re=O unit which corresponds to the strongest band in these spectra. Why?
- Could the two bands shown in the dd region (Problem VI.6) be ascribed to a spin-orbit splitting? Argue for or against this assignment.

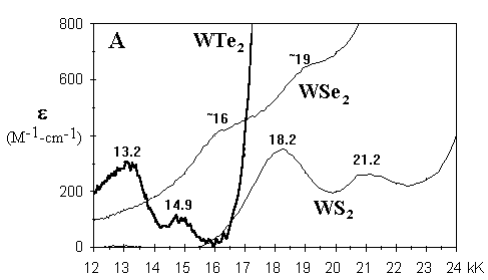

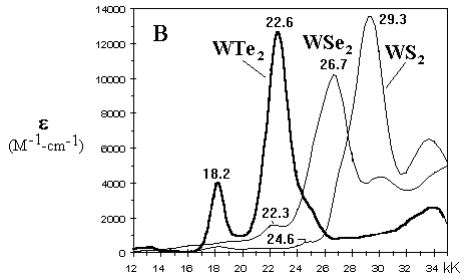

VI.8 Resonance Raman Scattering

There are several excellent reviews on resonance Raman and an excellent example featuring inorganic chemistry.[4] We will present here only a very qualitative overview. The experimental difference between normal Raman scattering (section IV.10) and resonance Raman scattering (RRS) is that in the former the exciting line is far removed from any electronic absorption while, in the latter, excitation is in resonance with an electronic transition. As a result, the RRS process is coupled to the electronic process with an enhancement of the Raman signal which can be orders of magnitude depending on the extinction coefficient of the electronic band and how close to resonance the excitation is. Thus, pure solids are studied in normal Raman while RRS from μM solutions have been reported.

Typically, the scattering tensor is written as $\boldsymbol{\alpha = A + B}$, where **A** is the Franck-Condon (one-state) scattering term and **B** is the Herzberg-Teller (two-state) scattering term.[5]

A-term scattering: The A-term is the dominant term in the scattering process and in many instances is the only enhancement mechanism observed. Since the photon is in resonance with an excited state, the molecule begins to move toward the excited state geometry during the scattering process and the modes it uses to achieve the excited state geometry are the ones that gain enhancement *via* the **A**-term. Since the only modes that can be displaced are the totally symmetric modes, they are the only ones that can be enhanced by the A-term. The more displaced the upper surface is along a coordinate, *i.e.*, the larger are the Franck-Condon factors for the vibration, the more enhanced the mode is and the more likely will be the observation of overtones. If the enhancement is plotted as a function of excitation energy, an *excitation profile* is obtained. This excitation profile will typically trace the absorption band. Finally, the extent of enhancement varies with the square of transition moment of the electronic absorption so that enhancement factors observed for RRS in resonance with strong absorption are greater than those observed from weak bands.

B-term scattering: Enhancement of non-totally symmetric modes results from the B-term. If two electronic states lie close in energy to the Raman excitation energy, an enhancement of those modes with the symmetry to couple the two states can be observed. B-term contributions are usually masked by the much stronger A-term. However, some

[4]Clark, R.J.H.; Stewart, B., *Struc. and Bonding*, **1979**, 36, 1-80.

[5]There are higher terms, but they are seldom observed.

cases have been observed. Perhaps, the most studied example is that of porphyrins, discussed in detail in section VII-5, where two E_u states are strongly coupled and absoption into them gives rise to a Q- and a Soret band. The A-term will result in a_{1g} modes of the D_{4h} molecule being enhanced while the B-term will enhance modes of the correct symmetry to couple the two E_u states ($E_u \otimes E_u = a_{1g} + a_{2g} + b_{1g} + b_{2g}$). Resonance Raman when probing the Soret band is typically due to the A-term as only a_{1g} modes are observed. Probing the Q-band results in the modes expected for the B-term contributions.

The visible absorption spectrum of TiI_4 and the resonance Raman spectra observed with three exciting lines probing the lowest energy band are given in Figure VI-10. The Raman spectra are normalized to the cyclohexane peak at 806 cm^{-1} which is maintained at the same intensity for all spectra. The resonance Raman spectrum at 647 nm is pre-resonance and the strongest peak in the spectrum is the cyclohexane reference peak while ν_1, the symmetric Ti-I stretching mode is relatively weak. As the exciting line is moved into resonance conditions at 568 nm, the Ti-I stretch is now comparable in intensity to the solvent mode and its first overtone is becoming pronounced. On resonance at 514 nm, ν_1 dominates the spectrum being about 5-times stronger than the solvent band. In addition, a progression in ν_1 out to $4\nu_1$ is readily observed. From these results, it can be concluded that the Ti-I bond length is substantially changed in the excited state which is populated at 514 nm.

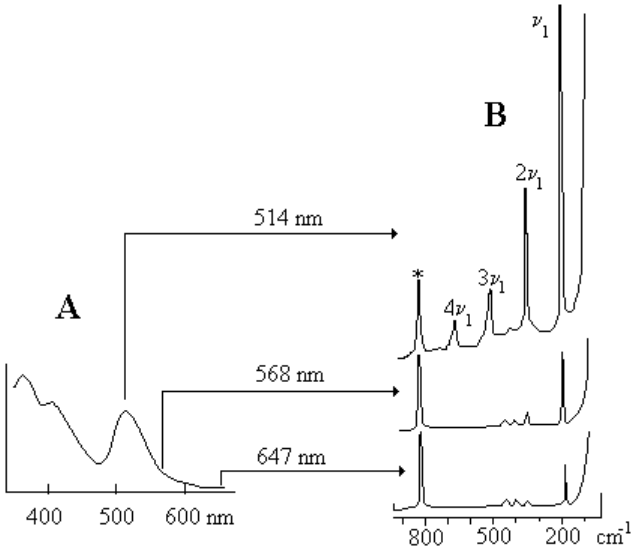

Figure VI-10. (A) The visible portion of the electronic spectrum of TiI_4. (B) Resonance Raman spectra of TiI_4 in cyclohexane reported at three exciting lines, 647, 568 and 514 nm. The spectra are normalized so that the cyclohexane reference peak at 806 cm^{-1} retains the same intensity in each spectrum.

Thus, resonance Raman can be viewed as high resolution vibronic spectroscopy. As such it is useful in determining the nature of excited states and in assigning electronic spectra. One of the topics to be discussed in detail at the end of the course is the localized nature of the metal to ligand charge transfer (MLCT) excited states of $Ru(bpy)_3^{2+}$. As implied in the name, charge is transferred from the metal to the bipyridine in this transition, and the question being considered was whether that charge was localized on a single bipyridine or delocalized in a π-MO spread over the entire molecule. The electrochemistry of these species is quite rich and stable reduction products are easily obtained. In our work in this field, we examined the spectroscopy of these reduced species to determine the effect of reduction. Upon reduction,

π–π* transitions in the bipyridine are found in the visible and it is difficult to determine the position of the MLCT bands. In the case of $Fe(bpy)_3^{2+}$, however, these peaks are well resolved.[6] Figure VI-11A shows the visible spectrum of $Fe(bpy)_3^{2+}$ and its one-electron reduction product, $Fe(bpy)_3^{1+}$. After a quick comparison of the general features of the visible spectrum, it would be tempting to assign the features at 19.0 and 20.2 kK in the reduced species to the MLCT and a vibronic side band in keeping with the assignment of the parent. The band at 16.5 kK would then be the $\pi \rightarrow \pi^*$ transition. This assignment would then indicate only a small shift in the MLCT with reduction. The resonance Raman spectra (RRS) of these complexes is shown in figure VI-11B. The RRS observed for the parent when probing into the maximum of the MLCT band is dominated by bipyridine vibrations indicating that the bipyridines are distorted in the excited state of the transition. This is to be expected since the transition is putting electron density into a bpy-$\pi*$ orbital. The RRS of the singly reduced species observed at 19.0 kK is different as most of the frequencies and relative intensities are different. When the low energy band at 16.6 kK is probed, however, an RRS essentially identical to that observed for the parent is observed. The conclusion, then is that the MLCT band red-shifts by about 2.4 kK upon reduction down to 16.6 kK. The band at 19.0 kK in the reduced species is then a $\pi \rightarrow \pi^*$ transition localized in the reduced bipyridine. The Raman frequencies observed when exciting at 19.0 kK are then due to a reduced bipyridine which results in a shift. Thus, the assignment of these electronic bands was greatly facilitated by the use of RRS. In addition, the observation of RRS from unreduced and reduced bipyridines in the same sample supports the contention that the redox orbital is indeed localized on an indidual bipyridine ligand and not spread out over all three ligands. We will revisit this problem in more detaila in the next chapter.

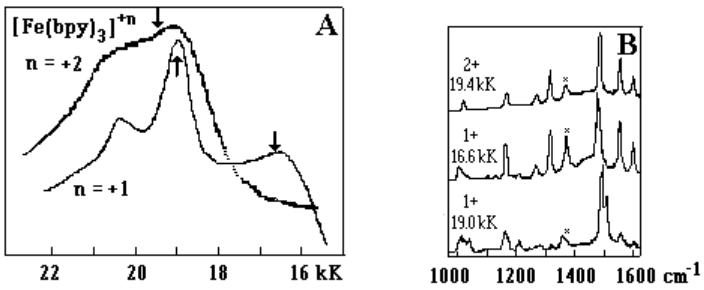

Figure VI-11. (A) The visible spectrum of $Fe(bpy)_3^{2+}$ and its one electron reduction product $Fe(bpy)_3^{+}$. (B) The resonance Raman spectrum of $Fe(bpy)_3^{2+}$ using 19.4 kK excitation and of $Fe(bpy)_3^{+}$ using 16.6 and 19.0 kK excitation. The arrows in (A) are the excitation energies used in (B).

Problem VI.8 Account for the 2400 cm^{-1} shift in the MLCT upon reduction of one of the bipyridines.

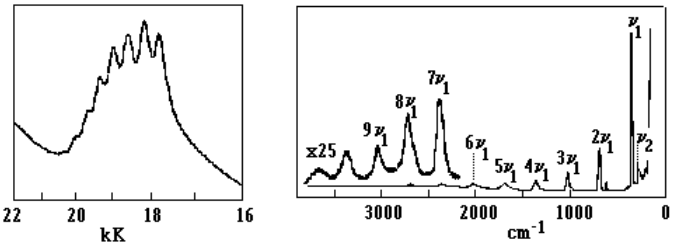

Figure VI-12. The absorption spectrum and the RRS of $Mo_2Cl_8^{4-}$

[6] Angel, S.M.; DeArmond, M.K.; Donohoe, R.J.; Wertz, D.W., *J. Phys. Chem.*, **1985**, 89, 282).

As another example of RRS consider the spectra of $Mo_2Cl_8^{4-}$ given in problem IV.4 and shown above. Here, the RRS was recorded using excitation at 19.4 kK, *i.e.*, into the band shown at the left. Since a long progression in the Mo-Mo stretch was observed in both the electronic absorption spectrum and in the resonance Raman, it was concluded that the excited state geometry had a substantially different Mo-Mo bond length. Since the stretching frequency is much less in the excited state (peak separations in the absorption spectrum) than in the ground state (RRS) it was concluded that the Mo-Mo bond lengthened upon excitation. The absorption band was therefore assigned as the $\delta \rightarrow \delta^*$ transition which results in a lowereing of the Mo-Mo bond order.

VI.9 Relaxation Pathways

There are a variety of relaxation mechanisms by which can lose the energy gained in an electronic absorption. They are represented in figure VI-13, a Jablonski diagram.

- **Vibrational relaxation (R)**: molecules in vibrationally excited states relax to the vibrational ground state by collisions with the solvent. This is the most rapid process (10^{-11} - 10^{-9}s) and therefore the first process to occur. All of the subsequent relaxation processes will occur from the ground vibrational level of the electronic manifold. This is a non-radiative process which results in heat.
- **Internal conversion (IC)**: The excess electronic energy of one manifold is converted into excess vibrational energy of a lower lying manifold of the same spin.
- **Intersystem crossing (ISC)**: The same process as internal conversion except the two electronic states are of different spin.
- Emission can be a spin allowed **Fluorescence (F)**, a spin forbidden **Phosphorescence (P)** or a **Luminescence** for strongly spin orbit coupled systems.
- **Photochemistry:** the excess electronic energy is oftentimes in very anti-bonding mo's which can lead to extensive bond weakening which can, in turn, lead to reactions.

In the following discussion, it is assumed that all electrons in the ground state are paired so the ground state is a singlet (S_0) while the excited states are either singlet (S_1 being the lowest excited singlet) or triplet (T_1 being the lowest lying triplet). Since highly excited electronic states are very short lived, the molecule typically does not spend sufficient time in these states to undergo a spin forbidden ISC or emission. As a result, vibrational relaxations and internal conversions occur very quickly to bring the sytem to the S_1 manifold by heating up the sample. This is sometimes referred to as **Kasha's Rule:** it is from the v=0 level of S_1 that fluorescence, intersystem crossing to T_1, or photochemistry will occur. In the following, we neglect photochemistry and consider only absorption into S_1.

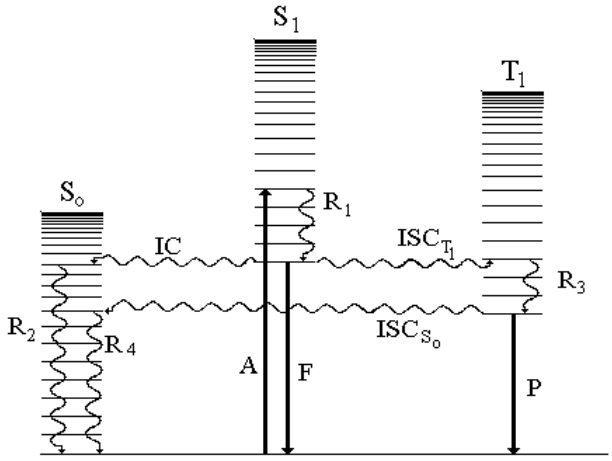

Figure VI-13. Jablonski Diagram showning some of the relaxation pathways after an absorption **A** into the lowest lying singlet, S_1.

The relaxation pathways available from the v=0 level of S_1:

1. **F**: spin allowed fluorescence - the excess energy is given off as a photon
2. **IC + R_2**: internal conversion to S_o followed by vibrational relaxation - energy is dissapated as heat.
3. **ISC_{T1} + R_3 + (P or ISC_{S_0} + R_4)**: Intersystem crossing to T_1 followed by vibrational relaxation followed by (either a spin forbidden phosphorescence or an intersystem crossing to S_o and subsequent vibrational relaxation).

The entire process is unimolecular, A*→A, so it obeys first order kinetics, *i.e.*, $[A^*]_t=[A^*]_0e^{-kt}$ where the rate constant, k is the sum of the rate constants for all of the competing pathways (all of which are first order). The lifetime is defined as $\tau = 1/k$ so $[A^*]_\tau=[A^*]_0e^{-1}$ or $[A^*]_\tau/[A^*]_0 = 1/e = 0.37$, *i.e.*, the lifetime is the time required for the concentration of the excited state species to fall to 37% of its original value.

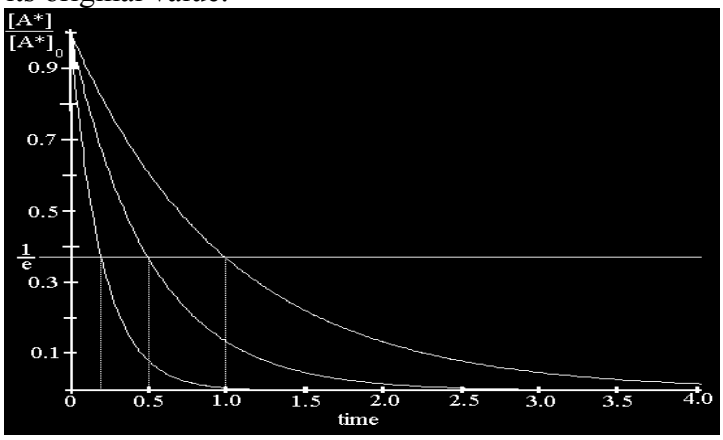

Figure VI-14. Exponential decay of A* with lifetimes of 0.2, 0.5, and 1.0 time units.

Thus the excited state decays exponentially. The importance of any pathway will depend on the rate constant for the process, the faster a process occurs, the more important the process is in the description of the relaxation. Because fluorescence is spin allowed, it is much faster ($10^{-4}s > \tau > 10^{-8}s$) than the spin forbidden phosphorescence ($10^{2}s > \tau > 10^{-4}s$). Since spin orbit coupling makes the term "spin forbidden" somewhat ambiguous, radiative decay with lifetimes in the regions of overlap between the two is called **luminescence**.

The rate of internal conversion or intersystem crossing will depend on the energy match of the two vibrational levels and the overlap of the vibrational wavefunctions. If the v=0 level of the S_1 manifold is close in energy to the v'=7 level of the S_0 manifold, one might expect the two extremes shown in figure VI-15. In figure VI-15A, the S_1 manifold is not displaced and thus there is very little positive overlap of the vibrational wavefunction in the S_0 state. In this case, internal conversion would be slow and the relaxation pathway would probably be dominated by fluorescence if the $S_1 \rightarrow S_0$ transition is orbitally allowed. In B, good overlap results and very rapid internal conversion would be expected so most of the relaxation would be non-radiative vibrational relaxation.

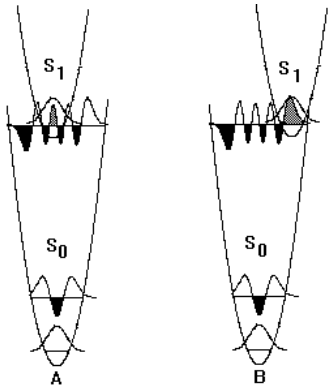

Figure VI-15. Overlap (dotted area) resulting between the v=0 level of the S_1 manifold with the v'=7 level of the S_0 manifold for two different amounts of displacements of S_1. Heavilly shaded areas represent regions where vibrational wavefunctions are negative.

VI.10 Bandshapes

The idealized spectrum presented for CO in figure VI-5 is seldom realized by the inorganic researcher. Usually bands are very broad (FWHM of 500 - 2000 cm^{-1} are common) and have shoulders rather than pronounced peaks. There are many factors contributing to the breadth of electronic transitions some of which are listed here.

- *Vibrational Coupling*. Vibrational progressions will necessarily broaden an electronic transition and in fluid solution, each of the vibrational peaks has associated with it a set of rotational lines so that each peak in the progression will itself be broadened. In a vibronically allowed transition there may be many false origins, each of which may have a progression in totally symmetric modes. In solid state spectra, lattice modes and combinations of lattice modes with the progressions will also broaden the peak.
- *Lifting of Degeneracies*. Spin-orbit coupling and Jahn-Teller distortions can both lift the degeneracy of a transition but the effect may not be great enough to resolve the resulting states so that the transition(s) simply appears to be broad. The same result can be observed if a complex is prepared in which the symmetry of the molecule is low, but the ligand substitution is such that the deviation from higher symmetry is small. If the deviation is small enough, degenerate modes will again be split but not split enough to be resolved.
- *Variations in Crystal Field Strength*. Dq is proportional to the $(R_{M-L})^5$ so Dq will vary during the metal-ligand vibrations and thus broaden dd bands.
- *Inhomogeneous Broadening*. The molecules are not all in the same environment. This usually contributes 10 to 15 cm^{-1} to every line in the band.
- *Homogeneous Broadening*. In addition to 0-0 band, hot-bands of the type 1-1, 2-2 etc. are also possible. For a harmonic oscillator all of these bands have the same energy, but anharmonicities will make them differ. Since these bands originate from excited vibrational levels, they will only be important for low frequency vibrations and should not be a factor at low temperatures.

In order to resolve the components of vibronic progressions it is usually necessary to reduce the bandwidths of the vibronic peaks. Thus, highly resolved spectra are usually shown at substantially lowered temperatures, 80K and 5K being typical. The purpose of the low temperature is to reduce the molecular rotations that result in rotational broadening of each of the vibrational lines and to eliminate the homogeneous broadening, but frozen samples are usually opaque and full of cracks precluding acquisition of good absorption spectra. There are

a number of solvent systems, however, that do not freeze but **glass** instead. A good glass will look like the solution, *i.e*. be transparent, but still substantially reduce molecular motion. Typically a good glassing solvent is one that has low symmetry and does not hydrogen bond extensively. The glassing solvent can be either a pure substance, *e.g*., ethanol or a mixture, *e.g*., a 4:1 ethanol:methanol mixture. Almost all spectra showing vibronic progressions of sharp peaks are reported at low temperatures (<80K) in glassy solutions.

VI.11 Emission *vs.* Absorption

Emission occurs from the v=0 level of the lowest lying excited electronic state of a given spin into the ground state manifold (Kasha's rule). Since the final vibrational level can be any level of the ground electronic manifold (depending on the Franck-Condon factors), the progression frequencies are those of the ground state unlike the absorption process which yields progressions in excited state frequencies. Indeed, the absorption peak and the corresponding emission peak often appear as mirror images. Based on the considerations made so far, one would expect the 0-0 bands for the emission and absorption to be at the same place with the absorption band having structure on the high energy side and the emission having low energy structure. Usually, however, the 0-0 bands of the emission and the absorption do not coincide - the difference between them being the **Stokes** shift. There are several reasons for a Stokes shift:

- Often times the emission is a phosporescence and much of the Stokes shift is due primarily to the singlet-triplet energy separation. See figure VI-16A.
- In the case of a very displaced oscillator, the 0-0 bands are not observed in which case several quanta of vibrational energy can contribute to the Stokes shift. See figure VI-16B.
- Due to the vertical nature of the absorption, the molecule ends up in the excited state with ground state geometry and solvation. A non-radiative relaxation to the excited state equilibrium geometry and solvation is then required. Emission occurs to the ground state, but the result is a molecule in the ground state with excited state geometry and solvation. See figure VI-16C.

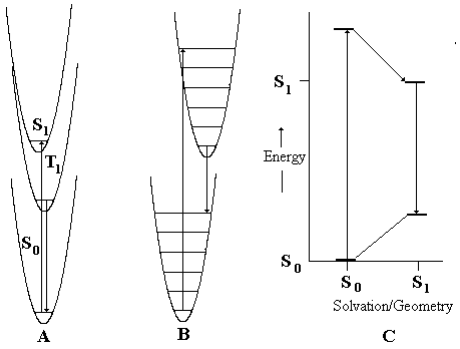

Figure VI-16. Contributions to the Stokes shift. (A) Absorption is into spin allowed manifold while emission is from lower lying spin forbidden manifold. (B) Excited state is so displaced that 0-0 band is not seen for emission or absorption. (C) Absorption is into excited state but with ground state geometry and solvation while emission is into ground state but with excited state geometry and solvation.

The non-radiative energy changes in figure VI-16C are the **reorganization energies** which can be inner-sphere (molecular geometry) or outer-sphere (solvent reorientation). The outer-sphere reorganization energy is large when the dipoles of the ground and excited states are different and the solvent is polar. Thus, transitions which involve large dipole changes are expected to show a solvent dependence (**solvatochromism**). There are essentially three types of electronic transitions in inorganic compounds: metal localized (LF); ligand localized (*e.g.*,

ππ*); and **charge transfer** transitions, *i.e*, transitions which involve movement of electron density from one region of the molecule to another,. Only the charge transfer (CT) transitions result in appreciable changes in dipole and thus show a marked dependence on the solvent - usually on the solvent dipole. As an example, consider a *ligand to metal charge transfer* on a hypothetical diatomic MBr where an electron is transferred from a Br p-orbital which has some π-bonding character to an empty t_{2g} orbital on the metal which has some π* character (refer to figure VI-17). Initially, the dipole on MBr is pointing to the electronegative bromine atom and the solvent dipoles are aligned so as to minimize the energy of the system. Upon charge transfer excitation, the M-Br bond elongates as the electron is promoted from a bonding to an antibonding orbital, *i.e*., the molecule undergoes an **innersphere reorganization**. In addition, the metal becomes electron rich while the bromine becomes electron deficient changing the direction of the dipole so the solvent molecules must rotate to realign the dipoles, *i.e*., the system undergoes an **outersphere reorganization**. Solvent effects are most notable for species which are polar to begin with and whose CT's result in a change in direction of the dipole. Non-polar species often show no solovent dependence in their CT bands.

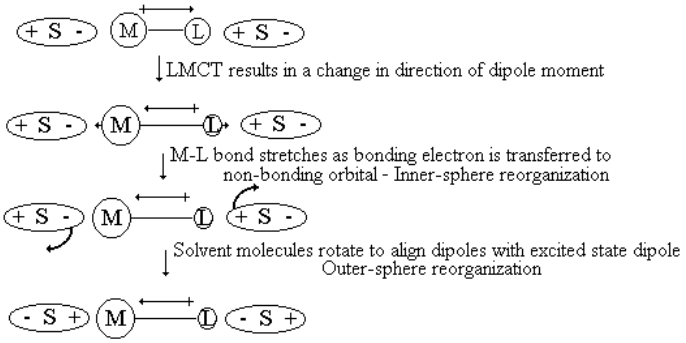

Figure VI-17. Inner- and outer-sphere reorganizations following an LMCT excitation.

Problem VI.9 Predict the direction of shift of MLCT emissions in going from the fluid to the glassy state (see section VI.9). Explain your answer.

VI.12 Ligand Field Spectra

The student should review section II.9 on the molecular orbital theory of transition metal complexes especially the factors influencing 10Dq and ligand field strengths. Ligand field (LF), crystal field (CF) and dd bands are three names for the same type of transitions - those between the d-orbitals on the metals which are formally forbidden in centrosymmetric molecules (Laporte forbidden) but are often observed as very weak bands (vibronically allowed). The energies of these transitions are clearly dependent on the crystal field splitting, but the observed peaks are between states not orbitals so the value of 10Dq for systems with more than one d electron is not simply the energy of an observed transition. In this section, the method for deducing the value of 10Dq from the observed spectra is presented. This will be done by examining the spectra of several $M(H_2O)_6^{m+}$ ions. As mentioned earlier, hole configurations and electron configurations can be treated in the same manner so in the following discussions we will do examples d^1 and d^9 together and then d^2 and d^8 together. The d^3 case is presented as a homework assignment.

d^1 - $Ti(H_2O)_6^{3+}$ & d^9 - $Cu(H_2O)_6^{+}$

The electron in the d^1 case is in a t_{2g} while the hole in the d^9 case is in an e_g orbital. In both cases, only one transition is expected either the $^2T_{2g} \rightarrow {}^2E_g$ or the $^2E_g \rightarrow$

$^2T_{2g}$. Both cases however are subject to Jahn-Teller distortion in both the ground and excited states. The determination of 10Dq which would be expected to be the energy of the transition in either case is therefore somewhat complicated.

$Ti(H_2O)_6^{3+}$ has a weak band at 20.1 kK (ε = 5.7) which was readilly assigned to this $^2T_{2g} \rightarrow {}^2E_g$ dd band. However, there is also a shoulder at 17.4 kK which was assigned to a Jahn-Teller distortion. As mentioned in section VI-5, $Ti(H_2O)_6^{3+}$ undergoes Jahn-Teller distortion in the ground state ($^2T_{2g} \rightarrow {}^2B_{2g} + {}^2E_g$), a tetragonal distortion involving either an equatorial elongation or an axial compression as it is this type of distortion that results in a $^2B_{2g}$ ground state. However, two bands separated by 2.7 kK cannot be attributed to a ground state distortion as this would imply substantial population of an energy level at ~10kT. Thus, there must also be a Jahn-Teller distortion of the excited state: $^2E_g \Rightarrow {}^2A_{1g}$ (z^2) + $^2B_{2g}$ (x^2-y^2) through the e_g vibration (see figure VI-8). The two observed bands then are assigned as $^2B_{2g} \rightarrow {}^2B_{1g}$ (17.4 kK) and $^2B_{2g} \rightarrow {}^2A_{1g}$ (20.1 kK). The value of 10Dq is not clear in this case but a rough estimate is ascertained from the average of the two transitions to be 10Dq ≈ 18.7 kK.

The distortion is so pronounced in $(NH_4)_2Cu(H_2O)_6(SO_4)_2$ that four dd bands have been assigned[7] to the orbital transitions: $z^2 \rightarrow x^2$-y^2 (6.4kK); xz & yz → x^2-y^2 (11.5 & 12.4 kK); xy → x^2-y^2 (10.7 kK).

Crystal field transitions involving metals with more than one d-electron are more difficult to assign since many states can arise from one orbital transition (see section VI.2). In order to determine 10Dq, the dd bands must be assigned, but the dd band energies depend on the value of 10Dq. Thus, the variation of the state energies with field strength must first be understood. A diagram displaying this variation for all of the states is referred to as a **correlation diagram**. We will consider the easiest example, that of the d^2 ion.

At the weak field extreme, the metal d-orbitals can be treated like the free ion. The terms arising from the d^2 ion are given by values of L, the total angular momentum, from $\ell_1 + \ell_2 = 2+2 = 4$ down to $|\ell_1 - \ell_2| = 2 - 2 = 0$ in increments of one. So for d^2, L = 4, 3, 2, 1, 0 for G, F, D, P and S terms. The multiplicity of each of the terms is determined by the Pauli exclusion principle. Thus the triplets cannot be derived from states in which $m_{\ell_1} = m_{\ell_2}$ so the 2+2 = 4 (G), 1+1 = 2 (D) and the 0+0 = 0 (S) are the singlets while the 2+1 = 3 (F) and the 1+0 = 1 (P) are the triplets. The states derived from a d^2 configuration are therefore ^1G, ^3F, ^1D, ^3P and ^1S. The energy ordering of the terms is determined by calculation to be $^3F < {}^1D < {}^3P < {}^1G < {}^1S$. The terms arising from a d^n configuration of the free ion (K_h symmetry) split in the presence of an octahedral field in the following manner:

Term	Components in O_h Field
S	A_{1g}
P	T_{1g}
D	$E_g + T_{2g}$
F	$A_{2g} + T_{1g} + T_{2g}$
G	$A_{1g} + E_g + T_{1g} + T_{2g}$
H	$E_g + T_{1g} + T_{1g} + T_{2g}$
I	$A_{1g} + A_{2g} + E_g + T_{1g} + T_{2g} + T_{2g}$

We now have the weak field side of our correlation diagram. For the strong field side, we simply determine the states derived from $(t_{2g})^2 < (t_{2g})^1(e_g)^1 < (e_g)^2$ configurations as we did in secton VI.2. A rough correlation diagram for this d^2 case is given in figure VI-18.

[7] Hitchman, M.A.; Waite,T.D., *Inorg. Chem*., **1976**, 15, 2150.

Examination of figure VI-18 allows us to conclude that, in the d^2 case, the two lowest energy, spin allowed transitions in a weak field would be the $^3T_{1g} \rightarrow {}^3T_{2g}$ and $^3T_{1g} \rightarrow {}^3A_{2g}$ while in a strong field they would be $^3T_{1g} \rightarrow {}^3T_{2g}$ and $^3T_{1g} \rightarrow {}^3T_{1g}$ and at some intermediate field strength the $^3T_{1g} \rightarrow {}^3A_{2g}$ and $^3T_{1g} \rightarrow {}^3T_{1g}$ are at similar energies and could give rise to one broad band.

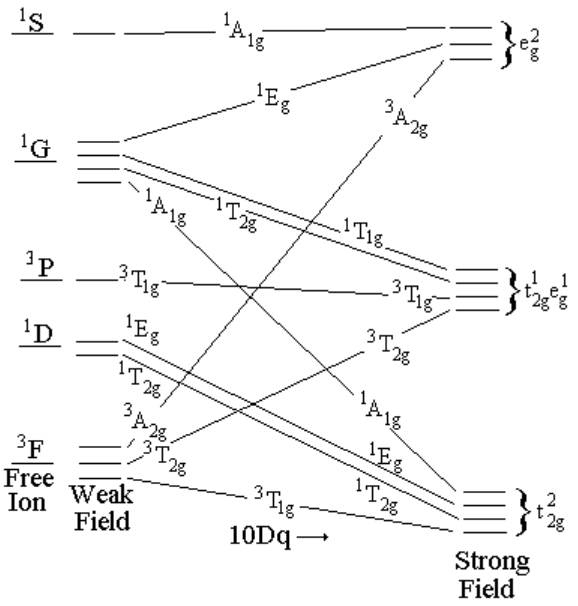

Figure VI-18. A rough correlation diagram for a d^2 ion showing how the state energies vary with the crystal field splitting, 10Dq. Energies are not to scale.

The assignment of crystal field bands is most easily accomplished with the use of **Tanabe-Sugano diagrams**.[8] Tanabe-Sugano diagrams are calculated correlation diagrams in which the ground state is always the abscissa at zero energy and where energies are given in terms of the dimensionless quantities E/B and 10Dq/B (B is a Racah parameter used to take into account interelectronic repulsions and will depend upon both the metal and the ligand and as such will be an unknown in the experiment). The Tanabe-Sugano diagrams used in this text are modified from those given by Offenhartz.[9] The state energies are functions of the ratio of the Racah parameters, C/B, which varies over the range of 3.5 to 4.5. The diagrams presented here are for a C/B ratio of 3.70 which differs from that presented in either Cotton or Huheey so care must be made in comparing these sets of diagrams and the parameters obtained from them with other diagrams and other derived parameters.

The procedure for assignment of dd bands:

1. Measure the energies of the observed dd bands.
2. Convert the energies to unitless quantities by taking ratios. These ratios can be either the ratios of the band energies to the lowest band energy or the ratios of differences between adjacent bands to the lowest energy band.
3. Use the diagram to find the best value of 10Dq/B to best fit the data.
4. Determine the value of E/B for the lowest energy transition at the value of 10Dq/B determined in #3. Since E is the observed band energy, B can be

[8] Tanabe, Y.; Sugano, S., *J. Phys. Soc. Japan*, **1954**, 753, 766. and *J. Phys. Soc. Japan*, **1965**, 20, 1155.

[9] Offenhartz, P. O'D, Atomic and Molecular Orbital Theory, McGraw Hill, NY, 1970.

determined from the value of E/B. Once B is known, 10Dq can be determined from 10Dq/B.

d^2 and d^8 - $V(H_2O)_6^{3+}$ and $Ni(H_2O)_6^{2+}$

V^{III} is d^2 while Ni^{II} is d^8 and the orbital occupancies for the possible states are given in figure VI-19.

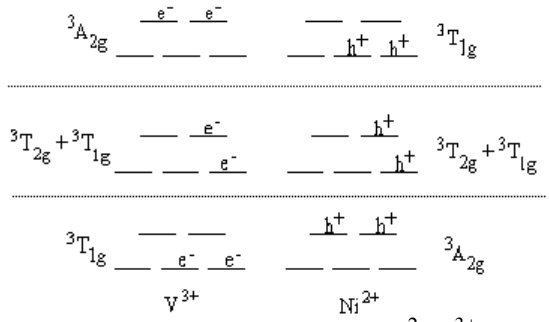

Figure VI-19. Orbital occupancies possible with d^2 (V^{3+}) and d^8 (Ni^{2+}) systems. The same states are derived in each case, but the order is reversed.

Hence, the following transitions are predicted:

	d^2	d^8
I	$^3T_{1g} \rightarrow {}^3T_{2g}$	$^3A_{2g} \rightarrow {}^3T_{2g}$
II	$^3T_{1g} \rightarrow {}^3T_{1g}$	$^3A_{2g} \rightarrow {}^3T_{1g}$
III	$^3T_{1g} \rightarrow {}^3A_{2g}$	$^3A_{2g} \rightarrow {}^3T_{1g}$

It should be noted that transition III involves a two electron transition and will be very weak if it is observed at all. It should also be noted that the order of the transitions II and III in the vanadium complex will depend upon the relative values of B and 10Dq. Simplified Tanabe-Sugano diagrams showing only the states involved in these transitions are shown in figure VI-20.

The observed dd bands are at the following energies in kK(ε):

$V(H_2O)_6^{3+}$[10]	$Ni(H_2O)_6^{2+}$[11]
17.8 (3.5)	8.5 (2)
25.7 (6.6)	13.8 (2)
?	25.3(5)

For the vanadium example, the energy differences between adjacent energy levels would be 17.8 and 25.7-17.8 = 7.9 kK and the ratios of the differences would be 17.8/7.9 = 2.3 : 1. We then refer to Tanabe-Sugano diagram for d^2 in figure VI-20 and move across the 10Dq/B line measuring vertical distances until the ratio between the two lowest triplets is 2.3:1. This occurs at 10Dq/B ≈ 30 where E/B for the lowest lying triplet is 28 but the lowest lying triplet occurs at 17.8 kK thus 17.8/B=28 so that B = 17.8/28 or 0.64 kK (640 cm^{-1}). 10Dq = 30B = 30(0.64) = 19 kK. Using these derived parameters and the diagram, we can calculate the second transition energy: E/B = 41 for the $^3T_{1g}$ state so the energy of the transition is 41(0.64) = 26 kK. The $^3A_{2g}$ state is not shown on the abbreviated diagram in

[10] Horner, S.M.; Tyree, S.Y.; Venexky, D.L., *Inorg. Chem.*, **1962**, 1, 844.
[11] Bose,A.; Chatterjee, R., *Proc. Phys. Soc.*, **1963**, 83, 23.

figure VI-20, but on more extensive diagrams its value at 10Dq/B = 30 is about 58 so E ≈ (0.64)(58) = 37 kK.

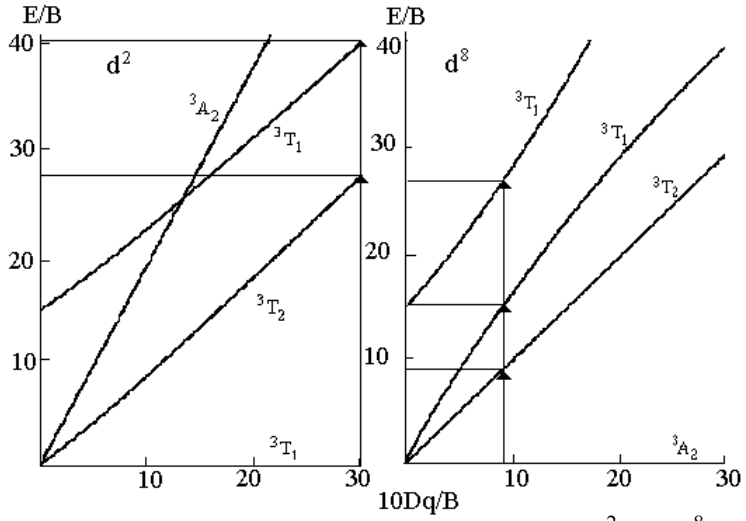

Figure VI-20. Simplified Tanabe-Sugano diagrams for the d^2 and d^8 systems showning only the allowed triplet states. The arrows represent the transitions observed for the $V(H_2O)_6^{3+}$ and $Ni(H_2O)_6^{2+}$ ions.

dd bands and asignments for $V(H_2O)_6^{3+}$
based on 10Dq=19 kK and B = 640 cm^{-1}

observed (kK)	Calculated (kK)	Assignments
17.8 (3.5)	17.8	$^3T_{1g} \rightarrow {}^3T_{2g}$
25.7 (6.6)	26	$^3T_{1g} \rightarrow {}^3T_{1g}$
?	37	$^3T_{1g} \rightarrow {}^3A_{2g}$

In the nickel case, the successive differences are 8.5, 5.3 and 11.5 kK which give ratios of 1 : 0.62 : 1.4 which yield 10Dq/B ≈ 9 at that point E/B is also 9 thus B = 8.5/9 = 0.94 kK. 10Dq = 9B = 8.5 kK. These values and the Tanabe-Sugano diagram can be used to calculate the next two transitions to be at 13 and 26 kK also in good agreement with the observed values. The results of this treatment are the assingments, and values for B and 10Dq:

dd bands and asignments for $Ni(H_2O)_6^{2+}$ based
on 10Dq=8.5 kK and B = 640 cm^{-1}

Observed (kK)	Calculated (kK)	Assignment
8.5 (2)	8.5	$^3A_{2g} \rightarrow {}^3T_{2g}$
13.8 (2)	13	$^3A_{2g} \rightarrow {}^3T_{1g}$
25.3(5)	26	$^3A_{2g} \rightarrow {}^3T_{1g}$

The effect of the ligand on the crystal field splitting can be seen by a comparison of the spectra of $V(H_2O)_6^{3+}$ with that of $V(CN)_6^{3-}$ which has dd bands at 22.2 (ε=27) and 28.6 (ε=50) kK.[12] The parameters derived from this data are 10Dq = 23.9 kK and B = 550 cm^{-1}. The much stronger field presented by the cyanide ligand increases the energy of the transitions some 3 to 4 kK and increases 10Dq by 7 kK. Remember that, in this case, not only are the e_g destabilized by σ-donation into them, but the metal t_{2g}'s are stabilized as a result of back bonding into the C≡N π*.

[12] Holloway, C.E.; Mabbs, F.E.; Smail, W.R., *J. Chem. Soc. (A)*, **1969**, 2330.

Problem VI.10 Refer to the Tanabe-Sugano diagram for d^3 in O_h field and assign the bands in the electronic spectrum of $Cr(H_2O)_6^{3+}$ [kK(ε): 14.0(2), 17.4(13), 24.6(15), 37.8(4)]. What is the value of 10Dq? Suggest reasons why the 14.0 kK bandsis so weak and broad.

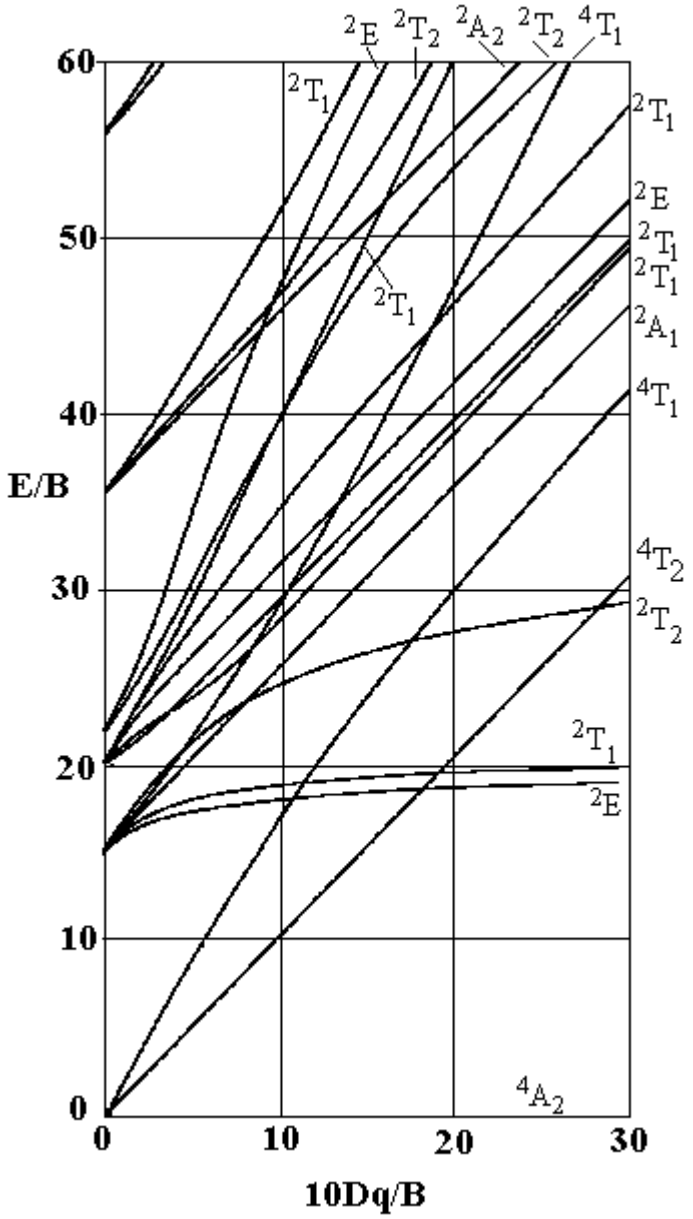

Tanabe-Sugano type diagram for a d^3 system on an O_h field.

VI.13 Charge Transfer Spectra

Since CT bands arise from transitions in which there is a transfer of electron density from a donor to an acceptor, a **favorable overlap between the orbitals is required**. The transition can be viewed as a redox process where the donor is oxidized and the acceptor is reduced, $AD \rightarrow A^-D^+$. In complexes which have MLCT bands in the visible, it is common to

observe both the metal oxidation and the ligand reduction in the cyclic voltammogram. The two processes are then,

$AD \rightarrow AD^+ + e^-$ $\quad E_{ox}$ - potential of donor

$AD + e^- \rightarrow A^-D$ $\quad E_{red}$ - potential of acceptor

and the difference between them is essentially the CT process

$AD \rightarrow A^-D^+$ $\quad E_{ox} - E_{red}$

In the cyclic voltammogram of $[Ru^{II}(bpy)_3]^{2+}$ the oxidation of Ru^{II} to Ru^{III} is observed at +1.29V while the reduction of bpy to bpy- occurs at -1.33V. Thus, $E_{ox} - E_{red} = 2.62V$ while the MLCT band is observed at 22.0 kK or 2.73 V. The reason that the MLCT energy will always exceed $E_{ox} - E_{red}$ is that the optical energy difference does not include reorganization while the much slower electrochemical process does (see section VI.11). The energy difference between the two is then the innersphere and outer- sphere reorganization energies in the excited state. If, however, one compares $E_{ox} - E_{red}$ with the emission energy the redox energy would be greater by the reorganization energy of the ground state - if the emission is from the same state that the absorption is into.

It should be clear from the above discussion and figure VI-21 that the more easily the metal (D) is oxidized (less positive E_{ox}) and the more easily the ligand (A) is reduced (more positive E_{red}), the lower will be the energy of the MLCT. To decrease the energy of LMCT's the opposite is required: a metal (Acceptor in LMCT) which is difficult to oxidize will be easier to reduce so the Acceptor orbital will be lower. Indeed, one way to distinguish LMCT from MLCT is the direction of the shift in the band as the oxidation state of the metal changes. Increases in the oxidation state stabilizes the metal orbitals and thus MLCT bands will increase in energy (blue shift) while LMCT bands will decrease in energy (red shift).

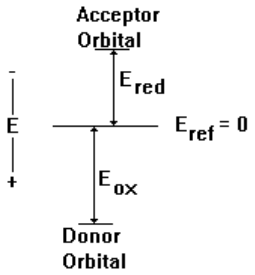

Figure VI-21. Oribital enerergies of donor and acceptor orbitals relative to a reference potential is the case where the acceptor reduction is at negative potential and the oxidation potential of the donor is at positive potential.

Charge transfer transitions *usually* result in a change in the direction and/or magnitude of the dipole and consequently in a substantial outersphere reorganization energy in polar solvents (section VI.11). Indeed, the more polar the solvent the greater the reorganization energy will be. As a result, CT bands are generally characterized by *solvatochromism*, solvent dependence of the absorption maxima. The more polar the solvent, the higher in energy is the CT band. Solvent dependence of a band is strong support for charge transfer character in the band, but lack of solvent dependence does not necessarily rule it out. In order to have a large solvatochromic effect, the charge transfer should result in a change in the direction of the dipole. Therefore, molecules with no permanent dipole in the ground state will usually not show a solvent dependence in their CT bands.

Problem VI.11 Discuss the effects on the CT spectrum of an octahedral d^6 ion as the metal is oxidized. Include MLCT and LMCT energies.

Problem VI.12 Assign the CT bands MLCT or LMCT in the spectra of CoX_4^{2-} shown below. Indicate the transitions on an energy diagram . Account for the trend in energy and complexity as X goes from Cl to I. Refer to Appendix D.

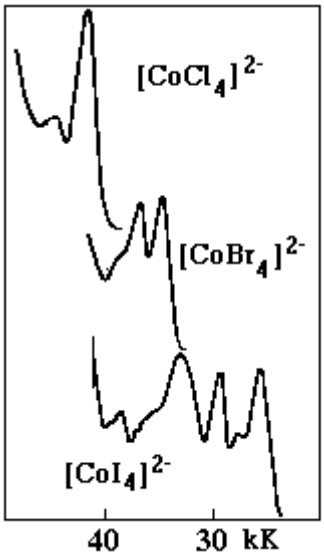

Problem VI.13 The near ir and visible spectra of the cations, bromotris-(methylmercapto-*o*-phenyl)phosphinenickel(II) $[Ni^{II}(TSP)Br]^+$ and bromotris-(dimethylarsino-*o*-phenyl)arsinenickel(II) $[Ni^{II}(QAS)Br]^+$ are given below.

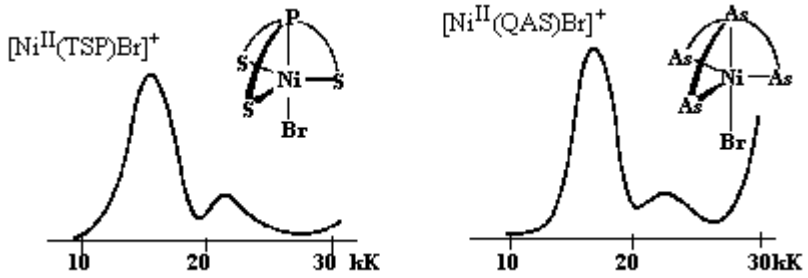

Assign the two bands (~15 and ~21 kK) as to the type of transition (dd, MLCT, LMCT or LC), the orbitals involved (e.g., xz → π*) and the states involved.

Problem VI.14 The electronic spectra of $[Re_2Cl_8]^{2-}$ measured on a single crystal at 5K in z-polarization (solid) and in xy polarization (dotted) and the ir and Raman spectra of the $[Re_2Cl_8]^{2-}$ and $[Re_2Br_8]^{2-}$ ions are given on the next page.

a. Draw the mo diagram for the Re-Re bond (use D_{4h} symmetry and see problem II.3). Construct a table in which the orbital types, orbital symmetries, state symmetries, and polarization of all possible transitions (not just allowed) within the Re-Re framework and originating from the HOMO or SHOMO.

b. Assign the features designated I, II and III in the electronic absorption spectrum. Note that band II undergoes a substantial red-shift in $[Re_2Br_8]^{2-}$ while I and III shift only slightly.
c. Draw symmetry coordinates for all **stretches** of the ion and give the symmetry of each. Suggest assignments for those which are observed.
d. Completely assign all of the vibronic peaks in band I. Identify the ground state and excited state frequencies of the Re-Re stretch. Clearly indicate your reasoning for each assignment.
e. Discuss the differences between the excited state and ground state geometries that can be deduced from the spectra. Is this picture consistent with the electronic assignments?
f. Is the Re-Re stretch strongly coupled to Re-Cl stretch? Remember that Pt-Pt stretch in Cl-Pt-Pt-Cl moiety was strongly coupled to Pt-Cl (section IV-6). Explain.

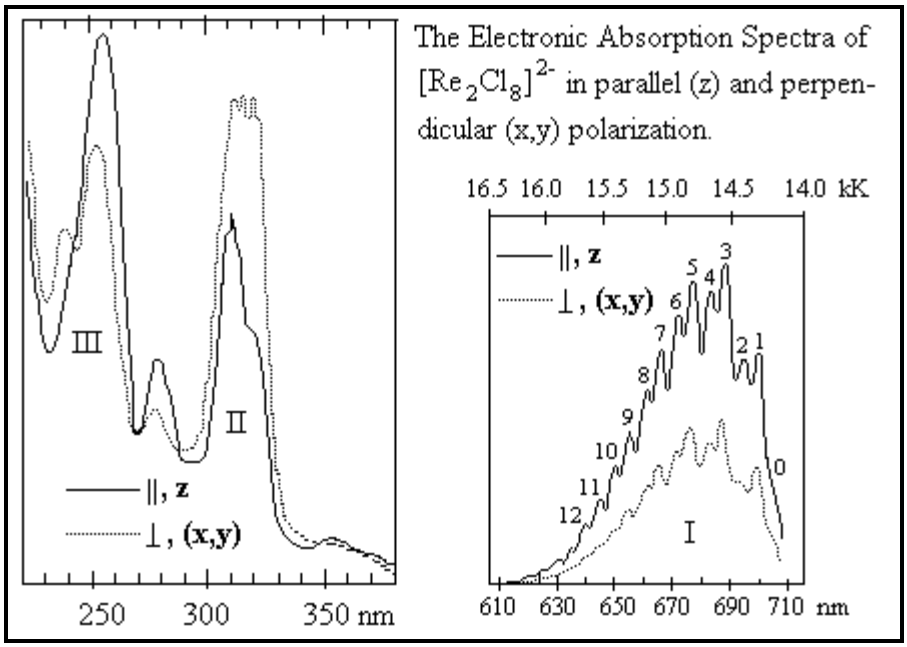

The observed wavelengths for the vibronic progressions observed on band I are given below.

Band #	λ (nm)	Band #	λ (nm)	Band #	λ (nm)	Band #	λ (nm)
0	705.06	4	682.41	7	665.06	11	644.12
1	699.41	5	676.24	8	660.00	12	639.00
2	694.13	6	671.00	9	654.35	13	634.29
3	687.65			10	649.29		

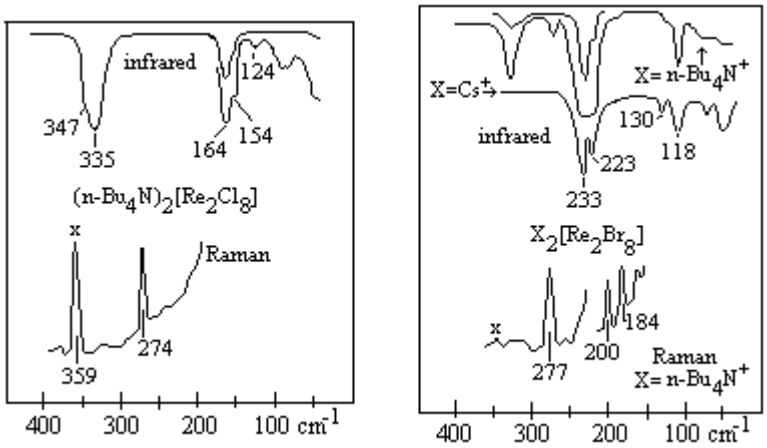

The Raman spectrum of $(n\text{-}Bu_4N)_2[Re_2Br_8]$ in CH_3CN indicated that the lines at 277 and 184 were polarized. There is a spurious laser line at the peak marked "x". However, comparison of the intensities of this peak in the bromide and cloride indicates that there is also a fundamental at this frequency in the choride.

Chapter VII. Electronic Spectroscopy

Part II. Examples

VII.1 Metal-ligand multiple bonding in *trans*-Dioxorhenium(V) Complexes

The structure (D_{4h}) and relative d-orbital energies of *trans*-$O_2Re(py)_4^+$ are shown in figure VII-1. Re(V) is d^2 with a ground state that is $(b_{2g})^2 = {}^1A_{1g}$. The lowest lying excited state, a dd state, is $(b_{2g})^1(e_g)^1 = {}^1E_g$ or ${}^3E_g$. The lowest lying, spin allowed transition then will be ${}^1A_{1g} \rightarrow {}^1E_g$ which is formally forbidden (Laporte) so that the 0-0 band is expected to be very weak or *missing entirely*. The transition can be allowed by an odd number of vibrational quanta of some ungerade modes through weak vibronic coupling.[1] The electric dipole spans $a_{2u} + e_u$ so the vibrations which can serve as false origins are those belonging to the irreducible representations of symmetry $e_g \otimes a_{2u} = e_u$ or $e_g \otimes e_u = a_{1u} + a_{2u} + b_{1u} + b_{2u}$, *i.e.*, any ungerade mode can serve as a **false origin**.

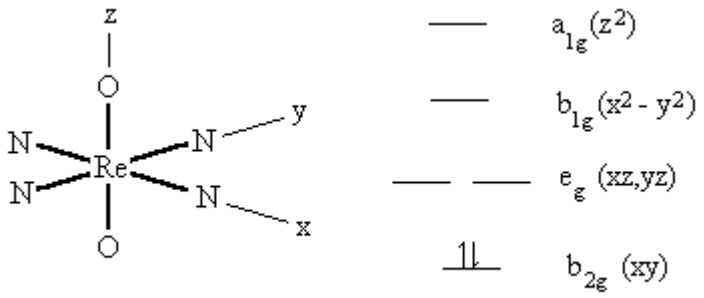

Figure VII-1. Structure and d-orbital energy scheme for *trans*-$O_2Re(py)_4^+$

The spectra of *trans*-$O_2Re(py)_4^+$ have been studied extensively by Gray *et al*.[2] and Hupp *et. al*.[3], and the spectra they report have been modified for presentation here. The room temperature, electronic absorption spectrum (Figure VII-2A) of a solution of *trans*-$O_2Re(py)_4^+$, consists of two features: a relatively strong band at 331 nm (30.2 kK, ε =19,400 M^{-1} cm^{-1}) and a much weaker band at 445 nm (22.5 kK, ε = 1200 M^{-1} cm^{-1}). The latter peak is also observed in the spectra of $O_2Re(CN)_4$ and $O_2Re(en)_2$ (figure VII-3) but with substantially reduced intensity (ε < 50 M^{-1} cm^{-1}) while the former band is not observed at all. The room temperature emission (figure VII-2E) consists of a broad featureless band centered near 640 nm (15.6 kK).

[1] The student should see section IV.3 pp 114-115 for a review of weak vibrational coupling.

[2] (a) Winkler, J.R.; Gray, H.B., *Inorg. Chem*., **1985**, 24, 346. (b) Thorp, H.H.; Challa, C.V.; Turro, N.J.; Gray, H.B., *J. Am. Chem. Soc*., **1989**, 111, 4364.

[3] Johnson, C.J.; Mottley, C.; Hupp, J.T.; Danzer, G.D., *Inorg. Chem*., **1992**, 31, 5143.

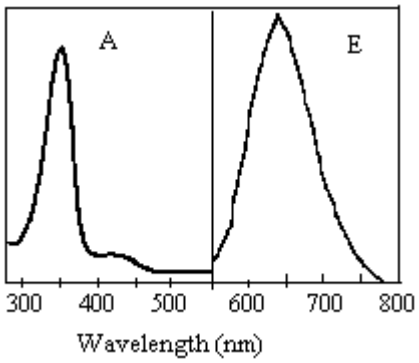

Figure VII-2. Room temperature electronic absorption spectrum (A) of an aqueous solution and the room temperature emission (E) from a CH_3CN solution of *trans*-$O_2Re(py)_4^+$.

The effect of reduced temperature on the band width can be appreciated by comparing these broad, structureless bands to the highly structured single-crystal spectra obtained at 30K. Both bands in the pyridine spectrum are too intense for measurement in the single crystal. However, a band near 445 nm is apparent as a highly structured band in the 30K, single-crystal spectrum of the ethlyenediamine complex (figure VII-3). In addition, there is a very weak feature centered near 550 nm in this spectrum that is too weak to be observed in the above spectra. It is *the analog to this latter, much weaker band on which we will focus in our discussion of the vibronic nature of the excited state of the pyridine complex*.

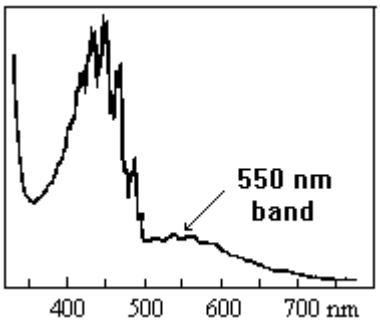

Figure VII-3. The single-crystal electronic absorption spectrum of $[ReO_2(en)_2]Cl$ at 30K.

The low temperature absorption and emission spectra of single-crystal of *trans*-$O_2Re(py)_4BPh_4$ (figure VII-4) and the vibronic peak maxima (tables VII.1 and VII.2) are given on the following page.

The band with a maximum near 500 nm is composed of a 780 cm^{-1} vibrational progression (I, II, III, IV & V) each of which is subdivided into vibronic maxima with spacings of 160-180 cm^{-1} (e.g., [1, 2, 3]; [4, 5, 6]; and [7, 8, 9]). The latter separations are not assigned to a single progression at ~170 cm^{-1} for two reasons: their relative intensities (peaks 1, 2, and 3)change with polarization (solid vs. dashed lines) and are not consistent with a harmonic Franck-Condon progression. Before a further examination of figure VII-4, the student should realize that **the absorbtion which displays the long progressions discussed and is centered near 500 nm is into a different state than that from which the emission spectrum originates**. There are actually three absorption peaks in this region: A, B and C. As will be shown, emission is from the state arrived at by the "A" absorption.

Spectral Features of a single-crystal of $ReO_2(py)_4BPh_4$

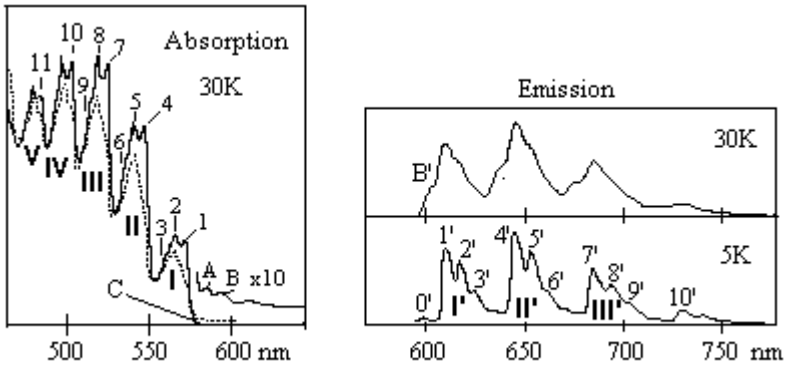

Figure VII-4. Absorption and emission spectra from a single crystal. Solid line absorption: parallel orientation of electric field and crystal needle axis. Dashed line absorption: perpendicular orientation of electric field and crystal needle axis.

Table VII.1. 30K absorption spectrum

Vibronic peak maxima

Peak Number	λ(nm) ±2 nm	ν (cm^{-1}) ±10 cm^{-1}
B	597.1	16748
A	590.1	16946
1	573.9	17425
2	568.2	17599
3	562.4	17781
4	549.2	18208
5	543.9	18386
6	539.0	18553
7	526.7	18986
8	521.8	19164
9	517.3	19331
10	505.9	19767
11	486.8	20542

Vibronic peak separations

Peak Numbers	Δν (cm^{-1})
2 - 1	174
3 - 2	182
5 - 4	178
6 - 5	167
8 - 7	178
9 - 8	167
4 - 1	783
7 - 4	778
10 - 7	781
11-10	775

Table VII.2. 5K emission spectrum

Vibronic Peak Maxima		
Peak Number	λ(nm) ±2 nm	ν (cm^{-1}) ±10 cm^{-1}
B'		16628
0'	599.6	16678
1'	609.4	16410
2'	616.6	16218
3'	623.8	16031
4'	645.0	15503
5'	652.8	15318
6'	661.0	15129
7'	684.6	14606
8'	693.6	14417
9'	703.0	14225
10'	731.6	13669

Vibronic Peak Separations	
Peak Numbers	Δν (cm^{-1})
1' - 2'	192
2' - 3'	187
4' - 5'	185
5' - 6'	189
7' - 8'	189
8' - 9'	192
1' - 4'	907
4' - 7'	897
7' - 10'	937

The 5K emission spectrum, however, is assigned to two vibrational progressions: one of 900 cm^{-1} (I', II', III') and another of 190 cm^{-1} (1', 2', 3'). The peak at 0' (16678 cm^{-1}) is approximately midway between peaks **A** and **1'** (~270 cm^{-1} from each) and is therefore

assigned as the electronic origin for the emitting state, *i.e.*, the 0-0 band for **A** (no Stokes shift). Peaks **A** and **1'** then correspond to the vibronic origins for the absorption and emission, *i.e.*, there is an ungerade mode near 270 cm^{-1} which weakly couples to this excited state making these formally forbidden transitions vibronically allowed. Since emission will be from the lowest lying excited state, peak **A** is the absorption into the $v_u = 1$ level of the lowest lying excited state. Each peak in the emission spectrum requires three vibrational quantum numbers for its description: one for the ungerade mode (v_u) and one for each of the progression forming a_{1g} modes, 190 (v_1) and 900 (v_2) cm^{-1}. Remember that vibrational relaxation to the ground vibrational level of the electronic excited state is the first process to occur upon absorption so that all emission peaks come from the level in which all three vibrational quanta are zero, (0,0,0). The transition labelled **1'** then corresponds to a transition from the lowest lying dd state in which all three vibrational quanta are zero to the ground electronic state where v_u=1,v_1=0, v_2=0, *i.e.*, (0,0,0) → (1,0,0) similarly 2' is (0,0,0) → (1,1,0) and 6' is (0,0,0) → (1,2,1). Thus, peak **6'** is 1 quantum of the ungerade mode (270 cm^{-1}) plus two quanta of the 190 cm^{-1} mode and one quantum of the 900 cm^{-1} mode or 270 + 380 + 900 = 1550 cm^{-1} lower than the electronic origin, *i.e.*, $\nu_{6'}$ = 16678 - 1550 = 15128 cm^{-1}.

With the above analysis in mind, let's go back to the stronger band centered near 500 nm. Remember that Winkler and Gray assign peaks 1, 2, and 3 to different vibronic origins not to a progression. They put the electronic origin for this band near 17200 cm^{-1} (~581 nm, **C** in figure VII-4) or about 500 cm^{-1} above **0'** - the reason for this asignment is unclear. With this origin, however, the vibrational frequencies of the bands labelled 1, 2 and 3 can be approximated as ($\nu_{vib} = \nu_{obs} - \nu_0$): 225 (1), 399(2) and 581(3). In this interpretation then, these three ungerade modes each serve as vibronic origins while the 780 cm^{-1} mode is an a_{1g} progression forming mode which forms progressions on all three origins. Thus four vibrational quantum numbers are needed to describe this system, v_1, v_2, v_3, v_s - the three ungerade modes and the symmetric mode. All absorption is from the ground vibrational level of the ground electronic state - (0,0,0,0). The final levels for several of the peaks shown in figure VII-4 are: peak **1**: (1,0,0,0); peak **2**: (0,1,0,0); peak **4**: (1,0,0,1) and peak **9**: (0,0,1,2). This description is very different from the one used to describe the emission even though the emission and absorption profiles appear to be the same at a casual glance.

The midpoint between peaks **B** and **B'** is at 16,688 cm^{-1} or approximately 10 cm^{-1} higher than 0'. If the frequency of the promoting mode is assumed to be the same in the ground and excited state, its frequency would be (16748-16628)/2 = 60 cm^{-1}. Note that the emitting and therefore lowest energy state is **A** but that absorption into **B** appears at a lower energy because only the false origins are observed and the promoting mode frequency for **B** is much less than the one for **A**! Since **B'** appears only at elevated temperatures, it must be due to an emission from a thermally accessible state. The origin of this higher state would be near 16,688 cm^{-1} or 10cm^{-1} above the lower emitting state. At 30K, kT ~ 21 cm^{-1} and the relative populations of the two states would be exp{-10/21} = 0.6 so that the population of the higher excited state comprises ~40% of the total (0.6/1.6) while at 4.5K, kT ~ 3 cm^{-1} and the relative poplulations become 0.03. It is not surprising that emission from a state with less than 3% of the population would not be observed.

The band systems **A**, **B**, **C** and the stronger sytem centered near 445 nm in the solution spectrum all arise from the lowest lying $b_{2g} \rightarrow e_g$ orbital transition which is expected to yield only two state transitions, $^1A_{1g} \rightarrow {}^1E_g$ and $^1A_{1g} \rightarrow {}^3E_g$. The ^3E_g state, however, is six-fold degenerate, but this degeneracy can be lifted by the spin-orbit coupling expected from a third

row transition metal. Winkler and Gray[1a] do a simple first-order spin-orbit coupling calculation and show that the six spin-orbit states derived from the ^3E_g are (B_{1g}, B_{2g}), E_g and (A_{1g}, A_{2g}) where pairs in parentheses remain degenerate at this level of approximation. Since the E_g level derived from the ^3E_g can gain singlet character by mixing with the ^1E_g, transitions into it should be the strongest "spin forbidden" transition (Band system **C**). The state level diagram is given in figure VII-5.

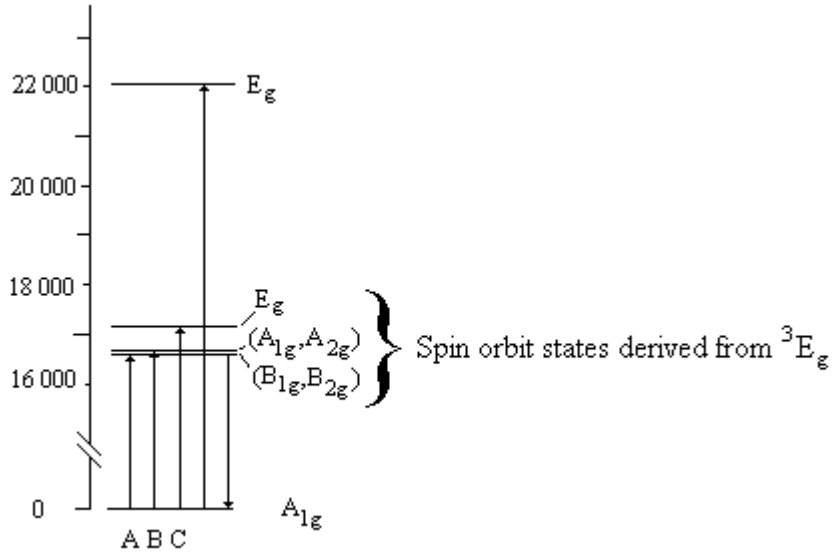

Figure VII-5. State level diagram for $ReO_2(py)_4^+$.

What can be deduced about the nature of this dd excited state? Geometry changes occur along totally symmetric modes and result in progressions of these modes in the absorption and emission spectra. Two progressions are observed in the emission: 190 and 900 cm^{-1} (ground state frequencies) but only one was assigned in the absorption: 780 cm^{-1} (excited state frequency). Substitution of ^{18}O results in a drop in the 780 and 900 cm^{-1} progression down to 740 and 850 cm^{-1}, respectively, consistent with the expected mass effect for the symmetric O=Re=O stretch. Since a progression in this mode is observed (up to v~4), the Re=O bond lengths are **different** in the ground and excited states. Since the mode is about 120 cm^{-1} lower in the excited state, we conclude that the bond **lengthens**. Indeed, a Franck-Condon analysis of the emission profile indicates that the Re=O bond lengthens by 70 pm in the excited state. Based on a study of metal pyridine complexes[4] the 190 cm^{-1} mode was assigned to the symmetric Re-N stretch. Thus, all of the Re-N bonds are either lengthened or shortened in this transition. The analysis of the spectra indicated that the ~170 cm^{-1} spacing in the absorption spectrum was not this mode, so we have no excited state frequency to compare with the 190 cm^{-1} and thus can not determine the direction of the change. However, the b_{2g} (xy) orbital is a Re-py π-bonding orbital (pyridines are in xz and yz planes) while the e_g (xz,yz) is a Re-O π*-antibonding orbital. Removal of electron density from the b_{2g} orbital should therefore weaken the Re-N bond while placing electron density into the e_g orbital will weaken the Re-O bond. Consistent with the conclusions based on the spectroscopy then, the $A_{1g} \rightarrow E_g$ transition is expected to increase both the Re-O and Re-N bond lengths with a corresponding decrease in the stretching force constants (frequencies).

[4] Clark, R.J.H.; Williams, C.S., *Inorg. Chem.*, **1965**, 4, 350.

The intensity of the band at 331 nm (30.2 kK, ε=19,400 $M^{-1}cm^{-1}$) argues for assignnment to a charge transfer band. Indeed, it has been assigned by different groups to either an MLCT into the pyridine or an LMCT from the oxygen. Its absence in the en and CN complexes certainly argues for the MLCT assignment. The question of the assignment, however, has been firmly established by resonance Raman scattering (RRS).[2] Figure VII-6 shows the RRS from $O_2Re(py)_4^+$ obtained "from a dilute sample contained in a spinning[5] NMR tube" with excitations of 356.4 and 406.7 nm. Hupp et al. actually measured the Raman spectra with eight different exciting lines between 647.1 and 356.4 nm but show only three in the paper.[6] The enhancement observed in the spectrum recorded at 356.4 is due to resonance with the charge transfer band while that recorded at 406.7 will involve *pre-resonance* enhancements from both the CT and dd bands. The strongest band in the 406.7 nm spectrum is at 907 cm^{-1} - the O=Re=O symmetric stretch that was the progression forming mode in the dd absorption band. The other modes designated by the dashed lines are pyridine modes. A plot of the extent of enhancement (intensity of a Raman line relative to some peak which is not enhanced - usually a solvent peak) versus the excitation energy or wavelength is referred to as an *excitation profile*. Figure VII-7 shows the excitation profiles for the observed bands. The profile for the 907 cm^{-1} mode has its peak in the excitation profile at 441.7 nm, *i.e.*, in the dd band, while the pyridine modes all appear to be heading for a maximum in the 331 nm band. The fact that the pyridine modes are strongly enhanced at the high energy excitation and appear to be reaching a maximum in the 331 nm band while the Re=O mode is very weak at 356 nm excitation and getting less enhanced as 331 nm is approached is clear evidence for the assignment of the 331 nm band to the Re→ py MLCT and precludes it being the O→Re LMCT.

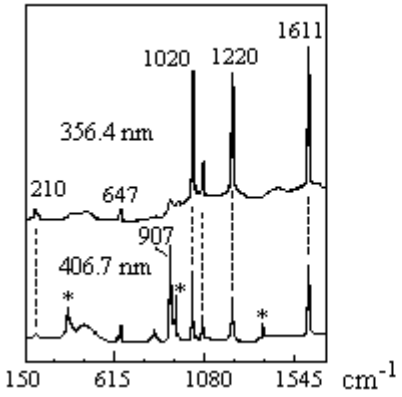

Figure VII-6. The RRS of $O_2Re(py)_4^+$ observed at the designated excitations.

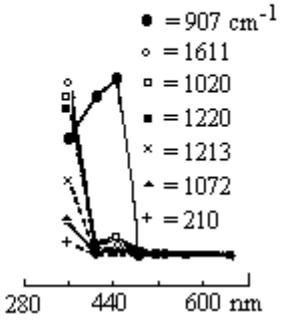

Figure VII-7. Excitation profiles for the modes observed in the RRS of $O_2Re(py)_4^+$

Peaks marked "*" are due to solvent.

VII.2 Metal-Metal Bonding in $Pt_2(\mu\text{-}P_2O_5H_2)_4^{4-}$

The structure of "platinum pop", $Pt_2(\mu\text{-}P_2O_5H_2)_4^{4-}$, which will be abbreviated as Pt_2 in this section is represented by figure VII-9. The pyrophosphito ligands each bridge the two

[5] Spinning the sample is common in RRS experiments to minimize photo-decomposition since one is irradiating the sample with a laser and into an electronic absorption.

[6] In addition to the two specta shown in figure VII-6, they report one recorded with 514.5 nm excitaion, but this line is off resonance and only solvent modes are obaserved.

metals through Pt-P bonds resulting in an anion which has a Pt-Pt separation of 292.5 pm, well under the sum of the van der Waals radii.[7]

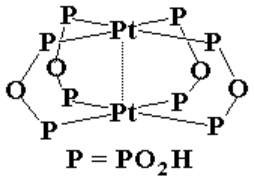

Figure VII-9. A schematic representation of the structure of $Pt_2(\mu\text{-}P_2O_5H_2)_4^{4-}$. The P-O-P group is simply a representation for the pyrophosphito ligand. Each of the ligands is attached to two of the other ligands via hydrogen bonding.

The electronic absorption and emission spectra[8] are shown in figure VII-10. The absorption spectrum consists of a strong band ($\varepsilon = 3.5x10^4$) at 367 nm (27.2 kK) and a much weaker band ($\varepsilon = 1.1x10^2$) at 452 nm (22.1 kK). Excitation at 367 nm results in a fluorescence (τ < 2ns) at 407 nm (24.6 kK) and a phosphorescence (τ = 9.8 ms) at 517 nm (19.3 kK).

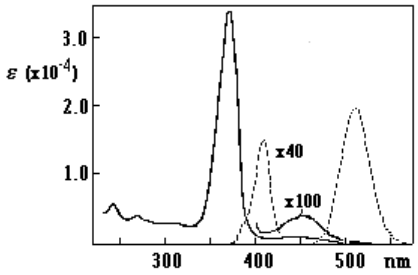

Figure VII-10. Absorption (solid line) and emission (dotted line) of Pt_2 at 25°C

The long lived phosphorescence is indicative of platinum involvement (heavy metal spin-orbit coupling), and the close proximity of the two platinum atoms and the presence of a Pt-Pt stretch at 116 cm^{-1} in the Raman spectrum[9] argue convincingly for a Pt-Pt bond. Interaction is along the z-axis and will involve predominantly the d_{z^2} and p_z orbitals because of their directional nature. However, the d_{xz} and d_{yz} might be expected to interact to a lesser extent. In the following discussion, the dihedral planes bisect the P-Pt-P bond and contain the C_2" axes while the vertical planes contain the P-Pt-P bonds and the C_2' axes. The dσ and pσ orbitals are each a_{1g} while the dσ* and pσ* orbitals are a_{2u}.

	E	$2C_4$	C_2	$2C_2'$	$2C_2''$	i	$2S_4$	σ_h	$2\sigma_v$	$2\sigma_d$	
dσ & pσ	1	1	1	1	1	1	1	1	1	1	a_{1g}
dσ* & pσ*	1	1	1	-1	-1	-1	-1	-1	1	1	a_{2u}

Figure VII-11 gives a qualitative picture of the orbital energy diagram for this system.

[7] The van der Waals radius of platinum is 170-180 pm.

[8] Che, C.-M.; Butler, L.G., Gray, H.B., *J. Am. Chem. Soc.*, **1981**, 103, 7796.

[9] Stein, P.; Dicksonb, M.K.; Roundhill, D.M. *J. Am. Chem. Soc.*, **1983**, 105, 3489. See also sect IV.7 this text.

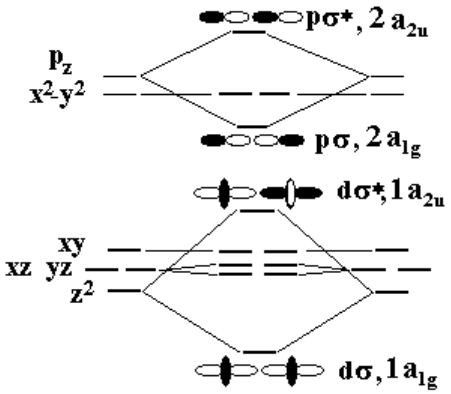

Figure VII-11. Orbital energy level diagram for the face-to-face interaction of two platinum atoms.

Since each platinum is d^8, both the $1a_{1g}$ and the $1a_{2u}$ orbitals are filled so a zero bond order is predicted and thus no Pt-Pt bond should result. However, interaction between orbitals of the same symmetry will stabilize the $1a_{1g}$ and the $1a_{2u}$ and destabilize the $2a_{1g}$ and $2a_{2u}$ with the $1a_{2u}$ orbital becoming essentially nonbonding. In this case, a weak Pt-Pt bond can result. All orbitals are filled so the ground state is $^1A_{1g}$ and the lowest orbital transition is the $d\sigma^* \rightarrow p\sigma$ which gives rise to $^1A_{2u}$ and $^3A_{2u}$ excited states. The $^1A_{1g} \rightarrow {}^1A_{2u}$ transition is fully allowed and is expected to be strong while the $^1A_{1g} \rightarrow {}^3A_{2u}$ transition is spin forbidden. However, due to the large size of the platinum, spin-orbit coupling is expected to be strong, so the spin forbidden transition could well be observed. If this bonding scheme is correct then the strong band at 367 nm would be assigned as the $^1A_{1g} \rightarrow {}^1A_{2u}$ while the much weaker band at 452 nm would be due to the $^1A_{1g} \rightarrow {}^3A_{2u}$. Both bands result from the $d\sigma^* \rightarrow p\sigma$ orbital transition. The two emissions are then assigned analagously: the fluorsescence at 407 nm is the spin allowed $^1A_{2u} \rightarrow {}^1A_{1g}$ while the phosphorescence at 517 nm is the "spin forbidden" $^3A_{2u} \rightarrow {}^1A_{1g}$.

To elucidate the properties of the long lived excited state, Che, Butler and Gray also examined the transient difference spectrum of Pt_2 shown in figure VII-12. In this experiment, a pulse of 355 nm (28.2 kK) radiation from a Nd:YAG laser was used to excite the $^1A_{2u}$ state of Pt_2. The $^1A_{2u}$ state is very short lived undergoes emission or intersystem crossing to the $^3A_{2u}$ state. The spectrometer then detects alternating signals from the ground state and the excited triplet state. In figure VII-12, peaks with positive optical density (OD) are due to the excited state while the peak with a negative OD between 330 and 340 nm is due to the ground state absorption. The intense peak at 325 nm was assigned to $d\sigma \rightarrow d\sigma^*$ of the $^3A_{2u}$ state.

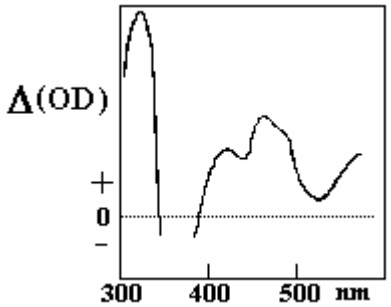

Figure VII-12. Transient difference spectrum of Pt_2 upon 355 nm excitation.

Another powerful method used to probe the nature of long-lived excited states is time resolved resonance Raman (TR^3). In a TR^3 experiment, the molecule is excited into a long lived excited state with an excitation laser and then the Raman spectrum is determined with a probe laser. Many times, the same laser can do both. In the TR^3 experiments on Pt_2, a 7ns pulse of 355 nm radiation from a Nd:YAG laser was used for both the excitation and the probing. Pulsed lasers have very high photon fluxes since all of the radiation is dumped out of the laser in bursts rather than only small portions coming out continuously as is the case for cw (continuous wave) lasers. At 355 nm, Pt_2 has an extinction coefficient of about 20 x 10^3 M^{-1} cm^{-1}, in addition Pt_2* (excited Pt_2) has a very strong band at 325 nm and will, therefore, also have a substantial extinction coefficient at this wavelength. Unfortunately, the actual absorption of the Pt_2* at this wavelength cannot be determined from figure VII-12 due to the bleaching by the ground state. Excitation of Pt_2 at 355 will result in absorption into the singlet state which can then fluoresce (τ<2ns) or undergo intersystem crossing to the triplet. Since the triplet is long lived (τ = 9.8 μs), and the photon flux is high, another photon may be Raman scattered by Pt_2* during the 7ns pulse and this Raman scattering is expected to show some resonance enhancement due to the $d\sigma \rightarrow d\sigma^*$ transition at 325nm. Some of the Pt_2 will resonance Raman scatter rather than absorb the photon so the resulting Raman spectrum will consist of a mixture of the ground state and excited state scattering. The top trace of figure VII-13 shows the TR^3 results obtained on Pt_2.[10]

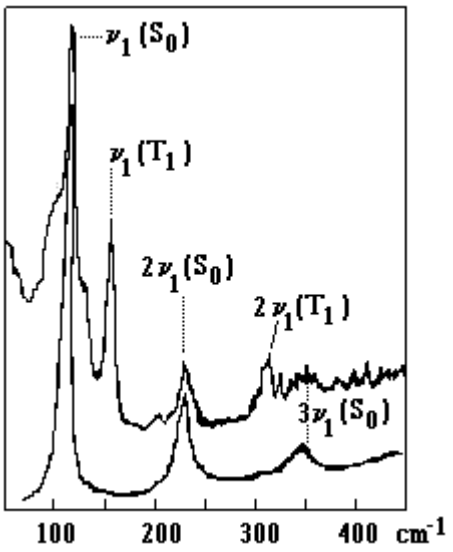

Figure VII-13. TR^3 scattering (top) of Pt_2 recorded with 7ns pulses of 355nm excitaiton, and ground state (bottom) recorded with the 356 nm cw line from a Kr^+ laser.

As can be seen, both ground state (S_0) and excited state (T_1) peaks are observed in the TR^3 while only ground state modes are observed when a cw laser is used. The Pt-Pt stretch (ν_1) is observed in both as would be expected since the orbital transitions involved in the resonance enhancement coupling are $d\sigma \rightarrow d\sigma^*$ and $d\sigma^* \rightarrow p\sigma$ both of which should change the Pt-Pt separation. ν(Pt-Pt) shifts from 118 cm^{-1} in the ground state to 156 cm^{-1} in the excited state.

Problem VII.1 The work of Roundhill *et al*[8] on the Raman spectra of Pt_2 and Pt_2X_2 (X=Cl, Br, I) reported that the Pt-Pt force constant in Pt_2 is 0.3 N/m while in Pt_2X_2 it increased substantially to 1.2 N/m and was independent of X. Account for the large increase in the Pt-Pt force constant with the addition of the halides. Also account for the increase in ν(Pt-Pt) in the excited state (156 cm^{-1}) relative to the ground state (118 cm^{-1}).

VII.3 Mixed Valence Species

In 1896, Werner[11] noted that substances which contained platinum in two oxidation states were considerably darker in color than those containing the metal in but one oxidation

[10] Che, C-M.; Butler, L.G.; Gray, H.B.; Crooks,R.M.; Woodruff, W.H., *J. Am. Chem. Soc.*, **1983**, 105, 5492.
[11] Werner, A., *Z. Anorg. Chem.*, **1896**, 12, 53.

state. It was not until 1950, however, that the color in these complexes was attributed to metal-metal interactions.[12] In the following year, it was suggested that the color was due to a metal to metal charge transfer (MMCT).[13] In 1967, Robin and Day[14] classified mixed valence complexes into three groups depending on the extent of electron delocalization:

Robin-Day Classification

Class	Degree of Delocalization	Spectral Properties
I	none, charge is localized on individual metal centers	spectra of independent centers
II	interemediate	spectra of two centers plus MMCT
III	completely delocalized	independent centers & MMCT are replaced by delocalized system

Later that year, Hush[15] proposed a semiclassical theory relating the energy, molar absorptivity and full width at half height to the extent of electronic coupling in mixed valence systems. The discussion of mixed valence systems that follows is an amalgam of Robin and Day, Hush and the more recent vibronic model present by Piepho, Krausz and Shatz[16] referred to as the PKS model which adds the complete absorption profile of the MMCT[17] by determining the energies and intensities of the complete vibronic manifold. We will apply the resulting model to the Creutz-Taube (CT) ion[18], $[(NH_3)_5Ru\text{-pyrazine-}Ru(NH_3)_5]^{5+}$. The question relevant to the CT ion is whether it is best described as a localized Class I RuII/RuIII system in which the two centers are completely independent; a delocalized Class III system in which the two centers are in identical oxidation states (+5/2 = 2.5); or somewhere in between (Class II) where the two centers have different oxidation states but do "communicate" with one another.

The MMCT process can be written as [2,3] → [3,2] which implies that there is a [3,2] state above the ground state. In the CT complex, the two states will have the same symmetry and thus can interact so the wavefunction for the ground state can be written as a mixture of the two states, *i.e.*, $\Psi_o = (1-\alpha^2)[2,3] + \alpha^2[3,2]$ where the mixing coefficient, α, will depend on the energy separation between the two states and the extent to which they are mixed, $\langle[2,3]|V|[3,2]\rangle$, where V is the interaction term that couples the two. V=0 and α=0 for Class I compounds. $\alpha^2 = (1-\alpha^2) = 0.5$ for a delocalized, Class III compound. For Class II, then, $0 < \alpha^2 < 0.5$. Thus, α^2 is often referred to as the degree of delocalization.

To understand this *electron transfer process*, one must look at the potential energy surfaces on the two centers. In the PKS model, two factors dictate the magnitude of α:

1. *Vibronic coupling*: a two-state vibronic coupling (see pages 120-121) which tends to localize the electron on one center and the hole on the other by introducing a barrier to electron transfer. The PKS model indicates that the normal coordinate to use is the antisymmetric combination of a symmetric monomer mode. In the CT complex, the Ru-N stretch is one choice as the Ru-N bonds are expected to be shorter on the Ru^{III} side. In a stongly coupled system, electron and nuclear motion cannot be separated. Remember the effects of vibronic coupling are to lower the

[12] Sedgwick, N.V., *The Chemical Elements and Their Compounds*, vol. II, Oxford Univ. Press, 1950, p. 1611.
[13] Wey., W.A., *J. Phys. Chem.*, **1951**, 55, 507.
[14] Robin, M.B.; Day P., *Adv. Inorg. Chem. Radiochem.*, **1967**, 10, 247.
[15] Hush, N.S., *Prog. Inorg. Chem.*, **1967**, 8, 301.
[16] Piepho, S.B.; Krausz, E.R.; Shatz, P.N., *J. Am. Chem. Soc.*, **1978**, 100, 2996.
[17] Optical transitions of this type are not confined to metals so MMCT is not always an appropriate term. Instead, the terms intervalence transition (IT) and intervalence charge transfer (IVCT) are often used.
[18] Creutz, C.; Taube, H., *J. Am. Chem. Soc.*, **1969**, 91, 3988; *ibid*, **1973**, 95, 1086.

energy of the minimum and to displace that minimum along the coordinate. The elements $\pm lQ$ in the secular determinant represent the vibronic contribution.

$$\begin{bmatrix} E^0 + \frac{kQ^2}{2} + lQ & V \\ V & E^0 + \frac{kQ^2}{2} - lQ \end{bmatrix}$$

2. *Exciton coupling*: the <[2,3]|V|[3,2]> term described above which tends to delocalize the system. The effect of this term is to move the two surfaces apart in energy, *i.e.*, stabilizing the ground state while destabilizing the excited state and to introduce an *avoided crossing*, *i.e.*, the two surface no longer intersect. The matrix elements V in the secular determinant represent the exciton or electronic coupling. Class III behavior results when $V \geq l^2/k$.

Refer to figure VII-14 in the following discussion. In the absence of any coupling, the two surfaces of the monomers are identical and have a minimum at Q=0 and E = D. The addition of vibronic coupling stabilizes the minima of the two surfaces and moves them apart (dotted lines) as the two monomer units adopt different Ru-N bond lengths. In the absence of any electronic coupling (V=0) there is a crossing at D (the previous minimum). These two surfaces would correspond to a Class I system. When electronic coupling is added to this system there is a stabilization of the lower surface by an amount V and a destabilization by V of the excited state surface (solid lines). Since the two surfaces are now coupled, there is an avoided crossing with a separation of 2V. The resulting surface would represent a Class II system with a thermal barrier to electron transfer (E_{th}), *i.e.*, the exciton[19] is vibronically trapped.

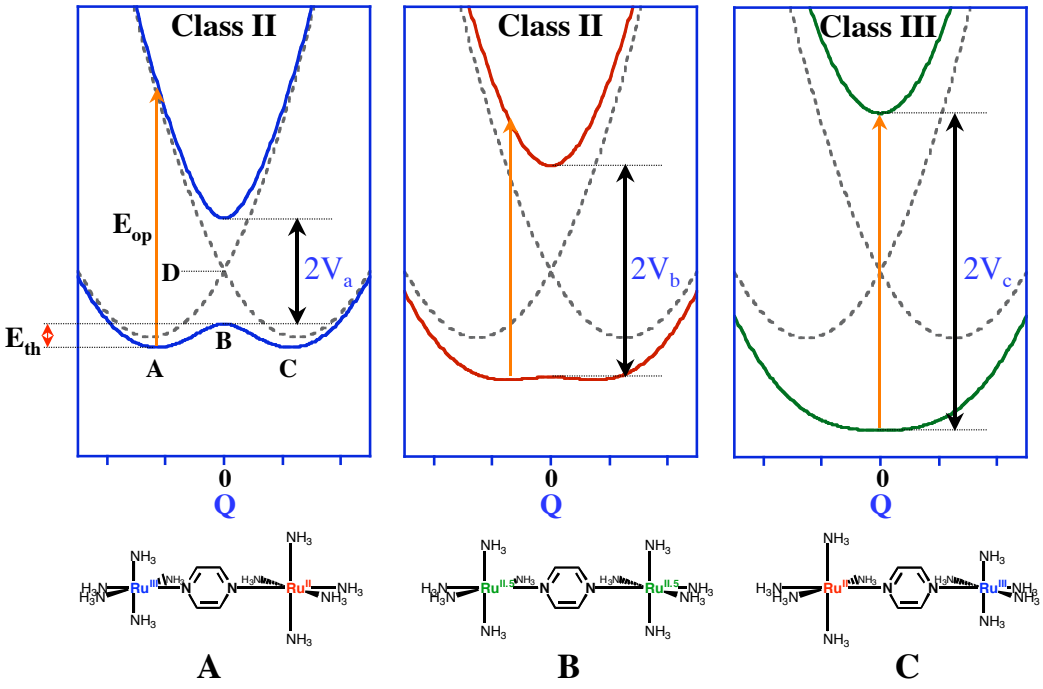

Figure VII-14. (Top) Potential energy diagrams for a mixed valence species with constant lQ and increasing V in going from left to right. (Bottom) metal-ligand bond lengths as the

[19] An exciton is an (electron + hole) pair. If the exciton is trapped then the hole is on one metal while the electron is on the other.

molecule proceeds along Q from the [3,2] to the [2,3] species. A, B, and C refer to points in the top left diagram. The dashed lines in the top left energy diagram would be for a Class I case.

The electron transfer process ([3,2]→[2,3]) can occur in either of two ways, optically or thermally. In the thermal electron transfer, the ion starts out at A with the geometry of [3,2] as shown in the figure to the right (shorter Ru-N bonds on Ru^{III} side). As the ion undergoes the Q normal mode, the shorter bonds begin to elongate while the longer bonds start to shorten; the (vibronic) energy of the ion increases and reaches a maximum at point B where the two halves of the ion are identical and there is no favorable side for the electron. At this point, the motion may proceed in either direction with equal probability. If the mode continues to the right, the electron is transferred and the new minimum at C is obtained, *i.e.*, the [2,3]. Alternatively, the transfer can occur optically with the absorption of a photon, $h\nu = E_{op}$. The Hush model views this transition as one between the two surfaces, *i.e.*, after the [3,2] species absorbs the energy it becomes the [2,3] species but still has the [3,2] geometry. Vibrational relaxation then results in the [2,3] minimum. In the PKS formulation, the upper surface is a delocalized surface with a minimum at Q=0, [2.5,2.5]. Relaxation from this excited state can be to either minimum in the ground state.

The Hush equations apply to the nature of the optical absorption, E_{op} = MMCT or IVCT. They assume Gaussian band shapes and strong valence trapping, *i.e.*, their utility decrease as the class II/class III border is approached.

Hush Equations for Intervalence bands.

$$E_{op} = 4E_{th} \qquad \text{Eq. VII-1}$$

$$\frac{\Delta \bar{\nu}^2_{1/2}}{\nu_{max}} = 16kT\ln 2 = 2312cm^{-1} \text{ at 300K} \qquad \text{Eq. VII-2}$$

$$\alpha^2 = 4.24x10^{-4}\,\frac{\varepsilon_{max}\Delta\nu_{1/2}}{\nu_{max}R^2} \qquad \text{Eq. VII-3}$$

$\Delta\nu_{½}$ = the full width at half-max in cm^{-1}

ν_{max} = the wavenumber of the peak maximum

ε_{max} = the molar extinction coefficient

R = the distance between the metal centers in $\mathring{A}$.

Figure VII-15 shows the spectra obtained for the series $[(NH_3)_5Ru\text{-pyrazine-}Ru(NH_3)_5]^{n+}$, n=4, 5 and 6, *i.e*, for [2,2], [2,3] and [3,3] ions. Relevant to our discussion is the near-ir where a band is observed for the [2,3] species (λ_{max} = 1570 nm, ε_{max} = 6300 M^{-1}-cm^{-1}) but nothing is present in this region for either of the other two species.

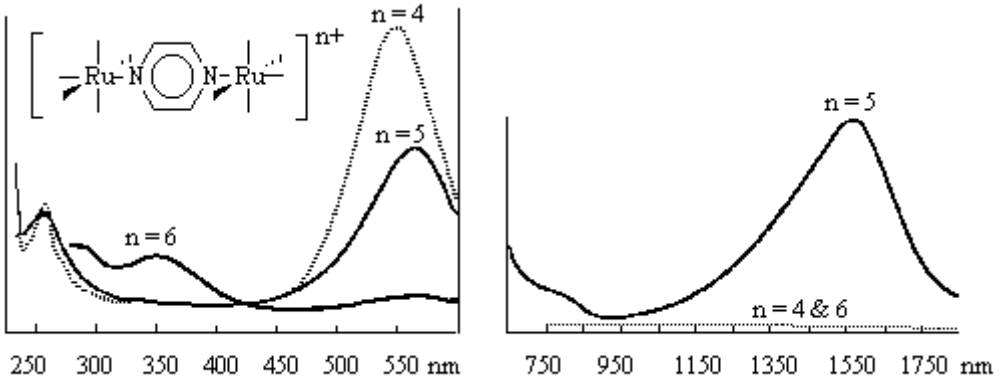

Figure VII-15. Spectra of $[(NH_3)_5Ru\text{-pyrazine-}Ru(NH_3)_5]^{n+}$ taken from reference 12a.

The near-ir band was attributed to the [2,3] → [3,2]* transition, *i.e.*, to the electron transfer process in which the resulting [3,2]* is in the environment of the [2,3]. $\nu_{max} = 1x10^4/1570 =$ 6.4 kK which would imply that the barrier to thermal electron transfer would be about 1.6 kK ($E_{op}/4$). The FWHM is reported to be 1250 cm^{-1}, but according to Equation VII-2, the FWHM at 300K should be $(2312\nu_{max})^{1/2} = (2312)(6400)^{1/2} = 3850$ cm^{-1} - **the observed bandwidth is about three times narrower than that predicted by Hush theory**. The PKS model uses parameters to fit the entire profile of the MMCT and from these parameters, a valence trapping barrier of only 57 cm^{-1} is deduced so that the lowest vibronic level is about 30 cm^{-1} above the barrier, *i.e.*, the degree of delocalization is quite high (nearly class III) and the Hush model is not expected to apply. The band also shows very little solvent dependence which is also indicative of a delocalized ground state, *i.e.*, the transition is not charge transfer in nature. Observed bandwidths much sharper than that predicted by the Hush model are typically indicative of large degrees of delocalization.

Problem VII.2 Assign the peaks in the UV/VIS portion of figure VII-15. Explain why the band maximum near 550 nm has different intensity and energy in the n=4 and n=5 spectra (Note that the weak absorption at 565 nm in n=6 is attributed to residual n=5).

n	λ_{max} nm	$\varepsilon_{max}x10^{-4}$ M^{-1}-cm^{-1}
4	547	3.0
5	565	2.1
6	353	0.58

The above should be contrasted to the results obtained for the near-ir band for the 4,4'-bipyridine bridged system[20]: $\nu_{max} = 9.71$ kK, $\varepsilon_{max} = 880$ M^{-1}-cm^{-1}, $\Delta\nu_{1/2} = 5.3$ kK. The calculated results then become: $5{,}300^2/9{,}710 =$ 2900 cm^{-1} (Hush theory regime); $E_{th} = 9.71/4 =$ 2.43 kK and $\alpha^2 = 0.00175$ (R was assumed to be 10.8 Å). The metals do not communicate across the bipyridine ligand while they are essentially delocalized across the pyrazine.

Problem VII.3 The following near-ir band, observed for $[(bpy)_2Cl\text{-}Ru(pyz)RuCl(bpy)_2]^{3+}$ but not for the 2+ or 4+ ions, has been assigned to the IT band.[21]

[20] Sutton, J.E.; Sutton, P.M.; Taube, H., *Inorg. Chem.*, **1979**, 18, 1017.

[21] Callahan, R.W.; Keene, F.R.; Meyer, T.J.; Salmon, D.J., *J. Am. Chem. Soc.*, **1977**, 99, 1064.

Discuss the extent of metal-metal communication in this ion. Be complete in your discussion. Assume a metal-metal separation of 6.9 Å.

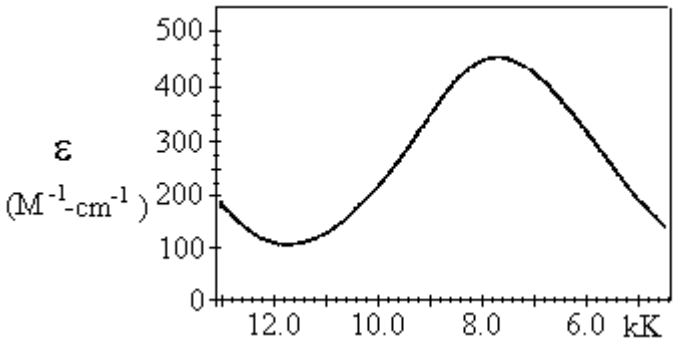

The separation between the metal oxidation potentials is often used in the discussion of metal-metal communication.

$$[2,2] \rightarrow [2,3] + e^- \qquad \Delta G_1 = FE_1$$[22]

$$[2,3] \rightarrow [3,3] + e^- \qquad \Delta G_2 = FE_2$$

The comproportionation constant, K_{comp}, is the equilibrium constant for the reaction

$$[2,2] + [3,3] \rightarrow 2[2,3]$$

which can be express by the difference between the oxidation reactions so (eq1-eq2)

$$\Delta G_{comp} = \Delta G_1 - \Delta G_2 = -F(E_2-E_1) = -F\Delta E_{ox}$$

$$K_{comp} = \exp\{-\Delta G/RT\} = \exp\{F\Delta E_{ox}/RT\}$$

$$\text{so, } K_{comp} = \frac{[2,3]^2}{[2,2][3,3]} = \exp\{F\Delta E_{ox}/RT\}$$

$$\text{or } \mathbf{\log K_{comp} = 16.9\Delta E_{ox}} \qquad \text{Eq. VII-4}$$

In the absence of any communication, the statistical value of $K_{comp} = 2^2/(1*1) = 4$ so at 25° C, ΔE_{ox} = 36 mV (Eq. VII-4, log4/16.9). As the metal-metal interactions increase, so too do K_{comp} and ΔE_{ox}.[23] The cyanogen bridged system has been characterized as delocalized since $K_{comp} \sim 10^{13}$ ($\Delta E_{ox} \sim 0.8$V).

Problem VII.4 The cyclic voltammogram for $[(bpy)_2ClRu(pyz)RuCl(bpy)_2]^{3+}$ showing the 3+/4+ and 4+/5+ couples is shown below (Roman numerals are the oxidation states of the Ru's at that potential). The $E_{1/2}$ values for the two waves are reported to be 0.89 and 1.01 V. Estimate the comproportionation constant for the ion. How does this result compare with the conclusions drawn from the near ir band in the previous problem?

[22] $\Delta G = +nFE$ since oxidation half-reactions are used. n is the number of moles of electrons transferred, F is the Faraday which is 9.65×10^4 C/mol, and E is the potential in volts (1V = 1J/C).

[23] In simple terms, if the two metals do not communicate, then they should both be oxidized at the same potential (36mV separation). If one metal does "sense" the other metal, however, the oxidation of one will affect the oxidation potential of the other.

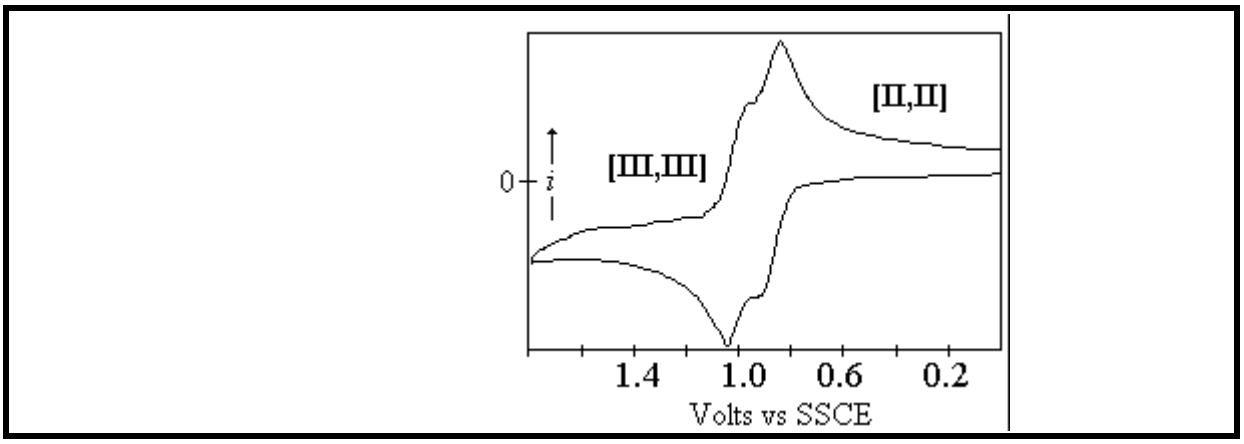

Problem VII.5 The mixed valent state, 2 [2,3], is always stabilized relative to the isovalent state, [2,2] + [3,3]. **Discuss** how electrostatic factors and back bonding affect the stability of the mixed valent state relative to the isovalent one.

VII.4 Spatially Isolated Orbitals in $Ru(bpy)_3^{2+}$

Figure VII-16A shows $Ru(bpy)_3^{2+}$ looking down the C_3 axis. The ion has D_3 symmetry with symmetrically equivalent bipyridine ligands. Thus the mo's would be expected to consist of SALC's constructed from linear combinations of all three bipyridines. The π and π* orbitals of bipyridine transform as either b_2 or a_2 in the C_{2v} point group depending upon whether they are antisymmetric or symmetric with respect to the C_2 rotation. Combining three b_2 bpy orbitals results in a_2 and e SALC's of the D_3 point group while combination of the three a_2 bpy orbitals results in SALC's of a_1 and e symmetry. As shown in figure VII-16B, the LUMO of bipyridine is b_2 in C_{2v} symmetry (plane rather than C_2 axis between the bpys) so the MO's derived from it in D_3 symmetry are A_2 + E. The dπ-orbitals transform as a_1 + e while the dσ's are E. A qualitative mo diagram[24] is presented in figure VII-16C.

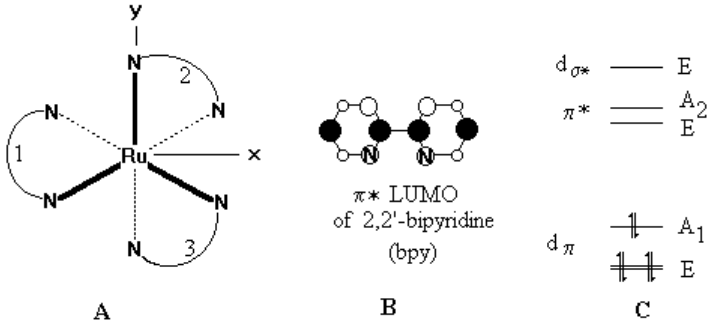

Figure VII-16. (A) $Ru(bpy)_3^{2+}$ viewed along the C_3 (z) axis. The Nitrogens with solid Ru-N bonds are out of the plane while the dotted bonds are behind the xy-plane. (B) Qualitative depiction of the LUMO of bipyridine. (C) Qualitative MO diagram of the Ru d-orbitals and low lying bipyridine π* orbitals involved in the MLCT and electrochemistry.

$Ru(bpy)_3^{2+}$ is deeply colored owing to a relatively strong ($\varepsilon \sim 10^4$) MLCT band centered near 22kK. Upon excitation into this ^{1}MLCT state, the ion undergoes rapid (< 1ps)

[24] Ohsawa, Y.; Whangbo, M.-H.; Hanck, K.W.; DeArmond, M.K., Inorg. Chem., **1984**, 23, 3426.

intersystem crossing to a long-lived, emissive ^{3}MLCT excited state ($\tau \sim 800$ ns in water at 300K, $\nu_{emis} \sim 17$ kK). The excited state is expected to be a strong oxidant and a strong reductant due to its charge transfer nature (see section VI.12). As a result of these properties, researchers have tried to develop systems based on $Ru(bpy)_3^{2+}$ that would serve as photocatalysts for the splitting of water - making it one of the most studied species in chemistry. Much of the debate in the literature centered around the nature of the excited state, *i.e.*, is the transferred charge delocalized in an mo spread over the symmetrically equivalent bipyridines as predicted from group theory

$$(Ru^{II}(bpy)_3^{2+} + h\nu \rightarrow [Ru^{III}(bpy^{-1/3})_3]^{2+*}$$

or is it localized on one bipyridine with perhaps a rapid hopping between the bipyridines?

$$Ru^{II}(bpy)_3^{2+} + h\nu \rightarrow [Ru^{III}(bpy^{-})(bpy)_2]^{2+*}.$$

Is the hole important in this description? If not, we are really asking about the nature of π^* orbital into which the charge is transferred. This π^* orbital is the LUMO and therefore the redox orbital, *i.e.*, the orbital which accepts electrons during the electrochemical reduction. The research into the nature of this orbital took two different directions: the excited state spectroscopy and the spectroelectrochemistry (spectroscopy of electrochemically generated species. We will take up the latter first.

The cyclic volatmmogram (CV) of $Ru^{II}(bpy)_3^{2+}$ shows six reversible one-electron processes[25] (figure VII-17A) occurring in two groups of three with the separation between members of a set being ~200mV while the two sets are separated by ~600 mV. This CV is certainly consistent with one-electron reductions of each of the bipyridines (first set of three waves) followed by the addition of a second electron into each bipyridine. In this picture, the 600 mV (~5000 cm^{-1}) separation would correspond to the pairing energy as second electron is added to the redox orbital. Further support for three spatially isolated bipyridine orbitals rather than mo's spread over all three bipyridines is found the the electronic spectra of the series[26] $[Ru(bpy)_3]^{(2-n)+}$ where n = 0, 1, 2, 3. Additional $\pi \rightarrow \pi^*$ transitions originating from the redox orbital complicate the visible region so the effect of reductions on the MLCT is not clear,[27] but

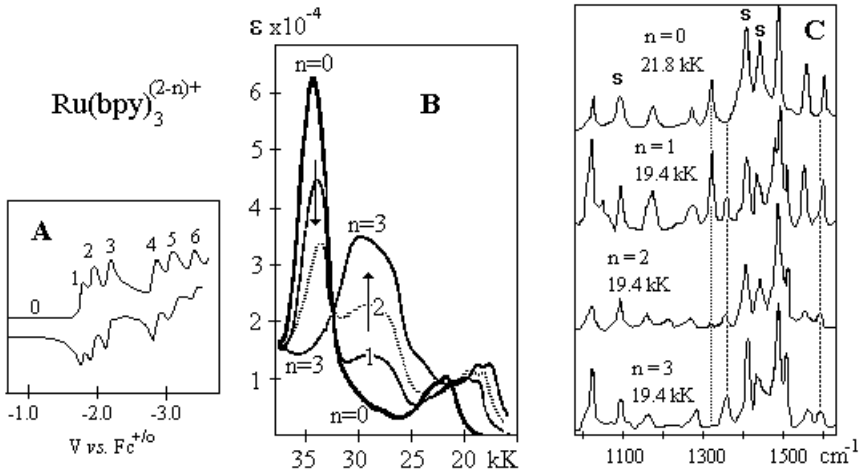

[25] Ohsawa, Y.; DeArmond, M.K.; Hanck, K.W.; Morris, D.E., *J. Am. Chem. Soc.*, **1983**, 105, 6522.

[26] Heath, G.A.; Yellowlees, L.J.; Braterman, P.S., *J. Chem. Soc. Chem. Comm.*, **1981**, 287.

[27] A one-electron reduction of $Fe(bpy)_3^{2+}$ results in a red shift of the MLCT by about 2500 cm^{-1}. See figure VI.8 and the discussion in section VI.6.

Figure VII-17. Spectroelectrochemistry of $Ru(bpy)_3^{(2-n)+}$. (**A**) The cyclic voltammogram[22] showing six reversible one-elecron processes. (**B**) The electronic spectra[23] of the parent and three reduction products. (**C**) Resonance Raman spectra[25] of the parent and three reduction products recorded at the indicated exciting lines.

the uv band centered near 34 kK is very informative. In the parent ion (n=0), this band has an extinction coefficient of about 64,000 M^{-1}-cm^{-1} upon reduction the intensity of this band drops by about 1/3 for each electron reaching 0 when n=3. Simultaneously, a new band near 28 kK grows in with its extinction coefficient increasing by about 12,000 M^{-1}-cm^{-1} with the addition of each electron. These spectra are completely incompatible with mo's spread over all of the bipyridines, but are precisely what would be expected for spatially isolated orbitals as shown in figure VII-18.

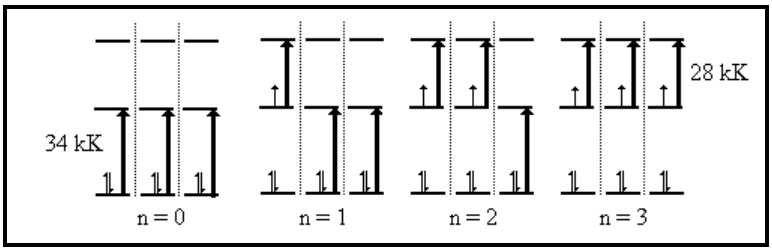

Figure VII-18. Orbital energy diagram for spatially isolated orbitals for $Ru(bpy)_3^{(2-n)+}$ and showing the disappearance of the 34 kK band with concurrent growth of the the 28 kK band with additional redox electrons.

In this model each bipyridine $\pi \rightarrow \pi^*$ transition **into** the redox orbital (34kK) has a molar extinction coefficient of about 20,000 M^{-1}-cm^{-1} while the transition originating **from** the redox orbital (28kK) has $\varepsilon \sim 12{,}000$ M^{-1}-cm^{-1}. For the n=2 case then, there are two reduced bipyridines so $\varepsilon(28kK) \sim 24{,}000$ M^{-1}-cm^{-1} and only one unreduced bipyridine so $\varepsilon(34kK) \sim 40{,}000$ M^{-1}-cm^{-1}. Another argument supporting this model is found in the resonance Raman spectra (RRS) for the reduction series (figure VII-17C). In the model predicted by group theory, the addition of electrons to an antibonding orbital should reduce the frequencies of most of the vibrations in a continuous manner, *i.e.*, the spectrum should shift slightly each time an electron is added. What is observed[28], however, is that the n=1 and n=2 spectra are composites of the n=0 and n=3 spectra, *i.e.*, the frequencies are those of either a reduced or an unreduced bipyridine and not those of -1/3 and -2/3 species. Finally EPR results[29] indicate the presence of an S=1/2 signal for all three reduction products (no coupling of electron spins) with a temperature dependent linewidth for the n=1 and n=2 species. The temperature dependence of the n=1 and n=2 species was attributed to a hopping of the redox electron between bipyridines, while in the n=3 case, all three bipyridines are reduced so the hopping ceases. A plot of ln(linewidth) *vs.* 1/T is linear and the slope was related to the barrier to electron hopping, $E_{th} \sim 1000$ cm^{-1}. This electron transfer process is similar to that described in the previous section for mixed valence species (bpy/bpy- are two bpy's in different oxidation states, *i.e.*, mixed valent) and so an optical electron transfer ($bpy/bpy^- + h\nu \rightarrow bpy^-/bpy$) is predicted. Indeed, a very weak band near 4,500 cm^{-1} was later attributed to this

[28] Angel, S.M.; DeArmond, M.K.; Donohoe, R.J.; Hanck, K.W.; Wertz, D.W., *J. Am. Chem. Soc.*, **1984**, 106, 3688.
[29] Motten, A.G.; Hanck, K.; DeArmond, M.K., *Chem. Phys. Letts.*, **1981**, 79, 541.

transition.[30] It is interesting to note that, consistent with Hush theory, the optical electron transfer is observed at about four times the thermal barrier found in EPR, *i.e.*, $E_{op} \sim 4E_{th}$.

Figure VII-19A shows the electronic absorbption spectum[31] of the emitting state of $Ru(bpy)_3^{2+}$ while figure VII-19B is the RRS.[32] The RRS of the excited state (TR^3) was done in q manner similar to that described in section VII-2 for Pt_2: the third harmonic (355 nm) of a Nd:YAG laser (1-5 mJ/pulse, 10 Hz pulse rate and a 7ns pulsewidth) was used as both the pump and probe beam. The 364 nm line of an Ar^+ laser was used for the cw (continuous wave) experiment. Woodruff *et al.* conclude that the "realistic formulation of the ^{3}MLCT state is $[Ru^{III}(bpy)_2(bpy^{-}\bullet)]^{2+}$". The two most important reasons for this conclusion are: (i) the large frequency shifts in bpy modes in the MLCT state and (ii) the TR^3 spectrum observed exhibits peaks due to both neutral and radical-like bipyridine.

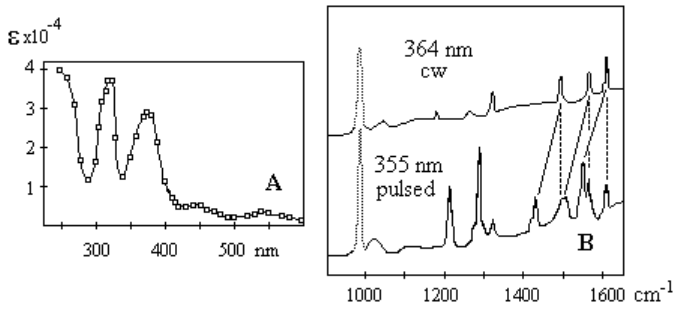

Figure VII-19. Excited state spectroscopy of $Ru(bpy)_3^{(2-n)+}$. (**A**) Excited state electronic spectrum.[24] (**B**) Resonance Raman spectra[25] recorded with CW irradiation which represents the ground state and with pulsed irradiation which consists predominantly (>90%) of the excited state. Dashed lines are to unshifted bpy peaks while solid lines are to the corresponding bpy* peaks. The dotted peak at 984 cm^{-1} is the symmetric S-O stretching in 0.50M SO_4^{2-}.

The evidence for spatially isolated orbitals in $Ru(bpy)_3^{2+}$ is quite strong and the concept is now generally accepted. Thus, as was the case in vibrational treatments, **group theory only predicts what can couple, not what will couple.**

VII.5 Metalloporphyrins

VII.5a Electronic Spectroscopy of Metalloporphyrins

Porphyrin (or *porphine)* spectra are ubiquitous in bioinorganic spectroscopy and are excellent examples of "configuration interaction" and two state coupling in resonance Raman scattering. The spectroscopy of porphyrins is rich and thorougly studied and has been extensively reviewed so in this section we will refer to only enough examples to familiarize you with the terms that are frequently encountered. Most of what follows is from Gouterman.[33]

The basic porphyrin ring (P) has D_{4h} symmetry (figure VII.20). The 18-electron, 16-membered ring at the center of the structure is responsible for the unique optical spectra of porphyrins which are perturbed by substitution at the pyrrole positions (R_1-R_8), the methine positions (meso, *m*) and/or upon chelation to a metal. Commonly studied

[30] Heath, G.; Yellowlees, L.; Braterman, P., *Chem. Phys. Letts.*, **1982**, 89, 297.

[31] Braterman, P.; Harriman, A.; Heath, G.A.; Yellowlees, L.J., *J.Chem. Soc. Dalton Trans.*, **1983**, 1801.

[32] Bradley, P.G.; Kress, N.; Hornberger, B.A.; Dallinger, R.F.; Woodruff, W.H., *J. Am. Chem. Soc.*, **1981**, 103, 7441.

[33] Gouterman, M. in *The Porphyrins*, Dolphin, D., Ed., Academic Press, New York, 1978; Vol III, pp 1-165.

porphyrins include octaethylporphyrin (OEP, substitution of ethyl groups at R_1 - R_8) and tetraphenylporphyrin (TPP, substition of phenyls at the meso positions). Porphyrin as shown is a dianion. The neutral species contains two protons coordinated to the pyrrole nitrogens and is referred to as the free-base porphyrin, H_2P.

The color of porphyrins is attributed to $\pi \rightarrow \pi^*$ transitions in the highly conjugated system. Metalloporphyrins often have two absorption bands in the visible (500 - 600 nm, $\varepsilon \sim 10^4$ M^{-1}-cm^{-1}) and a more intense band in the violet (380 - 420 nm, $\varepsilon \sim 10^5$ M^{-1}-cm^{-1}). These bands have been referred to by biochemists in order of increasing energy as the α, β, and Soret bands. The α and β bands are very weak for fully allowed $\pi \rightarrow \pi^*$ transitions and are considered to be only ***Q****uasi*-allowed and are therefore also referred to as Q-bands. Typically, they separated by about 1250 cm^{-1} and are assigned as the electronic origin (Q_0) and a vibrational satellite (Q_1) of the lowest lying $\pi\pi^*$ singlet. The Soret is also referred to as the "B-band".

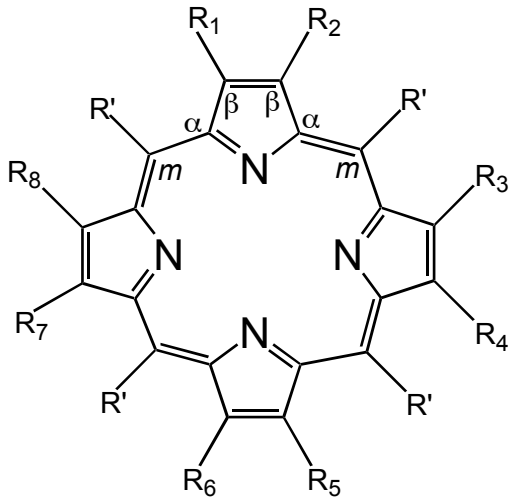

FigureVII.20. Structure of Porphyrin

Calculations indicate that the two top-filled orbitals, the $3a_{2u}(\pi)$ and the $1a_{1u}(\pi)$, are almost degenerate and their relative energies depend on substitution while the two lowest-empty orbitals, the $4e_g(\pi^*)$, are exactly degenerate. These orbitals are represented qualitatively in figure VII.21.

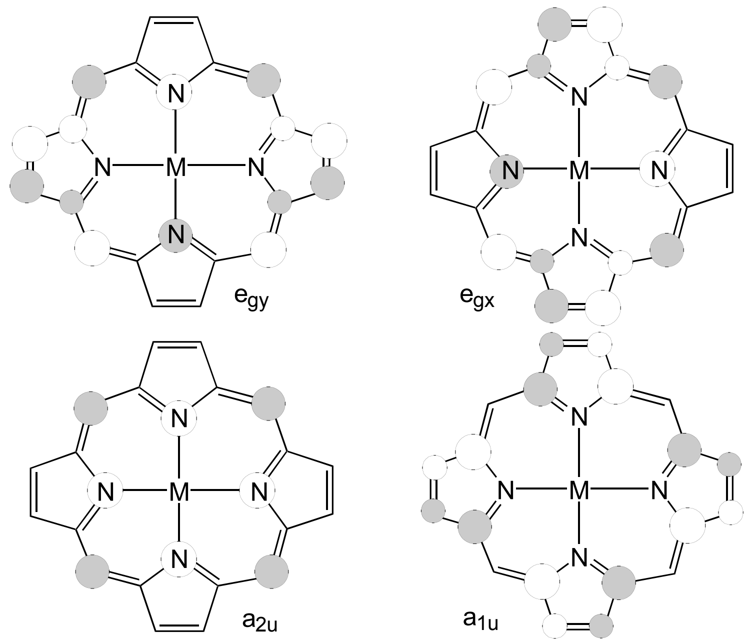

Figure VII.21. The two highest filled (e_g) and two lowest unfilled (a_{1u} & a_{2u}) molecular orbitals of a metalloporphyrin. These four form the basis of the "four orbital model".

The two lowest lying orbital transitions are the $3a_{2u} \rightarrow 4e_g$ and the $1a_{1u} \rightarrow 4e_g$ which were assigned to the Q and Soret bands, respectively, in porphine.[34] However, calculations also predict that the two transitions should have nearly equal intensity. Thus, a simple molecular orbital model was inadequate to explain the results, but a model which includes *configuration interaction* does account for most of the spectral properties.[35]

The resulting excited state configurations are ($a_{1u}e_g$) and ($a_{2u}e_g$), both of which yield E_u states. Because these excited states (configurations) are close in energy and are of the same symmetry, they can mix, *i.e.*, undergo *configuration interaction* - state not orbital mixing. The result of this interaction is that the Soret band is fully allowed while the Q-band is very weak. The resulting energy level diagram is shown in figure VII.22.

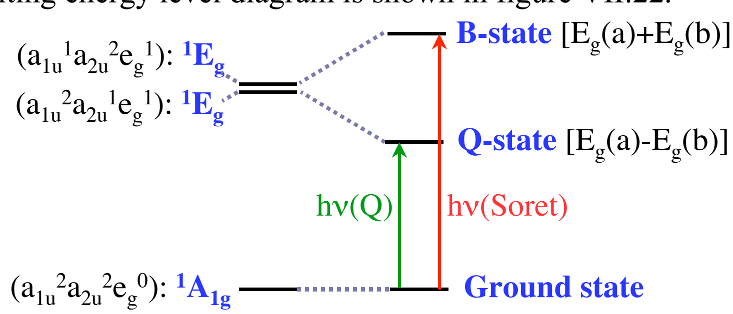

Figure VII.22. Energy level scheme showing the Q and B (Soret) states derived from a configuration interaction of the $a_{1u}e_g$ and $a_{2u}e_g$ configurations.

Metalloporphyrins are classified as *regular* or *irregular*.

- **Regular metals** have closed shells and little effect on the porphyrin spectrum, *i.e.*, the spectral properties are determined by the π electrons of the porphyrin as discussed above.

---

[34] Longuet-Higgins, H.; Rector, C.; Platt, J., *J. Chem. Phys*., **1950**, 18, 1174.

[35] (a) Gouterman, M., *J. Mol. Spectrosc*., **1961**, 6, 138. (b) Gouterman, M.; Wagniere, G.; Snyder, L., *J. Mol. Spectrosc*., **1963**, 11, 108.

- **Irregular metals** contain unfilled shells which interact with the porphyrin π-system and thus perturb the spectrum substantially resulting either *hypso* or *hyper* absorption.
  - **Hypsoabsorption** spectra appear to be very similar to those of regular porphyrins but are blue shifted.
  - **Hyperabsorption** spectra show additional, strong bands (ε>1000 M^{-1}-cm^{-1}) with λ > 320 nm ($\bar{\nu}$ < 31 kK).

The hypsochromic effect can be attributed to backbonding from the metal to the porphyrin as mixing the dπ and π* will destabilize the π* and blue-shift the porphyrin bands. The additional band in the hyperporphyrins is a charge transfer which is either a *p*- or a *d*-type. *p*-types are found in lower oxidation state main group metals and the CT band are attributed to an MLCT $a_{2u}(np_z, \text{metal}) \rightarrow e_g(\pi^*, \text{ring})$. d-type spectra are observed with transition metals with unfilled dπ orbitals and the transition is assigned to an LMCT, $a_{1u}(\pi)$ or $a_{2u}(\pi) \rightarrow e_g(d\pi, \text{metal})$. Thus Fe(II)porphyrins with weak field ligands (high spin and occupied dπ's) are hypsoporphyrins while those with strong field ligands (low spin, unoccupied dπ's) are hyperporphyrins. In D_{4h} symmetry, the $\pi(a_{2u}) \rightarrow z^2(a_{1g})$ transition ($^1A_{1g} \rightarrow {}^1A_{2u}$) is also allowed so an additional LMCT can be observed for those metals in which the d_{z^2} orbital is fairly low. Figure VII.23 shows the types of transitions expected for irregular metalloporphyrins. Note that the π→π* transition is shown to be at higher energy for the d-type than for the p-type since the d-orbital energies are expected to be much lower in the p-type and thus less energetically compatible.

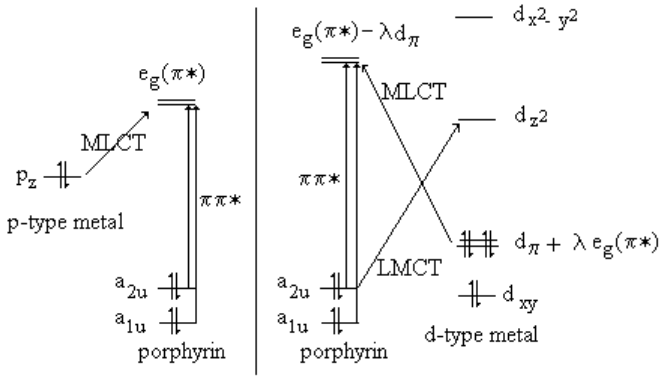

Figure VII.23. Transitions expected for p-type (left) and d-type (right) hyperporphyrins.

Figure VII.24 shows some sample spectra. H_2(OEP) is the free-base octaethyl-porphyrin. The two protons lower the symmetry to D_{2h} which lifts the degeneracy of the Q states. Note that both Q_x and Q_y have the vibronic side bands which are common to Q-bands, but the relative intensities of the two envelopes are quite different. The very strong band near 380 nm (B) is the Soret band. The two very weak peaks labelled **M** and **N** are typical of metalloporphyrins and are also attributed to π→π*. The spectrum of vanadyl OEP is very similar to that of the free-base except that the degeneracy of the Q-states is not lifted. It is therefore, a regular porphyrin.

The spectrum of Pb(II)(OEP) is that of a p-type hyperporphyrin. The CT state $[a_{2u}(6p_z) \rightarrow e_g(\pi^*)]$ is close in energy and has the same symmetry as the Soret state and, depending on the energy of the $6p_z$, can mix with the Soret state by configuration interaction. Thus the energies and relative intensities of bands A and B are quite variable. **C** is then assigned as the Q-band.

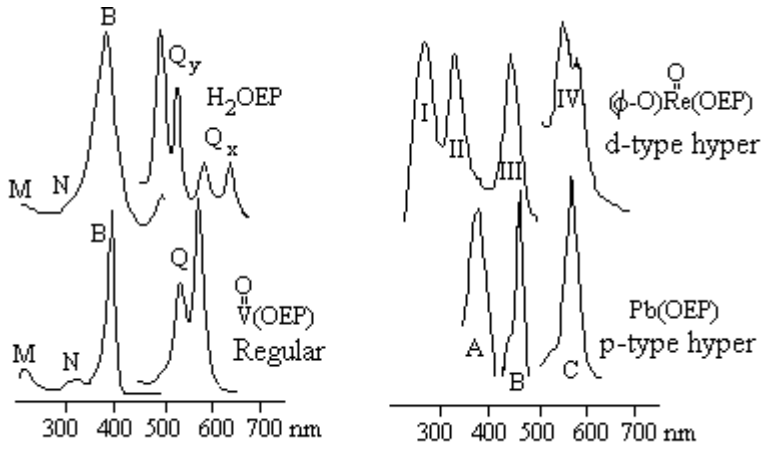

Figure VII.24. The spectra of the indicated porphyrins. Note the discontinuities in the spectra with the low energy peak being much weaker. The ratio of peak intensities in the spectrum Pb(OEP) is A:B:C =10:20:1.

(ϕ-O)Re^{V}(O)(OEP) is an example of a d-type hyperporphyrin. Band IV is the Q-band with its vibronic shoulder. Band III is assigned to a $[a_{1u}(\pi), a_{2u}(\pi)] \rightarrow e_g(d_\pi)$ CT. Band II is the Soret. Once again, there is a CT state close in energy and with the same symmetry as the Soret so that a configuration interaction between the states might be expected. Consistent with this mixing, the relative intensities of bands II and III are variable.

Problem VII.5. Band I in the spectrum of (ϕ-O)Re^{V}(O)(OEP) is not observed in the corresponding spectra of Mo^{V} or W^{V}. Suggest an assignment.

VII.5b Vibrational Spectroscopy of Metalloporphyrins

The vibrational spectra of porphyrins are extremely complicated as even the simplest porphyrin, porphin, has 3x37 - 6 = 105 normal modes. At D_{4h} symmetry, there are 102 vibrational degrees of freedom predicted for the free base porphine. The irreps for the in-plane modes can be determined in the usual way:

D_{4h}	E	$2C_2$	C_2	$2C_2'$	$2C_2''$	i	S_4	σ_h	$2\sigma_v$	$2\sigma_d$	
Γ_{xy}	72	0	0	0	0	0	0	72	0	0	$9a_{1g}, 8a_{2g}, 9b_{1g}, 9b_{2g}, 17e_u$

$$a(a_{1g}) = \frac{1}{16}\left[(1 \bullet 1 \bullet 72) + (1 \bullet 1 \bullet 72)\right] = 9a_{1g}$$

$$a(a_{2g}) = \frac{1}{16}\left[(1 \bullet 1 \bullet 72) + (1 \bullet 1 \bullet 72)\right] = 9a_{2g}$$

$$a(b_{1g}) = \frac{1}{16}\left[(1 \bullet 1 \bullet 72) + (1 \bullet 1 \bullet 72)\right] = 9b_{1g}$$

$$a(b_{2g}) = \frac{1}{16}\left[(1 \bullet 1 \bullet 72) + (1 \bullet 1 \bullet 72)\right] = 9b_{2g}$$

$$a(e_g) = \frac{1}{16}\left[(1 \bullet 2 \bullet 72) + (1 \bullet -2 \bullet 72)\right] = 0e_g$$

$$a(a_{1u}) = \frac{1}{16}\left[(1 \bullet 1 \bullet 72) + (1 \bullet -1 \bullet 72)\right] = 0a_{1u}$$

$$a(a_{2u}) = \frac{1}{16}\left[(1 \bullet 1 \bullet 72) + (1 \bullet -1 \bullet 72)\right] = 0a_{2u}$$

$$a(b_{1u}) = \frac{1}{16}\left[(1 \bullet 1 \bullet 72) + (1 \bullet -1 \bullet 72)\right] = 0b_{1u}$$

$$a(e_u) = \frac{1}{16}\left[(1 \bullet 2 \bullet 72) + (1 \bullet 2 \bullet 72)\right] = 18e_u$$

Since the rotation and translations transform as a_{2g} and e_u respectively, then the in-plane vibrations transform as: $9a_{1g}$, $8a_{2g}$, $9b_{1g}$, $9b_{2g}$, $17e_u$. The a_{1g}, b_{1g}, and b_{2g} modes are Raman-only active, while the a_{2g} is resonance-Raman active, and the e_u mode is IR active.

The irreps for the out-of-plane modes are likewise determined:

D_{4h}	E	$2C_2$	C_2	$2C_2'$	$2C_2''$	i	S_4	σ_h	$2\sigma_v$	$2\sigma_d$	
Γ_z	36	0	0	-4	-2	0	0	-36	4	2	$8e_g, 3a_{1u}, 5a_{2u}, 4b_{1u}, 5b_{2u}$

$$a(a_{1g}) = \frac{1}{16}\left[(1\bullet 1\bullet 36)+(2\bullet 1\bullet -4)+(2\bullet 1\bullet -2)+(1\bullet 1\bullet -36)+(2\bullet 1\bullet 4)+(2\bullet 1\bullet 2)\right] = 0a_{1g}$$

$$a(a_{2g}) = \frac{1}{16}\left[(1\bullet 1\bullet 36)+(2\bullet -1\bullet -4)+(2\bullet -1\bullet -2)+(1\bullet 1\bullet -36)+(2\bullet -1\bullet 4)+(2\bullet -1\bullet 2)\right] = 0a_{2g}$$

$$a(b_{1g}) = \frac{1}{16}\left[(1\bullet 1\bullet 36)+(2\bullet 1\bullet -4)+(2\bullet -1\bullet -2)+(1\bullet 1\bullet -36)+(2\bullet 1\bullet 4)+(2\bullet -1\bullet 2)\right] = 0b_{1g}$$

$$a(b_{2g}) = \frac{1}{16}\left[(1\bullet 1\bullet 36)+(2\bullet -1\bullet -4)+(2\bullet 1\bullet -2)+(1\bullet 1\bullet -36)+(2\bullet -1\bullet 4)+(2\bullet 1\bullet 2)\right] = 0b_{2g}$$

$$a(e_{g}) = \frac{1}{16}\left[(1\bullet 2\bullet 36)+(2\bullet 0\bullet -4)+(2\bullet 0\bullet -2)+(1\bullet -2\bullet -36)+(2\bullet 0\bullet 4)+(2\bullet 0\bullet 2)\right] = 9e_{g}$$

$$a(a_{1u}) = \frac{1}{16}\left[(1\bullet 1\bullet 36)+(2\bullet 1\bullet -4)+(2\bullet 1\bullet -2)+(1\bullet -1\bullet -36)+(2\bullet -1\bullet 4)+(2\bullet -1\bullet 2)\right] = 3a_{1u}$$

$$a(a_{2u}) = \frac{1}{16}\left[(1\bullet 1\bullet 36)+(2\bullet -1\bullet -4)+(2\bullet -1\bullet -2)+(1\bullet -1\bullet -36)+(2\bullet 1\bullet 4)+(2\bullet 1\bullet 2)\right] = 6a_{2u}$$

$$a(b_{1u}) = \frac{1}{16}\left[(1\bullet 1\bullet 36)+(2\bullet 1\bullet -4)+(2\bullet -1\bullet -2)+(1\bullet -1\bullet -36)+(2\bullet -1\bullet 4)+(2\bullet 1\bullet 2)\right] = 4b_{1u}$$

$$a(b_{2u}) = \frac{1}{16}\left[(1\bullet 1\bullet 36)+(2\bullet -1\bullet -4)+(2\bullet 1\bullet -2)+(1\bullet -1\bullet -36)+(2\bullet 1\bullet 4)+(2\bullet -1\bullet 2)\right] = 5b_{2u}$$

$$a(e_{u}) = \frac{1}{16}\left[(1\bullet 2\bullet 36)+(2\bullet 0\bullet -4)+(2\bullet 0\bullet -2)+(1\bullet 2\bullet -36)+(2\bullet 0\bullet 4)+(2\bullet 0\bullet 2)\right] = 0e_{u}$$

Since the rotations and translation transform as e_g and a_{2u} respectively, then the out-of-plane vibrations transform as: $8e_g$,$3a_{1u}$, $5a_{2u}$, $4b_{1u}$, $5b_{2u}$. The e_g modes are Raman active, while the a_{2u} modes are IR active. The a_{1u},, b_{1u}, and b_{2u} modes are inactive. To summarize:

22 IR-only modes ($17e_u + 5a_{2u}$)
35 Raman modes ($9a_{1g} + 9b_{1g} + 9b_{2g} + 8e_g$)
8 resonance Raman-only modes ($8a_{2g}$)
12 inactive modes ($3a_{1u}$, $4b_{1u}$, $5b_{2u}$)

Despite their complexity and due to their importance, porphyrins have been extensively studied in both the IR and in the Raman and excellent reviews are available.[36] Due to the strong absorption in the visible, metalloporphyrins are ideal for resonance Raman studies with strong contributions from both the A- and B-terms.[37] The A-term derives from one-state coupling and results in enhancement of the a_{1g} modes which are active due to either/both the isotropy, G^o, and the symmetric anisotropy, G^s, with $0 < \rho \leq 3/4$, since:

$$\rho = \frac{3G^s}{10G^o + 4G^s}$$

The B-term derives from two-state coupling of the Q- and Soret states each of which is of E_u symmetry. Thus, the vibrations active in the B-term are $E_u \otimes E_u = a_{1g} + a_{2g} + b_{1g} + b_{2g}$. The a_{1g} modes are active due to either/both the isotropy, G^o, and the symmetric anisotropy, G^s, as

[36] Kitagawa, T.; Ozaki, Y., Struct. Bonding, 1987, 64,71. Nakamoto, K., **Infrared and Raman Spectra of Inorganic and Coordination Compounds**, 4th Ed., John Wiley and Sons, NY, 1986.

[37] See sections IV.10 and VI.8 for reviews of normal and resonance Raman, respectively.

such they are polarized with $0 < \rho \leq 3/4$. The b_{1g} and b_{2g} modes are active due to contributions from the symmetric anisotropy only ($G^0=0$) and will be depolarized:

$$\rho = \frac{3G^s}{10G^o + 4G^s} = \frac{3G^s}{4G^s} = \frac{3}{4}$$

The a_{2g} modes result from the anitsymmetric anisotropy, G^a, only and will, therefore, be observed to be active only under resonance conditions and with anomalous polarization, *i.e.*,

$$\rho = \frac{5G^a}{\lim_{G^0 \to 0} 10G^o} = \infty$$

The electronic absorption and resonance Raman spectra observed while probing the Soret and the vibrational satellite of the Q band are shown in figure VII.25. A few comments about these spectra will exemplify several points of resonance Raman. Typically, probing the Soret band (406 nm) results in enhancement of modes *via* the A-term, *i.e.*, totally symmetric modes and in this region of the spectrum four a_{1g} modes are expected.[38] The three polarized, very strong peaks at 1603, 1519 and 1383 cm^{-1} are readily assigned as a_{1g}. The fourth fundamental must be one of the remaining polarized peaks 1025, 1260 or 1139 cm^{-1}. After careful study, it was concluded that the 1260 and 1139 cm^{-1} bands could be assigned to overtones or combinations so the 1025 cm-1 band must be due to the remaining a_{1g} mode. The bands at 1655 and 1220 cm^{-1} are depolarized and thus not of a_{1g} symmetry. The spectrum observed with 514 nm excitation has anomalously polarized peaks at 1603, 1397, 1308 and 1121 cm^{-1} which must be a_{2g}. Note that there are two separate peaks near 1600 cm^{-1}- 1603 (a_{1g}) and 1602 (a_{2g}). Kitagawa, Abe, et.al [39,40] examined the spectra of the meso-deuterated and the ^{15}N-substituted derivatives of NiOEP and assigned some 90 overtones and combintation bands to aid in the assignment of the fundamentals. Their normal coordinates are the generally accepted set.

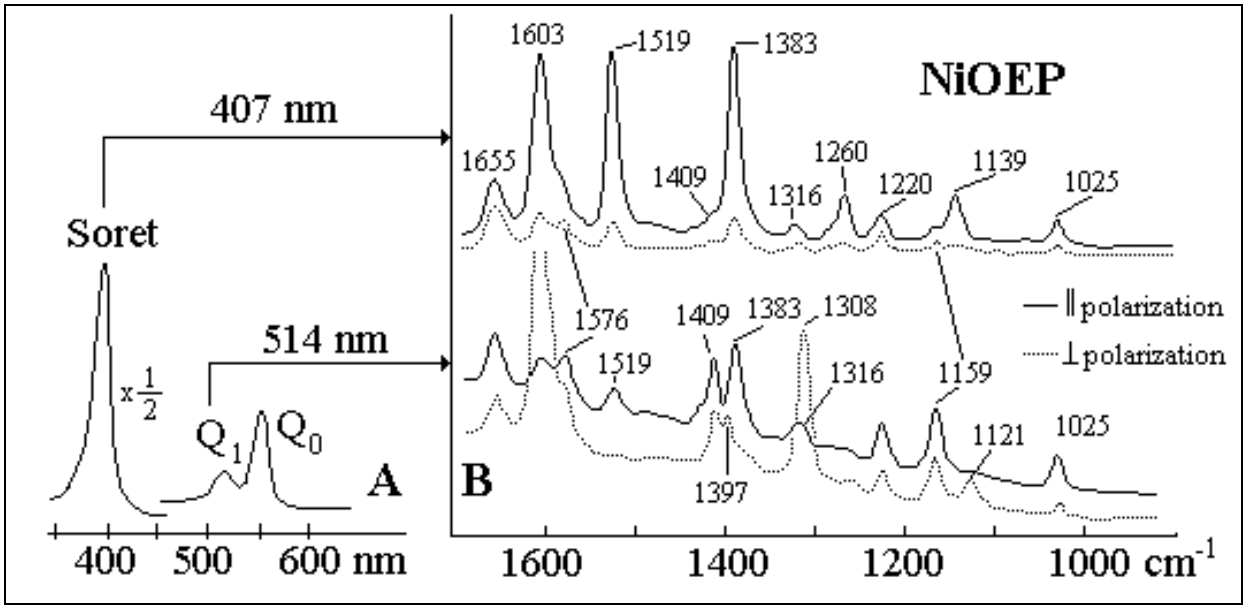

[38] There are $9a_{1g}$ modes, but one is a ν(C-H) which expected near 3000cm^{-1} and four are bending modes which are typically below 1000 cm^{-1}

[39] Kitagawa, T.; Abe, M., Ogoshi, H., *J. Chem. Phys*., **1978**, 69, 4516.

[40] Abe, M.; Kitagawa, T., Kyogoku, Y., *J. Chem. Phys.*, **1978**, 69,4526.

Figure VII.25. (A)The visible region of the electronic spectrum of NiOEP in CH_2Cl_2. (B) Resonance Raman spectra of NiOEP in CH_2Cl_2 recorded with 514 nm (bottom) and 406 nm (top) excitation. Both parallel (solid) and perpendicular (dotted) polarizations are shown.

There has been such a great amount of work done on the vibrational spectra of porphyrins that several *empirical trends* have emerged in regard to the structural implications of the vibrational frequencies of some of the bands. These bands are referred to as *marker bands* and serve as indicators for the coordination number, spin- and oxidation-states of the metal, and the core size.[41] The normal modes[36] corresponding to these marker bands are given in figure VII.26 and their sensitivities and potential energy distributions are summarized in Table VII.3. All of the modes are stretches with the exception of ν_7 which has substantial deformation character and is essentially a breathing of the 16-membered porphyrin ring. As such, it is strong for planar systems and weak for non-planar or *domed* systems. As the spin state of the iron is increased, the porphyrin tends to expand or be domed[42] which will weaken the C_α-C_m bond and those modes which contain substantial contribution from the stretch of this bond (ν_3, ν_4 and ν_{10}) will be sensitive to the spin state with a high spin state associated with lower frequencies.

[41] The core size is defined as the distance from the center of the porphyrin to the pyrrole nitrogens.

[42] A domed porphyrin is one that is non-planar as a result of the pyrroles tilting toward a metal which is out of the porphyrin plane.

Table VII.3. Structural Sensitivity of the marker bands of OEP

mode	cm^{-1}	PED (%)	Sensitivity
ν_3	1509	$\nu(C_\alpha C_m)$ 41; $\nu(C_\alpha C_\beta)$ 35	spin, oxidation
ν_4	1383	$\nu(C_\alpha N)$ 53; $\nu(C_\alpha C_m)$ 21	oxidation, metal
ν_7	674	$\delta(C_\beta C_\alpha N)$ 20; $\nu(C_\alpha C_\beta)$ 19	porphyrin ring doming
ν_{10}	1655	$\nu(C_\alpha C_m)$ 49; $\nu(C_\alpha C_\beta)$ 17	spin, oxidation
ν_{11}	1576	$\nu(C_\beta C_\beta)$ 57; $\nu(C_\beta Et)$ 16	substituent
ν_{19}	1603	$\nu'(C_\alpha C_m)$ 67; $\nu'(C_\alpha C_\beta)$ 18	spin

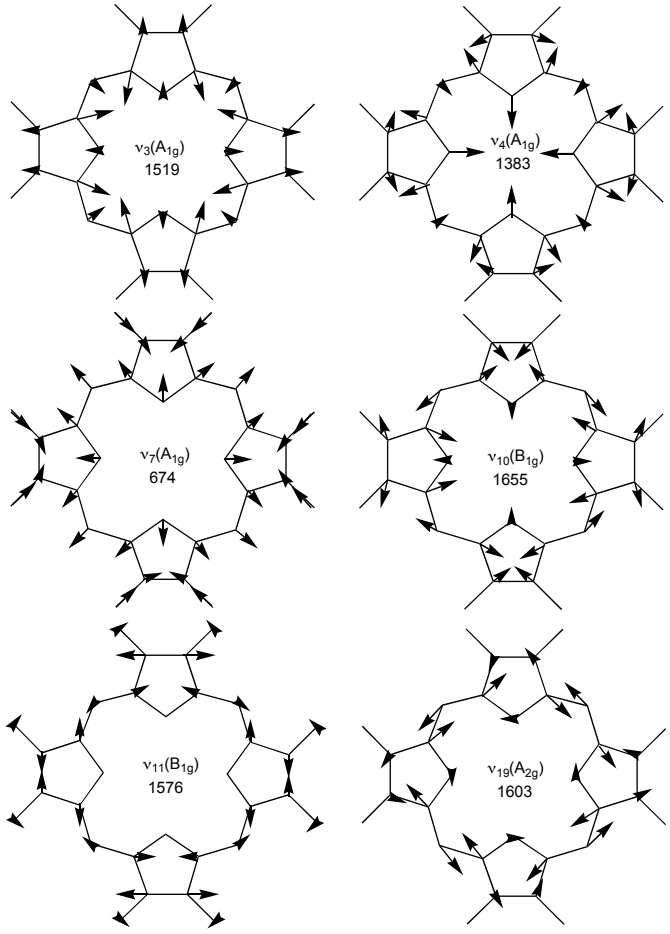

Figure VII.26. Normal modes of vibration of structure sensitive bands of NiOEP from reference 40.

Figure VII.27 shows how the marker band frequencies vary with the core size of Ni(OEP) and a series of derivatives of Fe(OEP). The variations are 576, 495, 414, 288 and 322 cm^{-1}/A.[43] for ν_{19}, ν_{10}, ν_3, ν_{11} and ν_2, respectively. The deviations of $Fe(OEP(Im)_2$ from the line have been attriubuted to increased π-back donation.

[43] Osaki, Y.; Iriyama, K.; Ogoshi, H.; Ochiai, T.; Kitagawa, T., *J. Phys. Chem*., **1986**, 90, 6105.

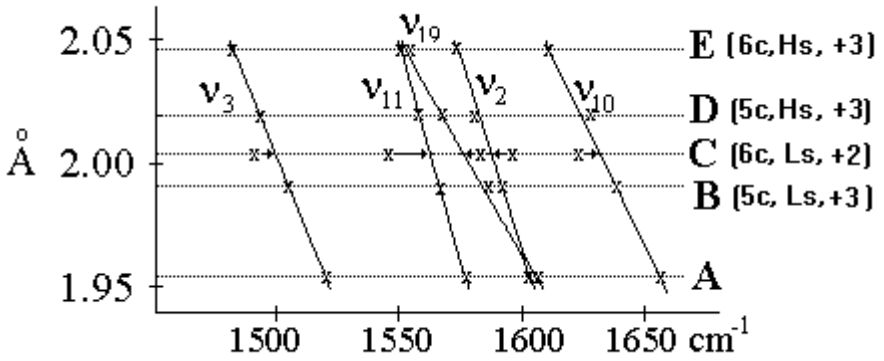

Figure VII.27. Correlations of the marker bands with the porphyrin core-size from reference 38. A = Ni(OEP); B = [Fe(OEP)(Im)$_2$]Br; C = Fe(OEP(Im)$_2$; D = Fe(OEP)Br; E = [Fe(OEP)(Me$_2$SO)]ClO$_4$; Im = imidazole. (6c, Hs, +3) = 6-coordinate, high spin Fe(III).

Appendix A. Character Tables for selected point groups.

C_s	E	σ_h		
A'	1	1	x,y,R_z	x^2,y^2,z^2,xy
A"	1	-1	z,R_x,R_y	yz,xz

C_i	E	i		
A_g	1	1	R_x,R_y,R_z	x^2,y^2,z^2,xy,xz,yz
A_u	1	-1	x,y,z	

C_2	E	C_2		
A	1	1	z,R_z	x^2+y^2,z^2
B	1	-1	x,y,R_x,R_y	yz,xz

D_2	E	$C_2(z)$	$C_2(y)$	$C_2(x)$		
A	1	1	1	1		x^2,y^2,z^2, xy
B_1	1	1	-1	-1	z,Rz	xy
B_2	1	-1	1	-1	y, Ry	xz
B_3	1	-1	-1	1	x,Rx	yz

D_3	E	$2C_3$	$3C_2$		
A_1	1	1	1		x^2+y^2, z^2
A_2	1	1	-1	z,R_z	
E	2	-1	0	(x,y);(R_x,R_y)	(xz,yz); (x^2-y^2,xy)

C_{2v}	E	C_2	$\sigma_v(xz)$	$\sigma_v(yz)$		
A_1	1	1	1	1	z	x^2,y^2,z^2
A_2	1	1	-1	-1	R_z	xy
B_1	1	-1	1	-1	x,R_y	xz
B_2	1	-1	-1	1	y,R_x	yz

C_{3v}	E	$2C_3$	$3\sigma_v$		
A_1	1	1	1	z	x^2+y^2, z^2
A_2	1	1	-1	R_z	
E	2	-1	0	(x,y), (R_x,R_y)	(x^2-y^2,xy), (xz,yz)

C_{4v}	E	$2C_4$	C_2	$2\sigma_v$	$2\sigma_d$		
A_1	1	1	1	1	1	z	x^2+y^2, z^2
A_2	1	1	1	-1	-1	R_z	
B_1	1	-1	1	1	-1		x^2-y^2
B_2	1	-1	1	-1	1		xy
E	2	0	-2	0	0	(x,y) (R_x,R_y)	(xz,yz)

C_{2h}	E	C_2	i	σ_h		
A_g	1	1	1	1	R_z	x^2,y^2, z^2, xy
B_g	1	-1	1	-1	R_x, R_y	xz, yz
A_u	1	1	-1	-1	z	
B_u	1	-1	-1	1	x, y	

D_{2h}	E	$C_2(z)$	$C_2(y)$	$C_2(x)$	i	$\sigma(xy)$	$\sigma(xz)$	$\sigma(yz)$		
A_g	1	1	1	1	1	1	1	1		x^2, y^2,z^2
B_{1g}	1	1	-1	-1	1	1	-1	-1	R_z	xy
B_{2g}	1	-1	1	-1	1	-1	1	-1	R_y	xz
B_{3g}	1	-1	-1	1	1	-1	-1	1	R_x	yz
A_u	1	1	1	1	-1	-1	-1	-1		
B_{1u}	1	1	-1	-1	-1	-1	1	1	z	
B_{2u}	1	-1	1	-1	-1	1	-1	1	y	
B_{3u}	1	-1	-1	1	-1	1	1	-1	x	

$\mathbf{D_{3h}}$	E	$2C_3$	$3C_2$	σ_h	$2S_3$	$3\sigma_v$		
A_1'	1	1	1	1	1	1		x^2+y^2, z^2
A_2'	1	1	-1	1	1	-1	R_z	
E'	2	-1	0	2	-1	0	(x,y)	(x^2-y^2, xy)
A_1''	1	1	1	-1	-1	-1		
A_2''	1	1	-1	-1	-1	1	z	
E''	2	-1	0	-2	1	0	(R_x,R_y)	(xz,yz)

$\mathbf{D_{4h}}$	E	$2C_4$	C_2	$2C_2'$	$2C_2''$	i	$2S_4$	σ_h	$2\sigma_v$	$2\sigma_d$		
A_{1g}	1	1	1	1	1	1	1	1	1	1		x^2+y^2, z^2
A_{2g}	1	1	1	-1	-1	1	1	1	-1	-1	R_z	
B_{1g}	1	-1	1	1	-1	1	-1	1	1	-1		x^2-y^2
B_{2g}	1	-1	1	-1	1	1	-1	1	-1	1		xy
E_g	2	0	-2	0	0	2	0	-2	0	0	(R_x, R_y)	(xz, yz)
A_{1u}	1	1	1	1	1	-1	-1	-1	-1	-1		
A_{2u}	1	1	1	-1	-1	-1	-1	-1	1	1	z	
B_{1u}	1	-1	1	1	-1	-1	1	-1	-1	1		
B_{2u}	1	-1	1	-1	1	-1	1	-1	1	-1		
E_u	2	0	-2	0	0	-2	0	2	0	0	(x,y)	

$\mathbf{D_{5h}}$	E	$2C_5$	$2C_5^2$	$5C_2$	σ_h	$2S_5$	$2S_5^3$	$5\sigma_v$		
A_1'	1	1	1	1	1	1	1	1		x^2+y^2, z^2
A_2'	1	1	1	-1	1	1	1	-1	R_z	
E_1'	2	$2\cos72^o$	$2\cos144^o$	0	2	$2\cos72^o$	$2\cos144^o$	0	(x,y)	
E_2'	2	$2\cos144^o$	$2\cos72^o$	0	2	$2\cos144^o$	$2\cos72^o$	0		(x^2-y^2, xy)
A_1''	1	1	1	1	-1	-1	-1	-1		
A_2''	1	1	1	-1	-1	-1	-1	1	z	
E_1''	2	$2\cos72^o$	$2\cos144^o$	0	-2	$-2\cos72^o$	$-2\cos144^o$	0	(R_x, R_y)	(xz, yz)
E_2''	2	$2\cos144^o$	$2\cos72^o$	0	-2	$-2\cos144^o$	$-2\cos72^o$	0		

$\mathbf{D_{6h}}$	E	$2C_6$	$2C_3$	C_2	$3C_2'$	$3C_2''$	i	$2S_3$	$2S_6$	σ_h	$3\sigma_d$	$3\sigma_v$		
A_{1g}	1	1	1	1	1	1	1	1	1	1	1	1		x^2+y^2, z^2
A_{2g}	1	1	1	1	-1	-1	1	1	1	1	-1	-1	R_z	
B_{1g}	1	-1	1	-1	1	-1	1	-1	1	-1	1	-1		x^2-y^2
B_{2g}	1	-1	1	-1	-1	1	1	-1	1	-1	-1	1		xy
E_{1g}	2	1	-1	-2	0	0	2	1	-1	-2	0	0	(R_x,R_y)	(xz,yz)
E_{2g}	2	-1	-1	2	0	0	2	-1	-1	2	0	0		
A_{1u}	1	1	1	1	1	1	-1	-1	-1	-1	-1	-1		
A_{2u}	1	1	1	1	-1	-1	-1	-1	-1	-1	1	1	z	
B_{1u}	1	-1	1	-1	1	-1	-1	1	-1	1	-1	1		
B_{2u}	1	-1	1	-1	-1	1	-1	1	-1	1	1	-1		
E_{1u}	2	1	-1	-2	0	0	-2	-1	1	2	0	0	(x,y)	
E_{2u}	2	-1	-1	2	0	0	-2	1	1	-2	0	0		

$\mathbf{D_{2d}}$	E	$2S_4$	C_2	$2C_2'$	$2\sigma_d$		
A_1	1	1	1	1	1		x^2+y^2, z^2
A_2	1	1	1	-1	-1	R_z	
B_1	1	-1	1	1	-1		x^2-y^2
B_2	1	-1	1	-1	1	z	xy
E	2	0	-2	0	0	(x,y); (R_x,R_y)	(xz,yz)

$\mathbf{D_{3d}}$	E	$2C_3$	$3C_2$	i	$2S_6$	$3\sigma_d$		
A_{1g}	1	1	1	1	1	1		x^2+y^2, z^2
A_{2g}	1	1	-1	1	1	-1	R_z	
E_g	2	-1	0	2	-1	0	(R_x,R_y)	$(x^2-y^2,xy);(xz,yz)$

A_{1u}	1	1	1	-1	-1	-1		
A_{2u}	1	1	-1	-1	-1	1	z	
E_u	2	-1	0	-2	1	0	(x,y)	

S_4	E	S_4	C_2	S_4^3		
A	1	1	1	1	R_z	x^2+y^2, z^2
B	1	-1	1	-1	z	x^2-y^2, xy
E	1	±i	-1	-(±i)	(x,y); (R_x,R_y)	(xz,yz)

T_d	E	$8C_3$	$3C_2$	$6S_4$	$6\sigma_d$		
A_1	1	1	1	1	1		$x^2+y^2+z^2$
A_2	1	1	1	-1	-1		
E	2	-1	2	0	0		($2z^2-x^2-y^2$, x^2-y^2)
T_1	3	0	-1	1	-1	(R_x, R_y,R_z)	
T_2	3	0	-1	-1	1	(x,y,z)	(xz,yz.xy)

O_h	E	$8C_3$	$6C_2$	$6C_4$	$3C_2$ (=C_4^2)	i	$6S_4$	$8S_6$	$3\sigma_h$	$6\sigma_d$		
A_{1g}	1	1	1	1	1	1	1	1	1	1		$x^2+y^2+z^2$
A_{2g}	1	1	-1	-1	1	1	-1	1	1	-1		
E_g	2	-1	0	0	2	2	0	-1	2	0		($2z^2-x^2-y^2$,x^2-y^2)
T_{1g}	3	0	-1	1	-1	3	1	0	-1	-1	(R_x,R_y,R_z)	
T_{2g}	3	0	1	-1	-1	3	-1	0	-1	1		(xz,yz,xy)
A_{1u}	1	1	1	1	1	-1	-1	-1	-1	-1		
A_{2u}	1	1	-1	-1	1	-1	1	-1	-1	1		
E_u	2	-1	0	0	2	-2	0	1	-2	0		
T_{1u}	3	0	-1	1	-1	-3	-1	0	1	1	(x,y,z)	
T_{2u}	3	0	1	-1	-1	-3	1	0	1	-1		

Appenidix B. Constants & Useful Energy Conversions

Planck's Constant, $h = 6.626 \times 10^{-34}$ J-s
Boltzman's Constant, $k = 1.381 \times 10^{-23}$ J/K = 0.6950 cm^{-1}/K
speed of light, $c = 2.998 \times 10^{8}$ m/s

1 eV = 1.60219×10^{-19} J = 96.485 kJ/mol = 22.58 kcal/mol = 8065.5 cm^{-1}
1 cm^{-1} = 11.96 J/mol = 2.859 cal/mol = 0.1240 meV

Appendix C. Some Direct Products

Note that is some instances, g and u must be added (gxg=uxu=g; gxu=u), some subscripts must be omitted and ' and " must be added (' x ' = " x" = '; ' x " = ")

D_2, D_{2h}	A	B_1	B_2	B_3
A	A	B_1	B_2	B_3
B_1		A	B_3	B_2
B_2			A	B_1
B_3				A

C_{2v}	A_1	A_2	B_1	B_2
A_1	A_1	A_2	B_1	B_2
A_2		A_1	B_2	B_1
B_1			A_1	A_2
B_2				A_1

C_{3v}, D_3, D_{3d}, D_{3h}	A_1	A_2	E
A_1	A_1	A_2	E
A_2		A_1	E
E			A_1+[A_2]+E

C_4, C_{4h}, S_4	A	B	E
A	A	B	E
B		A	E
E			[A]+A+E

C_{4v}, D_4, D_{2d}, D_{4h}	A_1	A_2	B_1	B_2	E
A_1	A_1	A_2	B_1	B_2	E
A_2		A_1	B_2	B_1	E
B_1			A_1	A_2	E
B_2				A_1	E
E					A_1+[A_2]+B_1+B_2

C_{5v}, , D_5, D_{5h},$_{5d}$	A_1	A_2	E_1	E_2
A_1	A_1	A_2	E_1	E_2
A_2		A_1	E_1	E_2
E_1			A_1+[A_2]+E_2	E_1+E_2
E_2				A_1+[A_2]+E_1

C_6, C_{6h}	A	B	E_1	E_2
A	A	B	E_1	E_2
B		A	E_2	E_1
E_1			[A]+A+E_2	2B+E_1
E_2				[A]+A+E_2

C_{6v}, D_6, D_{6h}	A_1	A_2	B_1	B_2	E_1	E_2
A_1	A_1	A_2	B_1	B_2	E_1	E_2
A_2		A_1	B_2	B_1	E_1	E_2
B_1			A_1	A_2	E_2	E_1
B_2				A_1	E_2	E_1
E_1					A_1+[A_2]+E_2	B_1+B_2+E_1
E_2						A_1+[A_2]+E_2

O_h, T_d	A_1	A_2	E	T_1	T_2
A_1	A_1	A_2	E	T_1	T_2
A_2		A_1	E	T_2	T_1
E			A_1+[A_2]+E	T_1+T_2	T_1+T_2
T_1				A_1+E+[T_1]+T_2	A_2+E+T_1+T_2
T_2					A_1+E+[T_1]+T_2

Appendix D. Standard Valence Orbital H_{ii} values (eV).

Atom	ns	np	(n-1)d	n
H	-13.6			1
B	-15.2	-8.5		2
C	-21.4	-11.4		
N	-26.0	-13.4		
O	-32.3	-14.8		
F	-40.0	-18.1		
Si	-17.3	-9.2		3
P	-18.7	-14.0		
S	-20.0	-13.3		
Cl	-26.3	-14.2		
Sc	-8.9	-2.8	-8.5	4
Ti	-9.0	-5.4	-10.8	
V	-8.8	-5.5	-11.0	
Cr	-8.7	-5.2	-11.2	
Mn	-9.8	-5.9	-11.7	
Fe	-9.1	-5.3	-12.6	
Co	-9.2	-5.3	-13.2	
Ni	-9.2	-5.2	-13.5	
Cu	-11.4	-6.1	-14.0	
Zn	-12.4	-6.5		
Ga	-14.6	-6.8		
Ge	-16.0	-9.0		
As	-16.2	-12.2		
Se	-20.5	-13.2		
Br	-22.7	-13.1		
Mo	-8.3	-5.2	-10.5	5
Ru	-10.4	-6.9	-14.9	
Rh	-3.09	-4.6	-12.5	
Pd	-7.3	-3.8	-12.0	
Sb	-18.8	-11.7		
I	-18.0	-12.7		
Te	-20.8	-13.2		6
W	-8.3	-5.2	-10.4	
Re	-9.36	-6.0	-12.7	
Os	-8.5	3.5	-11.0	
Pt	-9.1	-5.5	-12.6	
Au	-10.9	-5.6	-15.1	